AD-A122 744 POST-CRAZING STRESS ANALYSIS OF GLASS-EPOXY LAMINATES 1/2
(U) TENNESSEE TECHNOLOGICAL UNIV COOKEVILLE DEPT OF
ENGINEERING S.. D G SMITH ET AL. MAY 79 TTU-ESM-79-1

UNCLASSIFIED DAAK40-78-C-0165 F/G 11/9 NL

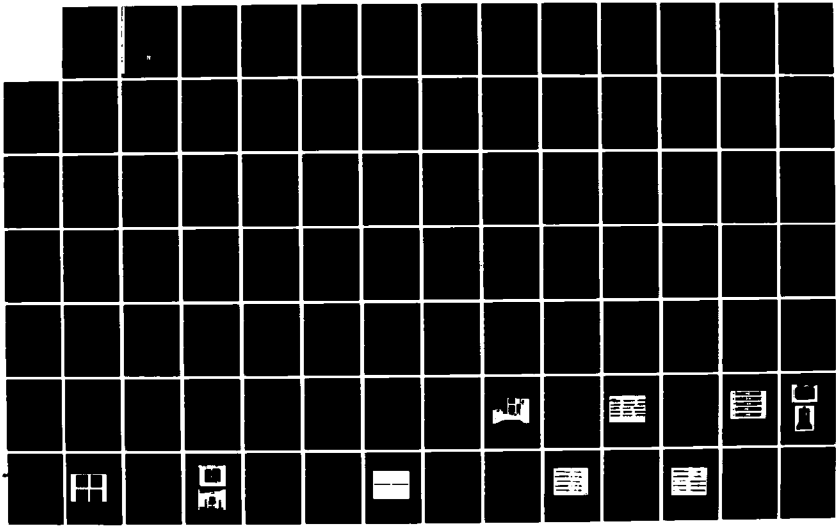

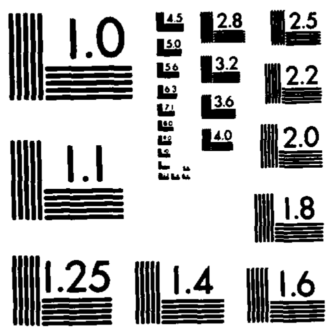

MICROCOPY RESOLUTION TEST CHART
NATIONAL BUREAU OF STANDARDS-1963-A

TTU-ESM-79-1

(1)

AD A122744

POST-CRAZING STRESS ANALYSIS OF GLASS-EPOXY LAMINATES

Dallas G. Smith and Ju-Chin Huang

PREPARED FOR

U. S. ARMY MISSILE RESEARCH AND DEVELOPMENT COMMAND

REDSTONE ARSENAL

ALABAMA

CONTRACT NUMBER DAAK40-78-C-0165

MAY 1979

TENNESSEE TECHNOLOGICAL UNIVERSITY

DEPARTMENT OF ENGINEERING SCIENCE AND MECHANICS

COOKEVILLE, TENNESSEE 38501

DISCLAIMER

The findings of this report are not to be construed as an official Department of the Army position unless so designated by other authorized documents.

50272-101

REPORT DOCUMENTATION PAGE	1. REPORT NO. TTU-ESM-79-1	2.	3. Recipient's Accession No.

4. Title and Subtitle Post-Crazing Stress Analysis of Glass-Epoxy Laminates	5. Report Date May 1979
	6.
7. Author(s) Dallas G. Smith and Ju-Chin Huang	8. Performing Organization Rept. No. TTU-ESM-79-1
9. Performing Organization Name and Address Tennessee Technological University Department of Engineering Science and Mechanics Cookeville, Tennessee 38501	10. Project/Task/Work Unit No.
	11. Contract(C) or Grant(G) No. (C) DAAK40-78-C-0165 (G)
12. Sponsoring Organization Name and Address U. S. Army Missile Research & Development Command DRDMI-TLA Redstone Arsenal, AL 35809	13. Type of Report & Period Covered Final, 5/78 - 5/79
	14.

15. Supplementary Notes

16. Abstract (Limit: 200 words)

A glass-epoxy material known as Scotchply XP-250 was characterized. The material's various strengths and stiffnesses were determined in tension, compression, and shear. The three-rail fixture was used for the shear tests. A modified IITRI fixture was used for compression. Glass-epoxy laminates having the following layups were tested in tension: $[\pm30]_s$, $[\pm45]_s$, $[\pm60]_s$, and $[0/\pm45/90]_s$. The stress-strain behavior in the pre- and post-crazing regions was predicted with a lamination program which employed the nonlinear ply shear curve. These predicted and test results were compared.

A finite element program was written for obtaining stress analysis of laminated structures with stress concentrations. The program used a doubly-curved, isoparametric, thick-plate or thick-shell element. A number of example problems were solved. The finite element results were compared to test results for a $[0/\pm45/90]_s$ tension coupon containing a hole.

17. Document Analysis a. Descriptors

Angle plys
Shear testing
Compression testing
Stress concentrations
Finite elements
Isoparametric element
Doubly-curved element
Thick-shell element
Thick-plate element

b. Identifiers/Open-Ended Terms

Glass-epoxy
Laminates
Composite materials
Failure analysis

c. COSATI Field/Group

18. Availability Statement:	19. Security Class (This Report)	21. No. of Pages
Distribution unlimited	Unclassified	
	20. Security Class (This Page) Unclassified	22. Price

(See ANSI-Z39.18) See Instructions on Reverse OPTIONAL FORM 272 (4-77)
(Formerly NTIS-35)
Department of Commerce

DO NOT PRINT THESE INSTRUCTIONS AS A PAGE IN A REPORT

INSTRUCTIONS

Optional Form 272, Report Documentation Page is based on Guidelines for Format and Production of Scientific and Technical Reports, ANSI Z39.18–1974 available from American National Standards Institute, 1430 Broadway, New York, New York 10018. Each separately bound report—for example, each volume in a multivolume set—shall have its unique Report Documentation Page.

1. Report Number. Each individually bound report shall carry a unique alphanumeric designation assigned by the performing organization or provided by the sponsoring organization in accordance with American National Standard ANSI Z39.23–1974, Technical Report Number (STRN). For registration of report code, contact NTIS Report Number Clearinghouse, Springfield, VA 22161. Use uppercase letters, Arabic numerals, slashes, and hyphens only, as in the following examples: FASEB/NS–75/87 and FAA/RD–75/09.
2. Leave blank.
3. Recipient's Accession Number. Reserved for use by each report recipient.
4. Title and Subtitle. Title should indicate clearly and briefly the subject coverage of the report, subordinate subtitle to the main title. When a report is prepared in more than one volume, repeat the primary title, add volume number and include subtitle for the specific volume.
5. Report Date. Each report shall carry a date indicating at least month and year. Indicate the basis on which it was selected (e.g., date of issue, date of approval, date of preparation, date published).
6. Sponsoring Agency Code. Leave blank.
7. Author(s). Give name(s) in conventional order (e.g., John R. Doe, or J. Robert Doe). List author's affiliation if it differs from the performing organization.
8. Performing Organization Report Number. Insert if performing organization wishes to assign this number.
9. Performing Organization Name and Mailing Address. Give name, street, city, state, and ZIP code. List no more than two levels of an organizational hierarchy. Display the name of the organization exactly as it should appear in Government indexes such as Government Reports Announcements & Index (GRA & I).
10. Project/Task/Work Unit Number. Use the project, task and work unit numbers under which the report was prepared.
11. Contract/Grant Number. Insert contract or grant number under which report was prepared.
12. Sponsoring Agency Name and Mailing Address. Include ZIP code. Cite main sponsors.
13. Type of Report and Period Covered. State interim, final, etc., and, if applicable, inclusive dates.
14. Performing Organization Code. Leave blank.
15. Supplementary Notes. Enter information not included elsewhere but useful, such as: Prepared in cooperation with . . . Translation of . . . Presented at conference of . . . To be published in . . . When a report is revised, include a statement whether the new report supersedes or supplements the older report.
16. Abstract. Include a brief (200 words or less) factual summary of the most significant information contained in the report. If the report contains a significant bibliography or literature survey, mention it here.
17. Document Analysis. (a). Descriptors. Select from the Thesaurus of Engineering and Scientific Terms the proper authorized terms that identify the major concept of the research and are sufficiently specific and precise to be used as index entries for cataloging.

    (b). Identifiers and Open-Ended Terms. Use identifiers for project names, code names, equipment designators, etc. Use open-ended terms written in descriptor form for those subjects for which no descriptor exists.

    (c). COSATI Field/Group. Field and Group assignments are to be taken from the 1964 COSATI Subject Category List. Since the majority of documents are multidisciplinary in nature, the primary Field/Group assignment(s) will be the specific discipline, area of human endeavor, or type of physical object. The application(s) will be cross-referenced with secondary Field/Group assignments that will follow the primary posting(s).
18. Distribution Statement. Denote public releasability, for example "Release unlimited", or limitation for reasons other than security. Cite any availability to the public, with address, order number and price, if known.
19. & 20. Security Classification. Enter U.S. Security Classification in accordance with U.S. Security Regulations (i.e., UNCLASSIFIED).
21. Number of pages. Insert the total number of pages, including introductory pages, but excluding distribution list, if any.
22. Price. Enter price in paper copy (PC) and/or microfiche (MF) if known.

*U.S. Government Printing Office: 1978—261-647/3308

REPORT DOCUMENTATION PAGE

READ INSTRUCTIONS BEFORE COMPLETING FORM

1. REPORT NUMBER	2. GOVT ACCESSION NO. AD-A122 744
3. RECIPIENT'S CATALOG NUMBER	
4. TITLE (and Subtitle) Post-Crazing Stress Analysis of Glass-Epoxy Laminates	5. TYPE OF REPORT & PERIOD COVERED Technical Report 5-31-78 to 5-31-79
	6. PERFORMING ORG. REPORT NUMBER TTU-ESM-79-1
7. AUTHOR(s) Dallas G. Smith and Ju-Chin Huang	8. CONTRACT OR GRANT NUMBER(s) DAAK40-78-C-0165
9. PERFORMING ORGANIZATION NAME AND ADDRESS	10. PROGRAM ELEMENT, PROJECT, TASK AREA & WORK UNIT NUMBERS 62303A 1L162303A214 0 0 369J20G641
11. CONTROLLING OFFICE NAME AND ADDRESS Tennessee Technological University Department of Engineering Science and Mechanics Cookeville, TN 38501	12. REPORT DATE May 1979
	13. NUMBER OF PAGES 178
14. MONITORING AGENCY NAME & ADDRESS(if different from Controlling Office) Commander U. S. Army Missile Research & Development Command ATTN: DRDMI-TLA Redstone Arsenal, AL 35809	15. SECURITY CLASS. (of this report) Unclassified
	15a. DECLASSIFICATION/DOWNGRADING SCHEDULE

16. DISTRIBUTION STATEMENT (of this Report)

Approved for public release; distribution unlimited.

17. DISTRIBUTION STATEMENT (of the abstract entered in Block 20, if different from Report)

18. SUPPLEMENTARY NOTES

19. KEY WORDS (Continue on reverse side if necessary and identify by block number)

Glass-Epoxy	Angle Plys	Finite Elements
Laminates	Shear Testing	Isoparametric Element
Composite Materials	Compression Testing	Doubly-Curved Element
Failure Analysis	Stress Concentrations	Thick-Shell Element
		Thick-Plate Element

20. ABSTRACT (Continue on reverse side if necessary and identify by block number)

A glass-epoxy material known as Scotchply XP-250 was characterized. The material's various strengths and stiffnesses were determined in tension, compression, and shear. The three-rail fixture was used for the shear tests. A modified IITRI fixture was used for compression. Glass-epoxy laminates having the following layups were tested in tension: $[\pm 30]_s$, $[\pm 45]_s$, $[\pm 60]_s$, and $[0/\pm 45/90]_s$. The stress-strain behavior in the pre- and post-crazing regions was predicted with a lamination program which employed the nonlinear

Block 20

ply shear curve. These predicted and test results were compared.

A finite element program was written for obtaining stress analysis of laminated structures with stress concentrations. The program used a doubly-curved, isoparametric, thick-plate or thick-shell element. A number of example problems were solved. The finite element results were compared to test results for a $[0/\pm45/90]_s$ tension coupon containing a hole.

SECURITY CLASSIFICATION OF THIS PAGE(When Data Entered)

ACKNOWLEDGMENTS

A number of persons at Tennessee Tech contributed to this work. A few are singled out here for their especially valuable contributions. Mr. Pen-Hsi Huang, M. S. candidate, conducted many of the tests and performed most of the test data reduction. Messrs. Vichen Nopratvarakorn and Chih-Chung Chao, doctoral students, carried out a great deal of the finite element computer programming. Mr. Charlie Hunter of the ESM shop skillfully fabricated the shear and compression test fixtures. Mr. Ban-Wei Chang, M. S. student, drew many of the figures. Mrs. Jo Ann Boling and Mrs. Charlotte Hethcoat competently typed the report. In addition, the authors benefited from a number of technical conversations with Mr. Richard Thompson of the U. S. Army Missile R and D Command. The writers extend their appreciation to all of these.

TABLE OF CONTENTS

Page

Chapter I. INTRODUCTION 1

Chapter II. MATERIAL CHARACTERIZATION TESTS 3

2.1 Introduction 3

2.2 Tension Tests 4

2.3 Shear Tests 6

2.4 Compression Tests 8

2.5 Summary of Material Properties 12

Chapter III. POST-CRAZING CHARACTERIZATION OF GLASS-EPOXY LAMINATES 13

3.1 Introduction 13

3.2 Failure Theories 15

3.3 Failure Surfaces for Glass-Epoxy Laminates 18

3.4 Laminate Response by the Method of Rowlands 19

3.5 Laminate Response with a Nonlinear Lamina Shear Curve . . .26

3.6 Test Laminate Response Compared with Predicted Response Using Ply Nonlinear Shear Behavior 27

3.7 Conclusions on Glass-Epoxy Laminate Response 31

Chapter IV DEVELOPMENT OF THE FAILURE ANALYSIS METHOD--A DOUBLY CURVED, ISOPARAMETRIC, THICK-SHELL FINITE ELEMENT . . .33

4.1 Introduction 33

4.2 Isoparametric Elements 34

4.3 The Elasticity Matrix 39

4.4 Element Stiffness Matrix 43

4.5 Body Loads, Surface Loads 45

4.6 Computer Implementation 46

4.7 Yield Criteria 48

Page

4.8 Mesh Generation 49

Chapter V. LAMINATE STRESS ANALYSIS BY THE FINITE ELEMENT MODEL . . 51

5.1 Description of the Computer Program 51

5.2 Verification of the Computer Model 51

5.3 Response of a $[0/\pm 45/90]_s$ Glass-Epoxy Laminate with a Hole. 53

REFERENCES 54

TABLES 57

FIGURES 63

APPENDIX A 125

APPENDIX B 131

LIST OF TABLES

Table | Page

1. Summary of Ply Properties from $[0^\circ]_S$ Tension Tests on XP-250 Glass-Epoxy 57

2. Summary of Ply Properties from $[90^\circ]_S$ Tension Tests on XP-250 Glass-Epoxy 58

3. Summary of Ply Shear Properties for XP-250 Glass-Epoxy from Three-Rail Shear Tests of Unidirectional Panels 59

4. Summary of Ply Compressive Properties for XP-250 Glass-Epoxy from Tests of $[0^\circ]_S$ Coupons 60

5. Summary of Ply Compressive Properties for XP-250 Glass-Epoxy from Tests of $[90^\circ]_S$ Coupons 61

6. Central Deflection of Simply Supported Square Plate 62

LIST OF FIGURES

Figure — Page

1. Test Set-Up 63
2. Typical Stress-Strain Response for $[0]_s$ Tensile Specimen . . . 64
3. The Failed $[0]_s$ Tensile Specimens 65
4. Typical Stress-Strain Response for $[90]_s$ Tensile Specimen . . . 66
5. The Failed $[90]_s$ Specimens. 67
6. Two Views of the Three-Rail Shear Fixture 68
7. The Shear Stress Distribution Across the Length of the Three-Rail Shear Specimen for a $[\pm 45]_s$ Graphite-Epoxy Laminate. . . 69
8. The Failed $[0]_s$ Three-Rail Shear Specimens 70
9. The Shear Stress-Strain Response for the Unidirectional $[0]_s$ Laminate 71
10. Two Views of the Compression Fixture 72
11. An Exploded View Drawing of the Compression Fixture 73
12. Dimensions of Compression Specimen 74
13. Compression Specimen Instrumented with Strain Rosettes. 75
14. The Load-Time and Longitudinal Strain-Time Response for 2024-T4 Aluminum Obtained with the Compression Fixture 76
15. The Measured Compressive Strain Response Compared with the Tensile Strain Response for Aluminum 2024-T4 77
16. The Failed $[0]_s$ Compressive Specimens 78
17. A Sample Stress-Strain Curve for a $[0]_s$ Specimen Under Compressive Loading 79
18. The Failed $[90]_s$ Compressive Specimens 80
19. A Sample Stress-Strain Curve for a $[90]_s$ Specimen Under Compressive Loading 81

Figure | Page

20. Predicted Strength of Glass-Epoxy Off-Axis Unidirectional Tension Coupon by the Tsai-Wu and Hill Failure Theories . . . 82

21. Predicted Strength of Glass-Epoxy Angle Ply Tension Coupon by Tsai-Wu and Hill Failure Theories 83

22. Failure Envelope for a $[\pm 45]_s$ Glass-Epoxy Laminate 84

23. Failure Envelope for a $[\pm 35]_s$ Glass-Epoxy Laminate 85

24. First Quadrant Failure Envelopes for Several Glass-Epoxy Angle Plys 86

25. Failure Envelope for a $[0/90]_s$ Glass-Epoxy Laminate 87

26. Notation for Symmetric Laminate Subjected to a Biaxial Test . . 88

27. Strain Response for the 0-degree Loading of a $[0_2/\pm 45]_s$ Graphite-Epoxy Laminate 89

28. Strain Response for the 90-degree Loading of a $[0_2/\pm 45]_s$ Graphite-Epoxy Laminate 90

29. Strain Response for the 24-degree Loading of a $[0_2/\pm 45]_s$ Graphite-Epoxy Laminate 91

30. Strain Response for the 45-degree Loading of a $[0_2/\pm 45]_s$ Graphite-Epoxy Laminate 92

31. Strain Response for the 0-degree Loading of a $[0/\pm 45/90]_s$ Graphite-Epoxy Laminate 93

32. Strain Response for the 30-degree Loading of a $[0/\pm 45/90]_s$ Graphite-Epoxy Laminate 94

33. Strain Response for a $[0/90/\pm 45]_s$ Boron-Epoxy Laminate Loaded at 15 degrees Off-Axis 95

34. Strain Response for a $[0/90/\pm 45]_s$ Boron-Epoxy Laminate Loaded at 30 degrees Off-Axis 96

35. Strain Response for a $[\pm 45]_s$ Boron-Epoxy Laminate Loaded 15 degrees Off-Axis. 97

36. Strain Response for a $[\pm 45]_s$ Boron-Epoxy Laminate Loaded 30 degrees Off-Axis. 98

37. Strain Response for a $[0/90_2]_s$ Glass-Epoxy Laminate 99

38. Effect of Failed-Ply Unloading on the Computed Response of the $[0/90_2]_s$ Glass-Epoxy Laminate 100

Figure		Page
39.	Predicted and Test Strain Response for a $[0/\pm 45/90]_s$ Glass-Epoxy Laminate	101
40.	Effect of Failed-Ply Unloading on the Computed Response of the $[0/\pm 45/90]_s$ Glass-Epoxy Laminate	102
41.	Stress-Strain Response of the $[\pm 30]_s$, XP-250 Glass-Epoxy Laminate	103
42.	The $[\pm 30]_s$ XP-250 Glass-Epoxy Tension Coupons After Failure.	104
43.	Stress-Strain Response of the $[\pm 45]_s$, XP-250 Glass-Epoxy Laminate-Initial Portion	105
44.	Stress-Strain Response of the $[\pm 45]_s$, XP-250 Glass-Epoxy Laminate-Full Curve	106
45.	The $[\pm 45]_s$, XP-250 Glass-Epoxy Tension Coupons After Failure	107
46.	Stress-Strain Response of the $[\pm 60]_s$, XP-250 Glass-Epoxy Laminate	108
47.	The $[\pm 60]_s$, XP-250 Glass-Epoxy Tension Coupons After Failure	109
48.	Stress-Strain Response of the $[0/\pm 45/90]_s$, XP-250 Glass-Epoxy Laminate	110
49.	Effect of Failed-Ply Unloading on the Computed Strain Response of the $[0/\pm 45/90]_s$, XP-250 Glass-Epoxy Laminate .	111
50.	The $[0/\pm 45/90]_s$, XP-250 Glass-Epoxy Tension Coupons After Failure	112
51.	The 16-Node Solid Element	113
52.	Local and Global Coordinates	113
53.	The Lamina Principal Axes of Elastic Symmetry	114
54.	Relationship of Lamina Principal Axes to Shell Coordinates .	114
55.	Intrisic Shell Coordinate Axes	115
56.	Possible Region for the Quadrilateral	115
57.	The Flow Chart of the Computer Program	116
58.	The Sides of a Quadrilateral Region	117

Figure Page

59. A Connected Set of Quadrilateral Regions 117

60. Influence of Transverse Shear on Maximum Deflection of a Homogeneous Simply Supported Plate 118

61. A Cylindrical Shell Roof 119

62. Midspan Vertical Displacement for the Cylindrical Shell Roof 120

63. The Geometry of a Hyperbolic Paraboloid 121

64. Vertical Deflection Across the Midspan of a Clamped Hyperbolic Paraboloid Under Uniform Load 122

65. Coupon Dimensions for the $[0/\pm45/90]_s$ Glass-Epoxy Laminate with a Hole 123

66. Mesh Layout for the $[0/\pm45/90]_s$ Coupon with a Hole 123

67. Comparison of the Computed and Test Strain Near a Hole in a $[0/\pm45/90]_s$ Glass-Epoxy Laminate 124

Chapter I

INTRODUCTION

Glass fiber reinforced epoxy is an effecient structural material, coupling high strength with light weight. This favorable strength-weight ratio makes the material attractive for some flight structures as well as other machines and structures where weight is an important consideration. In recent years the material has undergone considerable development, and it has experienced a moderate amount of use for some components. Presently, its use is hampered by the difficulty in predicting the material's behavior under loads which approach the breaking load. Whereas many materials exhibit near-linear behavior up to failure, glass-epoxy laminates typically exhibit a considerable amount of nonlinear deformation prior to gross fracture. Zones of increasing material damage occur in the form of crazing, ply cracking, and ply delamination. In some applications, efficient use of the material requires employing the material at stress levels well into the nonlinear portion of the laminate's stress-strain curve. Questions then arise relative to a precise definition of exactly what constitutes failure, the form of the stress distribution around notches and holes, and the laminate's stress-strain response in the post-crazing region.

These questions provided the impetus for this research. The overall purpose of the work was to obtain information that would contribute to rational methods of strength predictions and design of glass-epoxies. Toward this end, a joint program of material testing and numerical

investigation of glass-epoxy laminates was undertaken. The specific objectives were to determine the appropriate stress-strain behavior for various glass-epoxy laminates, develop a finite element computer model for determining the stress distribution around stress raisers, such as notches and holes, and determine ways to apply these results to the failure mechanisms to predict the strength of laminated glass-epoxy structures.

A specific material, Scotchply XP-250, was selected as a test material. This material was characterized with respect to its ply properties in tension, compression and shear. For verification of prediction methods, three angle ply laminates--$[\pm 30]_s$, $[\pm 45]_s$, and $[\pm 60]_s$--and one quasi-isotropic laminate, $[0/\pm 45/90]_s$, were tested in tension. Finally, the $[0/\pm 45/90]_s$ laminate containing a hole was tested to failure. These tests were compared to the finite element results.

The finite element program contains a doubly-curved, thick-shell, isoparametric element. The program will predict the stress distribution in both thick and thin plates and shells loaded transversely or inplane. The shape of the crazed or yielded region around stress raisers can be mapped and the change, with increasing load, in the shape and size of this damage zone can be determined on up to complete failure.

Chapter II.

MATERIAL CHARACTERIZATION TESTS

2.1 Introduction

The material chosen for this work is known as Scotchply XP-250 manufactured by the 3M Company. It is a high-strength, moldable, epoxy-glass prepreg. For the present tests it was obtained in unidirectional cured sheet form, having either 8 or 14 plys. The nominal ply thickness is 0.009 inch and the fiber volume ratio is about 50 percent.

To obtain lamina characterization of the material, five types of unidirectional tests were run. Tension tests at 0 and 90 degrees to the fiber direction were used to determine the stiffness properties $E_{11}{}^{T}$, $E_{22}{}^{T}$, and $\nu_{12}{}^{T}$ together with the ultimate strengths $X_1{}^{T}$ and $X_2{}^{T}$ parallel and transverse to the fiber direction. Shear tests were used to determine the shear stiffness G_{12} and ultimate shear strength S_{12}. Compression tests were used to find the compressive stiffness properties $E_{11}{}^{c}$, $E_{22}{}^{c}$, and $\nu_{12}{}^{c}$ together with the compressive ultimate strengths $X_1{}^{c}$ and $X_2{}^{c}$.

Specimens for all tests were cut oversize (1/16 to 1/8 inch) with a band saw. Final dimensions were obtained by grinding, with water flowing over the cutting area. All specimens were instrumented with 350-ohm strain gages. Because of the small gage section, 1/16-inch-long tee rosettes were used on the compression specimens. Gages 1/4 inch long were used on all other specimens. All tests were conducted at room temperature of about 70°F and room humidity of about 50 percent.

All specimens were tested in an Instron testing machine using a fixed cross-head speed. The Instron machine chart-recorded load versus time. Strain data were recorded by the use of a four-channel strain gage signal conditioner together with two two-channel strip chart recorders. Figure 1 shows the test set up. The load-time and strain-time curves are digitized by use of a Tektronics 4051 Computer Graphics System. A pen is moved along the load-time curve taking load readings at certain time intervals. The pen is then moved along the strain-curve, reading strain values at the same time intervals as for the load curve. The Tektronics computer was programmed to construct stress-strain curves from these data and to compute the required stiffness parameters.

2.2 Tension Tests

Five tension tests were conducted on 8-ply unidirectional specimens loaded at 0 degrees to the fiber direction. Specimen dimensions were fixed by the ASTM standards, reference 1. The specimens were 9 inches long and 0.5 inch wide equipped with 1.5-inch-long load tabs made from printed circuit board material. Tabs were attached before final machining with Eastman 910 cement. Specimens were equipped with longitudinal and transverse strain gages. Cross-head speed was 0.05 inch/minute. A typical stress-strain curve is shown in Figure 2. The elastic modulus E_{11}^{T} was determined from a first-order least squares curve fit of only the initial points on the stress-strain curve.

The failed 0-degree specimens are shown in Figure 3 and the test results are summarized in Table 1. The desired "shaving brush" failure is exhibited by specimens 2 and 5 and by specimen 3, although somewhat imperfectly. Note from Table 1 the resulting high ultimate stress for specimens 2 and 5. Tab bond failure occurred on specimen 1, possibly

depressing its measured ultimate strength. Ultimate strength was not obtained from specimen 4 because a strain gage was broken prior to the ultimate load and the test was stopped to investigate. The specimen was broken later. The average values for the elastic modulus and ultimate strength of 5.64×10^6 psi and 134 ksi respectively agree well with the values of 5.70×10^6 psi and 130 ksi published by the 3M Company, reference 2.

Five unidirectional tensile tests were conducted at 90 degrees to the fiber direction. The specimen dimensions were the same as for the 0-degree tests except for the width which was 1.000 inch instead of 0.500 inch, in accordance with ASTM. A typical stress-strain curve is shown in Figure 4. The five failed specimens are shown in Figure 5, and the test results are summarized in Table 2. The specimens 6, 7, and 10 exhibit the desired type of failure, i.e. away from the end tabs. The failure stress, however, of specimen 9, which failed at the tabs, was the highest of all and the failure stress of specimen 11, which also failed at the tabs, was among the highest. This suggests that for 90-degree specimens, failure near the tabs causes no serious error in the measured ultimate stress.

Poisson's ratio $\nu_{21}{}^T$ was calculated from $\nu_{21} = \nu_{12} E_{22}/E_{11}$. For comparison the measured value of ν_{21} is shown. The difference in the two-- 0.078 measured as compared to 0.092 calculated-- is not surprising, considering that the measured values are obtained from a very small transverse strain. Even a small error in this strain would account for the difference in the measured and calculated values. From Table 2 it can be seen that the material has an elastic modulus of $E_{22}{}^T = 1.74 \times 10^6$ psi and fails at an ultimate stress of 7.55 ksi.

2.3 Shear Tests

In determining lamina shear properties, the three-rail fixture was used. Shear testing has been the subject of considerable controversy and a number of fixtures or specimens have been used, including the ± 45-degree specimen (see references 3 and 4), the 10-degree off-axis specimen (see references 5 and 6), and the two-and three-rail fixtures. Currently the two- and three-rail fixtures are being considered by ASTM Committee D-30 as standard fixtures for finding inplane shear properties.

Figure 6 shows two views of the three-rail specimen. The test plate is clamped between stationary rails on the edges while a third rail, clamping the plate at the center, is pushed down by the test machine, loading the specimen in shear parallel to the fibers. Two strain gages are attached to the specimen at 45 degrees to the fiber direction. From the strain transformation equations the normal strain ε_{45} at 45 degrees is related to the shearing strain γ_{12} referred to the material's axis by

$$\gamma_{12} = 2\,\varepsilon_{45} \qquad (1)$$

The shearing stress τ_{12} between the rails is assumed to be uniform throughout the specimen length from top to bottom. So assumed, the shearing stress is given by

$$\tau_{12} = \frac{P}{2bh} \qquad (2)$$

where P is the load, b is the specimen shear length, which was 6 inches, and h is the plate thickness. It is apparent that, while this expression may be accurate, it is not exact since the shearing stress must go to zero at the top and bottom free edges of the plate. Because of this, the accuracy of the average stress, Equation (2), has been questioned, especially for laminates with angle plys. A Fourier series solution by

Whitney et al [7] indicated that for a $[\pm 45]_s$ laminate the shear stress near the edge increased from zero to a peak value 50 percent greater than the average at a distance of only one-tenth the plate length from the edge. A recent finite element solution by Bergner [8], however, disagrees with this. This is shown in Figure 7, taken from [8]. Bergner's results indicate that the average shear distribution is indeed an accurate estimate of the actual shear stress distribution. The present finite element computer results (see Chapter IV) are also shown on Figure 7. The present finite elements results are slightly lower than Bergner's but they essentially show that a condition of uniform shearing stress exists along the length of the three-rail fixture.

For the three-rail fixture two equal test sections exist on either side of the middle rail. Thus to fully utilize the specimen, strain gages are placed on both sides and strain data are recorded from both. The three-rail specimens must be used with care. The rails hold the specimen by clamping friction rather than by bearing on the bolts. In fact, the rails have emery cloth bonded to them and the rail bolts are torqued to 70 ft-lbs to prevent slipping. The holes in the test plate are considerably larger than the bolts -- 1/2 inch as compared to 3/8 inch for the bolts. As a consequence, it is possible to assemble the specimen and fixture with considerable misalignment, with the middle rail tilted from vertical, say. This would destroy the assumed equality of the test sections on each side of the middle rail, compounded by the fact that the load head would now push down at the top on one side of the middle rail rather than at the rail's center. To alleviate this problem, cylindrical spacers with diameters equal to the width of the test section were used to align the rails during bolt-up. These spacers

are visible in the top picture of Figure 6. To further decrease misalignment the top of the center rail was machined so as to leave only a small area 1/2 inch in diameter for the load head to push against.

Four specimens were tested, yielding eight sets of data. The failed specimens are shown in Figure 8 and the test results are summarized in Table 3. The average lamina shear modulus, G_{12}, was 0.68×10^6 psi and the ultimate shear stress, S_{12}, was 7.23 ksi. The shear stress-strain curves exhibited considerable nonlinearity. For predicting laminate behavior it was decided that use would be made of the full stress-strain curve rather than just the initial slope. To permit this, all the shear data were plotted and fitted with a second order least-squares curve, Figure 9. This curve now becomes the master shear curve for use in the laminate programs.

2.4 Compression Tests

Compression testing was carried out using a fixture similar to the IITRI compression fixture, reference [9]. Two views of the fixture are shown in Figure 10. An exploded view drawing is shown in Figure 11. While the IITRI fixture was discussed in reference [9] no dimensions were given, and so the fixture has been re-designed here. It was built in-house requiring 283 man-hours of shop time. The fixture was built from cold-rolled steel. The two main parts of the fixture are guided together by two rods 0.750 inch in diameter which fit into linear bearings in the upper half. The specimen is gripped by wedges which are bolted to the specimen prior to the test. The wedge angle is 11 degrees. The sloping surfaces of the wedges were lubricated prior to testing to increase the wedging action. The wedges were 2.500 inches in length and

1.500 inches in width. They were slotted on the straight side to receive the tabbed test specimen. These slots were given gripping "teeth" by punching the slot surface numerous times with an impact punch.

Specimens were prepared for testing at both 0 and 90 degrees to the fiber direction. The dimensions of both types of specimens were the same. To minimize buckling the specimens were 14 plys thick. The specimens were 0.25 inch wide and 5.5 inches long, equipped with crossply end tabs 2.50 inches long. This leaves a gage section which measures only 0.5 inch by 0.25 inch--a small area for a strain rosette. Specimen dimensions are shown in Figure 12. A photograph of a specimen instrumented with strain rosettes and lead wires on both sides is shown in Figure 13.

The compression fixture was checked by conducting a test on a 2024-T4 aluminum specimen. The same specimen was then used in a tension test and the stress-strain curves for tension and compression were compared. For the compression test the longitudinal strain was monitored on both sides of the specimen to assess the degree of bending. The load-time curve and the two longitudinal strain-time curves are shown together in Figure 14. At point A it appears that minute grip adjustment occurred so that the two strain curves abruptly crossed, one increasing while the other decreased with no change in load. This suggests that one of the tabs on one side of the specimen slipped slightly while its opposing neighbor held firm. This would introduce bending into the specimen even without fixture misalignment. The strain on either side deviated from the average strain by about 6 percent. The "flat spot" on the load-time curve at B does not indicate grip slippage or tab failure but instead results from crosshead backlash when the testing machine is loaded

in compression.

The average compressive strain was used to construct the stress-strain curve shown in Figure 15. That figure also contains the tensile stress-strain curve. Aluminum is known to possess very nearly the same stress-strain behavior in tension as compression. Thus friction in the compression fixture would result in a stress-strain curve whose slope is too steep and the measured value of E would be larger than that for tension. The good comparison shown in Figure 15 means this does not happen, indicating that friction in the compression fixture is negligible. The gripping problem reflected by point A in Figure 14, however, is a source of error which can affect the measured values of E if the strain is monitored on only one side of the specimen. Moreover, any induced bending will tend to depress the measured values of the compressive ultimate strength.

Six compression tests were run on 0-degree specimens. The failed specimens are shown in Figure 16. A sample stress-strain curve is shown in Figure 17. In that test--test 17--as well as two other tests, strain gages were mounted on both sides of the specimen. The longitudinal strain from both sides is shown in Figure 17. They are not quite the same, as ideally would be the case if no bending or buckling were present. The two values of $E_{11}{}^{c}$ obtained from both strains are 6.39×10^{6} psi and 5.73×10^{6} psi. This was the highest difference in E_{11} obtained from the three specimens instrumented on both sides. A summary of the 0-degree test results is shown in Table 4. For test 18 the values obtained for $E_{11}{}^{c}$ are 5.35×10^{6} psi and 5.88×10^{6} psi and for test 19 both values for $E_{11}{}^{c}$ are 5.97×10^{6} psi. The strains from opposite sides of a specimen usually agreed fairly well

until some type of failure (perhaps fibers breaking) began to occur. This initial failure, marked by audible noise and a small drop in the load, usually occurred near two-thirds of the ultimate load. After this initial damage or failure had occurred symmetry was lost. The strain suddenly increased in a step fashion on one side of the specimen while suddenly decreasing on the other side, indicating a sudden application of bending strain. It may be that failure of a bundle of fibers on one side of the specimen causes a load eccentricity on the remaining effective net section, hence bending must occur. Minute uneven slippage of the tabs in the grips as already discussed could cause the same behavior. Too, it must be remembered that the gage section is short and that failure sometimes initiated underneath a gage, which could cause erratic gage behavior. In any case, the data obtained after the initial failure--a sudden decrease in load accompanied by a sudden increase or decrease or both in strain--must be viewed with suspicion, since the assumed symmetry of the test is lost at that point. For this reason the measured ultimate strains were not recorded in Table 4. The average measured value of E_{11}^{c} was 5.87×10^{6} psi, slightly higher than the value of E_{11}^{T}, which was 5.64×10^{6} psi. Poisson's ratio, too, was slightly higher in compression than tension--0.317 as compared to the tensile value of 0.299.

Five compression tests were run on 90-degree specimens. The failed specimens are shown in Figure 18. A sample stress-strain curve is shown in Figure 19, and results are summarized in Table 5. More than for any other tests, the 90-degree compressive stress-strain

curves exhibited an early nonlinearity. Considering this, a secant definition of E_{22}^c might be appropriate, however, for the sake of consistency with the other tests, the slope of the initial portion of the curve was used for E_{22}^c. This made the determination of E_{22}^c difficult, since for this method, E_{22}^c depends strongly upon the first few points of the curve. This accounts for some of the variation in E_{22}^c shown in Table 5. Bending, however, was a problem; test 28, monitored with gages on both sides, exhibited considerable bending as can be noted from two considerably different values of E_{22}^c for that test.

2.5 Summary of Material Properties

For handy reference, the various lamina properties determined from the characterization tests for the XP-250 material are summarized below:

$E_{11}^T = 5.64 \times 10^6$ psi	$e_1^T = 24{,}000\ \mu\varepsilon$
$E_{22}^T = 1.74 \times 10^6$ psi	$X_1^c = 112$ ksi
$\nu_{12}^T = 0.299$	$X_2^T = 7.55$ ksi
$G_{12} = 0.680 \times 10^6$ psi	$e_2^T = 4{,}760\ \mu\varepsilon$
$E_{11}^c = 5.87 \times 10^6$ psi	$X_2^c = 25.0$ ksi
$E_{22}^c = 2.12 \times 10^6$	$e_2^c = 18{,}600\ \mu\varepsilon$
$\nu_{12}^c = 0.317$	$S_{12} = 7.23$ ksi
$X_1^T = 134$ ksi	$e_{12} = 19{,}700\ \mu\varepsilon$

Chapter III.

POST-CRAZING CHARACTERIZATION OF GLASS-EPOXY LAMINATES

3.1 Introduction

A laminate contains a number of laminae (plys) oriented at various angles to the primary load direction. For loads limited to the linear range, given the lamina properties the usual lamination theory [10] gives accurate estimates of the overall stiffness and compliance of a given laminate. With increasing loads, however, certain plys within the laminate begin to fail by matrix cracking and splitting between the fibers. In glass epoxies the onset of matrix cracking gives the laminate a hazy, milky, light-colored appearance, sometimes referred to as crazing. Beyond the onset of crazing the laminate compliance increases with increasing load; the crazing area in a ply grows and may extend to plys of other angles before the ultimate laminate load is reached. Depending upon the laminate's layup, the onset of crazing may occur at loads which are rather low compared to the laminate's ultimate load. For many structural applications the laminate's reserve strength beyond crazing may safely be utlized. For confident design in much cases it is important to have knowledge of the post-crazing stress-strain response of the laminate.

Efforts at forming a lamination theory of failure have generally been only moderately successful. The usual approach is to numerically apply the laminate stress or strain in increments. After each load

increment some selected failure theory is applied to each ply. The load increments are continued until a ply fails, after which the stiffness of that ply is modified to reflect its reduced load carrying capacity. This reduced ply stiffness is then used to assemble the overall laminate stiffness and the load increments are continued until other plys fail, after which their stiffnesses are also reduced. This process is continued until, by some definition, enough plys have failed to constitute laminate failure. This approach has been lucidly discussed by Rowlands [11] in the proceedings from a ASME Symposium on inelastic behavior of composite materials (see also the Rowlands report [12]); papers by Sandhu [13], Hahn and Tsai [14] and Chow et al [15, 16] illustrate aspects of this approach. While this approach is conceptionally clear and logically sound, in its application a number of problems must be resolved. In the first place, a ply may fail in a number of modes--e.g. splitting or crushing of the matrix between the fibers due to large transverse tension or compression, fiber failure in tension or compression, etc. How should the failed ply's various stiffness constants be modified for each mode of failure? In other words, how does the ply unload after its failure. Evidence indicates that in situ ply strength and post-failure stiffness properties may vary considerably from those of a unidirectional test coupon [17]. Futhermore, a uniform definition of laminate failure, applicable to a number of layups, is lacking. In some cases laminate failure is assumed to occur once fiber failure (as distinct from matrix failure) has occurred in two or more plys. This definition may be adequate for, say, a $[0/\pm 45]$, layup but totally inappropriate for an angle ply layup of, say, $[\pm 45]_s$. In other instants laminate failure

is assumed to occur once the modified laminate stiffness become singular. Each definition may apply, albeit, each to a different class of layups.

The above method of laminate behavior prediction--here loosely referred to as Rowland's method although a number of researchers have used it--is investigated in detail in the following. The method is assessed by applying it to a number of materials--graphite-epoxy, boron epoxy and glass-epoxy--having various layups. Biaxial failure response of several glass epoxies is illustrated.

3.2 Failure Theories

A number of failure theories are available for predicting ply failure. An exhaustive review of failure theories for anisotropic materials was provided by Sandhu [18]; Rowlands [11] also discussed several. Only two were considered in the present work: the Hill theory [19] and the Tsai-Wu theory [20].

For an orthotropic ply in plane stress the Hill theory takes the form,

$$\left(\frac{\sigma_1}{X_1}\right)^2 - \frac{\sigma_1\sigma_2}{(X_1)^2} + \left(\frac{\sigma_2}{X_2}\right)^2 + \left(\frac{\tau_{12}}{S_{12}}\right)^2 = 1 \qquad (3)$$

where X_1 and X_2 are the uniaxial strengths parallel and transverse to the fibers and S_{12} is the ply shear strengths. The Hill theory does not distinguish between the tensile strengths X_1^T, X_2^T and the compressive strengths X_1^c, X_2^c. Some writers have made this distinction by using X_1^c when σ_1 is negative and X_1^T when σ_1 is positive and similarly for σ_2.

The Tsai-Wu failure criterion accounts for both tensile and compressive strengths. In addition to quadratic terms it contains linear terms which distinguishes between negative and positive stresses. For plane stress conditions the criterion is expressed as,

$$F_1\sigma_1 + F_2\sigma_2 + F_6\tau_{12} + F_{11}\sigma_1^2 + F_{22}\sigma_2^2 + 2F_{12}\sigma_1\sigma_2 + F_{66}\tau_{12}^2 = 1 \quad (4)$$

where

$$F_1 = \frac{1}{X_1^T} - \frac{1}{X_1^c} \; ; \; F_2 = \frac{1}{X_2^T} - \frac{1}{X_2^c} \; ; \; F_6 = \frac{1}{S_{12}^+} - \frac{1}{S_{12}^-}$$

$$F_{11} = \frac{1}{X_1^T X_1^c} \; ; \quad F_{22} = \frac{1}{X_2^T X_2^c} \; ; \quad F_{66} = \frac{1}{S_{12}^+ S_{12}^-}$$

As before X_1^T, X_1^c are the ply longitudinal tensile and compressive strengths and X_2^T, X_2^c are the ply transverse tensile and compressive strengths. S_{12}^+ and S_{12}^- are the ply strengths in positive and negative inplane shear. For most composite materials $S_{12}^+ = S_{12}^- = S_{12}$ so that $F_6 = 0$. The interaction term F_{12} cannot be expressed in terms of the unaxial strength properties, but must instead be determined from biaxial tests. Since the accuracy of F_{12} is sensitive to the type of test used to find it, accurate values of F_{12} are difficult to obtain. Certain stability conditions limit the range of F_{12} such that $F_{11}F_{22} - F_{12}^2 \geq 0$. For a glass-epoxy material having the properties

$$X_1^T = 154 \text{ ksi} \quad X_1^c = 88.5 \text{ ksi}$$

$$X_2^T = 4.56 \text{ ksi} \quad X_2^c = 17.04 \text{ ksi}$$

$$S_{12} = 9.00 \text{ ksi} \quad (5)$$

the limiting values of F_{12} become,

$$F_{12} = \pm \sqrt{F_{11}F_{22}} = \pm 9.717 \times 10^{-10} \text{ in}^4/\text{lb}^2 \tag{6}$$

For a unidirectional off-axis tension coupon the value of F_{12} has little effect on the predicted strength as shown in Figure 20. For that case the Tsai-Wu theory predicts about the same strength whether $F_{12} = 0$, $F_{12} = + \sqrt{F_{11}F_{22}}$ or $F_{12} = - \sqrt{F_{11}F_{22}}$. For this reason the off-axis test is known to be an unsatisfactory test for finding F_{12} [21, 22]. Since the influence of F_{12} for the off-axis test is small the suggestion is that F_{12} may be set equal to zero without losing accuracy. This has been common practice for graphite-epoxy and will be adopted here for glass-epoxy as well. Figure 20 also contains a strength prediction based on the Hill theory. The Hill theory prediction agrees well the Tsai-Wu prediction for the off-axis coupon.

For angle ply test coupons the Hill and Tsai-Wu theories are compared again in Figure 21. The value of F_{12} which gives the best comparison iwth the Hill theory is $F_{12} = - \sqrt{F_{11}F_{22}}$. In the region, $0^\circ > \alpha > 35^\circ$, the Hill theory predicts a significantly lower failure load than does the Tsai-Wu theory. Beyond $\alpha = 35^\circ$ the two agree fairly well. The value of F_{12} which agreed best with the Hill prediction was $F_{12} = - 9.717 \times 10^{-10}$.

The Tsai-Wu failure theory, because of its generality and because it provides for a difference in tensile and compressive strengths was selected for the following work.

3.3 Failure Surfaces for Glass-Epoxy Laminates

To illustrate the failure response to biaxial stress, the failure surfaces of several glass-epoxy laminates are shown in Figures 22 thru 25. The failure strengths were predicted for various values of the stress ratio σ_x/σ_y using the Tsai-Wu failure theory. The failure behavior of a $[\pm 45]_s$ angle-ply laminate is shown in Figure 22. The failure surface is seen to be an ellipse. This is as expected since the Tsai-Wu failure theory applied to an orthotropic lamina in two-dimensional stress space is an ellipse and since the $[\pm 45]_s$ laminate is essentially an orthotropic plate. The laminate's strength for hydrostatic compression, the third quadrant, is great compared to its strength for hydrostatic tension, the first quadrant. In general the laminate's predicted strength is great for negative applied stresses. The failure surface of a $[\pm 35]_s$ laminate is shown in Figure 23. This laminate is stronger along the x-direction than the y-direction and thus the long axis of the failure surface is skewed toward the σ_x axis in stress space. As for the $[\pm 45]$, laminates, abundant strength is exhibited in the third quadrant compared to the first quadrant. Although complex structural shapes and complex loads sometimes result in a laminate loaded in quadrants 2, 3 or 4, most laminates are utilized in the first quadrant of the stress space. That is, thin laminates are primarily tension structures. The failure surfaces for a number of angle plys were computed for the first quadrant only. These are shown in Figure 24. The surfaces for $\alpha = 60^\circ$ and 55° are the same as for 30° and 35° if σ_x and σ_y are interchanged. The $[\pm 15]_s$ and $[\pm 75]_s$ laminates extend off the graph exhibiting considerable longitudinal strength and relative transverse weakness on the x- and y-directions respectively.

The character of the failure behavior for a $[0/90]_s$ glass-epoxy laminate is shown in Figure 25. Actually, three surfaces are shown. The inside curve--dotted line--represents the first ply failure (FPF) in the matrix material of one set of plys. At this value of the load the stiffness properties of the damaged ply were reduced (see the following section for details) and load application was continued until matrix failure occurred in the remaining plys--solid lines. The stiffness values of these plys were likewise reduced and load application was continued until longitudinal (fiber) failure occurred in one of the sets of plys; this is shown by the outside line. In quadrant one, great reserve strength exists beyond matrix failure of the first two sets of plys. In quadrants 2, 3, and 4, however, the curve for longitudinal failure mostly coincides with the curve for second matrix failure; longitudinal failure is simultaneous with second matrix failure.

3.4 Laminate Response by the Method of Rowlands

Since the method of Rowlands [12] deals with stresses rather than strain energy and uses the usual lamination theory the method has strong appeal for engineers. The method is conceptionally simple and well founded within the framework of lamination theory. It was decided to investigate this approach for a wide range of materials and layup configurations. The purpose was to assess its applicability in general for predicting laminate strength and to investigate its ability for predicting specifically the strengths of glass-epoxy laminates.

A computer program was written similar to that described by Rowland in References [11] and [12]. The program predicts the inplane stress-strain response of a symmetric laminate test coupon subjected to a biaxial test, Figure 28. The program contains both the Hill and Tsai-Wu failure criteria

although only the Tsai-Wu theory is used in the following examples. The laminate stress in the x-direction is applied in increments, $\Delta\sigma_x$. The laminate stress in the y-direction is given by $\Delta\sigma_y = \beta\Delta\sigma_x$. The average shearing stress is given by either $\Delta\tau_{xy} = \gamma\Delta\sigma_x$ or by τ_{xy} = constant. The operator selects the values of β and γ for a desired stress ratio. The provision τ_{xy} = constant allows one to obtain a failure curve for a constant value of shearing stress.

For each increment of stress, the incremental laminate strain components $\Delta\varepsilon_x$, $\Delta\varepsilon_y$, and $\Delta\gamma_{xy}$ are calculated using the laminate compliance matrix from the previous stress increment. These strain increments are then used to calculate increments of stress $(\Delta\sigma_x)_k$, $(\Delta\sigma_y)_k$ and $(\Delta\tau_{xy})_k$ for each k ply using the stiffness matrices from the previous load increment. These stress increments are transformed to the 1-2 direction for each ply yielding $(\Delta\sigma_1)_k$, $(\Delta\sigma_2)_k$, and $(\Delta\tau_{12})_k$. The current ply stresses are then given by adding the incremental stresses for the (n+1) cycle to the stresses for the n load cycle:

$$
\begin{aligned}
\sigma_1(n+1)_k &= \sigma_1(n)_k + \Delta\sigma_1(n)_k \\
\sigma_2(n+1)_k &= \sigma_2(n)_k + \Delta\sigma_2(n)_k \\
\tau_{12}(n+1)_k &+ \tau_{12}(n)_k + \Delta\tau_{12}(n)_k
\end{aligned}
\tag{7}
$$

The total strains for the n+1 load increment are given by

$$
\begin{aligned}
\varepsilon_x(n+1) &= \varepsilon_x(n) + \Delta\varepsilon_x \\
\varepsilon_y(n+1) &= \varepsilon_y(n) + \Delta\varepsilon_y \\
\gamma_{xy}(n+1) &= \gamma_{xy}(n) + \Delta\gamma_{xy}
\end{aligned}
\tag{8}
$$

The average laminate stresses, of course, are given by

$$\sigma_x(n+1) = \sigma_x(n) + \Delta\sigma_x$$

$$\sigma_y(n+1) = \sigma_y(n) + \Delta\sigma_y$$

$$\tau_{xy}(n+1) = \tau_{xy}(n) + \Delta\tau_{xy} \quad (9)$$

The components $(\sigma_1)_k$, $(\sigma_2)_k$, and $(\tau_{12})_k$ are used in either the Hill or Tsai-Wu formula to investigate the failure of each ply. Once failure, as predicted by the formula, is reached the ply is next investigated to determine if the failure is matrix or fiber in nature. This is done by comparing $(\sigma_1)_k$ with the ultimate tensile stress and ultimate compressive stress. If $(\sigma_1)_k$ exceeds neither of these, it is assumed that the failure is in the ply matrix. After matrix failure if $(\sigma_2)_k$ is positive, the failure is designated as "RESIN FAILURE IN TENSION." If $(\sigma_2)_k$ is negative, the failure is designated as "RESIN FAILURE IN COMPRESSION." Once resin failure occurs, the constants E_{22} and G_{12} are set equal to near zero (i.e., 100) and E_{11} retains its original value. Actually, E_{22} and G_{12} can be modified differently for resin failure in tension and resin failure in compression although they are modified the same way in the following examples. The resulting value of ν_{21} is approximately zero since $\nu_{21} = \nu_{12}E_{22}/E_{11}$. If $(\sigma_1)_k$ exceeds the compressive or tensile ultimate strength then the failure is in the fiber and it is assumed that all stiffness of the ply is lost. Thus E_{11}, E_{22}, and G_{12} are all set approximately equal to zero. After ply stiffness is modified as above, linear lamination theory is used to calculate new values for the laminate stiffness and compliance matrices for use in the next load increment.

Once fiber failure has occurred in more than one ply, then laminate failure is assumed and computations are stopped. In addition to the laminate stresses and strains the program indicates the stresses in each ply, indicates the laminate load at which a ply fails and tells how the ply failed--i.e. whether the failure was a transverse failure in the matrix or a longitudinal failure of the fibers. Thus the laminate stress-strain curve is constructed. This curve is piece-wise linear, changing its slope at each ply failure. In some laminates several plys fail tranversely so that laminate stiffness becomes very low and the laminate compliance becomes exceedingly large, resulting in large laminate strains--strains of order 1 or greater. This is also taken to be laminate failure since essentially all stiffness is lost.

In the following, the method of Rowlands, as explained above, is compared with several test results taken from the literature for graphite-epoxy, boron-epoxy and glass-epoxy laminates.

Graphite-Epoxy. Rowlands [12] compared his predicted strain response with test results on $[0_2/\pm 45]_s$ graphite-epoxy loaded at several off-axis angles to obtain various biaxial stress ratios. As an exposition of his method as used in the present report, the experimental data from five of his figures are repeated here. Figure 27 shows the ε_x strain response for the 0-degree loading of the $[0_2/\pm 45]_s$ laminate. Data from five tests are compared with predicted test response. Two possible failure loads, 76 ksi and 139 ksi are indicated, one corresponding to transverse failure of the $\pm 45^\circ$ plys and one corresponding to longitudinal failure of the 0° plys. Neither is very close to the actual failure load of 100.2 ksi. (The present failure loads, 76 and 139 ksi, differ somewhat from those stated by Rowlands in his report of 81 ksi and 184 ksi. The reason why

is not known; a difference in the applied stress increment will cause some variation but not enough to explain the difference.) The point to notice in Figure 27 is that Rowland's method gives a good strain response, but a poor estimate of the laminate's strength--whether one uses as laminate failure the initial transverse failure of the $\pm 45^{\circ}$ plys or the longitudinal failure of the 0° plys. Figure 27 also shows the ϵ_y strain response. Again, good strain response is indicated.

Response of the $[0_2/\pm 45]_s$ laminate loaded in the 90-degree direction along with the predicted response is shown in Figure 28. The responses for a loading of 24 degrees and 45 degrees respectively are shown in Figures 29 and 30.

Figure 31 shows a comparison of the Rowlands method with experimental data obtained by Daniel [6] for a $[0/\pm 45/90]_s$ test coupon. Only a few of the computed points are shown. The computed failure load of 80 ksi compares fairly well with the test value of 74 ksi. The method slightly overestimates the stiffness after the computed transverse failures of the 90° and $\pm 45^{\circ}$ plys. A definite change in the slope of the test curve is easily seen in the region where the computed failures of the 90° and $\pm 45^{\circ}$ plys occur.

Figure 32 shows a comparison of the Rowlands method with Daniel data for the $[0/\pm 45/90]_s$ laminate tested in uniaxial tension at 30° to the laminate axis. As computed, the 75° and -60° plys fail nearly at the same load--45 ksi and 47 ksi, respectively. The method considerably overestimates the laminate's strength; the predicted strength is 86 ksi and the tested strength was only 63 ksi.

Boron-Epoxy. Data for two boron epoxy laminates--$[0/90/\pm 45]_s$ and $[\pm 45]_s$ each tested at off-axis angles of 15 and 30 degrees--were taken from Coles and Pipes [23] for comparison with the Rowlands method. Figure

33 shows the test and computed results for the $[0/90/\pm45]_s$ laminate loaded at 15 degrees off the axis. The method grossly over estimates the strength. Test failure occurred at 26 ksi, before even the first computed transverse failure of any ply. Roughly, the same comparison is obtained for the 30° off-axis test shown in Figure 34.

The $[\pm45]_s$ laminate loaded 15 degrees off-axis is shown in Figure 35. Test failure occurs there near the load level of transverse failure for each of the plys, but at a much higher strain--about 20,000 $\mu\varepsilon$ for ε_x computed to 4,600 $\mu\varepsilon$ for a computed value of ε_x. The computed stiffness is much greater than the actual stiffness. The 30-degree off-axis case is shown in Figure 36. Test failure occurs just below transverse failure of the plys, but again at a higher strain than indicated by the results.

Glass-Epoxy. Test data of Hahn and Tsai [14] for a $[0/90_2]_s$ glass-epoxy laminate and test data for a $[0/\pm45/90]_s$ laminate from Chow et al [15] were compared with the method of Rowlands. Figure 37 shows the $[0/90_2]_s$ laminate. Good agreement is noted between the test results and the predicted results. Test failure occurs at 50 ksi and the predicted failure occurs at 56 ksi. The $[0/90_2]$ laminate is a particularity useful one for studying the unloading behavior of transversely failed plys. In the analysis used by Petit and Waddoups [24], negative values are assigned to certain stiffness moduli of the failed plys, thus as the applied load is increased in increments the failed plys gradually give up their stress, redistributing their load to the remaining unfailed plys. The negative moduli values are maintained until the ply's stress approaches zero at which time the moduli are equated to zero. In the method of Rowlands as explained in [11] and as used here, once a ply fails by either the Tsai-Wu or Hill theory the transverse stiffness moduli are equated to

zero. This means that a failed ply does not unload at all. As the applied load is increased in increments the failed ply maintains its load without either an increase or decrease in the affected stress. At the present, not much is known about the unloading response of failed plys; the response may depend upon the material properties, and the stacking sequence. A number of unloading hypotheses were tested by computing laminate strain response for various valued of the moduli of the failed plys. When E_{11}, E_{22}, G_{12} and ν_{12} of the transversely failed plys were equated respectively to E_{11}, -0.2 E_{22}, -0.2 G_{12}, and 0, excellent agreement resulted. This is shown on Figure 38. While the unloading factor of -0.2 is only an empirical quantity having no rational basis, the excellent agreement obtained in Figure 38 must be regarded as a clue in the unloading behavior of failed plys. A slight change in slope of the test curve can be seen near the computed transverse failure stress of the 0-degree plys.

Predicted and test results for the $[0/\pm 45/90]_s$ laminate are shown in Figure 39. The prediction of either the ultimate strength or the stiffness for the top portion of the curve is not as good as for the $[0/90_2]$ laminate. This is probably due to the addition of the ±45-degree plys with their associated shearing stresses. Lamina shearing stress-strain response is usually nonlinear.

Summary of the Comparisons. The Rowlands method allows for nonlinear laminate behavior by a loss in stiffness associated with the transverse failure of the various plys in a laminate. This results in a stress-strain curve piecewise linear--i.e. with a number of slope changes, each one corresponding to the failure of a ply. In the comparisons of Figures 27 -39 the method is seen to give reasonable estimates of stiffness following the initial ply failures for the graphite-epoxy and glass-

epoxy but not boron-epoxy. Much less accurate is the strength prediction. If one takes as the definition of failure, longitudinal fiber failure or singularity of the laminate stiffness matrix then the method in general considerably over estimates the failure strength of most of the laminates. One exception was the glass epoxy with the simple $[0/90_2]_s$ layup. For angle plys loaded along the matrix axis the method does not permit sufficient nonlinearity because various plys do not fail sequentially but instead fail all at once (when the $+\alpha$ plys fail so do the $-\alpha$ plys).

It was thought that the laminate nonlinear behavior could better be accomodated by using the full lamina stress-strain curve rather than just the initial slope of the curve. All of the various lamina stress-strain curves are reasonably linear except for the shear curve. Therefore, it was decided to use the full lamina stress-strain curve in the lamination program. This is discussed in the next section.

3.5 Laminate Response with a Nonlinear Lamina Shear Curve

In order to devise a method of laminate strength and stiffness prediction which would permit a higher degree of nonlinearity it was decided to use the full nonlinear lamina shear stress-strain curve together with lamination theory. This refinement was made for the lamina shear curve only since the ε_1 and ε_2 strain responses are very nearly linear and the shear strain response is usually highly nonlinear.

The lamina shear curve was used in a manner similar to that of Sandhu [13]. The actual shear stress-strain curve was approximated by a cubic spline function. This function was incorporated into the program described in Article 3.4. Using the full curve, after each increment of stress the laminate's compliance and stiffness are evaluated by

using the tangent modulus corresponding to the current slope of the ply shear stress-strain curve. Thus, general nonlinear laminate response is allowed over the full range of applied load values, including the region prior to first ply failure. The resulting laminate response, still exhibiting sharp changes in slope at each ply failure, will now be nonlinear between the neccessive ply failures and not piecewise linear as before. Except for making use of the full shear stress-strain curve the method is the same as explained in Article 3.4.

3.6 Test Laminate Response Compared with Predicted Response Using Ply Nonlinear Shear Behavior

Three angle ply laminates and one quasi-isotropic laminate of Scotch Ply XP-250 were tested to failure in uniaxial tension. The laminate layups were, $[\pm 30]_s$, $[\pm 45]_s$, $[\pm 60]_s$, and $[0/\pm 45/90]_s$. Three tests were run for each layup. The coupon dimensions were the same as those used for the 90° unidirectional material characterization tests, 1 inch wide by 9 inches long with end tabs for gripping. Strain gages were used to record the longitudinal and transverse strains, ε_x and ε_y. The stress-strain response of each layup was determined and compared with the response predicted by the method explained in Article 3.5. The tensile stiffness properties of Article 2.5 were used in the predictions.

Figure 41 shows the stress-strain response of the $[\pm 30]_s$ laminate. The response is nonlinear almost from the beginning. The predicted longitudinal strain ε_x is somewhat greater than the measured strain although the difference is generally less than 10 percent. The agreement for the transverse strain is not as good. As a result of using the ply nonlinear stress-strain curve the computed curves in Figure 41 exhibit correctly

the decreasing stiffness with increasing load. For example, the initial stiffness E_{xx} of the laminate is about 3.34×10^6 psi, whereas the stiffness at the predicted failure load is only about 2.02×10^6 psi. The predicted ultimate stress is low, about 42 ksi as compared to an actual failure stress of about 60 ksi. Generally, strength predicitions using lamination theory fall below the actual strength for angle plys. Chamis and Sullivan [17] have indicated that this may be due to the difference in the in situ ply strength and the ply strength measured in unidirectional coupons. Use of the ply nonlinear shear curve improves the failure prediction only slightly. The failed $[\pm 30]_s$ coupons are shown in Figure 42. As can be seen, final fracture resulted from a combination of matrix splitting between fibers, fiber fracture, and delamination. Delamination, indicated by the light region around the fracture surface, was extensive. Final failure was sudden, with complete loss of load occurring almost instantaneously.

Figure 43 shows the initial portion of the stress-strain curve for the $[\pm 45]_s$ laminate; the full curve is shown in Figure 44. As noted by Rotem and Haskin [25] the $[\pm 45]_s$ laminates exhibits a singular amount of large deformation prior to ultimate failure. In Figure 44 it can be seen that this laminate yields at a stress of about 17 ksi. The specimen deforms by a scissoring action and the strain continues with little increase in load to a strain of about 35,000-40,000 $\mu\varepsilon$. Then the curve starts climbing again and failure finally occurs at a strain of near 100,000 $\mu\varepsilon$--a 10 percent elongation--four times the failure strain of the $[\pm 60]_s$ laminate. The transverse strain was practically equal to the longitudinal strain after the onset of

extensive yielding. This transverse contraction is visible in the pictures of Figure 45 by comparing the width of the tested specimen with the width of the end tabs, which originally were the same width as the specimen. As the scissoring action took place crazing spread over the whole specimen (still in evidence by the light appearance of the specimens). Failure occurred by a combination of delamination, fiber breakage and splitting between the fibers. Failure occurred near the end tabs where the scissoring action was restrained by the stiffness of the tabs. Figure 43 shows the predicted strain response. The transverse and longitudinal strains both agree well with the test values up to the predicted failure load of 12 ksi. The tangent modulus of the ε_x curve decreases from about 2.07×10^6 psi at the origin to about 1.13×10^6 psi at the predicted failure load of 12 ksi. The predicted failure load is too low, and the extensive straining beyond 17 ksi followed by a rising curve is not predicted. While the extensive strain ability of the $[\pm 45]_s$ laminate is interesting, for most structural applications the laminate could not be utilized beyond the 17 ksi knee because of the large deformations and material damage associated with a higher stress. It is felt that from a structural viewpoint the useful strength of the laminate is about 17 ksi rather than the higher figure.

The predicted and test response of the $[\pm 60]_s$ laminate is shown in Figure 46. While the correct trend is predicted, the overall predicted stiffness of the laminate is greater than the test stiffness. Transverse failure of all plys occurs at a stress of about 9 ksi. The actual failure stress was about 11 ksi. The predicted tangent modulus decreased from an initial value of 1.70×10^6 to a final value of 1.47×10^6 psi.

The fractured specimens are shown in Figure 47. Practically no delamination occurred on these specimens with the exception of a narrow region adjacent to the fracture surface. Rather, the fracture extends along the fibers of one set of the plys, breaking the fibers of the other set. Failure occurred by matrix splitting in, say, the +60-degree plys and by fiber failure in the -60-degree plys.

The strain response of the $[0/\pm 45/90]_s$ laminates is shown in Figure 48. Transverse failure of the 90-degree plys is predicted at a stress of 14 ksi followed by a transverse failure of the ±45-degree plys at a stress of 18 ksi. Final failure is predicted when longitudinal fiber failure occurs in the 0-degree plys at a laminate stress of 53 ksi. The actual test failure stress was about 41 ksi. In contrast to the case of the angle plys, for the $[0/\pm 45/90]$ laminate, the prediction method over estimates the strength. From a design viewpoint the method erred on the side of safety for angle plys but for the $[0/\pm 45/90]_s$ laminate the results are nonconservative. The stiffness of the laminate is predicted very well, however. The predicted longitudinal stiffness decreases from an initial predicted value of 3.01×10^6 psi to a final value of $1.88 \times .0^6$ psi. The strain response was also computed by setting E_{22}, G_{12}, and ν_{21} after the ply failure equal to -0.2 times their original values. The prediction is shown in Figure 49. The agreement on the failure load is improved to a value of 50 ksi. The stiffness of the upper portion of the curve seems slightly low, however. It has been noted before that the ply unloading factor of -0.2 resulted in good comparisons for some other materials. The failed coupons are shown in Figure 50. Half of the 45-degree plys failed by matrix splitting, the

other half by fiber failure. The 90-degrees plys of course failed by matrix splitting and the 0-degree plys failed by longitudinal fiber failure. A considerable amount of delamination can be seen. Crazing due to transverse failure of the matrix of the 90-degree plys can be seen throughout the length of the coupon.

3.7 Conclusions on Glass-Epoxy Laminate Response

In the present lamination method, after matrix failure the constants E_{22}, G_{12} where set approximately equal to zero under incremental loading. Using negative values for these constants (simulating unloading) resulted in no substantial improvement of predicted and test laminate stress-strain. Use of the nonlinear ply shear curve resulted in a better laminate stress-strain curve--one which was nonlinear between failures of the various plys and also nonlinear prior to first-ply-failure. Ply failure stresses and strains agreed well with abrupt changes in the slopes of the glass-epoxy test curves.

Two definitions of laminate failure were used: (1) longitudinal fiber failure in two or more plys (2) strains of order one (singularity of stiffness matrix). Definition (1) is appropriate only if a high percentage of the fibers correspond to the load direction. This definition over estimates the ultimate load in the $[0/\pm45/90]_s$ laminate by about 30 percent. For angle plys loaded along the principal axis, definition (1) does not apply. All plys fail in the matrix simultaneously leading to very high strains (singular laminate stiffness matrix) of 100 percent or more on the very next load increment. Hence, definition (2) was used. This resulted in failure predictions for angle plys which were low by 20 to 30 percent.

Improvements in the prediction of laminate ultimate loads are desirable. Lamination theory is inherently limited, omitting interlaminar shear behavior and making no distinction in stacking sequence. Given these, it may be that no rational refinement will result in any further improvement in lamination prediction of ultimate loads. The use of in situ ply strengths as suggested by Chamis and Sullivan [17] may in the future be a fruitful approach.

For the time being, the present method--using the nonlinear ply shear curve together with E_{22} and G_{12} equal near zero after matrix failure--yields a laminate stress-strain curve sufficiently accurate for many practical engineering applications. This stress-strain behavior will be employed in the finite element program and example problems of Chapter V.

Chapter IV.

DEVELOPMENT OF THE FAILURE ANALYSIS METHOD--
A DOUBLY-CURVED, ISOPARAMETRIC, THICK-SHELL FINITE ELEMENT

4.1 Introduction

Early theory on laminated plates and shells [26] was a direct extension of the classical thin plate and shell theory based on the so-called Kirchhoff assumptions. Later the bending-extension coupling was studied by Reissner and Stavsky [27]. In 1971 Pryor and Barker [28] developed a rectangular finite element for laminated plates. The shear deformation was included by the relaxation of part of Kirchhoff's assumptions. Later, in 1976, a quadrilateral element for laminated plates was presented by Nopratvarakorn [29]. The latter element is similar to but more versatile than the one developed by Pryor and Barker. The plate quadrilateral element is then further extended to model the shell structure. A plate element to model shells has the merit of simplicity, but a large number of elements are needed for modeling shell structures. Therefore, a doubly-curved, isoparametric, quadratic, 8-node, thick-shell element is developed in this study. The element is derived from the 16-node solid element by specializing the element so that strain energy of the stresses normal to the midsurface is ignored and by constraining lines initially normal to the midsurface to remain straight. Thus fewer degrees of freedom are needed to define the displacement field. The resulting element has 40 degrees of freedom--three displacements and two rotations for each of the eight nodes. Though the midsurface normals are to remain straight during

deformation, these lines need not remain normal to the deformed mid-surface. Therefore, the ability to model transverse shear deformation is retained. Transverse shear is thought to be significant for the laminated plates and shells.

4.2 Isoparametric Elements

Considering the geometry of the three-dimensional element in Figure 51, one notes that by means of the coordinate transformation

$$x = \Sigma N'_i x_i$$
$$y = \Sigma N'_i y_i$$
$$z = \Sigma N'_i z_i \qquad (10)$$

the element can have curved boundaries. This is an important advantage of the isoparametric formulation. In Equation (10) x, y, and z are the coordinates at any point of the element and x_i, y_i, z_i, i = 1, . . . n are the coordinates of the n nodes. The interpolation functions N_i are defined in the natural coordinate system of the element, which are functions of ξ, η, ζ that each vary from -1 to +1.

In the isoparametric formulation the element displacements are interpolated in the same way as the geometry; i.e., one assumes

$$u = \Sigma N'_i u_i$$
$$v = \Sigma N'_i v_i$$
$$w = \Sigma N'_i w_i \qquad (11)$$

where u, v, and w are the local element displacements at any point of the element and u_i, v_i, and w_i, i = 1, . . . n, are the corresponding element displacements at its nodes.

For a 16-node solid element the interpolation functions are defined to be

$$N_1' = 1/8(1-\xi)(1-\eta)(1-\zeta)(-\xi-\eta-1)$$

$$N_2' = 1/4(1-\xi^2)(1-\eta)(1-\zeta)$$

$$N_3' = 1/8(1+\xi)(1-\eta)(1-\zeta)(\xi-\eta-1)$$

$$N_4' = 1/4(1-\eta^2)(1+\xi)(1-\zeta)$$

$$N_5' = 1/8(1+\xi)(1+\eta)(1-\zeta)(\xi+\eta-1)$$

$$N_6' = 1/4(1-\xi^2)(1+\eta)(1-\zeta)$$

$$N_7' = 1/8(1-\xi)(1+\eta)(1-\zeta)(-\xi+\eta-1)$$

$$N_8' = 1/4(1-\eta^2)(1-\xi)(1-\zeta) \tag{12}$$

N_9' through N_{16}' can be obtained by replacing ζ with $-\zeta$. With the definition of N_i', the first of Equations (10) can be written as

$$x = \sum_{i=1}^{8} N_i \frac{(1-\zeta)}{2} x_i + \sum_{i=1}^{8} N_i \frac{(1+\zeta)}{2} x_{i+8}$$

or

$$x = \sum_{i=1}^{8} N_i \left(\frac{1-\zeta}{2}\right) x_{ip} + \sum_{i=1}^{8} N_i \left(\frac{1+\zeta}{2}\right) x_{iq}$$

where

$$N_i = 1/4(1+\xi\xi_i)(1+\eta\eta_i)(\xi\xi_i+\eta\eta_i-1) \quad \text{for } i = 1, 3, 5, 7$$

$$N_i = 1/2(1-\xi^2)(1+\eta\eta_i) \quad \text{for } i = 2, 6$$

$$N_i = 1/2(1+\xi\xi_i)(1-\eta^2) \quad \text{for } i = 4, 8$$

are the shape functionsof the 8-node two-dimensional element of the midsurface, and

$$\left.\begin{aligned} \xi_i &= -1, 0, 1, 1, 1, 0, -1, -1 \\ \eta_i &= -1, -1, -1, 0, 1, 1, 1, 0 \end{aligned}\right. \quad \text{for } i = 1, 2, \ldots 8$$

and x_{iq}, x_{ip}, etc., are global cartesian coordinates of the 16 nodes on $\zeta = -1$ and $+1$. Similar expressions can be written for y and z; i.e.,

$$\begin{Bmatrix} x \\ y \\ z \end{Bmatrix} = \sum_{i=1}^{8} N_i \left(\frac{1+\zeta}{2}\right) \begin{Bmatrix} x_{iq} \\ y_{iq} \\ z_{iq} \end{Bmatrix} + \sum_{i=1}^{8} N_i \left(\frac{1-\zeta}{2}\right) \begin{Bmatrix} x_{ip} \\ y_{ip} \\ z_{ip} \end{Bmatrix} \tag{13}$$

Following Ahmad [30] the full three-dimensional element is then reduced to the conventional representation by midsurface nodes only, preserving

most of the desirable characteristics of the solid element. The six degrees of freedom can be transformed into three mid-point translations and two mid-point rotations about two axes perpendicular to the normal, and a change of length of the normal itself. This yields a stiffness too high in bending due to the fact that the normal strain $\varepsilon_n = 0$. However, Ahmad replaced the linear ζ variation of the normal displacement with the condition $\sigma_n = 0$, the usual assumption for beam and plate theory. A linear assumption in the ζ direction for the in-plane displacements u and v is sufficiently good to represent membrane strain states exactly and transverse shear strains closely; therefore, all desired features are now included. Introducing the following

$$x_i = \frac{x_{ip}+x_{iq}}{2} \qquad y_i = \frac{y_{ip}+y_{iq}}{2} \qquad \vec{V}_{3i} = \begin{Bmatrix} x_{iq}-x_{ip} \\ y_{iq}-y_{ip} \\ z_{iq}-z_{ip} \end{Bmatrix} \qquad z_i = \frac{z_{ip}+z_{iq}}{2}$$

into Equation (13) yields a set of equations which define element geometry in terms of midsurface nodal coordinates and vectors $\vec{V}_{3i}$,

$$\begin{Bmatrix} x \\ y \\ z \end{Bmatrix} = \sum_{i=1}^{8} N_i \begin{Bmatrix} x_i \\ y_i \\ z_i \end{Bmatrix} + \sum_{i=1}^{8} N_i \frac{\zeta}{2} \vec{V}_{3i} \tag{14}$$

The global coordinate system x, y, z has z vertically upwards. The local ξ, η, ζ system is defined by the intrinsic shell coordinates. The five degrees of freedom of each node will be three translations u, v, w in the global x, y, z system and two rotations α, β about axes $\vec{V}_1$, $\vec{V}_2$. The directions of $\vec{V}_1 \vec{V}_2$ are in the tangential direction of the ξ, η coordinates respectively. $\vec{V}_3$ is drawn in the ζ direction of the ζ-axis to

form a triad with $\vec{V}_1$ and $\vec{V}_2$ at the node, Figure 52.

Consider a rotation α_i about axis $\vec{V}_{2i}$ and β_i about axis $\vec{V}_{1i}$. The displacement at any point ζ from the midsurface is

$$\frac{\zeta t_i}{2}\left(\frac{\alpha_i \vec{V}_{1i}}{|\vec{V}_{1i}|} - \frac{\beta_i \vec{V}_{2i}}{|\vec{V}_{2i}|}\right)$$

where t_i is the thickness of the shell at node i. Therefore the complete 40-degree-of-freedom element displacement field may be written as

$$\begin{Bmatrix} u \\ v \\ w \end{Bmatrix} = \sum_{i=1}^{8} N_i \begin{Bmatrix} u_i \\ v_i \\ w_i \end{Bmatrix} + \sum_{i=1}^{8} N_i \zeta [\mu_i] \frac{t_i}{2} \begin{Bmatrix} \alpha_i \\ \beta_i \end{Bmatrix} \tag{15}$$

where

$$[\mu_i] = \begin{bmatrix} \ell_{1i} & -\ell_{2i} \\ m_{1i} & -m_{2i} \\ n_{1i} & -n_{2i} \end{bmatrix} = \begin{bmatrix} \mu_{i11} & \mu_{i12} \\ \mu_{i21} & \mu_{i22} \\ \mu_{i31} & \mu_{i33} \end{bmatrix}$$

and $\ell_{1i}, m_{1i}, n_{1i}$, $\ell_{2i}, m_{2i}, n_{2i}$ are respectively the direction cosines of $\vec{V}_1$ and $\vec{V}_2$ at node i.

The strain-displacement transformation may be obtained by differentiating Equation (15). Since the displacement field is defined in the local $\xi\eta\zeta$ system, the derivatives in this system must be evaluated beforehand. Now at any point

$$\begin{bmatrix} \frac{\partial u}{\partial \xi} & \frac{\partial v}{\partial \xi} & \frac{\partial w}{\partial \xi} \\ \frac{\partial u}{\partial \eta} & \frac{\partial v}{\partial \eta} & \frac{\partial w}{\partial \eta} \\ \frac{\partial u}{\partial \zeta} & \frac{\partial v}{\partial \zeta} & \frac{\partial w}{\partial \zeta} \end{bmatrix} = \begin{bmatrix} \frac{\partial x}{\partial \xi} & \frac{\partial y}{\partial \xi} & \frac{\partial z}{\partial \xi} \\ \frac{\partial x}{\partial \eta} & \frac{\partial y}{\partial \eta} & \frac{\partial z}{\partial \eta} \\ \frac{\partial x}{\partial \zeta} & \frac{\partial y}{\partial \zeta} & \frac{\partial z}{\partial \zeta} \end{bmatrix} \begin{bmatrix} \frac{\partial u}{\partial x} & \frac{\partial v}{\partial x} & \frac{\partial w}{\partial x} \\ \frac{\partial u}{\partial y} & \frac{\partial v}{\partial y} & \frac{\partial w}{\partial y} \\ \frac{\partial u}{\partial z} & \frac{\partial v}{\partial z} & \frac{\partial w}{\partial z} \end{bmatrix} \tag{16}$$

or symbolically

$$[uvw_{\xi\eta\zeta}] = [J][uvw_{xyz}]$$

where [J] is the Jacobean of the transformation of x, y, z to ξ, η, ζ.

Thus

$$[uvw_{xyz}] = [J]^{-1}[uvw_{\xi\eta\zeta}] \tag{17}$$

Now the strains ε_{ij} are various combinations of $\frac{\partial u}{\partial x}$, $\frac{\partial v}{\partial x}$, $\frac{\partial w}{\partial x}$, $\frac{\partial u}{\partial y}$, $\frac{\partial v}{\partial y}$, $\frac{\partial w}{\partial y}$, $\frac{\partial u}{\partial z}$, $\frac{\partial v}{\partial z}$, $\frac{\partial w}{\partial z}$ and can be picked out of the matrix $[uvw_{xyz}]$ term-by-term or

$$\begin{Bmatrix} \varepsilon_x \\ \varepsilon_y \\ \varepsilon_z \\ \gamma_{xy} \\ \gamma_{yz} \\ \gamma_{zx} \end{Bmatrix} = \begin{bmatrix} 1 & 0 & 0 & 0 & 0 & 0 & 0 & 0 & 0 \\ 0 & 0 & 0 & 0 & 1 & 0 & 0 & 0 & 0 \\ 0 & 0 & 0 & 0 & 0 & 0 & 0 & 0 & 1 \\ 0 & 1 & 0 & 1 & 0 & 0 & 0 & 0 & 0 \\ 0 & 0 & 0 & 0 & 0 & 1 & 0 & 1 & 0 \\ 0 & 0 & 1 & 0 & 0 & 0 & 1 & 0 & 0 \end{bmatrix} \begin{Bmatrix} u,_x \\ u,_y \\ u,_z \\ v,_x \\ v,_y \\ v,_z \\ w,_x \\ w,_y \\ w,_z \end{Bmatrix} \tag{18}$$

Substituting Equations (16), (17) into Equation (18) leads to

$$\{\varepsilon\} = [B]\{\delta\} \tag{19}$$

where $\{\delta\}$ is the nodal displacement matrix. Matrix $[B]$ is a 6 x 40 and is built of eight 6 x 5 blocks. A typical block $[B_i]$ is of the form

$$[B_i] = \begin{bmatrix} a_i & 0 & 0 & A_i\mu_{i11}\frac{t_i}{2} & A_i\mu_{i12}\frac{t_i}{2} \\ 0 & b_i & 0 & B_i\mu_{i21}\frac{t_i}{2} & B_i\mu_{i22}\frac{t_i}{2} \\ 0 & 0 & c_i & C_i\mu_{i31}\frac{t_i}{2} & C_i\mu_{i32}\frac{t_i}{2} \\ b_i & a_i & 0 & (B_i\mu_{i11}\frac{t_i}{2}+A_i\mu_{i21}\frac{t_i}{2}) & (B_i\mu_{i12}\frac{t_i}{2}+A_i\mu_{i22}\frac{t_i}{2}) \\ 0 & c_i & b_i & (C_i\mu_{i21}\frac{t_i}{2}+B_i\mu_{i31}\frac{t_i}{2}) & (C_i\mu_{i22}\frac{t_i}{2}+B_i\mu_{i32}\frac{t_i}{2}) \\ c_i & 0 & a_i & (C_i\mu_{i11}\frac{t_i}{2}+A_i\mu_{i31}\frac{t_i}{2}) & (C_i\mu_{i12}\frac{t_i}{2}+A_i\mu_{i32}\frac{t_i}{2}) \end{bmatrix} \tag{20}$$

where

$$a_i = J^*_{11} \frac{\partial N_i}{\partial \xi} + J^*_{12} \frac{\partial N_i}{\partial \eta}$$

$$b_i = J^*_{21} \frac{\partial N_i}{\partial \xi} + J^*_{22} \frac{\partial N_i}{\partial \eta}$$

$$c_i = J^*_{31} \frac{\partial N_i}{\partial \xi} + J^*_{32} \frac{\partial N_i}{\partial \eta}$$

and $[J^*] = [J]^{-1}$

$$A_i = a_i \zeta + J^*_{13} N_i$$

$$B_i = b_i \zeta + J^*_{23} N_i$$

$$C_i = c_i \zeta + J^*_{33} N_i$$

4.3 The Elasticity Matrix

Consider each lamina or each layer of the composite behaving as a homogeneous orthotropic material. Nine independent elastic constants are required to describe the material. For the principal axes of elastic symmetry ($\theta^1\theta^2\theta^3$), Figure 53, which coincide with the reference axis ($x'y'z'$), the compliance relations for a typical layer of a composite are

$$\begin{Bmatrix} \varepsilon_1 \\ \varepsilon_2 \\ \varepsilon_3 \\ \gamma_{12} \\ \gamma_{23} \\ \gamma_{13} \end{Bmatrix}^{(\theta)} = \begin{bmatrix} \frac{1}{E_1} & -\frac{\nu_{12}}{E_2} & -\frac{\nu_{13}}{E_3} & 0 & 0 & 0 \\ -\frac{\nu_{21}}{E_1} & \frac{1}{E_2} & -\frac{\nu_{23}}{E_3} & 0 & 0 & 0 \\ -\frac{\nu_{31}}{E_1} & -\frac{\nu_{32}}{E_2} & \frac{1}{E_3} & 0 & 0 & 0 \\ 0 & 0 & 0 & \frac{1}{G_{12}} & 0 & 0 \\ 0 & 0 & 0 & 0 & \frac{1}{G_{23}} & 0 \\ 0 & 0 & 0 & 0 & 0 & \frac{1}{G_{13}} \end{bmatrix} \begin{Bmatrix} \sigma_1 \\ \sigma_2 \\ \sigma_3 \\ \tau_{12} \\ \tau_{23} \\ \tau_{13} \end{Bmatrix}^{(\theta)} \qquad (21)$$

where the coefficient matrix is symmetric. If the fiber arrangement

were such that the variation of the properties in the 2-3 plane were to be negligible, the number of constants reduces to five.

$$E_1 = E_L$$

$$E_2 = E_3 = E_T$$

$$\nu_{21} = \nu_{31} = \nu_{TL}$$

$$\nu_{23} = \nu_{TT}$$

$$G_{12} = G_{13} = G_{LT}$$

$$G_{23} = G_T = \frac{E_T}{2(1+\nu_{TT})} \qquad (22)$$

E and G are the Young's modulus and shear modulus. Poison's ratio ν_{ij} is defined as

$$\nu_{ij} = -\frac{\varepsilon_i}{\varepsilon_j}$$

due to a stress in the j-direction. Therefore, the determination of the five independent elastic constants E_L, E_T, ν_{TL}, G_{LT}, and ν_{TT} characterizes the transversely isotropic composite. If the expression for G_T does not hold, the number of independent elastic constants increases to six.

The constitutive relationship for the generally orthotropic composite is obtained by solving for $\{\sigma^\theta\}$ in Equation (21) and making use of Equations (22).

$$\begin{Bmatrix} \sigma_1 \\ \sigma_2 \\ \sigma_3 \\ \tau_{12} \\ \tau_{13} \\ \tau_{13} \end{Bmatrix}^{(\theta)} = \begin{bmatrix} C_{11} & C_{12} & C_{13} & 0 & 0 & 0 \\ C_{21} & C_{22} & C_{23} & 0 & 0 & 0 \\ C_{31} & C_{32} & C_{33} & 0 & 0 & 0 \\ 0 & 0 & 0 & C_{44} & 0 & 0 \\ 0 & 0 & 0 & 0 & C_{55} & 0 \\ 0 & 0 & 0 & 0 & 0 & C_{66} \end{bmatrix} \begin{Bmatrix} \varepsilon_1 \\ \varepsilon_2 \\ \varepsilon_3 \\ \gamma_{12} \\ \gamma_{23} \\ \gamma_{13} \end{Bmatrix}^{(\theta)} \tag{23}$$

where

$$C_{11} = E_L^2(1-\nu_{TT}^2)F$$

$$C_{12} = E_L E_T \nu_{TL}(1+\nu_{TT})F = C_{21} = C_{13} = C_{31}$$

$$C_{22} = E_T(E_L-\nu_{TL}^2 E_T)F$$

$$C_{23} = E_T(E_L\ {}_{TT}+E_T\nu_{TL}^2)F = C_{32}$$

$$C_{33} = E_T(E_L-E_T\nu_{TL}^2)F = C_{22}$$

$$C_{44} = G_{LT} = C_{66}$$

$$C_{55} = G_T$$

$$F = 1/[E_L(1-\nu_{TT}^2)-2E_T\nu_{TL}^2(1+\nu_{TT})] \tag{24}$$

The transverse normal strain can be found from Equation (23) as

$$\varepsilon_3^\theta = \frac{1}{C_{33}}(\sigma_3-C_{31}\varepsilon_1^\theta-C_{32}\varepsilon_2^\theta)$$

which can be used to eliminate ε_3 from the stress-strain relations for the K^{th} layer leaving

$$\begin{Bmatrix} \sigma_1 \\ \sigma_2 \\ \tau_{12} \\ \tau_{23} \\ \tau_{13} \end{Bmatrix}^{(\theta)}_{(K)} = \begin{bmatrix} Q_{11} & Q_{12} & 0 & 0 & 0 \\ Q_{21} & Q_{22} & 0 & 0 & 0 \\ 0 & 0 & Q_{44} & 0 & 0 \\ 0 & 0 & 0 & Q_{55} & 0 \\ 0 & 0 & 0 & 0 & Q_{66} \end{bmatrix}_{(K)} \begin{Bmatrix} \varepsilon_1 \\ \varepsilon_2 \\ \gamma_{12} \\ \gamma_{23} \\ \gamma_{13} \end{Bmatrix}^{(\theta)}_{(K)} \tag{25}$$

where σ_3 is neglected as in classical lamination theory

$$Q_{ij} = \begin{matrix} C_{ij} - \dfrac{C_{i3}C_{j3}}{C_{33}} & \text{if } i, j = 1, 2 \\ C_{ij} \quad \text{if } i, j = 4, 5, 6 & \end{matrix}$$

For an arbitrary orientation of a lamina, the principal axes of material will not coincide with the reference axes of the laminate. The transformation for expressing stresses in an $(\theta^1\theta^2\theta^3)$ coordinate system in terms of stresses in $(x'y'z')$ system, Figure 54, is

$$\begin{Bmatrix} \sigma_1 \\ \sigma_2 \\ \tau_{12} \\ \tau_{23} \\ \tau_{13} \end{Bmatrix}^{(\theta)}_{(K)} = \begin{bmatrix} \cos^2\phi & \sin^2\phi & 2\sin\phi\cos\phi & 0 & 0 \\ \sin^2\phi & \cos^2\phi & -2\sin\phi\cos\phi & 0 & 0 \\ -\sin\phi\cos\phi & \sin\phi\cos\phi & \cos^2\phi-\sin^2\phi & 0 & 0 \\ 0 & 0 & 0 & \cos\phi & \sin\phi \\ 0 & 0 & 0 & -\sin\phi & \cos\phi \end{bmatrix} \begin{Bmatrix} \sigma_{x'} \\ \sigma_{y'} \\ \tau_{x'y'} \\ \tau_{y'z'} \\ \tau_{x'z'} \end{Bmatrix}_{(K)} \tag{26}$$

or

$$\{\sigma^\theta\}_{(K)} = [T_\sigma]\{\sigma'\}_{(K)}$$

Hence, solving Equation (26) yields

$$\{\sigma'\}_{(K)} = [T_\sigma]^{-1}\{\sigma^\theta\}_{(K)}$$

where $[T_\sigma]^{-1}$ is obtained by replacing $\sin\phi$ with $-\sin\phi$ in $[T_\sigma]$. Similar transformations for the strain can be obtained as

$$\begin{Bmatrix} \varepsilon_1 \\ \varepsilon_2 \\ \gamma_{12} \\ \gamma_{23} \\ \gamma_{13} \end{Bmatrix}^{(\theta)}_{(K)} = \begin{bmatrix} \cos^2\phi & \sin^2\phi & \sin\phi\cos\phi & 0 & 0 \\ \sin^2\phi & \cos^2\phi & -\sin\phi\cos\phi & 0 & 0 \\ -2\sin\phi\cos\phi & 2\sin\phi\cos\phi & \cos^2\phi-\sin^2\phi & 0 & 0 \\ 0 & 0 & 0 & \cos\phi & \sin\phi \\ 0 & 0 & 0 & -\sin\phi & \cos\phi \end{bmatrix} \begin{Bmatrix} \varepsilon_{x'} \\ \varepsilon_{y'} \\ \gamma_{x'y'} \\ \gamma_{y'z'} \\ \gamma_{x'z'} \end{Bmatrix}_{(K)} \tag{27}$$

or

$$\{\varepsilon^\theta\}_{(K)} = [T_\varepsilon]\{\varepsilon'\}_{(K)}$$

and

$$\{\varepsilon'\}_{(K)} = [T_\varepsilon]^{-1}\{\varepsilon^\theta\}_{(K)}$$

where $[T_\varepsilon]^{-1}$ is obtained by replacing $\sin\phi$ with $-\sin\phi$ in $[T_\varepsilon]$ and the prime represents the principal axes system.

Equations (25) can now be rewritten as

$$\{\sigma^\theta\}_{(K)} = [Q]_{(K)}\{\varepsilon^\theta\}_{(K)} \tag{28}$$

Substituting Equations (26), (27) into (28) yields

$$\{\sigma'\}_{(K)} = [T_\varepsilon]^T[Q]_{(K)}[T_\varepsilon]\{\varepsilon'\}_{(K)} \tag{29}$$

or

$$\{\sigma'\}_{(K)} = [Q']_{(K)}\{\varepsilon'\}_{(K)}$$

where

$$[Q']_{(K)} = [T_\varepsilon]^T[Q]_{(K)}[T_\varepsilon]$$

and

$$[T_\varepsilon]^T = [T_\sigma]^{-1}$$

4.4 Element Stiffness Matrix

The strain energy of the element can be written as

$$U = \sum_{K=1}^{N} \tfrac{1}{2} \int_{V(K)} \{\varepsilon'\}^T_{(K)}\{\sigma'\}dV_{(K)} \tag{30}$$

where the $V_{(K)}$ denotes the volume of the K^{th} lamina. By substituting

Equation (29) into Equation (30), the element strain energy can be obtained as

$$U = \sum_{K=1}^{N} \tfrac{1}{2}\int_{V_{(K)}} \{\varepsilon'\}^T[Q']_{(K)}\{\varepsilon'\}dV_{(K)} \qquad (31)$$

where $\{\varepsilon'\}$ is equal to $\{\varepsilon'\}_{(K)}$, since the distribution of strain is assumed to be continuous throughout the entire thickness of the laminate. Matrix $[Q']_{(K)}$ is the stress-strain matrix for the K^{th} layer. One must ensure that $[Q]_{(K)}$ provides for zero stress normal to the shell. Let the reference shell coordinate x'y'z' have the same directions as $\vec{V}_1$, $\vec{V}_2$, $\vec{V}_3$ so that at each point of the shell z' is normal to the midsurface. Taking for example the K^{th} layer, the stress-strain relation

$$\{\sigma'\}_{(K)} = [Q']_{(K)}\{\varepsilon'\}$$

in x'y'z' coordinates is

$$\begin{Bmatrix} \sigma_{x'} \\ \sigma_{y'} \\ \sigma_{z'} \\ \tau_{x'y'} \\ \tau_{y'z'} \\ \tau_{z'x'} \end{Bmatrix}_{(K)} = \begin{bmatrix} Q'_{11} & Q'_{12} & 0 & 0 & 0 & 0 \\ Q'_{21} & Q'_{22} & 0 & 0 & 0 & 0 \\ 0 & 0 & 0 & 0 & 0 & 0 \\ 0 & 0 & 0 & Q'_{44} & 0 & 0 \\ 0 & 0 & 0 & 0 & Q'_{55} & 0 \\ 0 & 0 & 0 & 0 & 0 & Q'_{66} \end{bmatrix}_{(K)} \begin{Bmatrix} \varepsilon_{x'} \\ \varepsilon_{y'} \\ \varepsilon_{z'} \\ \gamma_{x'y'} \\ \gamma_{y'z'} \\ \gamma_{z'x'} \end{Bmatrix} \qquad (32)$$

This form of $[Q']_{(K)}$ provides for $\sigma_{z'} = 0$ and plane stress conditions in the x'y' plane. A coordinate transformation is applied to convert $\{\varepsilon'\}_{(K)}$ to matrix $\{\varepsilon\}_{(K)}$ in the global xyz coordinates; i.e., substituting

$$\{\varepsilon'\} = [T'_\varepsilon]\{\varepsilon\}$$

into Equation (31) yields

$$U = \tfrac{1}{2}\sum_{K=1} \int_{V_{(K)}} \{\varepsilon\}^T[T'_\varepsilon]^T[Q']_{(K)}[T'_\varepsilon]\{\varepsilon\}dV_{(K)} \qquad (33)$$

Introducing Equation (19) into (33) leads to

$$U = \tfrac{1}{2}\{\delta\}^T[k]\{\delta\} \tag{34}$$

where

$$[k] = \sum_{K=1}^{N} \int_{V_{(K)}} [B]^T[E]_{(K)}[B]dV_{(K)} \tag{35}$$

is the element stiffness matrix and

$$[E] = [T']^T[Q']_{(K)}[T']$$

in which $[T'_\varepsilon]$ is the transformation matrix between xyz and x'y'z' coordinates.

The integral of Equation (33) is evaluated by numerical integration with respect to the local ξ, η, ζ coordinates. Matrix [B] may be split into a part $[B_0]$ independent of ζ and a part $\zeta[B_1]$ linear in ζ. The products

$$\zeta[B_0]^T[E]_{(K)}[B_1]$$

and

$$\zeta[B_1]^T[E]_{(K)}[B_0]$$

are linear in ζ, representing the bending-membrane coupling effect. The product

$$[B_0]^T[E]_{(K)}[B_0]$$

and

$$[B_1]^T[E]_{(K)}[B_1]$$

are the membrane and bending effects respectively.

4.5 Body Loads, Surface Loads

Nodal loads resulting from body force and surface pressure will now be considered. The nodal loads associated with these applied forces may be found by usual procedures and only an outline is included here.

Equation (15) can be rewritten as follows:

$$\{f\} = \begin{Bmatrix} u \\ v \\ w \end{Bmatrix} = [\bar{N}]\{\delta\} \tag{36}$$

where $[\bar{N}]$ defines the nature of the displacement field. Matrix $[\bar{N}]$ is a 3 x 40 and is built of eight 3 x 5 blocks. A typical block $[\bar{N}_i]$ is of the form

$$[\bar{N}_i] = \begin{bmatrix} N_i & 0 & 0 & \frac{N_i \ell t_i \ell_{1i}}{2} & -\frac{N_i \ell t_i \ell_{2i}}{2} \\ 0 & N_i & 0 & \frac{N_i \ell t_i m_{1i}}{2} & -\frac{N_i \ell t_i m_{2i}}{2} \\ 0 & 0 & N_i & \frac{N_i \ell t_i n_{1i}}{2} & \frac{N_i \ell t_i n_{2i}}{2} \end{bmatrix}$$

The array of element nodal forces $\{r\}$ produced by body force and surface pressure in the element is [31]

$$\{r\} = \int_{Vol} [\bar{N}]^T \{P\} dV + \int_S [\bar{N}]^T \{p_n\} ds \qquad (37)$$

The first integral represents the body force and the last integral represents surface normal pressur .

4.6 Computer Implementation

First of all, consider the definition of the three mutually perpendicular vectors $\vec{V}_{1i}$, $\vec{V}_{2i}$, $\vec{V}_{3i}$ as shown in Figure 52. The rotation vectors β_i, α_i are colinear with $\vec{V}_{1i}$ and $\vec{V}_{2i}$ respectively. It is conceivable that in the assembled structure no two nodal rotation vectors will have the same direction. Vector $\vec{V}_{3i}$ may be defined by input data, and is presumed to span the thickness and be normal to the midsurface. This proves to be very time-consuming in preparation of data for a large-scale problem. In this study the following approach is adopted.

From the differential geometry, the tangent vector $\vec{e}_1$, $\vec{e}_2$ as shown in Figure 55 along the local intrinsic shell coordinates axes can be found by the following equations.

$$\vec{e}_1 = \frac{\partial x}{\partial \xi} \vec{i} + \frac{\partial y}{\partial \xi} \vec{j} + \frac{\partial z}{\partial \xi} \vec{K}$$

$$\vec{e}_2 = \frac{\partial x}{\partial \eta} \vec{i} + \frac{\partial y}{\partial \eta} \vec{j} + \frac{\partial z}{\partial \eta} \vec{K}$$

and

$$\vec{e}_3 = \vec{e}_1 \times \vec{e}_2$$

The direction cosines of $\vec{e}_3$ give the directions for $\vec{V}_{3i}$. $\vec{V}_{1i}$ could be defined by $\vec{e}_1$ or might be defined by input data so that it coincides with a principal direction of an orthotropic material and

$$\vec{V}_{2i} = \vec{V}_{3i} \times \vec{V}_{1i}$$

Next the element stiffness matrix given by Equation (35) will be integrated numerically with respect to the local ξ, η, ζ coordinates resulting in

$$[k] = \sum_K \int_{-1}^{1} \int_{-1}^{1} \int_{-1}^{1} [B]^T [E]_{(K)} [B] \det|J| d\xi d\eta d\zeta \tag{38}$$

When the Jacobian of the above equation is computed, it is found that ζ to the first power appears in certain terms. These terms may be neglected in comparison with terms to which they are added. In this study, these terms have been temporarily suppressed so that [J] becomes independent of ζ and explicit integration through the thickness is possible; and, as indicated in the previous section, [B] may be split into $[B_0] + \zeta[B_1]$. This integral results in

$$[k] = \int_{-1}^{1} \int_{-1}^{1} ([B_0][E][B_o]+[B_0][DE][B_1]+[B_1][DE][B_o]$$

$$+[B_1][D][B_1]) \times \det|J| d\xi d\eta$$

where [E] is the in-plane stiffness array, [D] is the flexural rigidity array, and [DE] is the coupling of membrane and bending stiffness array.

The average values of [E], [DE], and [D] are then computed and the ζ terms are restored in [J]. Two Gaussian points in the thickness direction are used for numerical integration; i.e.

$$[k] = \int_{-1}^{1} \int_{-1}^{1} \int_{-1}^{1} ([B_0][E][B_o]+[B_o][DE][B_1]+[b_1][DE][B_o]$$

$$+[B_1][D][B_1] \times \det|J| d\xi d\eta d\zeta$$

The cost of numerical integration is then doubled but the stiffness obtained is much better than the one obtained by neglecting ζ terms in [J].

In the final calculation of element stresses, the strains computed from

$$\{\varepsilon\} = [B]\{\delta\}$$

are referred to global coordinates x, y, and z. The strain is then transferred back to the x',y',z' coordinates by

$$\{\varepsilon'\} = [T_\varepsilon']\{\varepsilon\}$$

And, finally, the operation

$$\{\sigma'\}_{(K)} = [Q']_{(K)}\{\varepsilon'\}$$

gives stresses referred to the shell coordinates x',y',z'; and the stresses in the principal material direction are obtained by

$$\{\sigma^\theta\}_{(K)} = [T_\sigma]\{\sigma'\}_{(K)}$$

4.7 Yield Criteria

The Hill criterion as well as the Tsi-Wu tensor criterion are implemented in the computer program to assess the effect of stresses and strains on the structural integrity of the composite. Due to the thinness of the plates and shells in the θ^3-direction, plane stress is assumed; that is

$$\sigma_3 = \tau_{13} \simeq \tau_{23} \doteq 0$$

Also for a composite which has a regular fiber array in the θ^1-θ^2 plane it is usually assumed

$$(\sigma_3)_{y.p.} = (\sigma_2)_{y.p.}$$

With these conditions the Hill and Tsi-Wu criteria are essentially the same as used in the plane stress analysis. Incorporation into the computer code makes it possible to assess the structural integrity of the

plates and shells at discrete points due to the finite element approximation. At these discrete points the layer stresses σ_1, σ_2, τ_{12}, τ_{13}, τ_{23} are computed as described previously, and are substituted into either Equation (3) or Equation (4). The layer is yielded if the left-hand side of the equation is greater than or equal to 1.

4.8 Mesh Generation

The preparation of element data is a very time-consuming task. Incorrect element data is also a major source of errors when running finite element programs. The mesh generation subroutine is developed to generate the element data automatically. The MESH8 subroutine uses a group of either 8-node (quadratic) or 12-node (cubic) quadrilateral regions to define the body under consideration. This sub-program is capable of modeling two- or three-dimensional plates and shells midsurface domains that are composed of 8-node quadrilateral elements. The element nodes are numbered and the element nodal connectivities also generated. The 8-node quadrilateral region is available in MESH8. It can be used to generate a two- or three-dimensional quadrilateral element with eight nodes. The eight nodes that define the region are numbered as shown in Figure 56. Node 1 is always at the coordinate location $\xi = \eta = -1$.

The region is then subdivided into elements by considering eight nodes that form a quadrilateral such as the area in Figure 56 with the center node being omitted.

The size of the elements can be varied by placing nodes 2, 4, 6, or 8 at some point other than the center of the side. Movement of these nodes shifts the origin of the ξ-η coordinate system.

A domain is generally modeled by using several regions connected to one another along one or more sides. The possibility of a common boundary between two regions requires that proper connectivity data be given. These connectivity data convey to the computer how the region under consideration is connected to other regions.

Chapter V

LAMINATE STRESS ANALYSIS BY THE FINITE ELEMENT MODEL

5.1 Description of the Computer Program

The element is a general doubly-curved 8 node laminated thick-shell isoparametric element which can be used to model both thick and thin plates and shells, laminated or single layer. The material can be homogeneous isotropic or orthotropic. Both geometric and material non-linearity have been considered. The incremental procedure is employed. The load increments are of equal magnitude. The load is applied one increment at a time and during the application of each load increment the equations are assumed to be linear. The coordinates of the node are then updated and the adjusted coordinates are used in the computation of the stiffness for the next increment. The shear stress-strain curve of the composite material is highly nonlinear. The current tangent modulus is used in the calculations. The shear curve is fit by a cubic spline interpolation to define the shear modulus at a given strain. Figure 57 is a flow chart showing the sequence of operations performed by the program. Appendix A together with Figures 58 and 59 give an explanation of the data input for the program. Appendix B gives the program listing.

5.2 Verification of the Computer Model

This section presents the solutions of several problems which are intended to illustrate the capabilities and limitations of the finite element computer program. Examples included have known solutions, and thus provide good test cases for the program.

Homogeneous Simply Supported Square Plate. The first example is the well known Reissner thick plate problem. A nondimensional deflection parameter was calculated for various plate-thickness-to-lateral-dimension ratios. These results are presented in tabular form in Table 6 and in Figure 60. They show excellent agreement with the Reissner theory (see [29] or [32]). As the thickness to lateral dimension ratio gradually increases, the solutions of both the finite element method and Reissner theory disagree with the classical solution.

Cylindrical Shell Roof. This is a test example of application of the element to a shell in which bending action is severe, due to supports restraining deflection at the ends. The shell is supported on diaphragms as shown in Figure 61. These allow no displacements in their own plane, but offer no resistance to displacements perpendicular to it. Only a quarter of the shell was actually analyzed, by using symmetric boundary conditions along the two orthogonal planes of symmetry. Displacements of the shell in the vertical direction at the mid-span section are shown in Figure 62. The reference curve is that used by Pawsley [33]. The graphs show that this shell roof is well modelled by even one element.

Thin Hyperbolic Paraboloid Shell. The boundary of this shell is assumed to be rigidly held against both displacements and rotations. The shell is subjected to a uniform load. The geometry and material properties are shown in Figure 63. The entire hyperbolic paraboloid was modelled using only 4 elements. The results obtained are presented along with the results of Minch and Chamis [34]. These results show good agreement.

These comparisons all indicate a high degree of accuracy for the present method. The method will now be applied to a glass-epoxy laminate with a hole.

5.3 Response of a $[0/\pm45/90]_S$ Glass-Epoxy Laminate with a Hole

An example like that of Chow et al [16] was chosen. Three tensile coupons of XP-250 containing a hole were tested. The layup was $[0/\pm45/90]_s$, eight plys thick. During the load application the strain was monitored near the hole by a 1/16-inch strain gage. The coupon dimensions and gage location are shown in Figure 65.

Figure 66 shows the mesh layout for the computer simulation of this problem. The properties used in the input are those of Article 2.5. The tensile values of the stiffness properties were used in the input together with the nonlinear ply shear curve, Figure 9. After matrix failure in a given ply E_{22} and G_{12} were set approximately equal to zero as explained in Article 3.7. The computed response is compared with the three test responses in Figure 67. The two agree fairly well although test strain is slightly larger than the computed strain. The indicated computed failure was taken to be when two plys failed by fiber fracture. In this problem these failures occurred first, of course, in the elements on the hole edge. The slight disagreement in Figure 67 is probably due more to imperfect material characterization, as discussed in Article 3.7, than to the numerical method. The present finite element model, as already seen, appears to be quite precise.

REFERENCES

1. "Standard Test Method for Tensile Properties of Oriented Fiber Components," ANSI/ASTM D 3039-76, ASTM Annual Book of Standards, Part 32, 1976, pp. 706-711.

2. "Scotchply Reinforced Plastic Type XP-250, 3M Company Technical Data Sheet No. 4, December 1968.

3. Petit, P. H., "A Simplified Method of Determining the Inplane Shear Stress-Strain Response of Unidirectional Composites," Composite Materials: Testing and Design, ASTM STP 460, 1969, pp. 83-93.

4. Sims, D. F., "In-Plane Shear Stress-Strain Response of Unidirectional Composite Materials," Journal of Composite Materials, Vol. 7, January 1973, pp. 124-128.

5. Chamis, C. C. and Sinclair, J. H., "10° Off-Axis Tensile Test for Intralaminar Shear Characterization of Fiber Composites," NASA TN D-8215, April 1976.

6. Daniel, I. M., "Biaxial Testing of Graphite/Epoxy Composites Containing Stress Concentrations," Part I, AFML-TR-76-244, December 1976.

7. Whitney, J. M., Stansbarger, D. L., and Howell, H. B., "Analysis of the Rain Shear Test Applications and Limitations," Journal of Composite Materials, Vol. 5, JAnuary 1971, pp. 24-34.

8. Bergner, H. W., "Analysis of Shear Test Methods for Composite Laminates," Ph.D. Thesis, Virginia Polytechnic Institute and State University, April 1977.

9. Hofer, K. E. Jr., and Rao, P. N., "A New Static Compression Fixture for Advanced Composite Materials," Journal of Testing and Evaluation, Vol. 5, No. 4, July 1977, pp. 278-283.

10. Ashton, J. E., Halpin, J. C. and Petit, P. H., Primer on Composite Materials: Analysis, Technomic Publishing Co., 1969.

11. Rowlands, R. E., "Flow and Failure of Biaxially Loaded Composites," Inelastic Behavior of Composite Materials, Ed. Carl T. Herakovich, ASME, 1975, pp. 97-125.

12. Rowlands, R. C., "Analytical-Experimental Correlation of the Biaxial State of Stress in Composite Laminates (T-300/5208)," Air Force Flight Dynamics Laboratory, AFFDL-TR-75-11, April 1975.

13. Sandhu, R. S., "Ultimate Strength Analysis of Symmetric Laminates," Air Force Flight Dynamics Laboratory, AFFDL-TR-73-137, February 1974.

14. Hahn, H. T., and Tsai, S. W., "On the Behavior of Composite Laminates After Initial Failures," Journal of Composite Materials, Vol. 8, July 1974, pp. 288-305.

15. Chou, S. C., Orringer, O., and Rainey, J. H., "Post-Failure Behavior of Laminates: I -No Stress Concentration," Journal of Composite Materials, Vol. 10, October 1976, pp. 371-381.

16. Chou, S. C., Orringer, O., and Rainey, J. H., "Post-Failure Behavior of Laminates: II - Stress Concentration," Journal of Composite Materials, Vol. 11, January 1977, pp. 71-78.

17. Chamis, C. C. and Sullivan, T. L., "In Situ Ply Strength: An Initial Assessment," NASA TM-73771, 1978.

18. Sandhu, R. S., "A Survey of Failure Theories of Isotropic and Anisotropic Materials," Air Force Flight Dynamics Laboratory, AFFDL-TR-72-71, January 1972.

19. Hill, R., "A Theory of the Yielding and Plastic Flow of Anisotropic Metals," Proceedings of Royal Society of London (Series A), Vol. 193, 1948, pp. 281-297.

20. Tsai, S. W. and Wu, E. M., "A General Theory of Strength for Anisotropic Materials," Journal of Composite Materials, Vol. 5, January 1971, pp. 58-80.

21. Wu, E. M., "Optimal Experimental Measurements of Anisotropic Failure Tensors," Journal of Composite Materials, Vol 6, October 1972, pp. 472-489.

22. Pipes, R. B. and Cole, B. W., "On the Off-Axis Strength Test for Anisotropic Materials," Journal of Composite Materials, Vol. 7, April 1973, pp. 246-256.

23. Cole, B. W. and Pipes, R. B., "Filamentary Composite Laminates Subjected to Biaxial Stress Fields," IIT, Research Institute, AD-785 362, June 1974.

24. Petit, P. H. and Waddoups, M. E., "A Method of Predicting the Nonlinear Behavior of Laminated Composites," Journal of Composite Materials, Vol. 3, January 1969, pp. 2-19.

25. Rotem, A. and Hashin, Z., "Failure Modes of Angle Ply Laminates," Journal of Composite Materials, Vol. 9, April 1975, pp. 191-206.

26. Lechnitzki, S. G., Anisotropic Plates, translated from the second Russian edition by S. W. Tsai and T. Cheron, Gordon and Breach, 1968.

27. Reissner, E. and Stavsky, Y., "Bending and Stretching of Certain Types of Heterogeneous Aeolotropic Elastic Plates," Journal of Applied Mechanics, Vol. 28, No. 3, Trans. ASME, Vol 83, Series E, 1961, pp. 402-408.

28. Pryor, C. W., Jr., and Barker, R. M., "A Finite-Element Analysis Including Transverse Shear Effects for Applications to Laminated Plates," AIAA Journal, Vol. 9, No. 5, May 1971, pp. 912-917.

29. Nopratvarakorn, V., Analysis of Laminated Plates by Finite Element Method, M. S. Thesis, Tennessee Technological University, 1976.

30. Ahmad, S., Irons, B. M. and Zienkiewicz, O. C., "Curved Thick Shell and Membrans Elements with Particular Reference to Axisymmetric Problems," Proc. of Second Conference on Methods in Structural Mechanics, Wright-Patterson A.F.B. Ohio, 1968.

31. Cook, R. D., Concepts and Applications of Finite Element Analysis, John Wiley and Sons, 1974.

32. Pryor, Charles W. Jr., and Barker, R. M., "Finite Element Bending Analysis of Reissner Plates," Engineering Mechanics Division, ASCE, EM6, December 1970, pp. 967-983.

33. Pawsley, S. F., The Analysis of Moderately Thick to Thin Shells by the Finite Element Method, Report No. UCSESM 70-12, Dept. of Civil Engineering, University of California, 1970.

34. Minich, M. C. and Chamis, C. C., "Doubly-Curved Variable-Thickness Isoparametric Heterogeneous Finite Element," Computers and Structures, Vol. 7, 1975, pp. 295-301.

35. Choi, C. K. and Schnobrich, "Use of Non-conforming Modes in Finite Element Analysis of Plates and Shells," University of Illinois, UILU-ENGR-73-2019, 1073.

Table 1

Summary of Ply Properties from $[0°]_s$ Tension Tests on XP-250 Glass-Epoxy

Properties / Test No.	Young's Modulus E_{11}^T (psi)	Poisson's Ratio ν_{12}^T	Ultimate Stress X_1^T (ksi)	Ultimate Strain ε_1^T (μ Strain)
1	5.70×10^6	0.299	132	22,400
2	5.39×10^6	0.295	140	26,400
3	5.56×10^6	0.308	127	23,400
4	5.62×10^6	0.299	---[1]	------[1]
5	5.90×10^6	0.293	137	23,900
Mean Values	5.64×10^6	0.299	134	24,000

[1]Load application was stopped following strain gage failure.

Table 2

Summary of Ply Properties from $[90^\circ]_s$ Tension Tests on XP-250 Glass-Epoxy

Properties / Test No.	Young's Modulus E_{22}^T (psi)	Poisson's Ratio (Test Value) ν_{21}^T	Poisson's Ratio (Calculated Value)[1] ν_{21}^T	Ultimate Stress X_2^T (ksi)	Ultimate Strain e_2^T (μ strain)
6	1.72×10^6	0.061	0.091	7.20	4,580
7	1.91×10^6	0.069	0.101	7.88	4,770
9[2]	1.64×10^6	0.080	0.087	8.06	5,450
10	1.72×10^6	0.086	0.091	6.83	4,130
11	1.74×10^6	0.094	0.093	7.78	4,850
Mean Values	1.74×10^6	0.078	0.092	7.55	4,760

[1]Calculated value of Poisson's ratio $\nu_{21}^T = \nu_{12}^T \times E_{22}^T/E_{11}^T$, where $E_{11}^T = 5.64 \times 10^6$ psi and $\nu_{12}^T = 0.299$.

[2]Coupon no. 8 was broken while inserting into test machine.

Table 3

Summary of Ply Shear Properties for XP-250 Glass-Epoxy from Three-Rail Shear of Unidirectional Panels

Test No. \ Properties	Shear Modulus G_{12} (psi)	Ultimate Shear Stress S_{12} (ksi)	Ultimate Shear Strain e_{12} (μ strain)
12 (I)	0.60×10^6	6.48	18,200
12 (II)	0.63×10^6		14,300
13 (I)	0.69×10^6	7.60	20,300
13 (II)	0.76×10^6		18,200
14 (I)	0.58×10^6	6.76	19,200
14 (II)	0.78×10^6		15,000
15 (I)	0.74×10^6	8.10	25,900
15 (II)	0.66×10^6		26,300
Mean Values	0.68×10^6	7.23	19,700

Table 4

Summary of Ply Compressive Properties for XP-250 Glass-Epoxy from Tests of [0°] Coupons

Properties / Test No.	Young's Modulus E_{11}^{c} (psi)	Poisson's Ratio ν_{12}^{c}	Ultimate Stress X_{1}^{c} (ksi)
16	4.94×10^{6}	0.403	---[1]
17 (Channels 1, 2)	6.39×10^{6}	0.294	122
17 (Channels 3, 4)	5.73×10^{6}	0.309	
18 (Channels 1, 2)	5.35×10^{6}	0.277	---[1]
18 (Channels 3, 4)	5.88×10^{6}	0.325	
19 (Channels 1, 2)	5.97×10^{6}	0.330	121
19 (Channels 3, 4)	5.97×10^{6}	0.287	
20	5.19×10^{6}	0.324	99.8
21	6.38×10^{6}	0.305	105
Mean Values	5.87×10^{6}	0.317	112

[1]No ultimate load due to grip slippage.

Table 5

Summary of Ply Compressive Properties for XP-250 Glass-Epoxy from Tests of $[90°]_s$ Coupons

Properties / Test No.	Young's Modulus E_{22}^c (psi)	Ultimate Stress X_2^c (ksi)	Ultimate Strain e_2^c (μ strain)	Poisson's Ratio (Test Value) ν_{21}^c	Poisson's Ratio (Calculated Value)[1] ν_{21}^c
22	2.42×10^6	25.6	14,000	0.123	0.131
24	2.05×10^6	23.7	15,300	0.142	0.111
26	1.76×10^6	25.6	29,800	0.076	0.095
27	2.27×10^6	25.1	15,400	0.147	0.123
28 (Channels 1, 2)	2.71×10^6	24.8	13,100	0.121	0.146
28 (Channels 3, 4)	1.44×10^6	24.8	30,900	0.053	0.078
Mean Values[2]	2.12×10^6	25.0	18,600	0.122	0.115

[1]Calculated value of Poisson's ratio $\nu_{21}^c = \nu_{12}^c \times E_{22}^c/E_{11}^c$ where $E_{11}^c = 5.87 \times 10^6$ psi and $\nu_{12}^c = 0.317$.

[2]Test no. 28 excluded from mean values due to bending.

Table 6

Central Deflection of Simply Supported Square Plate. After Reference [29].

THICKNESS RATIO H/a	$\beta = W_{max}EH^3/qa^4$ UNIFORM LOAD, q		
	Present Finite Element	Reissner's Theory	Classical Theory
0.01	0.04481	0.04439	0.04437
0.05	0.04524	0.04486	0.04437
0.10	0.04686	0.04632	0.04437
0.20	0.05243	0.05217	0.04437
0.25	0.05698	0.05656	0.04437

Figure 1. Test Set-Up

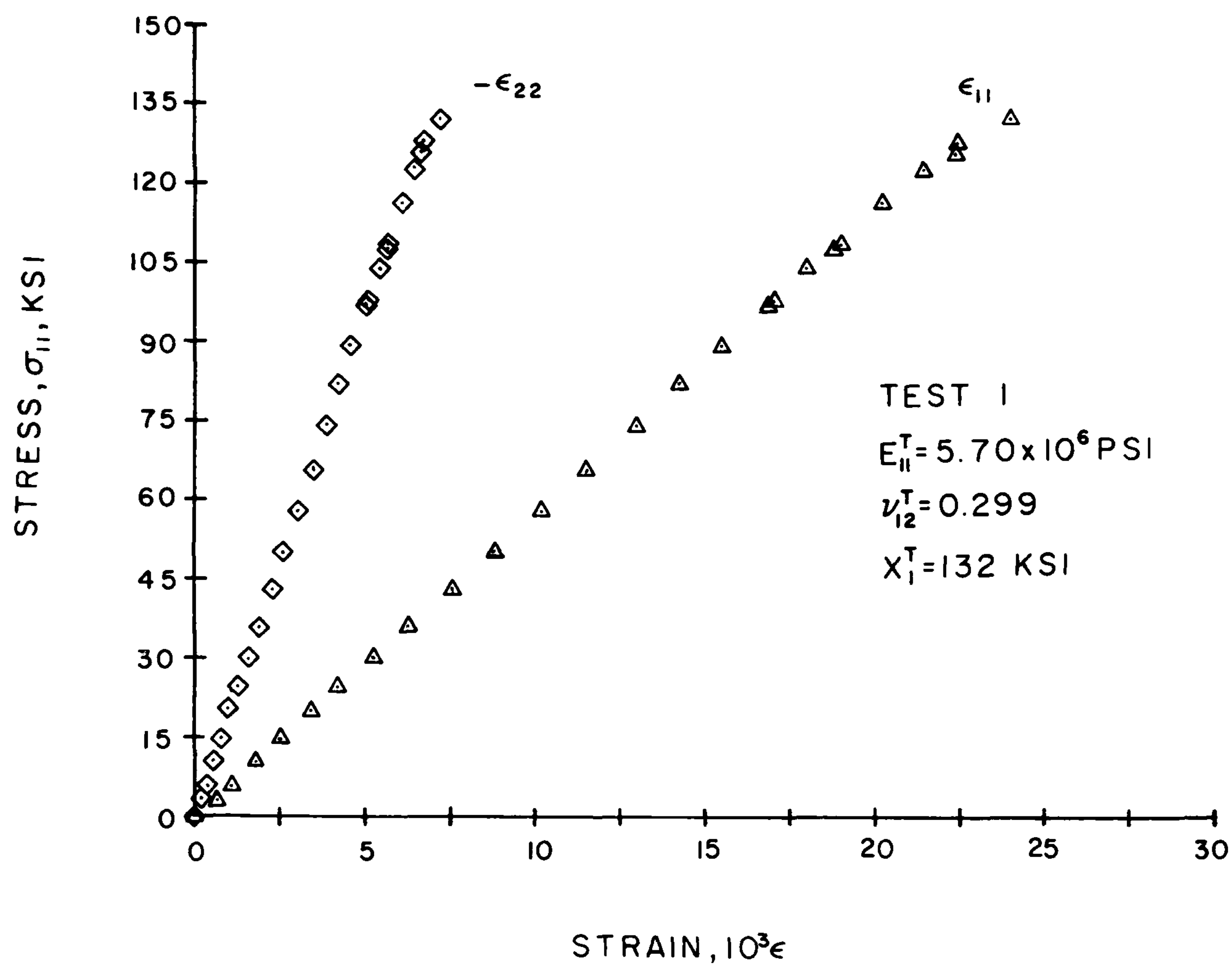

Figure 2. Typical Stress-Strain Response for $[0]_S$ Tensile Specimen

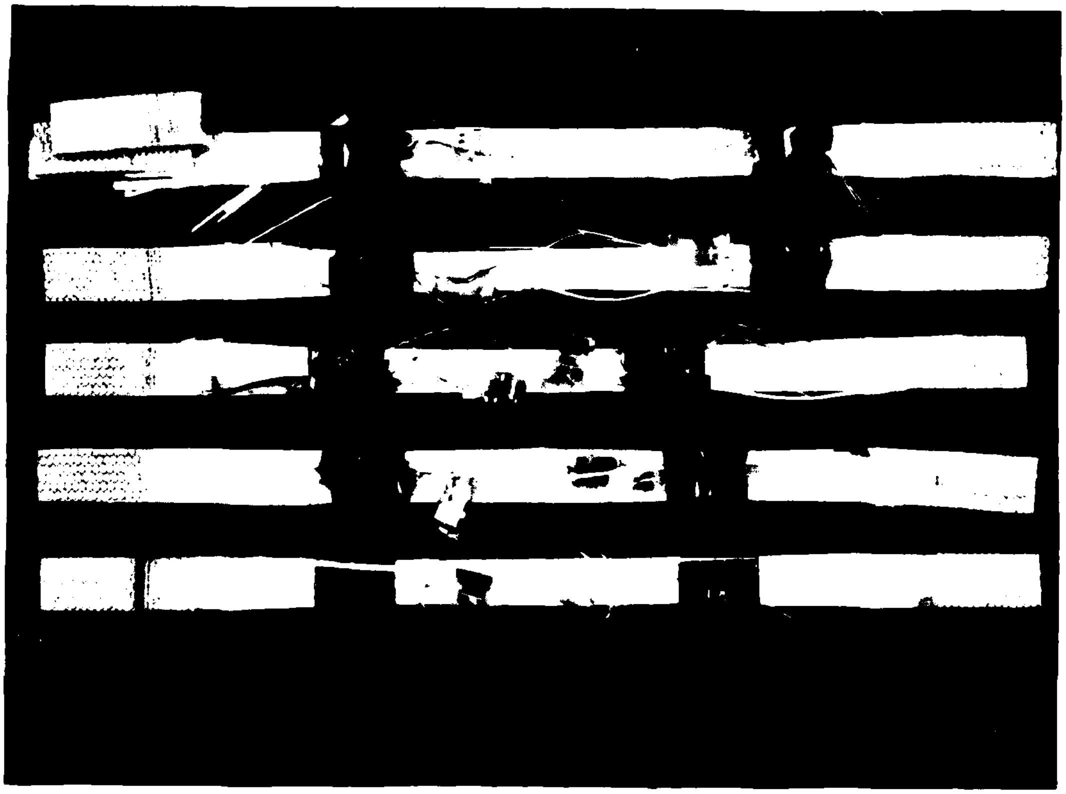

Figure 3. The Failed $[0]_s$ Tensile Specimens

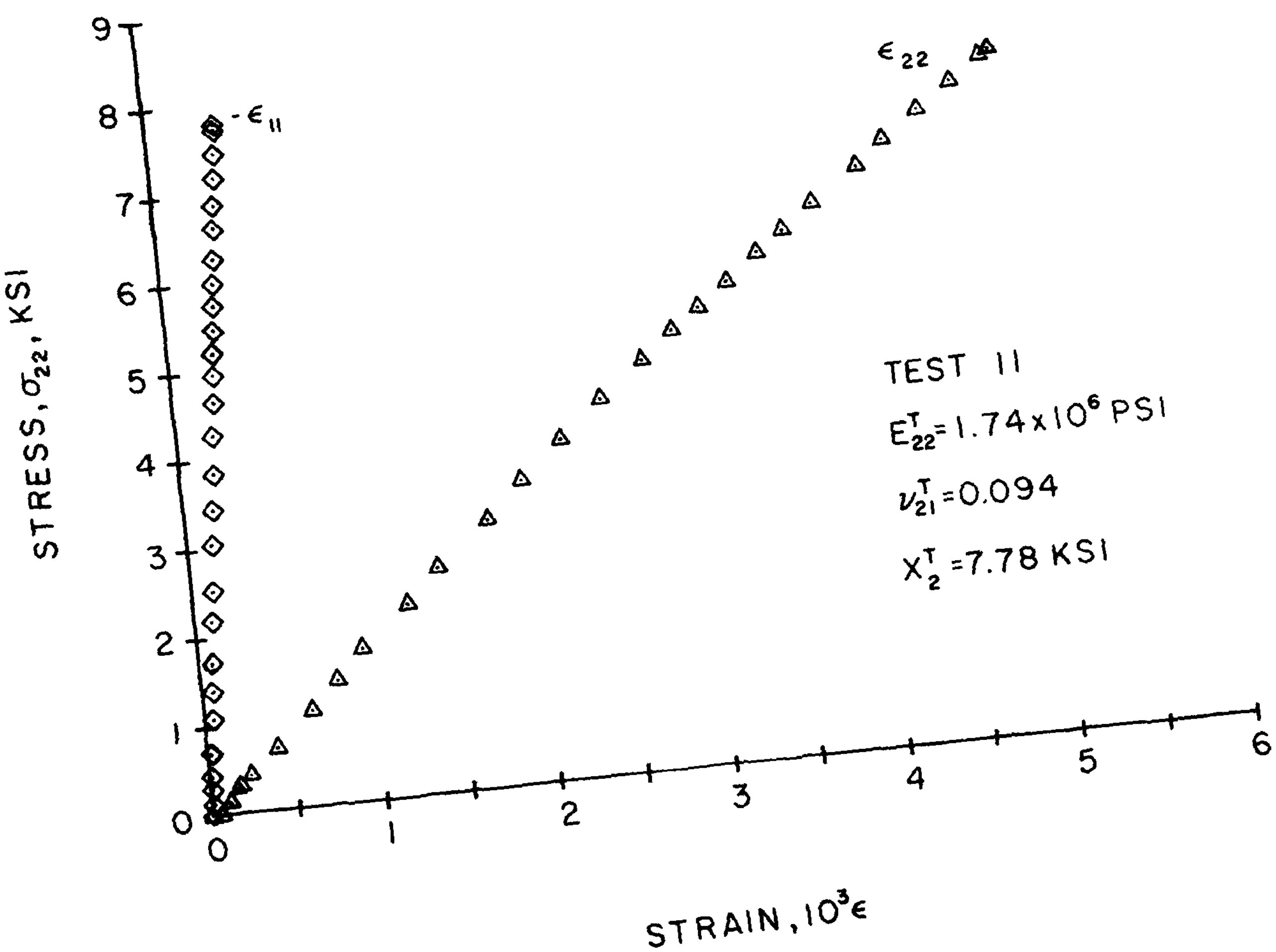

Figure 4. Typical Stress-Strain Response for $[90]_s$ Tensile Specimen

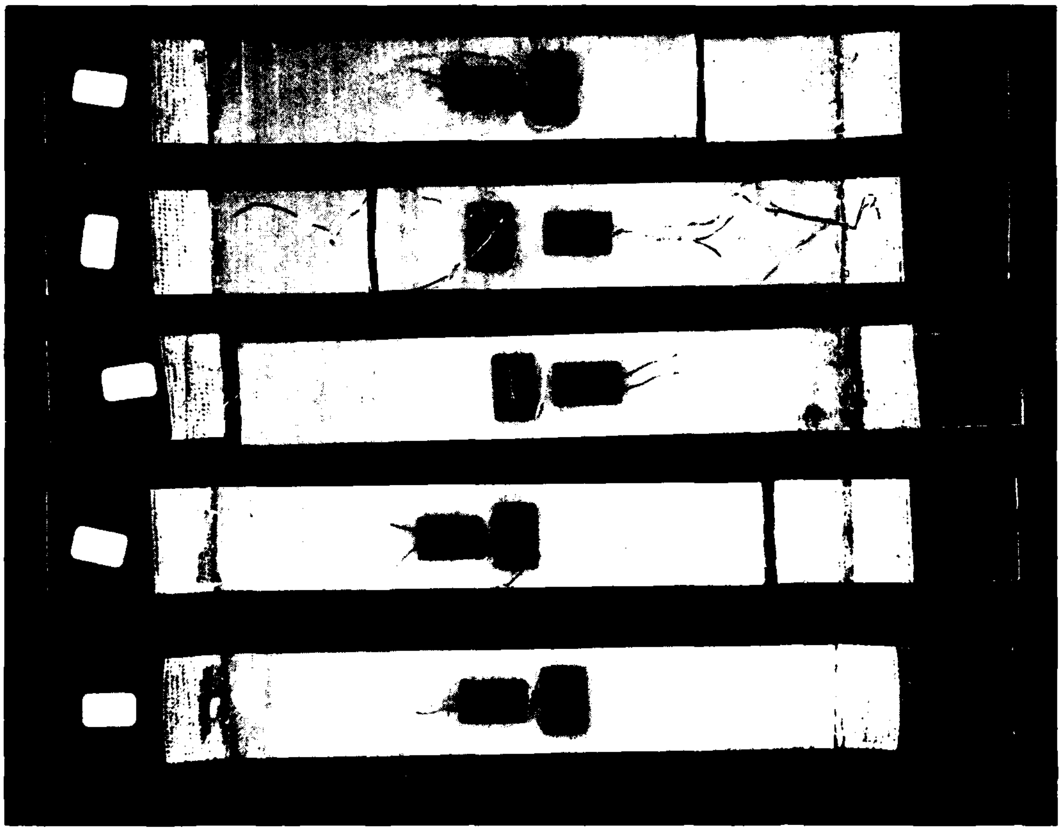

Figure 5. The Failed $[90]_s$ Specimens

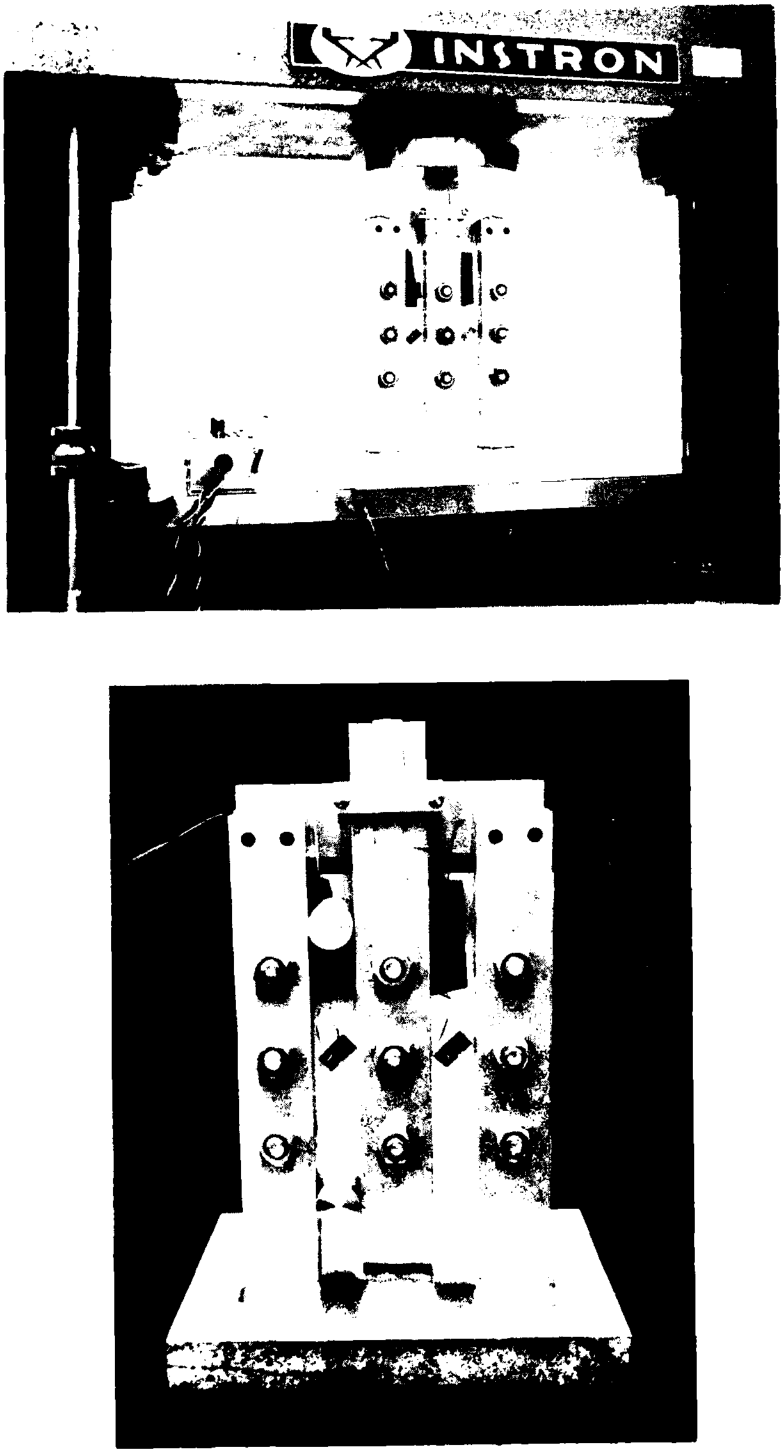

Figure 6. Two Views of the Three-Rail Shear Fixture

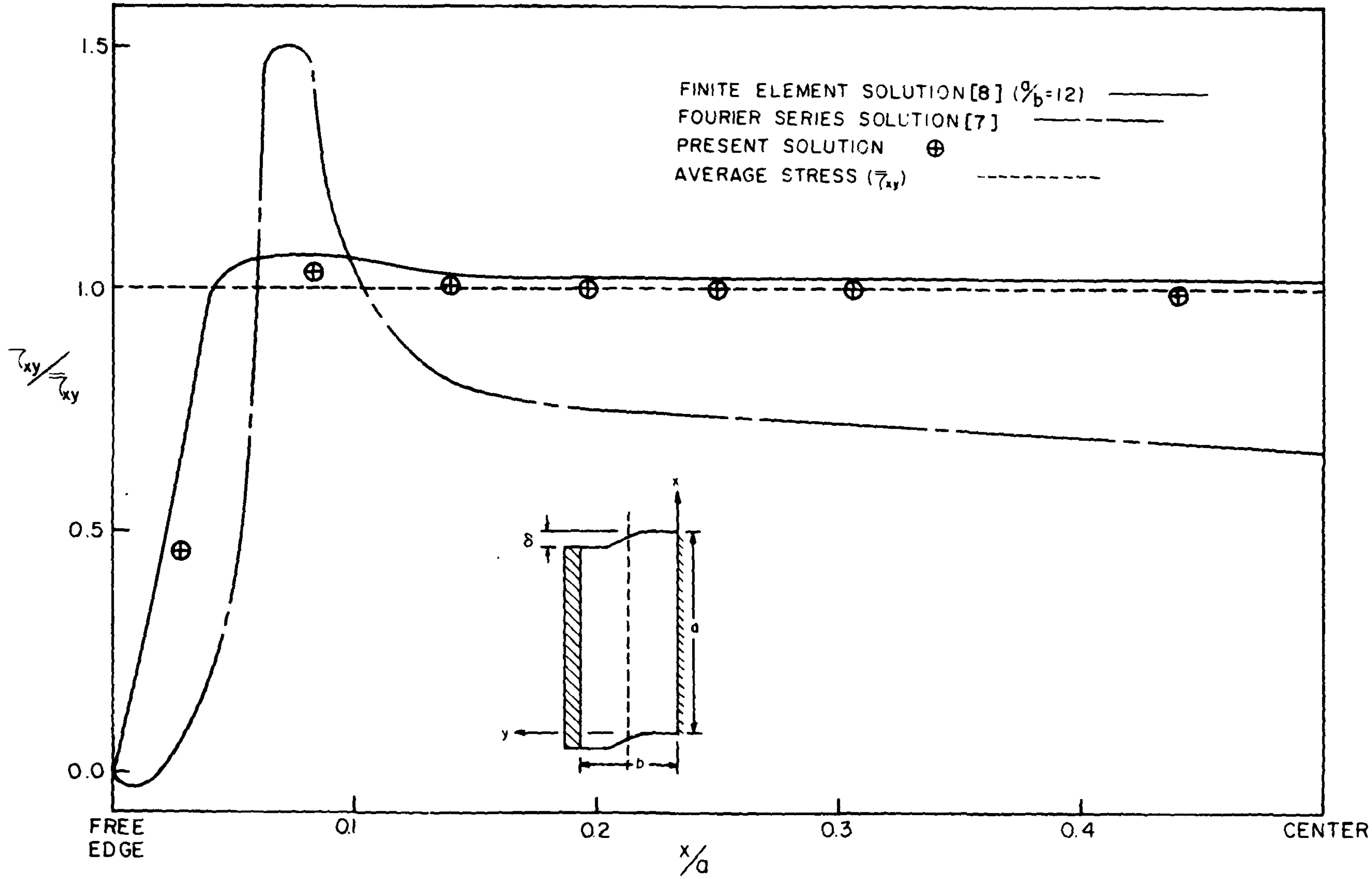

Figure 7. The Shear Stress Distribution Across the Length of the Three-Rail Specimen for a $[\pm 45]_s$ Graphite-Epoxy Laminate

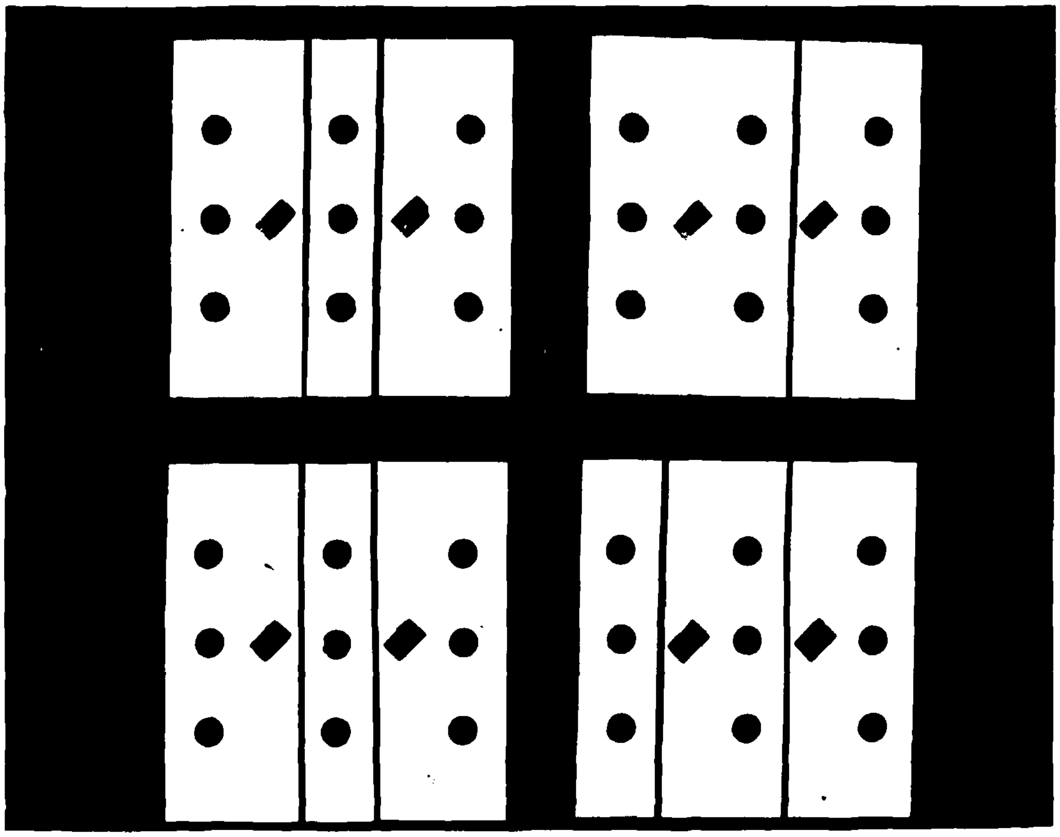

Figure 8. The Failed $[0]_s$, Three-Rail Shear Specimens

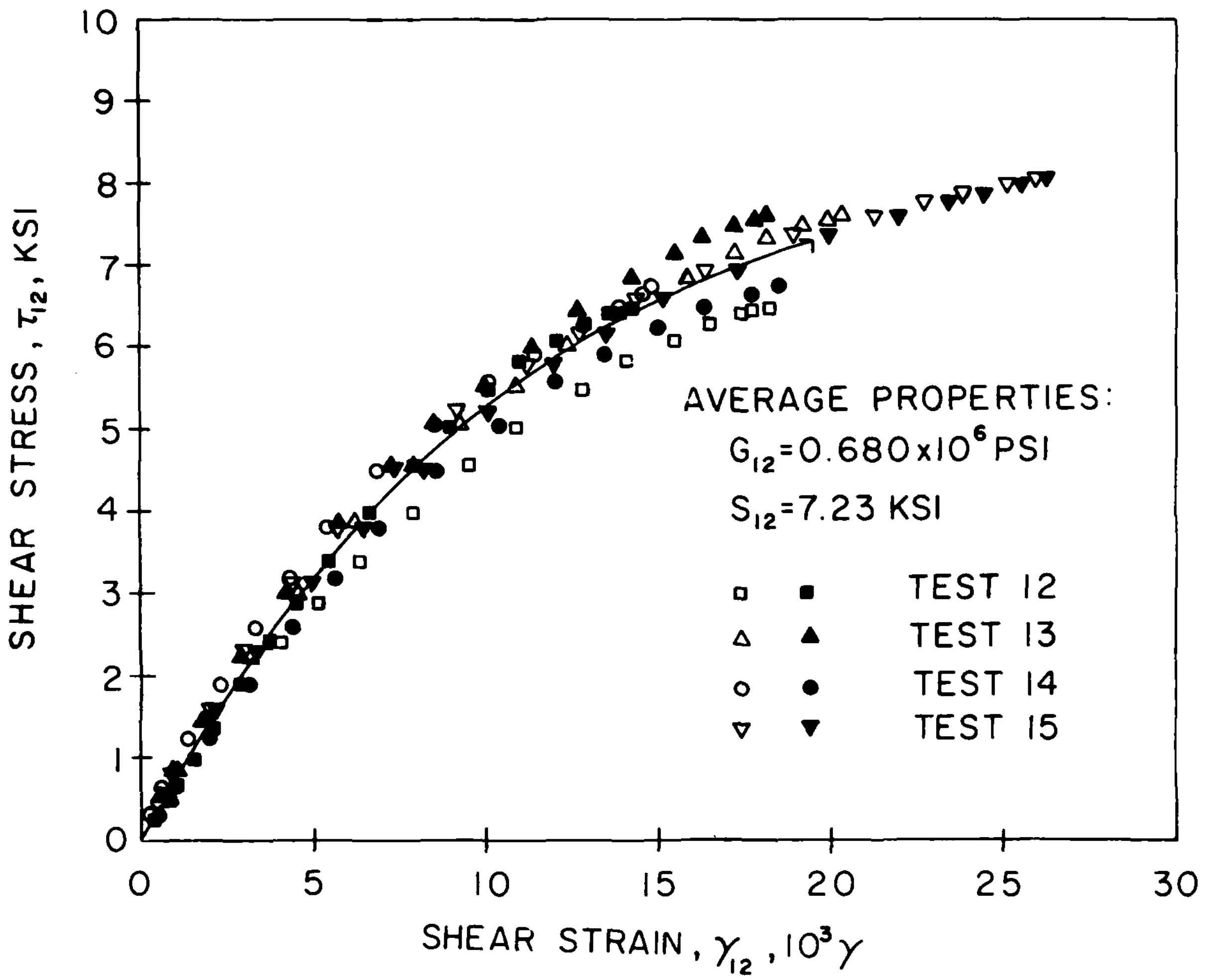

Figure 9. The Shear Stress-Strain Response for the Unidirectional $[0]_s$ Laminate

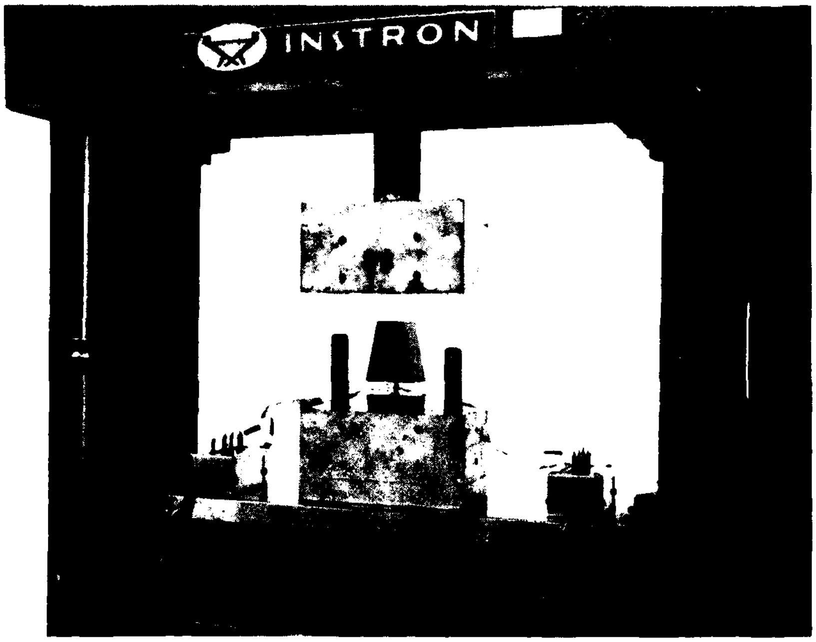

Figure 10. Two Views of the Compression Fixture

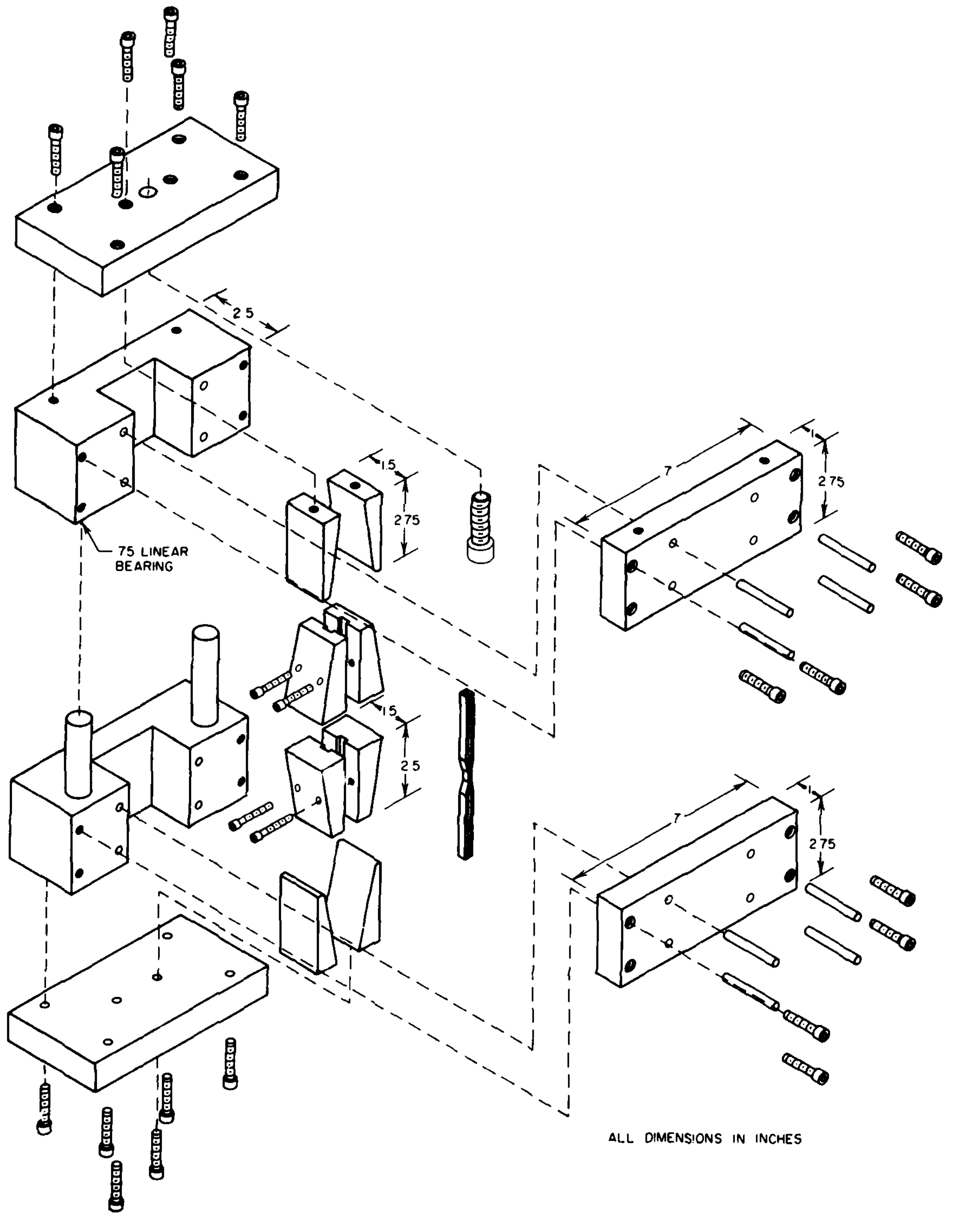

Figure 11. An Exploded View Drawing of the Compression Fixture

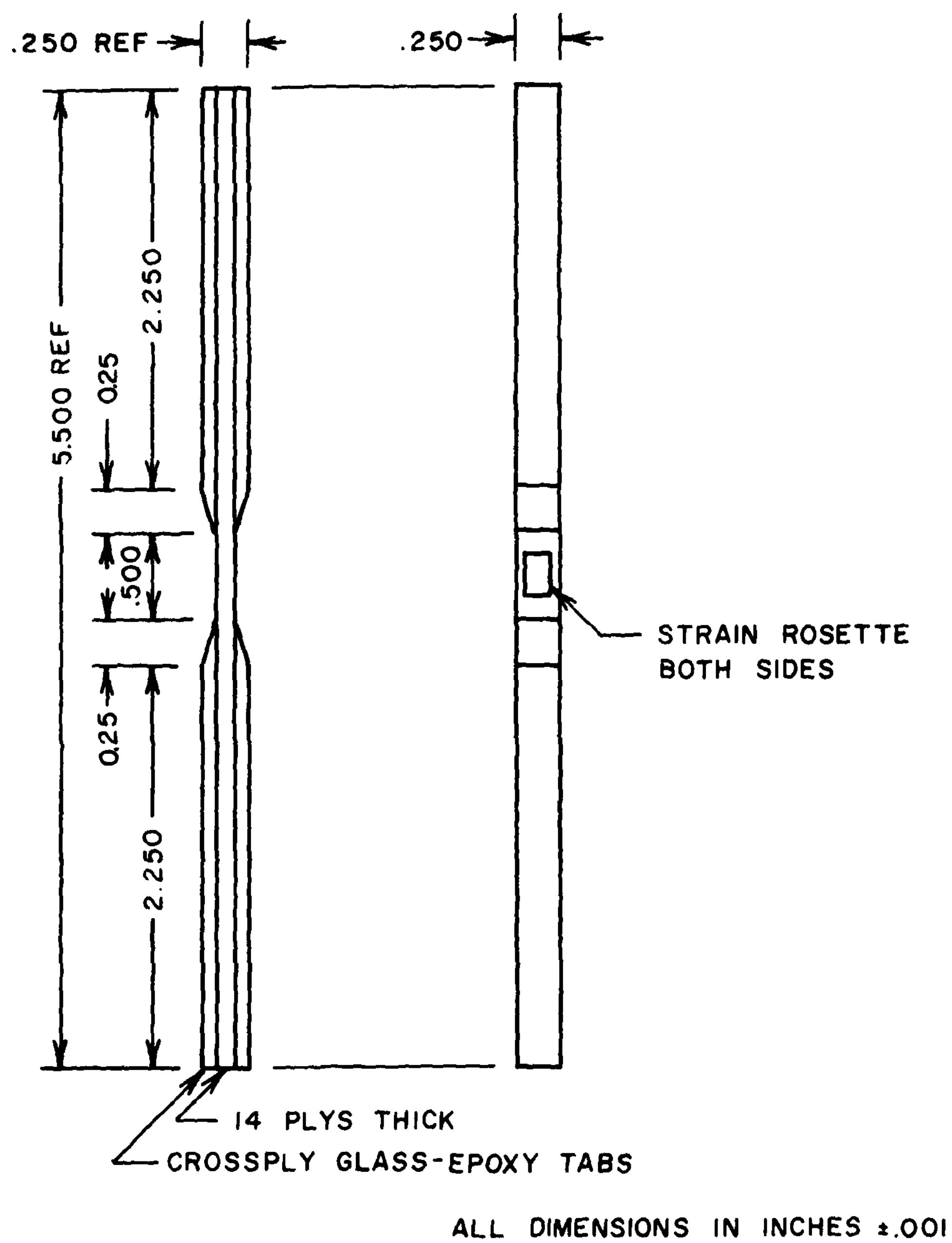

Figure 12. Dimensions of Compression Specimen

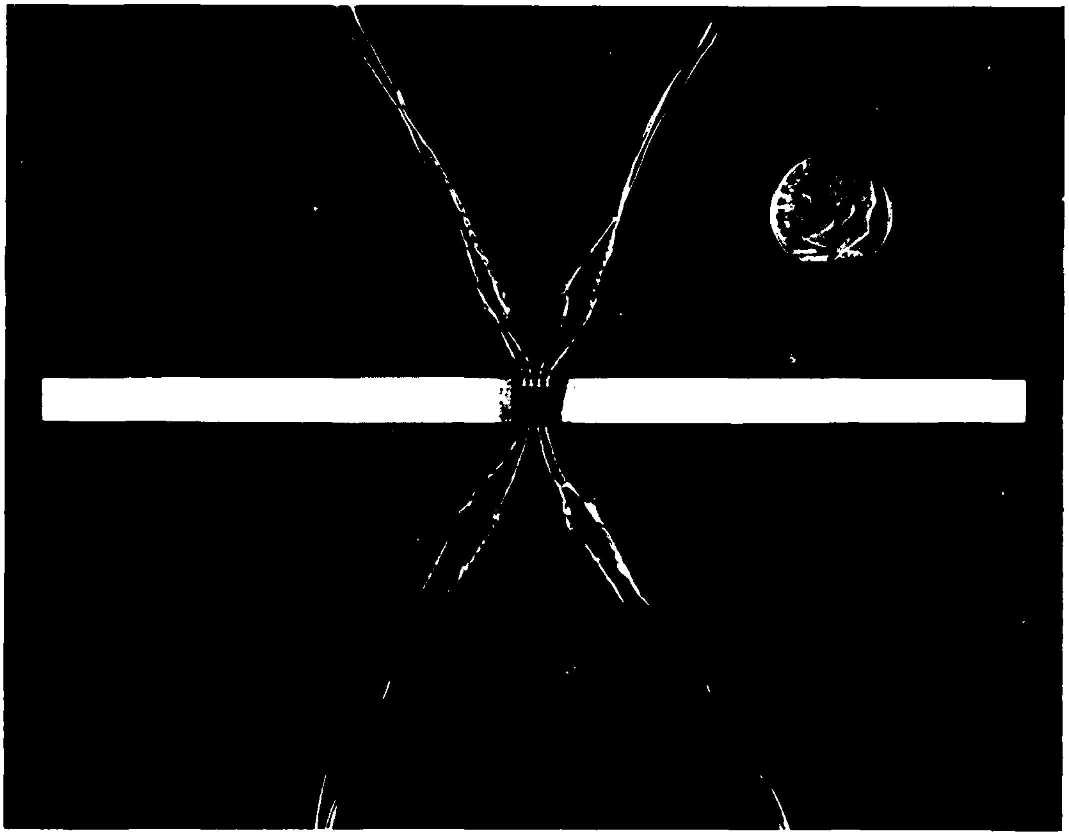

Figure 13. Compression Specimen Instrumented with Strain Rosettes

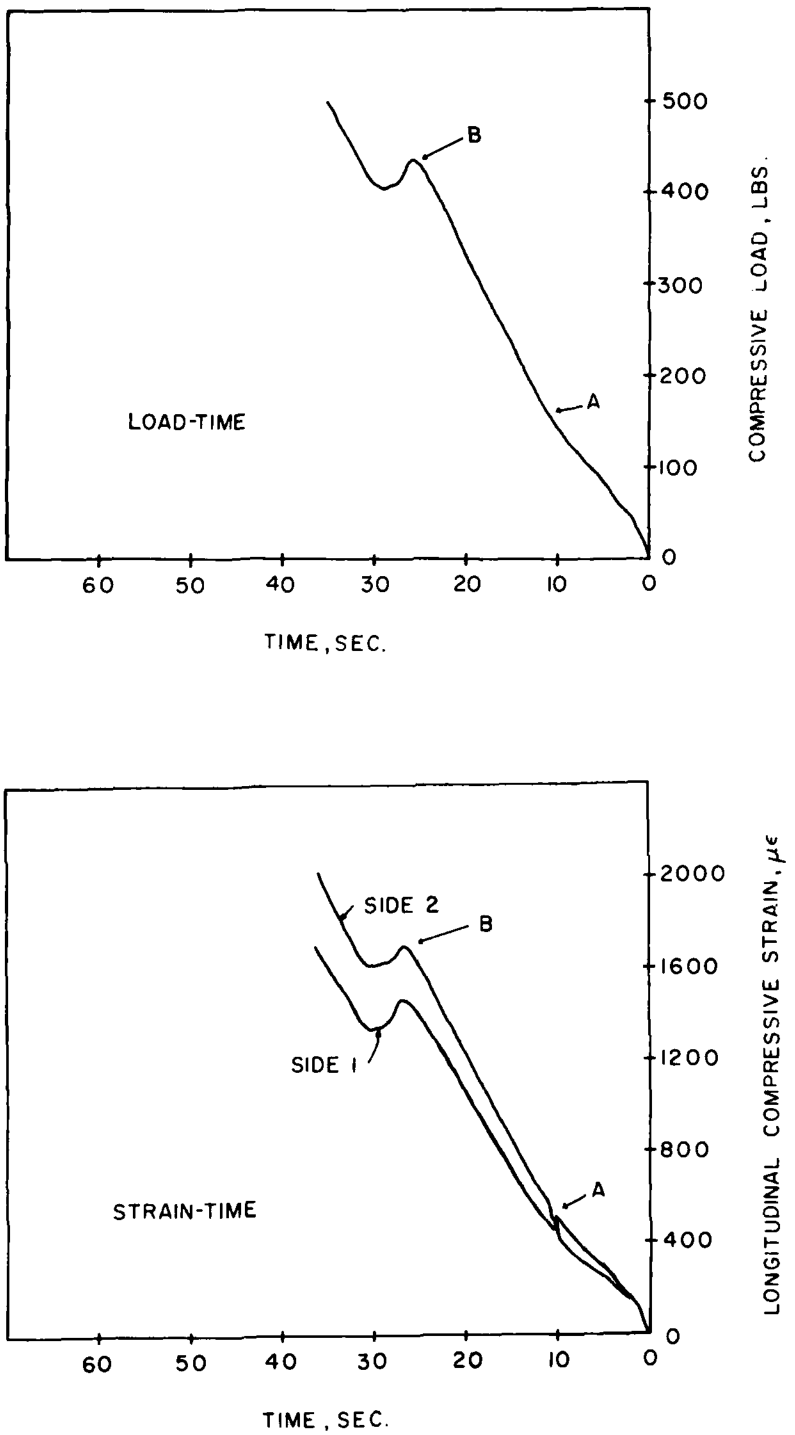

Figure 14. The Load-Time and Longitudinal Strain-Time Response for 2024-T4 Aluminum Obtained with the Compression Fixture

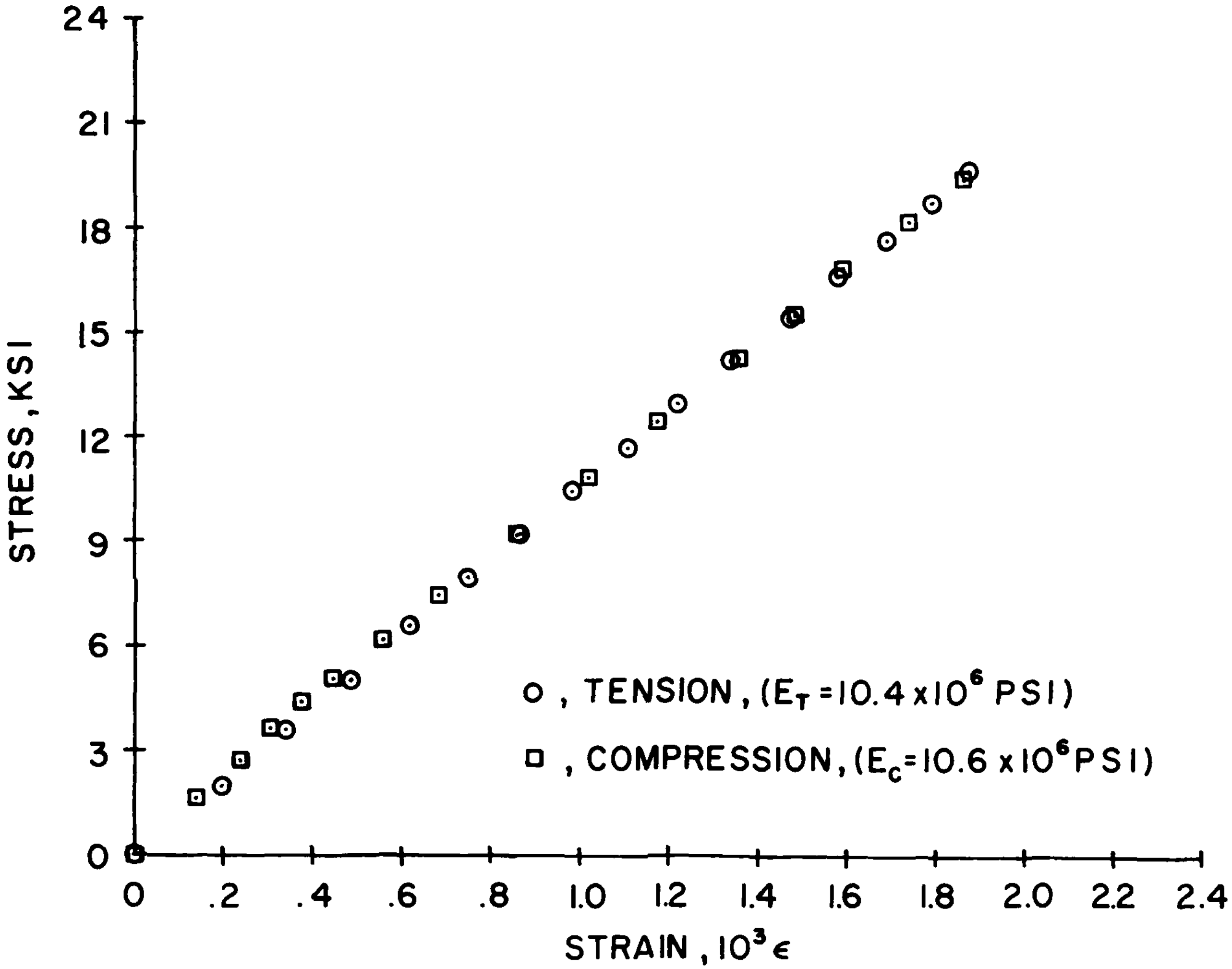

Figure 15. The Measured Compressive Strain Response Compared with the Tensile Strain Response for Aluminum 2024-T4

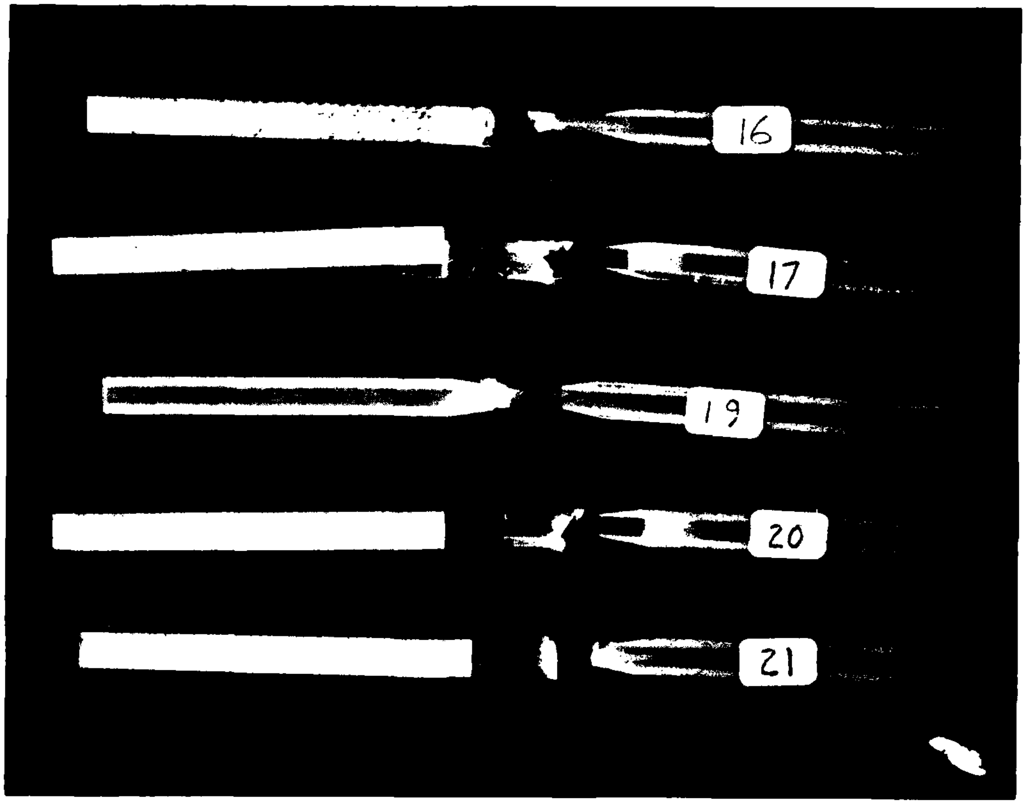

Figure 16. The Failed $[0]_s$ Compressive Specimens

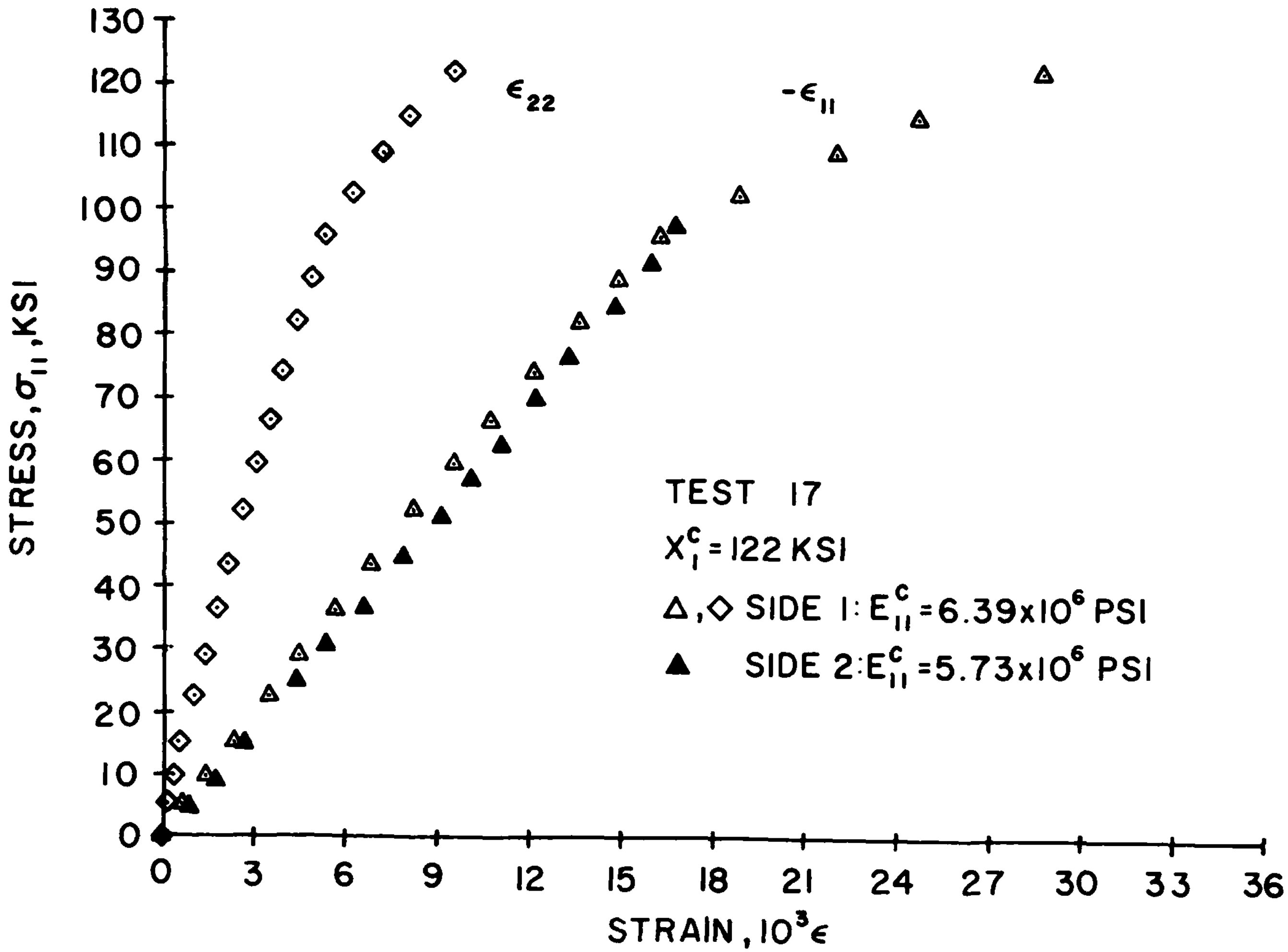

Figure 17. A Sample Stress-Strain Curve for a $[0]_s$ Specimen Under Compressive Loading

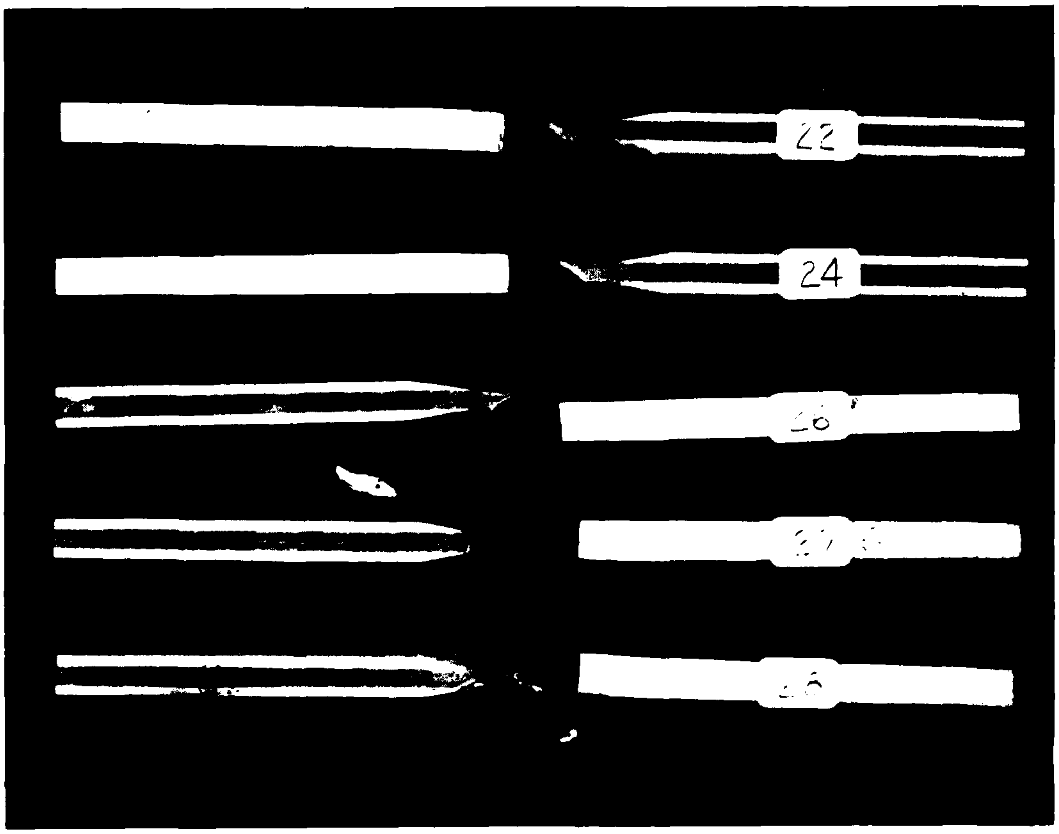

Figure 18. The Failed $[90]_s$ Compressive Specimens

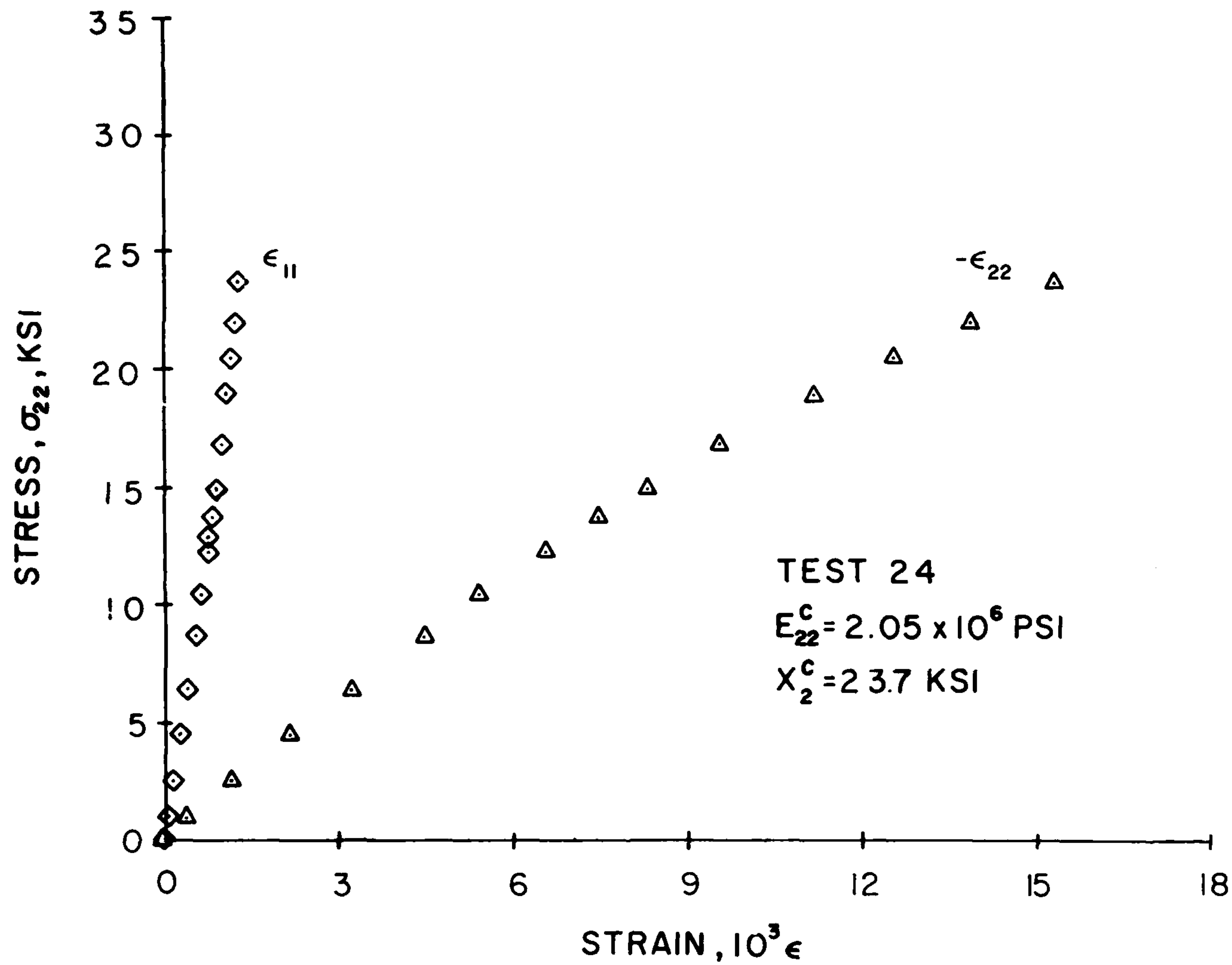

Figure 19. A Sample Stress-Strain Curve for a $[90]_s$ Specimen Under Compressive Loading

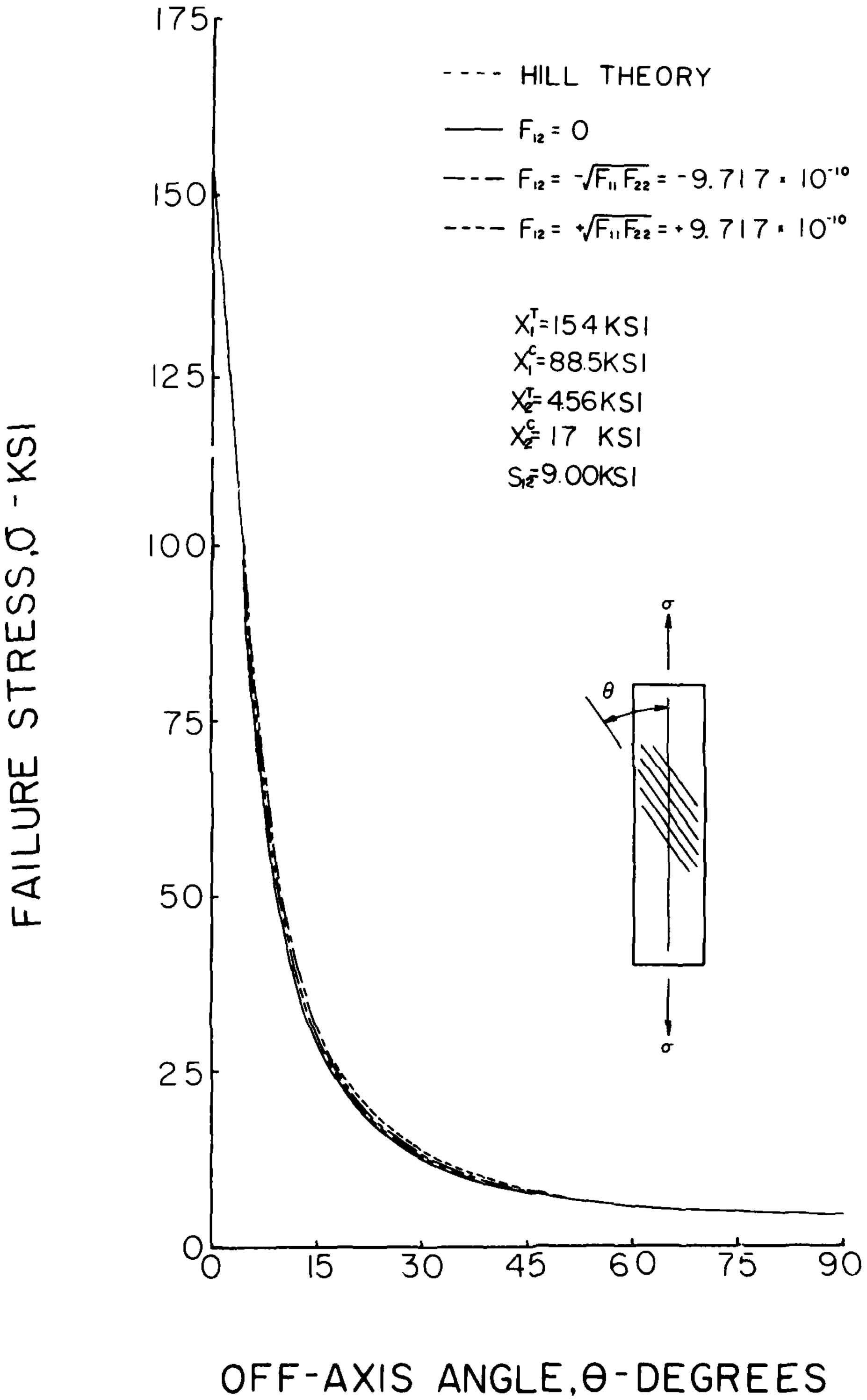

Figure 20. Predicted Strength of Glass-Epoxy Off-Axis Unidirectional Tension Coupon by the Tsai-Wu and Hill Failure Theories

AD-A122 744 POST-CRAZING STRESS ANALYSIS OF GLASS-EPOXY LAMINATES (U) TENNESSEE TECHNOLOGICAL UNIV COOKEVILLE DEPT OF ENGINEERING S.. D G SMITH ET AL. MAY 79 TTU-ESM-79-1 2/2

UNCLASSIFIED DAAK40-78-C-0165 F/G 11/9 NL

END

FILMED

DTIC

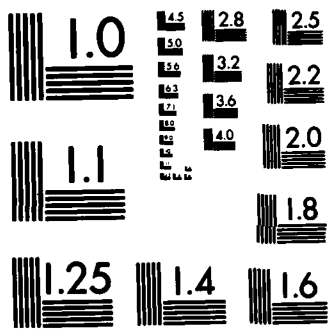

MICROCOPY RESOLUTION TEST CHART
NATIONAL BUREAU OF STANDARDS-1963-A

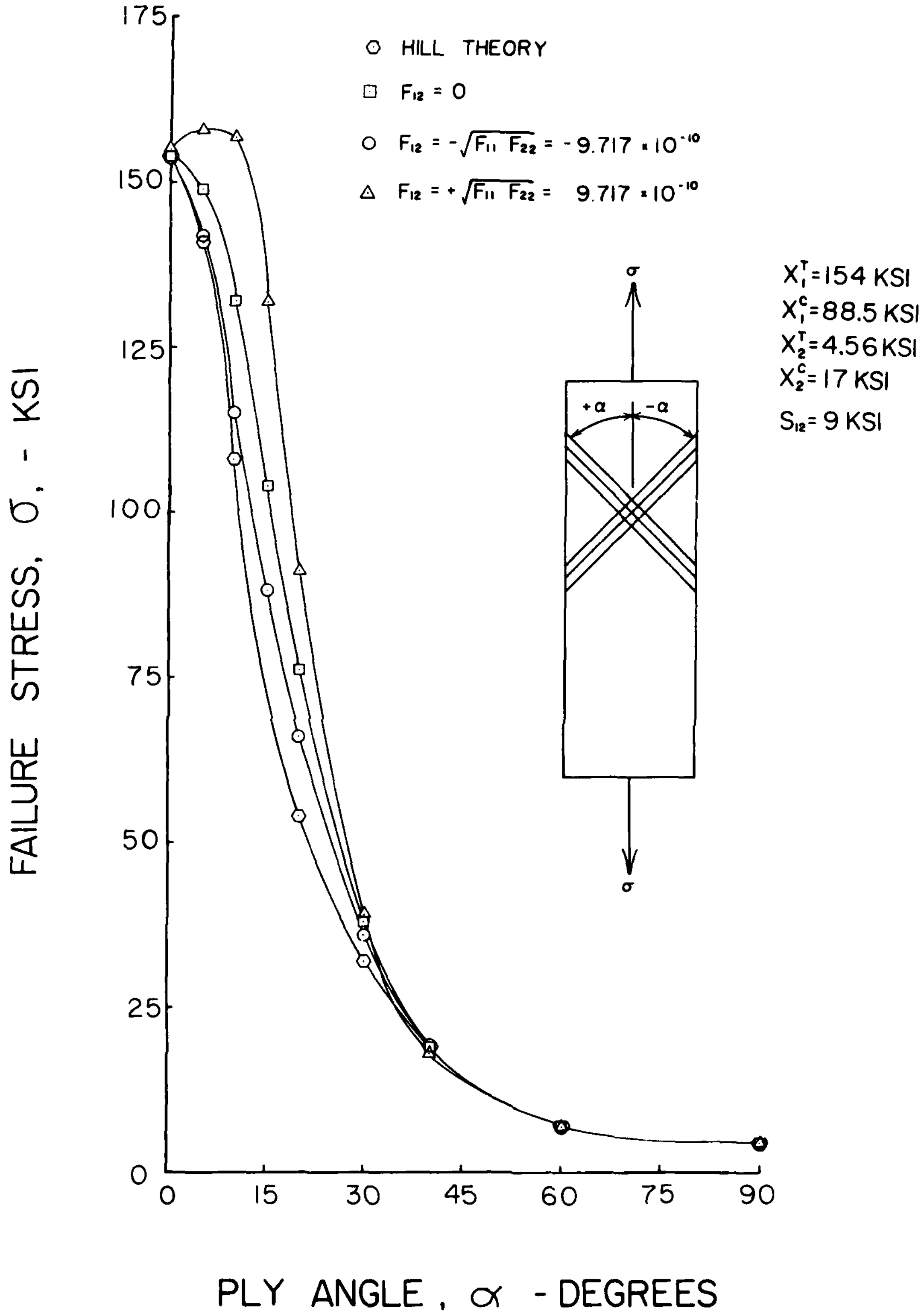

Figure 21. Predicted Strength of Glass-Epoxy Angle Ply Tension Coupon by Tsai-Wu and Hill Failure Theories

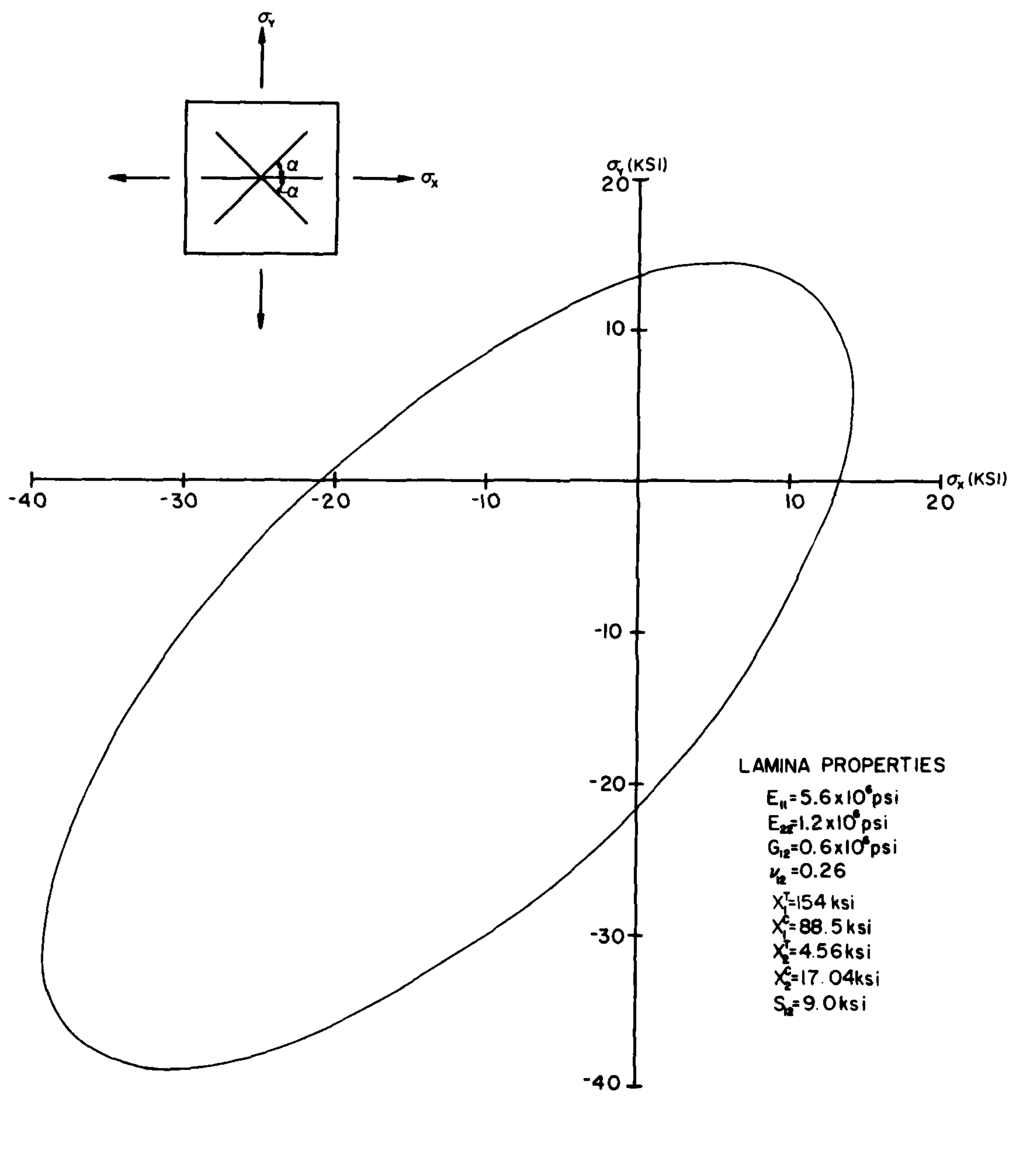

Figure 22. Failure Envelope for a $[\pm 45]_s$ Glass-Epoxy Laminate

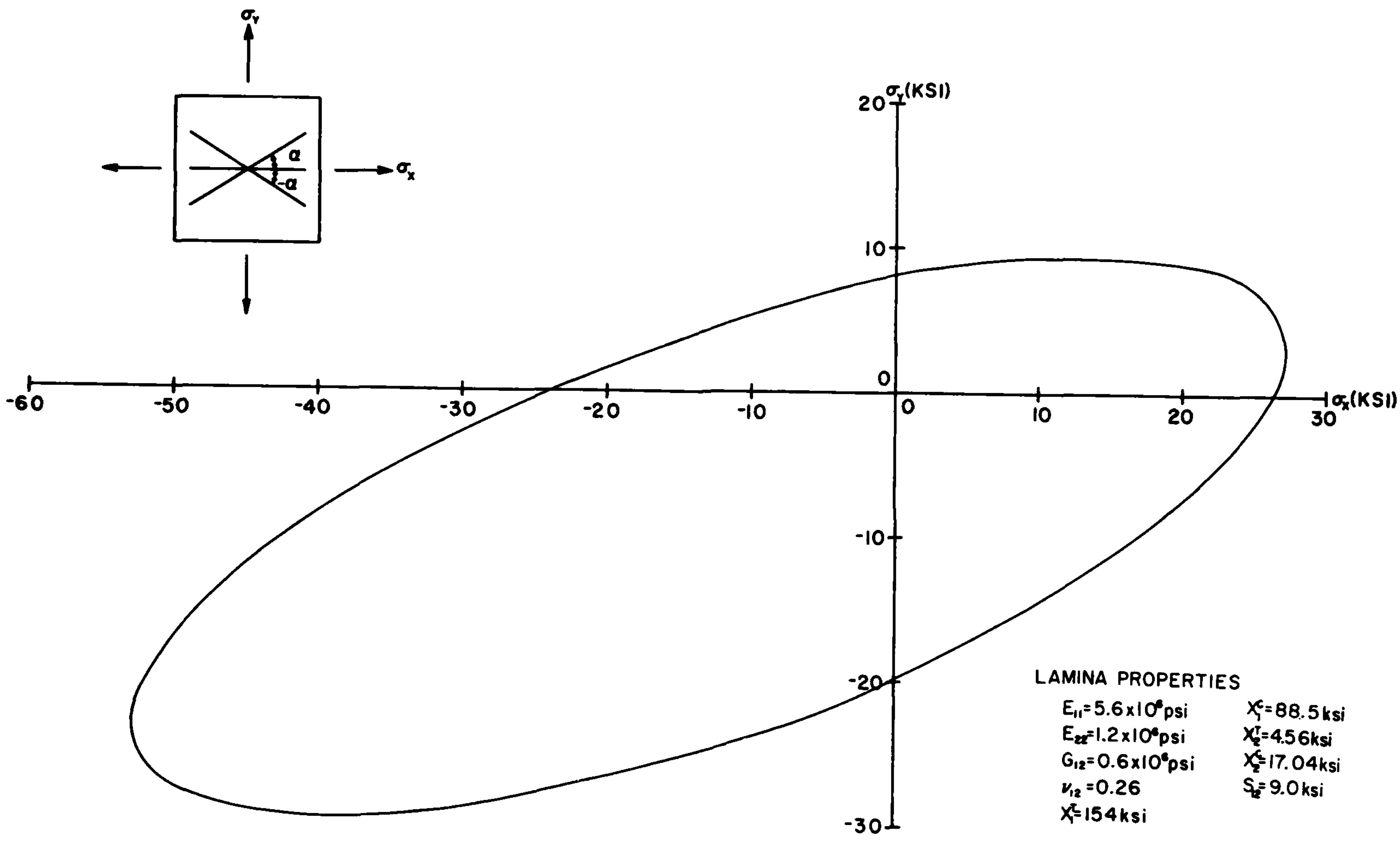

Figure 23. Failure Envelope for a $[\pm 35]_s$ Glass-Epoxy Laminate

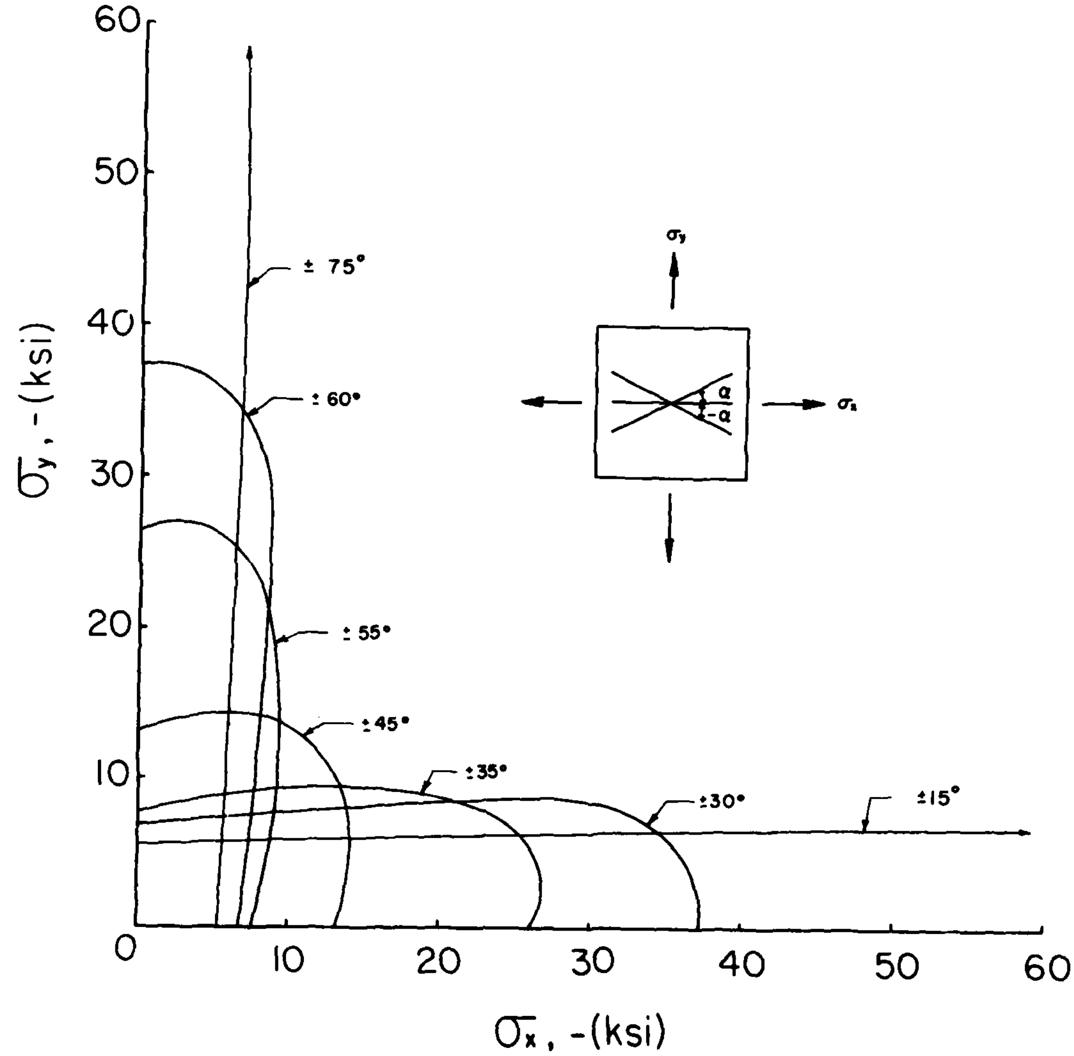

Figure 24. First Quadrant Failure Envelopes for Several Glass-Epoxy Angle Plys

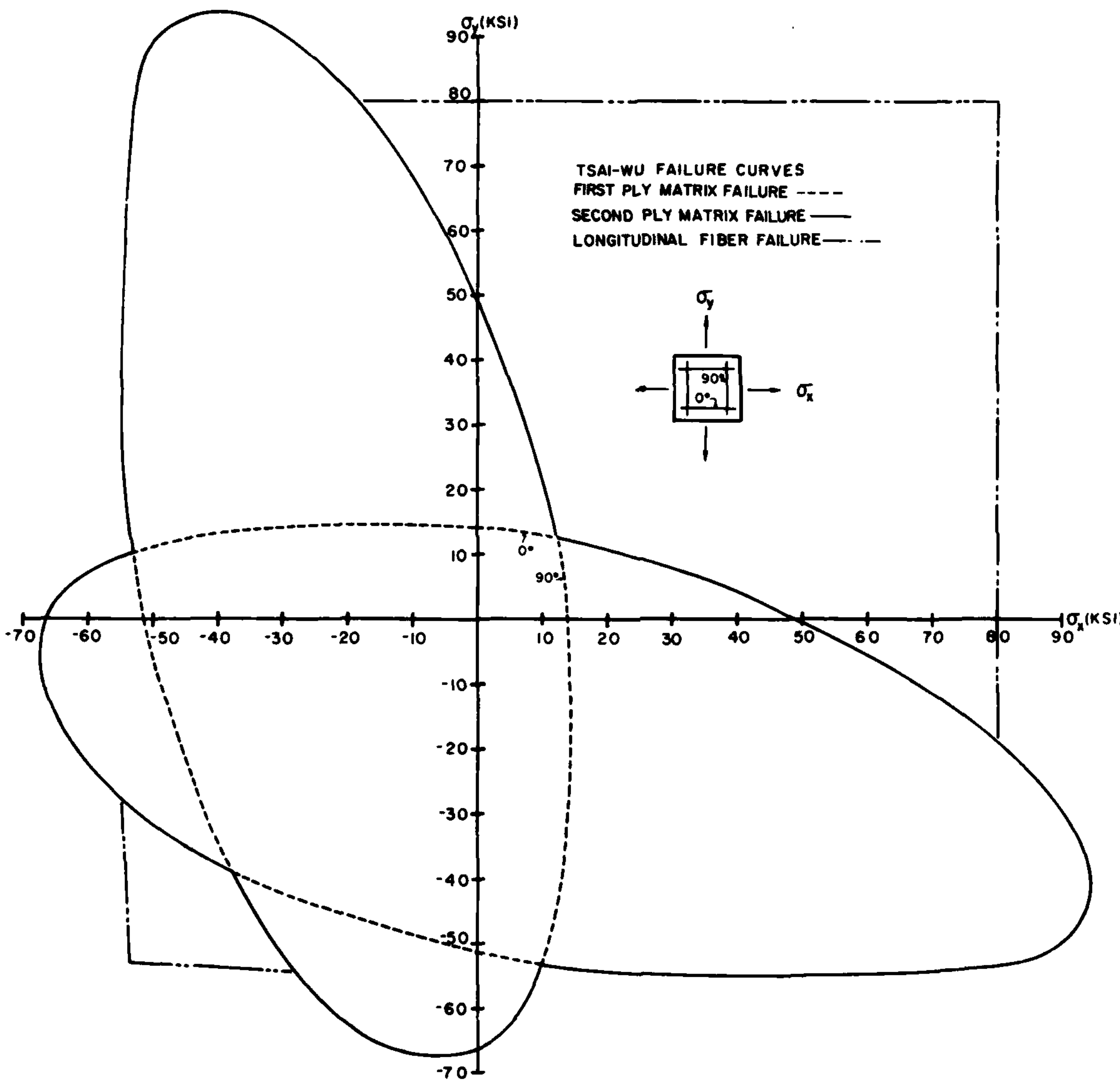

Figure 25. Failure Envelope for a $[0/90]_s$ Glass-Epoxy Laminate

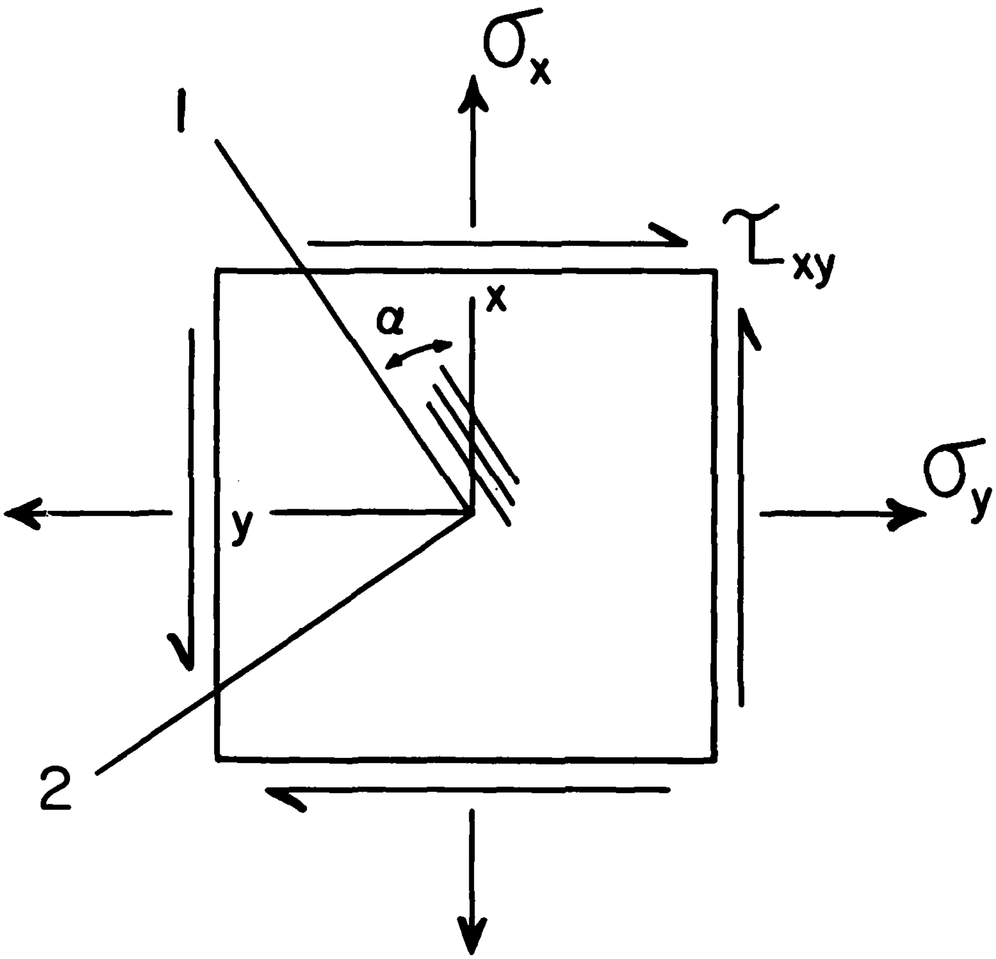

Figure 26. Notation for Symmetric Laminate Subjected to a Biaxial Test

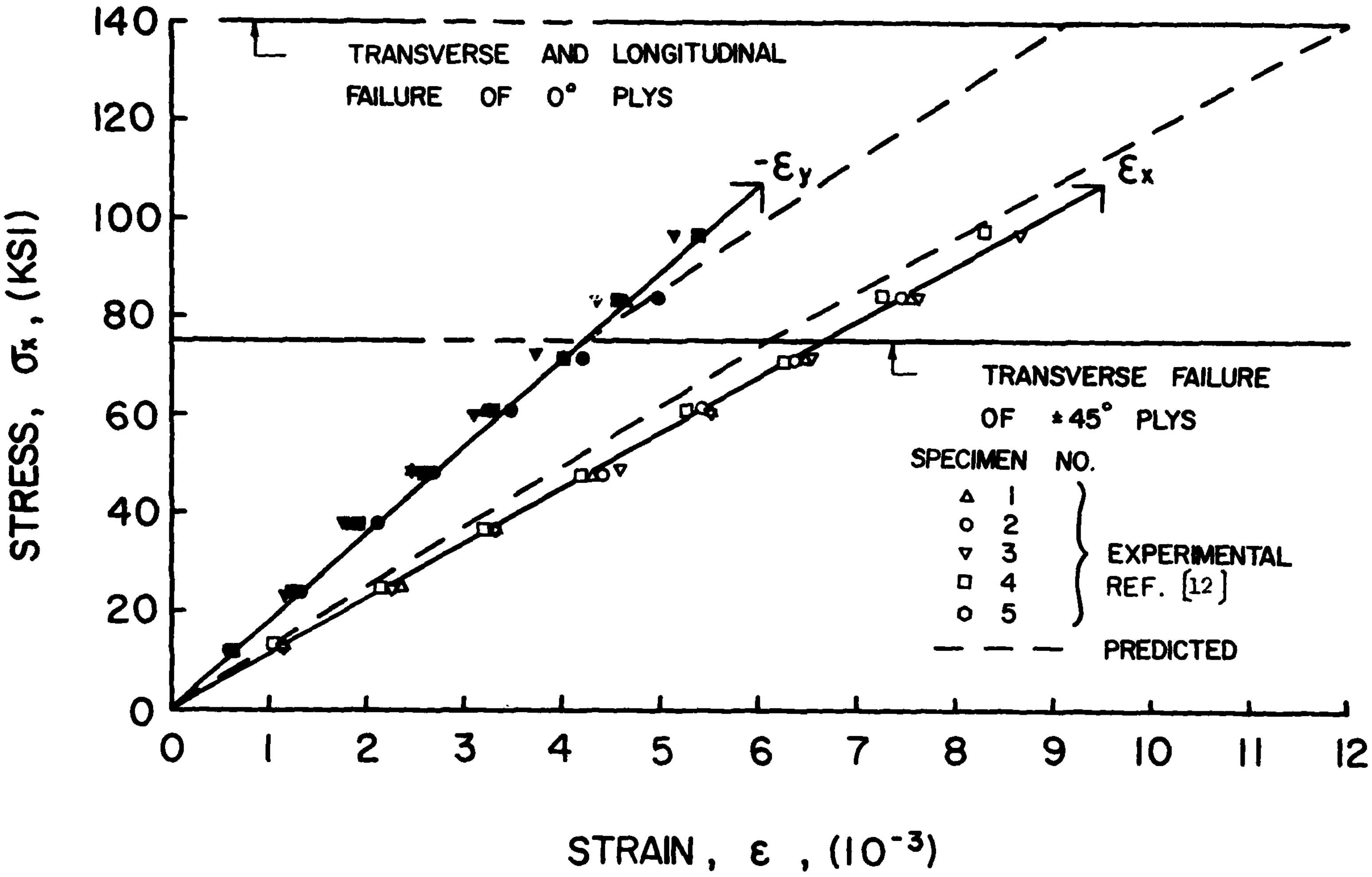

Figure 27. Strain Response for the 0-degree Loading of a $[0_2/\pm45]_s$ Graphite-Epoxy Laminate

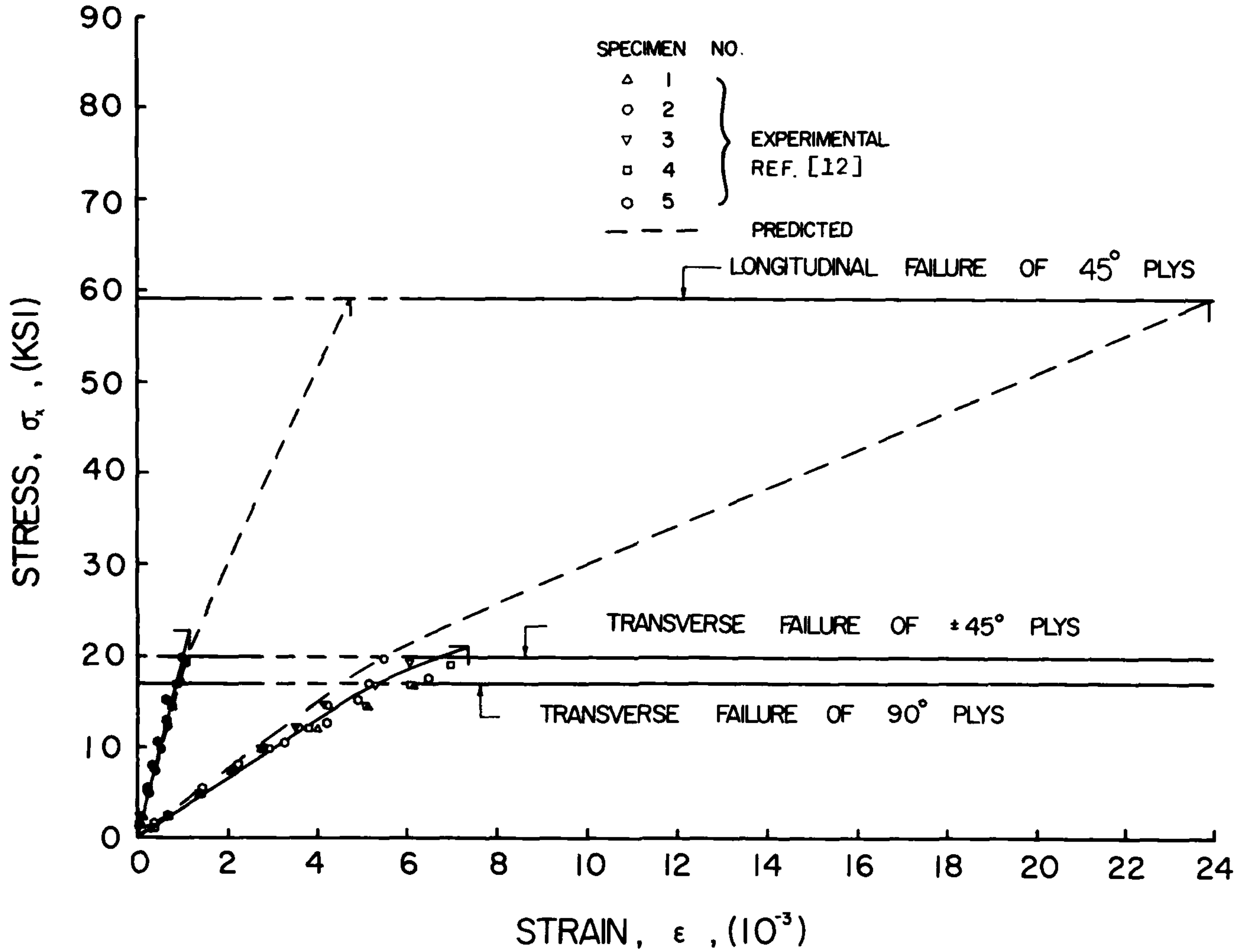

Figure 28. Strain Response for the 90-degree Loading of a $[0_2/\pm45]_s$ Graphite-Epoxy Laminate

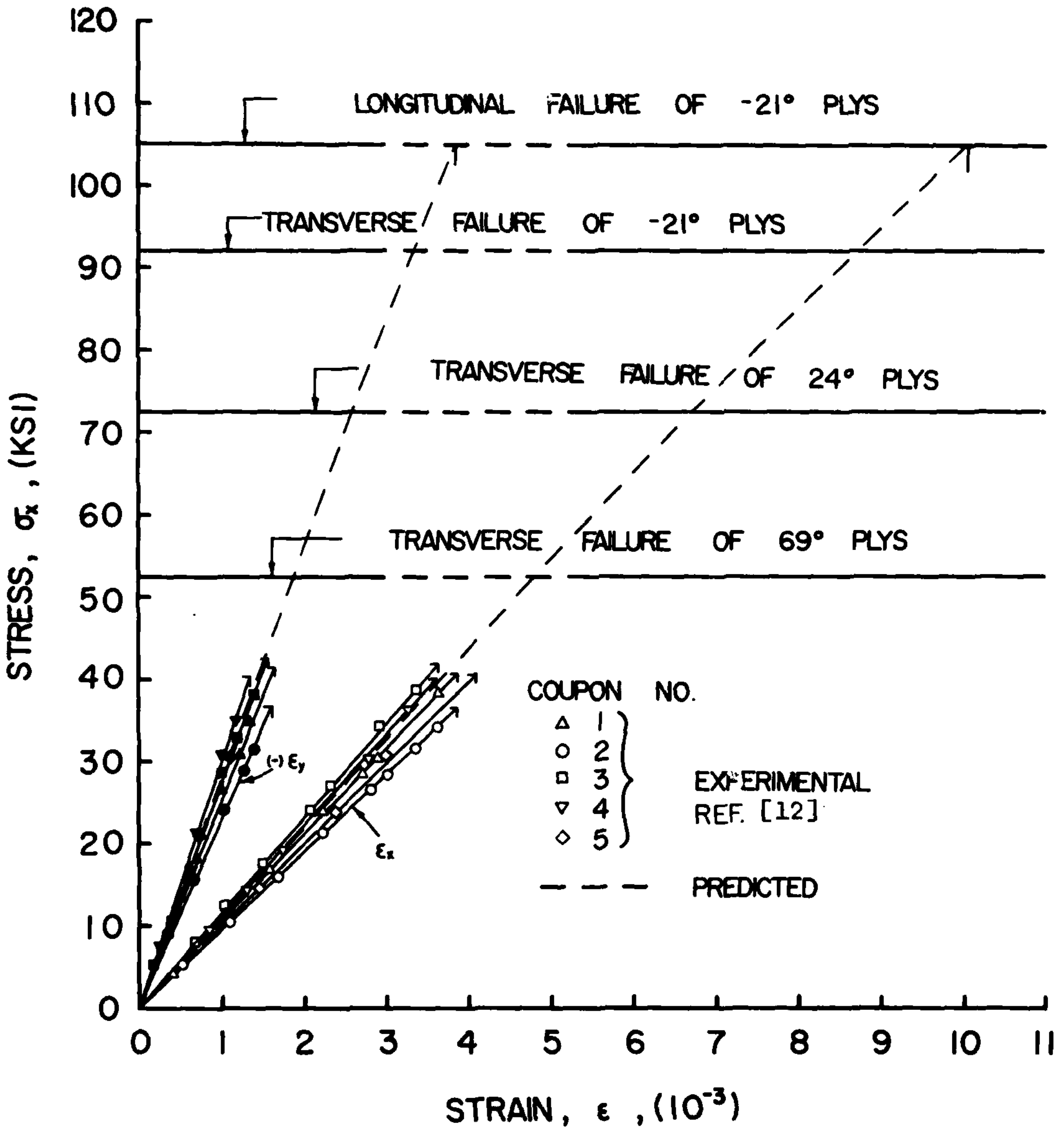

Figure 29. Strain Response for the 24-degree Loading of a $[0_2/\pm45]_s$ Graphite-Epoxy Laminate

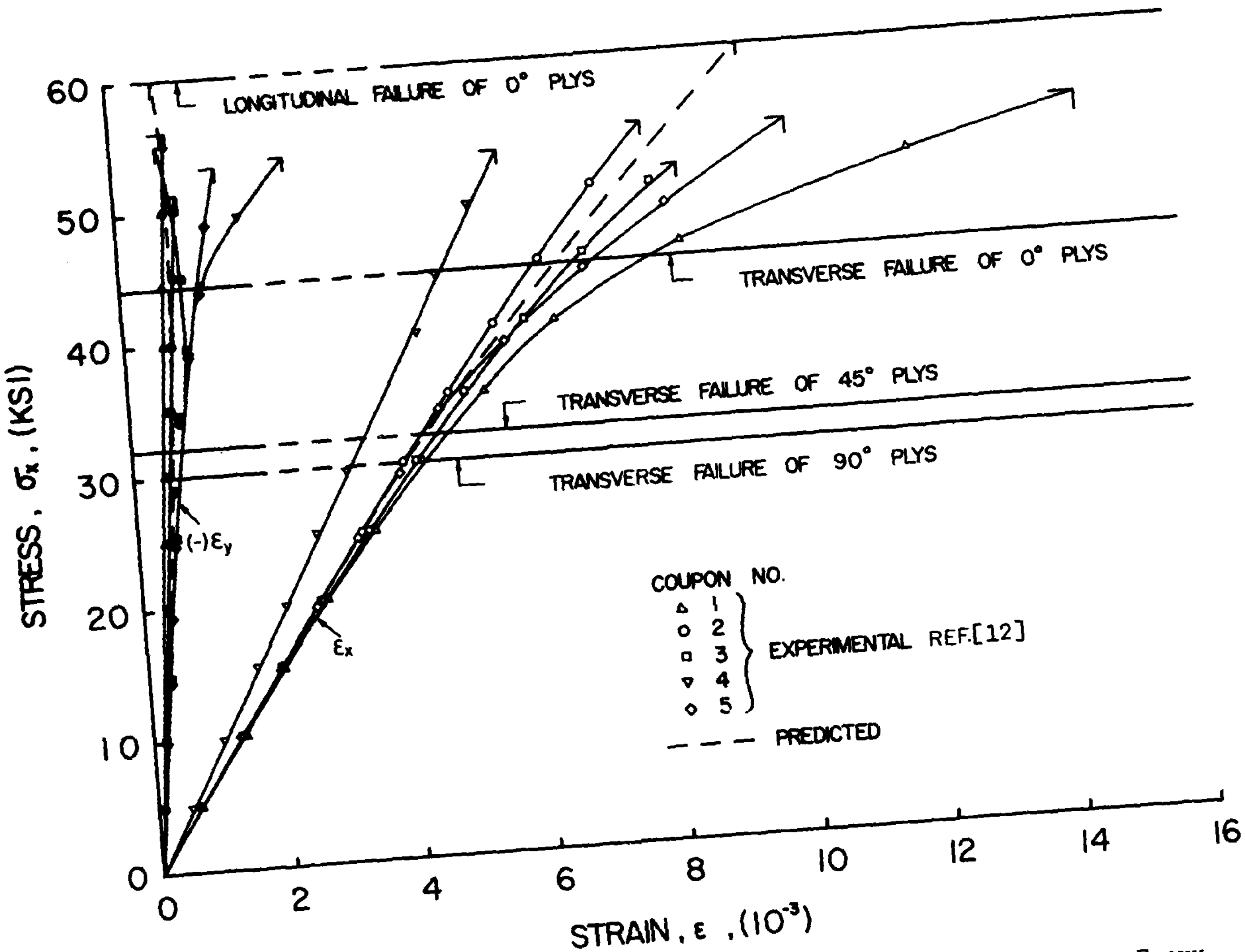

Figure 30. Strain Response for the 45-degree Loading of a $[0_2/\pm45]_s$ Graphite-Epoxy Laminate

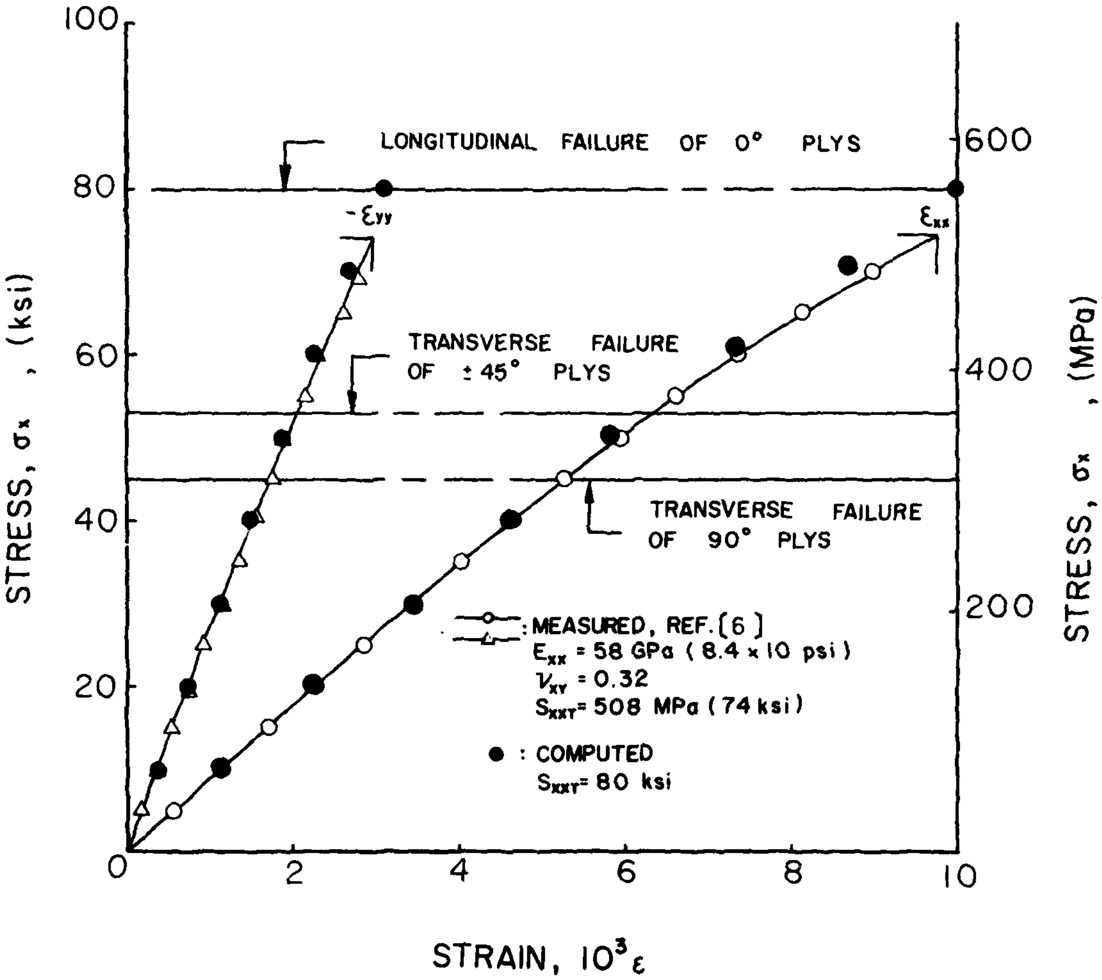

Figure 31. Strain Response for the 0-degree Loading of a $[0/\pm45/90]_s$ Graphite-Epoxy Laminate

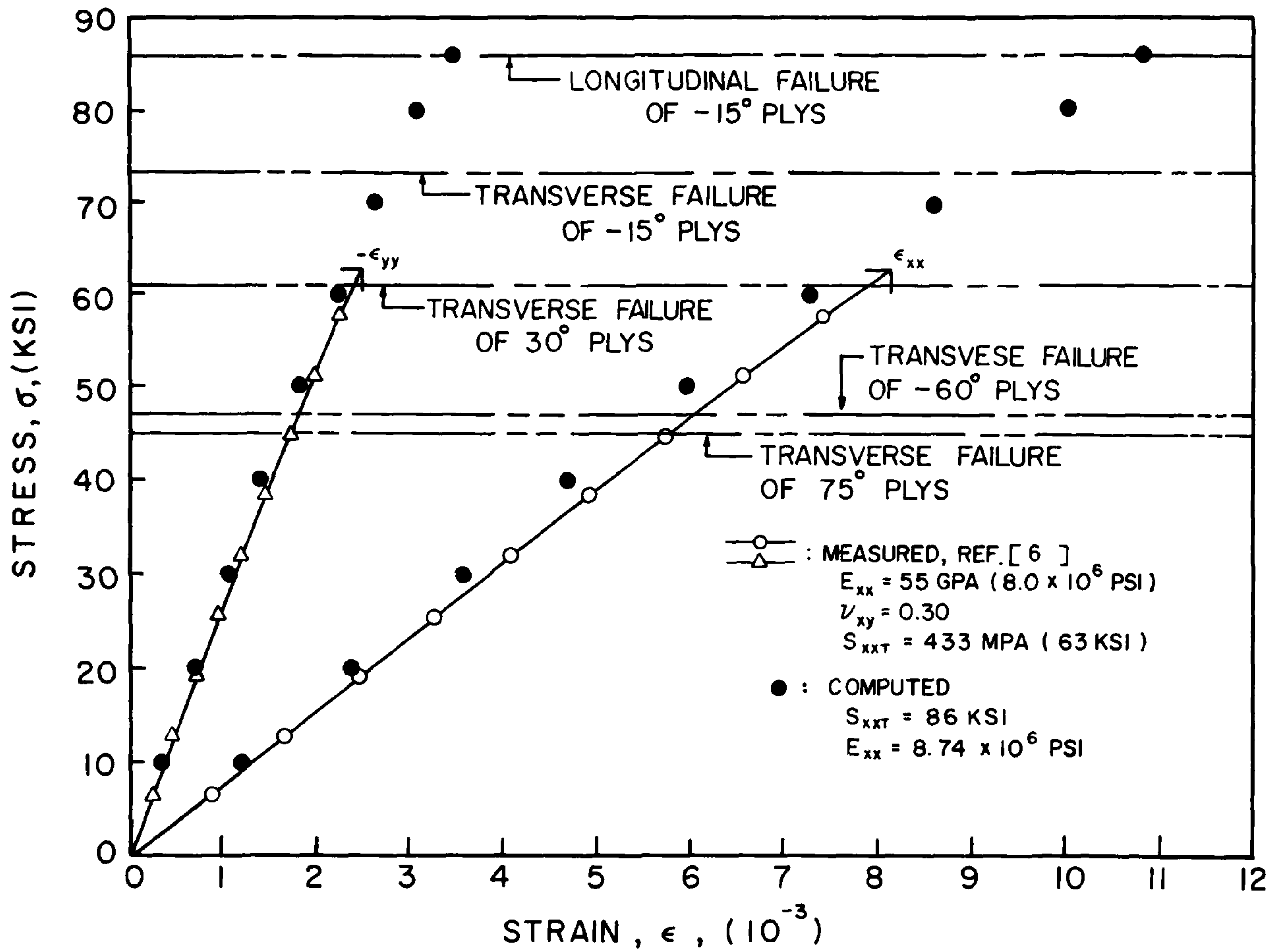

Figure 32. Strain Response for the 30-degree Loading of a $[0/\pm45/90]_s$ Graphite-Epoxy Laminate

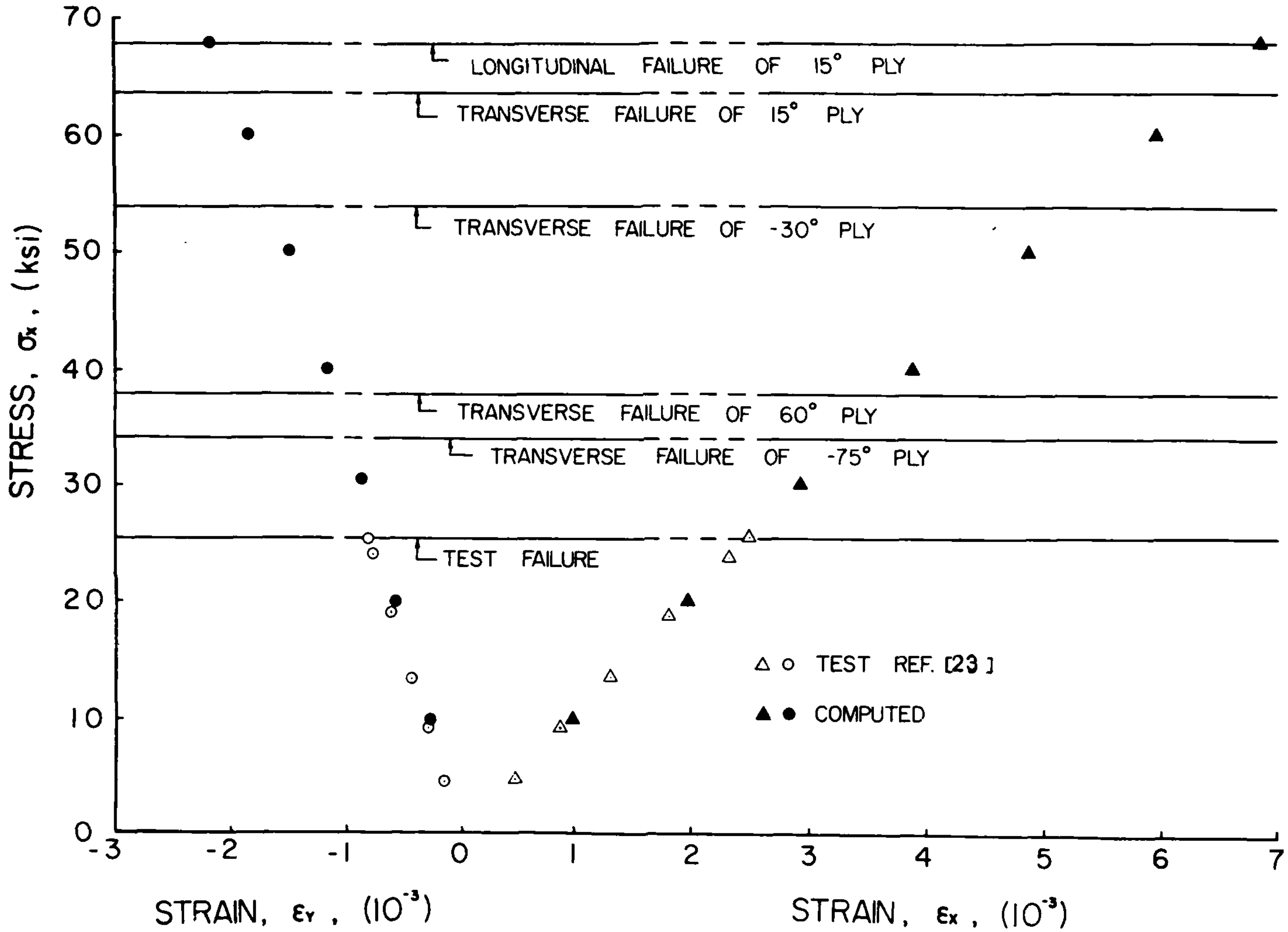

Figure 33. Strain Response for a $[0/90/\pm45]_s$ Boron-Epoxy Laminate Loaded at 15 Degrees Off-Axis

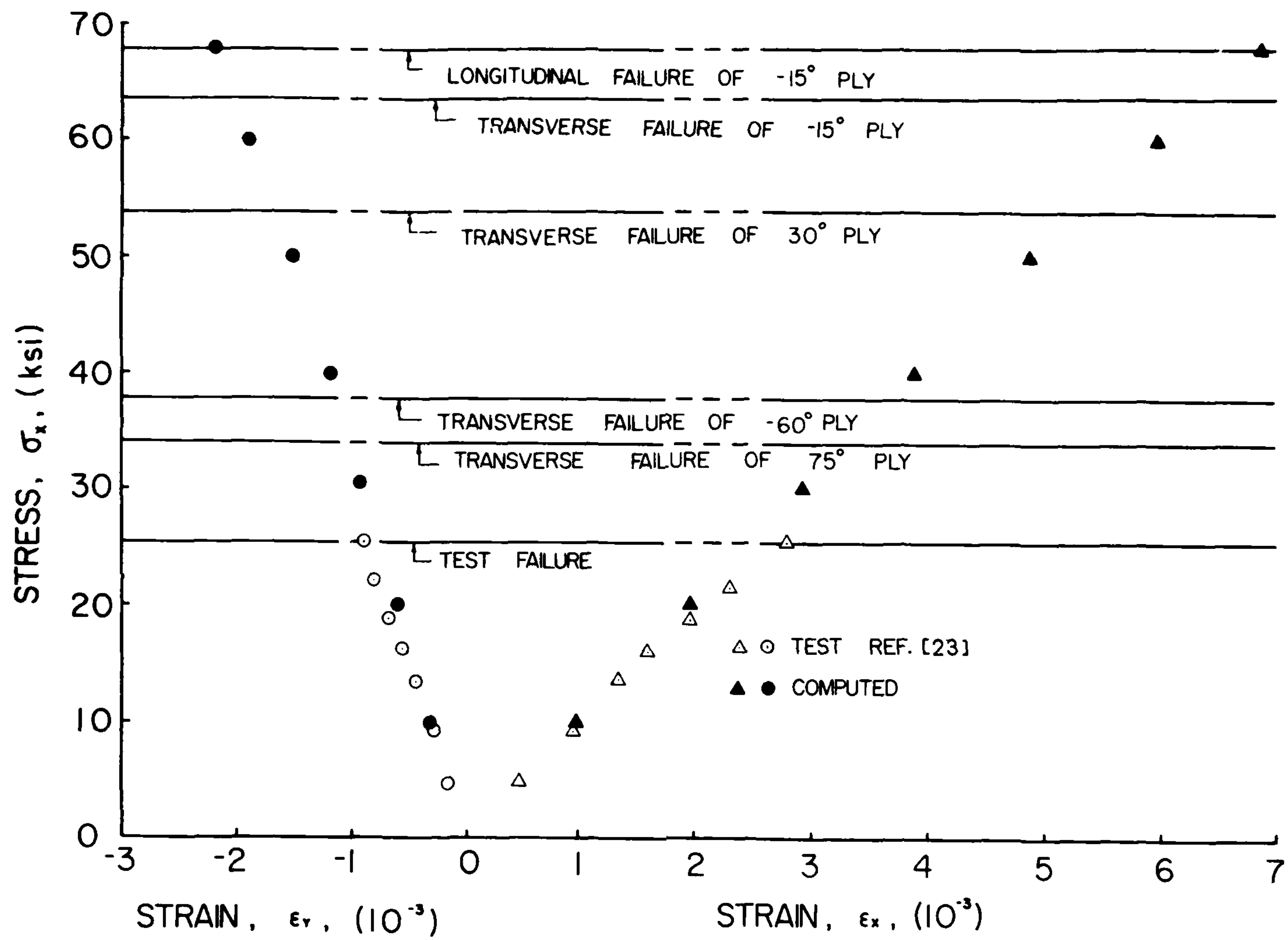

Figure 34. Strain Response for a $[0/90/\pm45]_s$ Boron-Epoxy Laminate Loaded at 30 Degrees Off-Axis

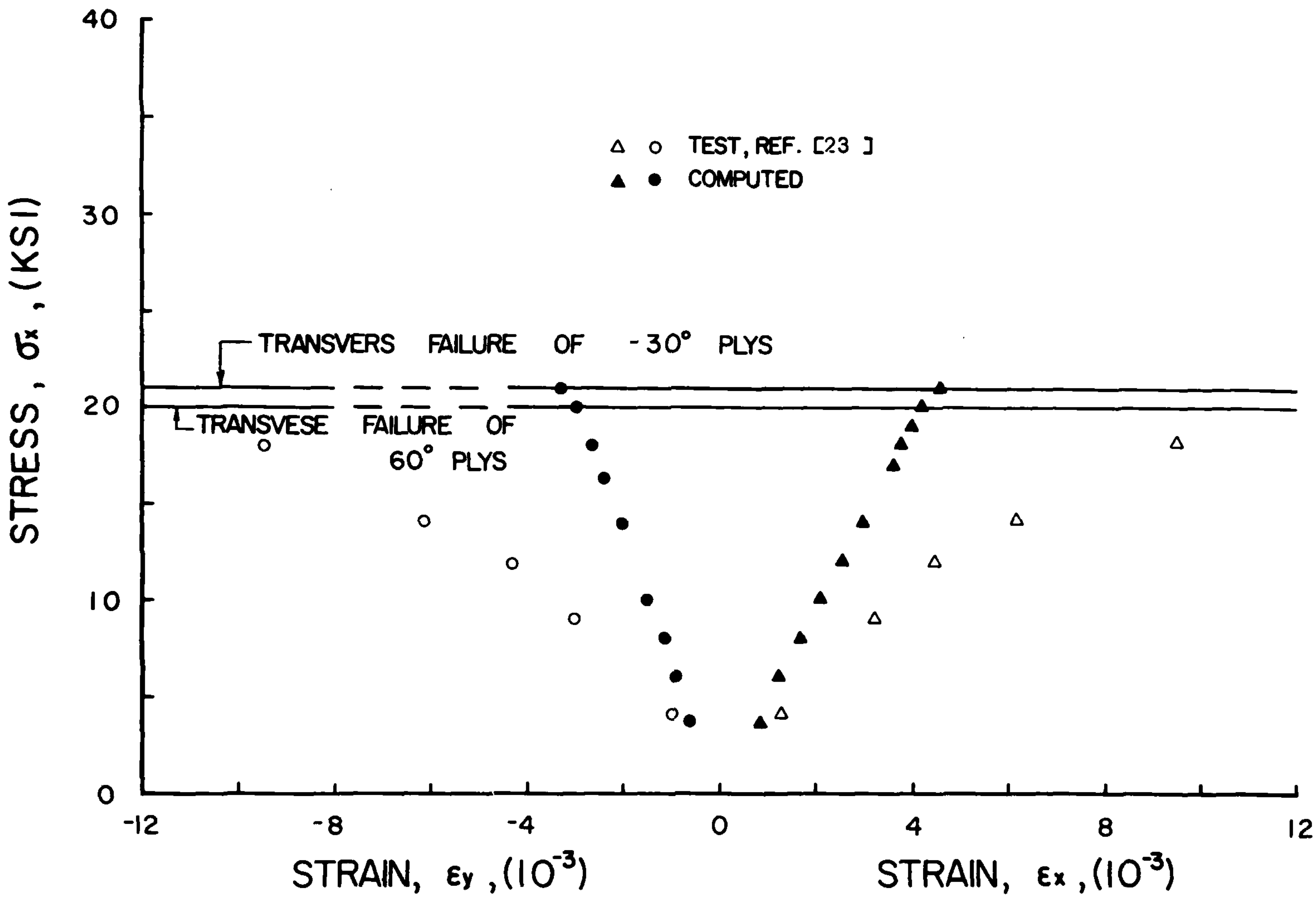

Figure 35. Strain Response for a $[\pm 45]_s$ Boron-Epoxy Laminate Loaded 15 Degrees Off-Axis

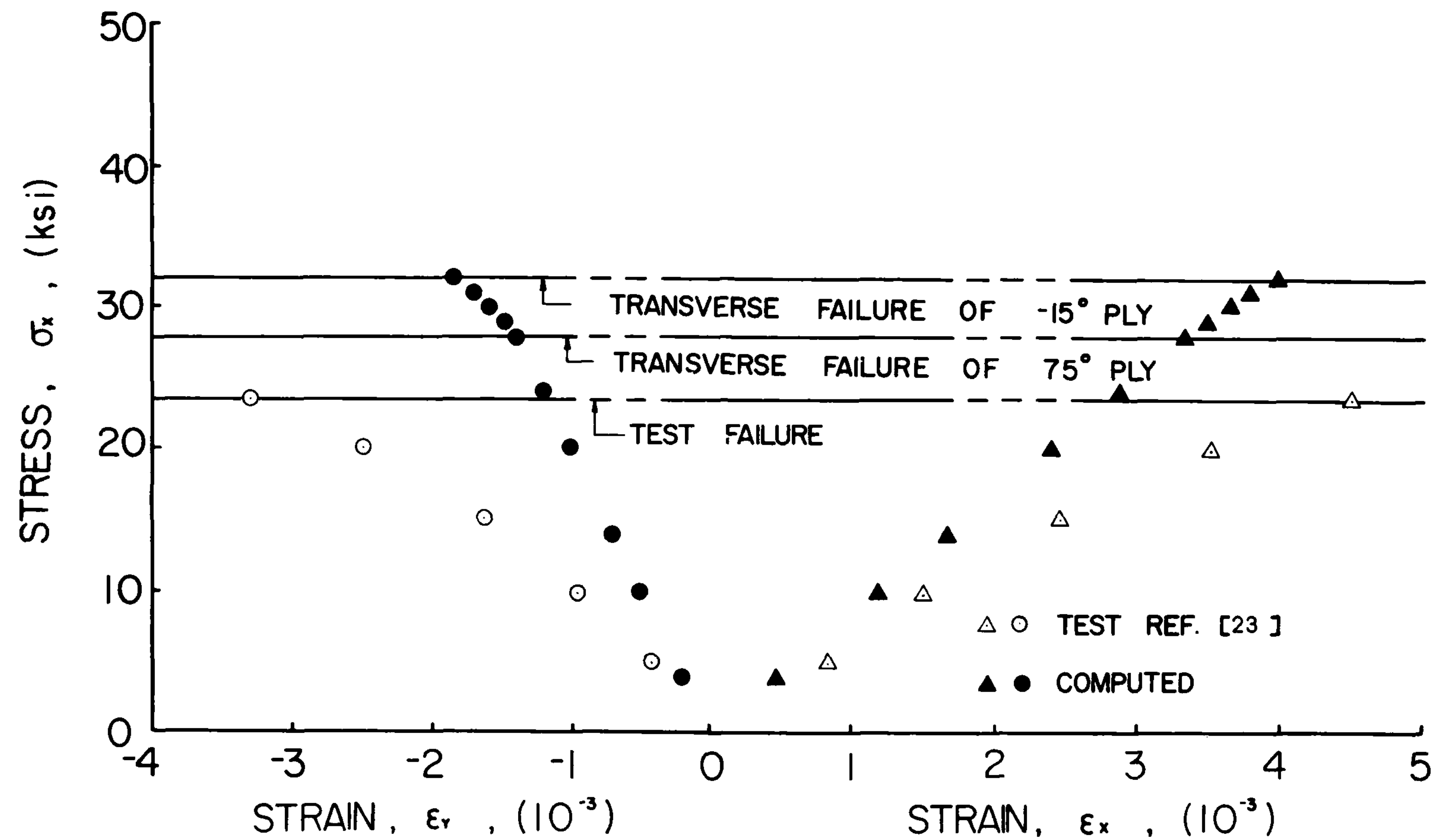

Figure 36. Strain Response for a $[\pm 45]_s$ Boron-Epoxy Laminate Loaded 30 Degrees Off-Axis

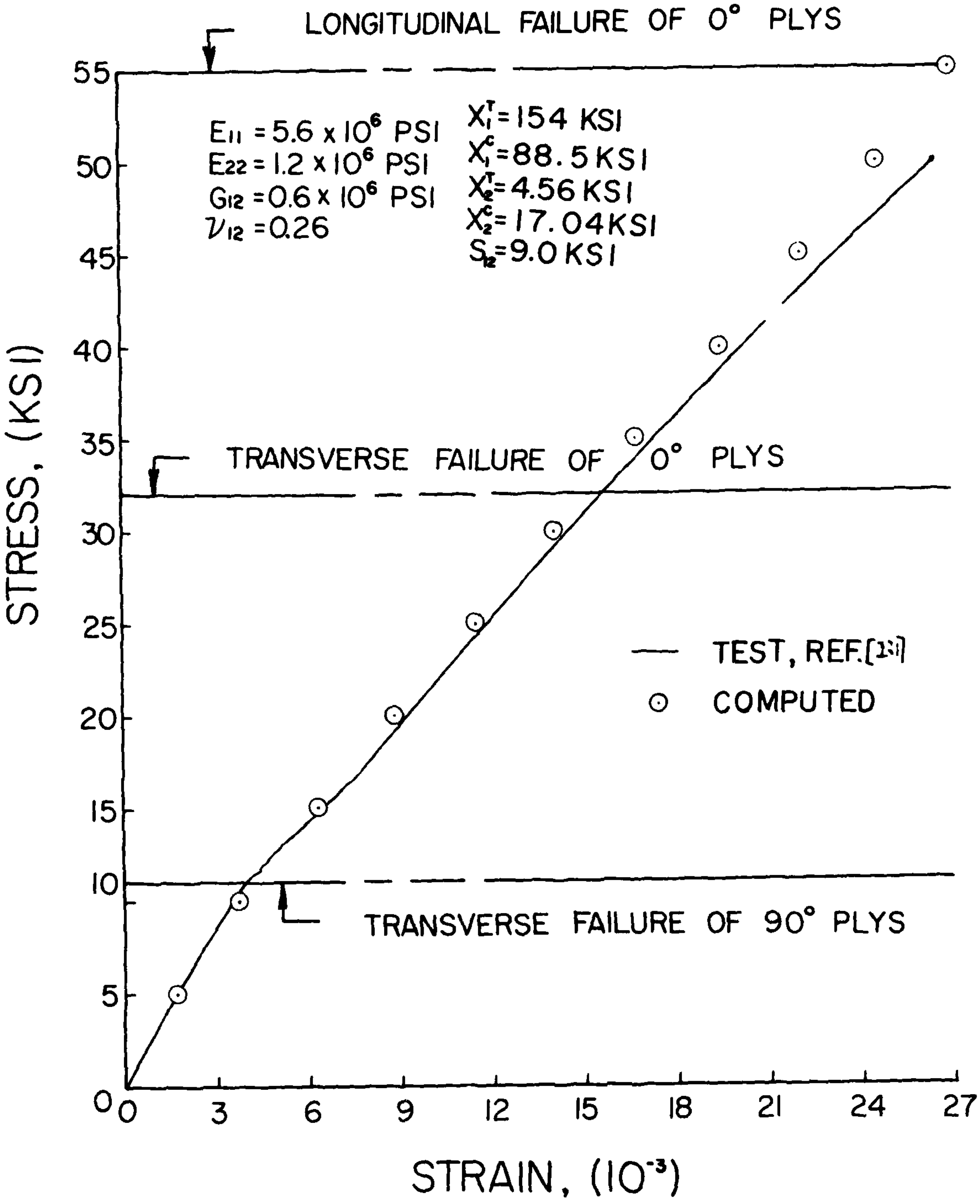

Figure 37. Strain Response of a $[0/90_2]_s$ Glass-Epoxy Laminate

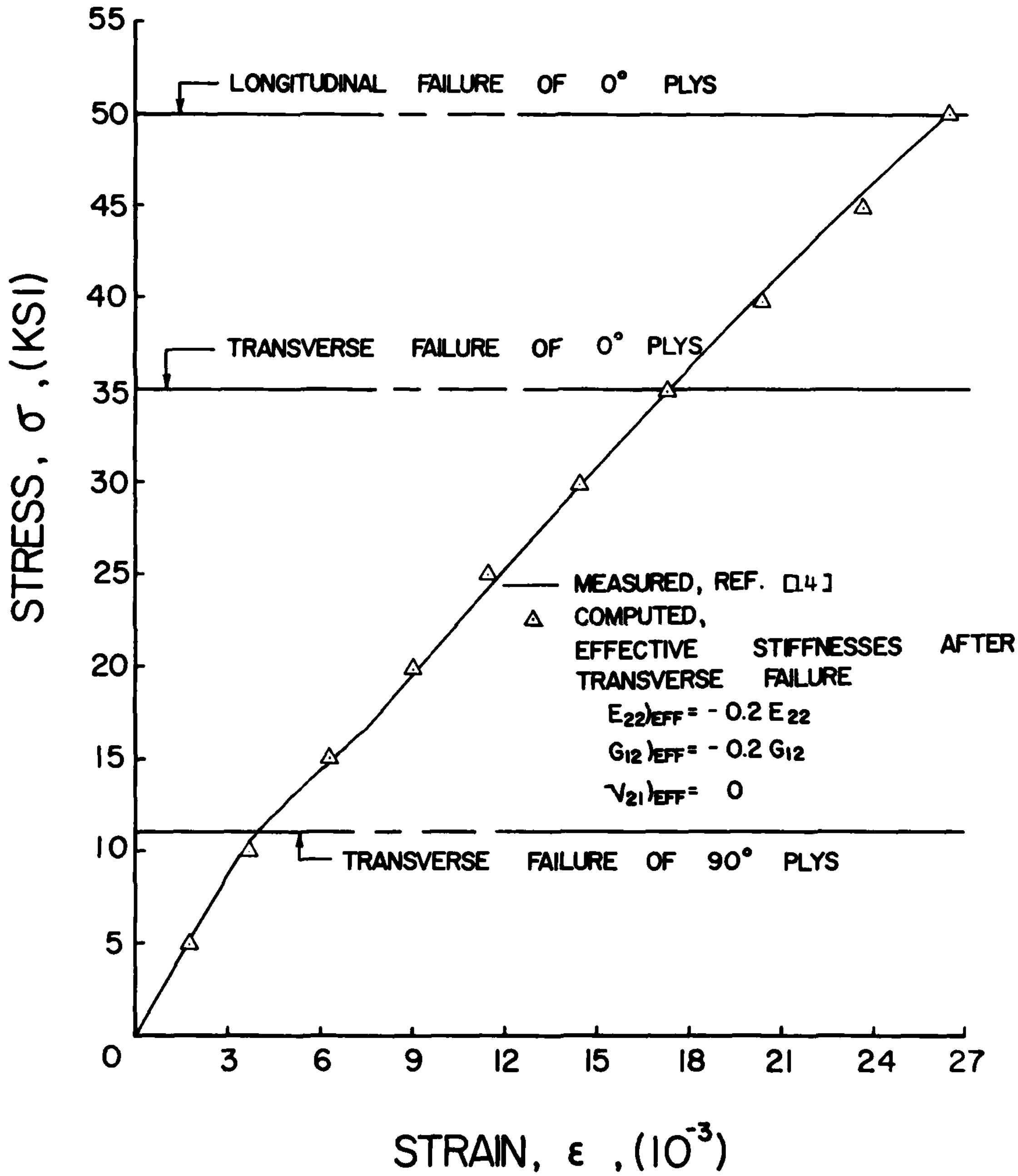

Figure 38. Effect of Failed-Ply Unloading on the Computed Response of the $[0/90_2]_s$ Glass-Epoxy Laminate

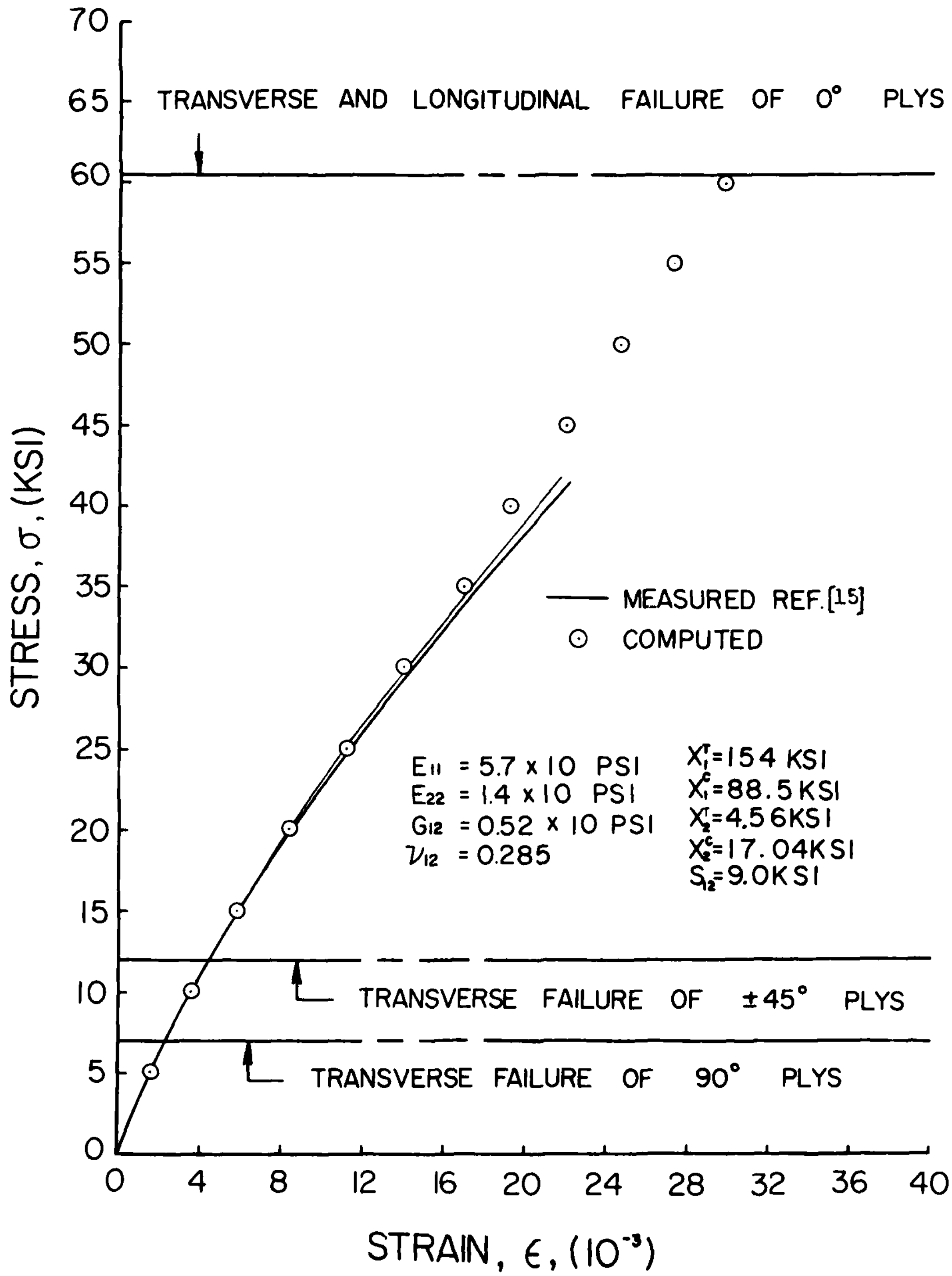

Figure 39. Predicted and Test Strain Response for a $[0/\pm45/90]_s$ Glass-Epoxy Laminate

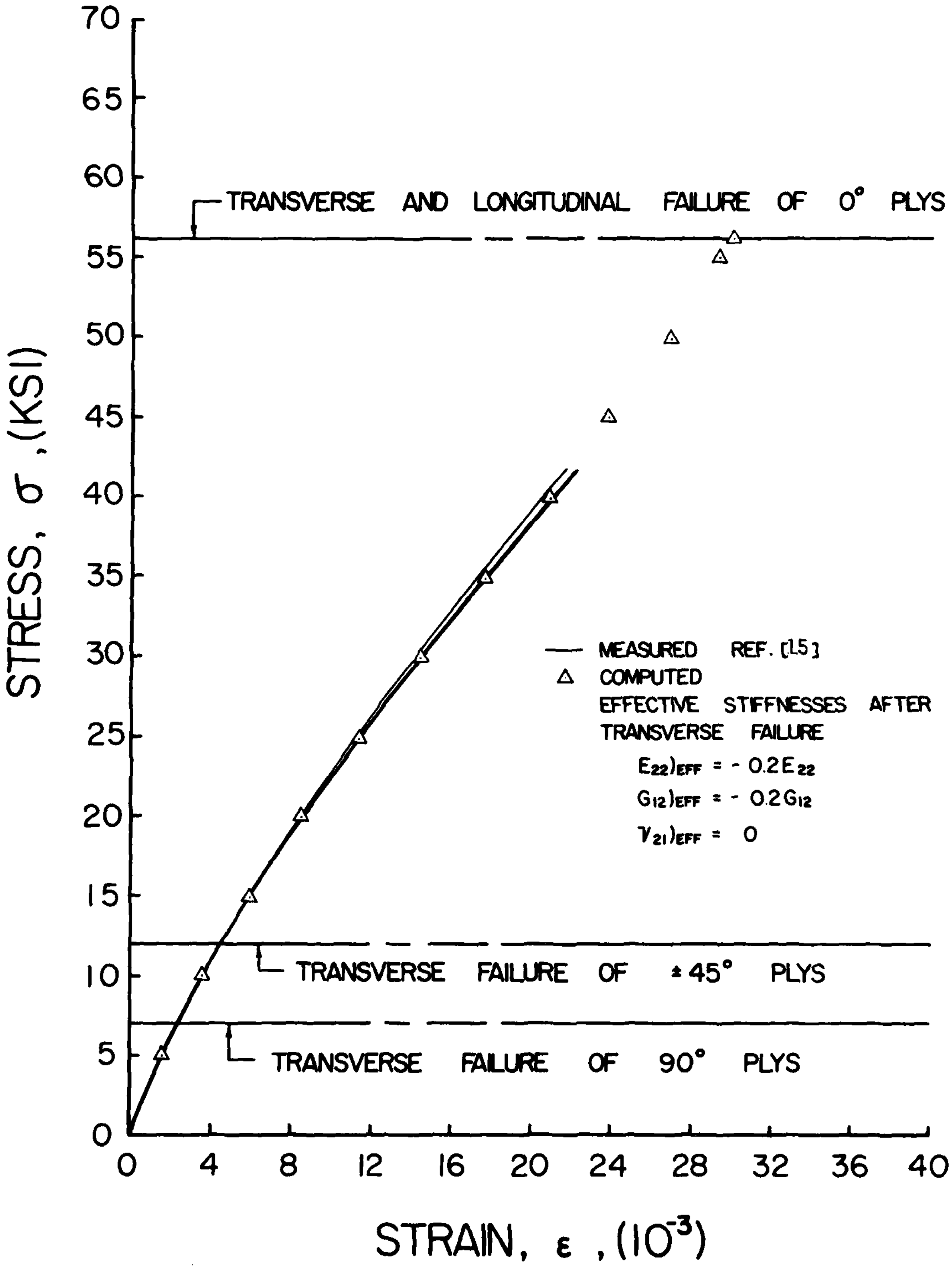

Figure 40. Effect of Failed-Ply Unloading on the Computed Response of the $[0/\pm45/90]_s$ Glass-Epoxy Laminate

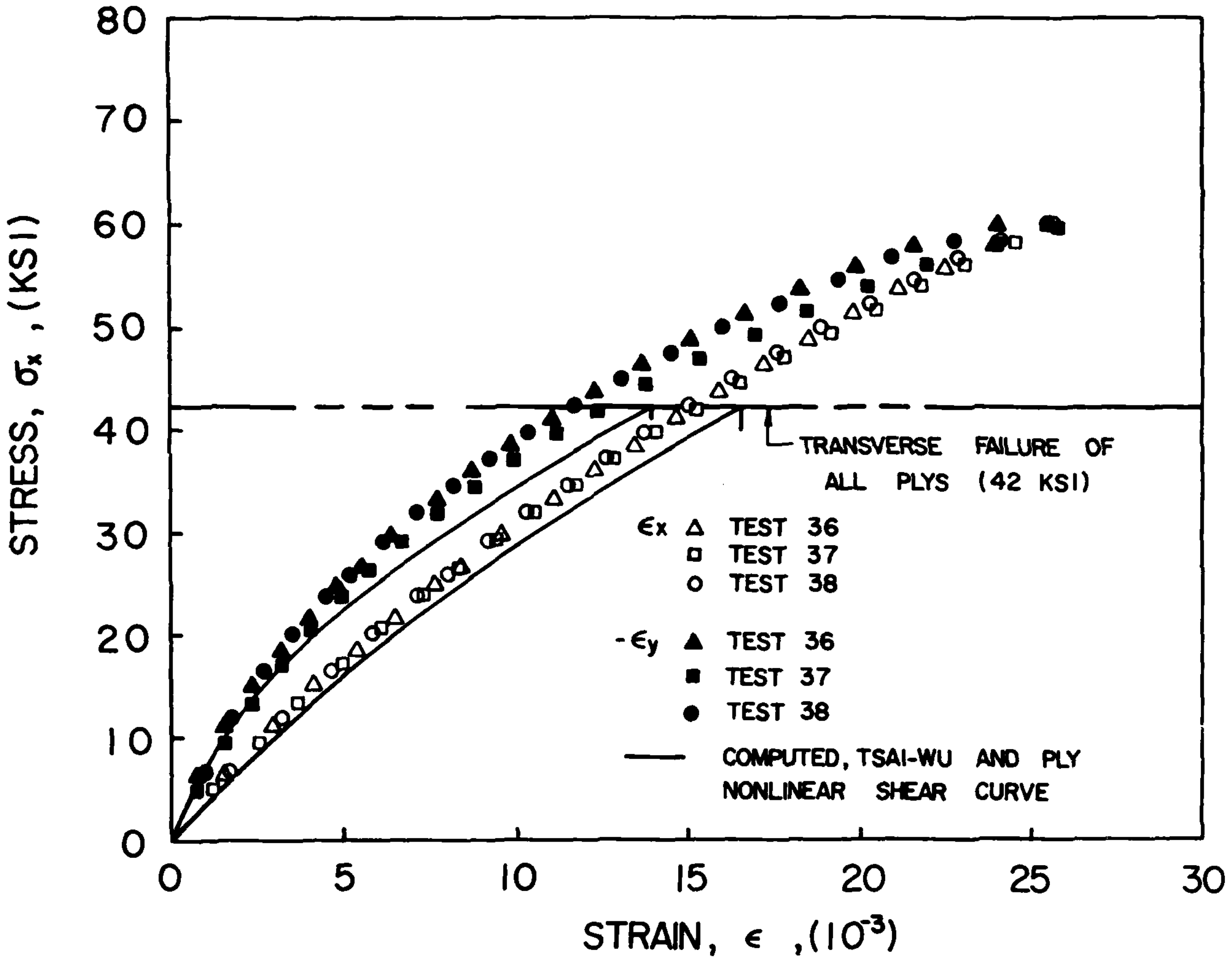

Figure 41. Stress-Strain Response of the $[\pm 30]_s$, XP-250 Glass-Epoxy Laminate

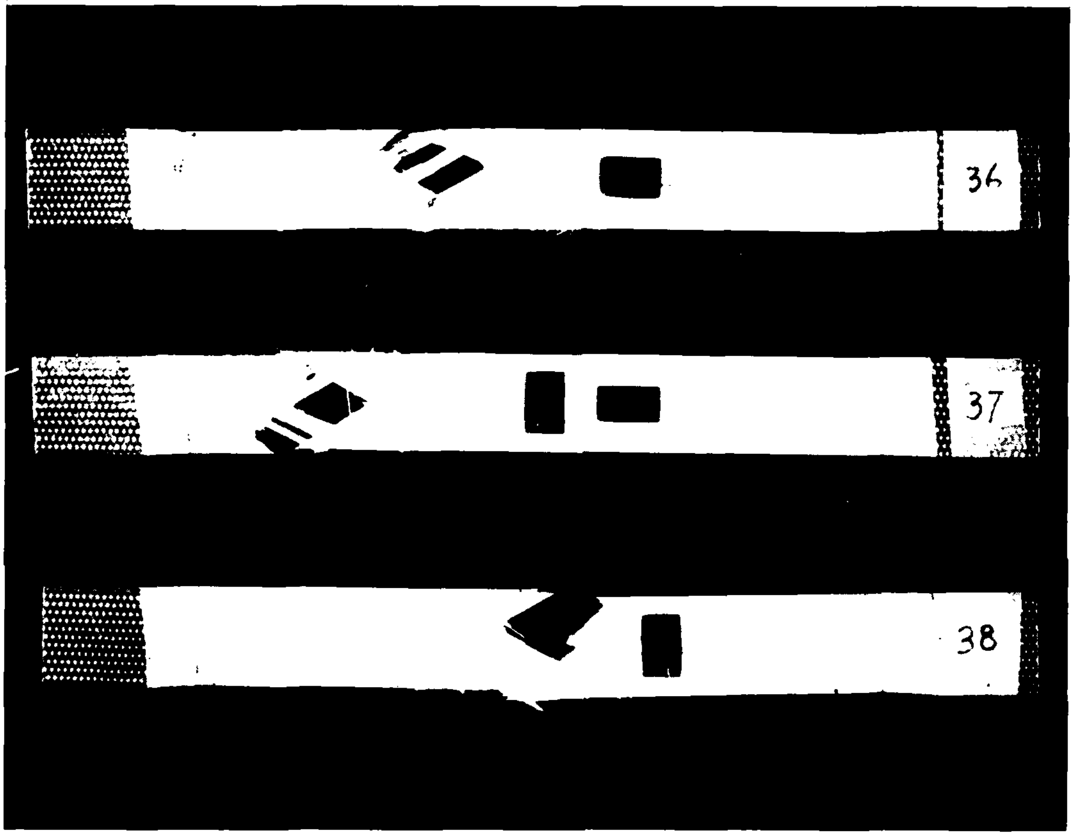

Figure 42. The $[\pm 30]_s$ XP-250 Glass-Epoxy Tension Coupons After Failure.

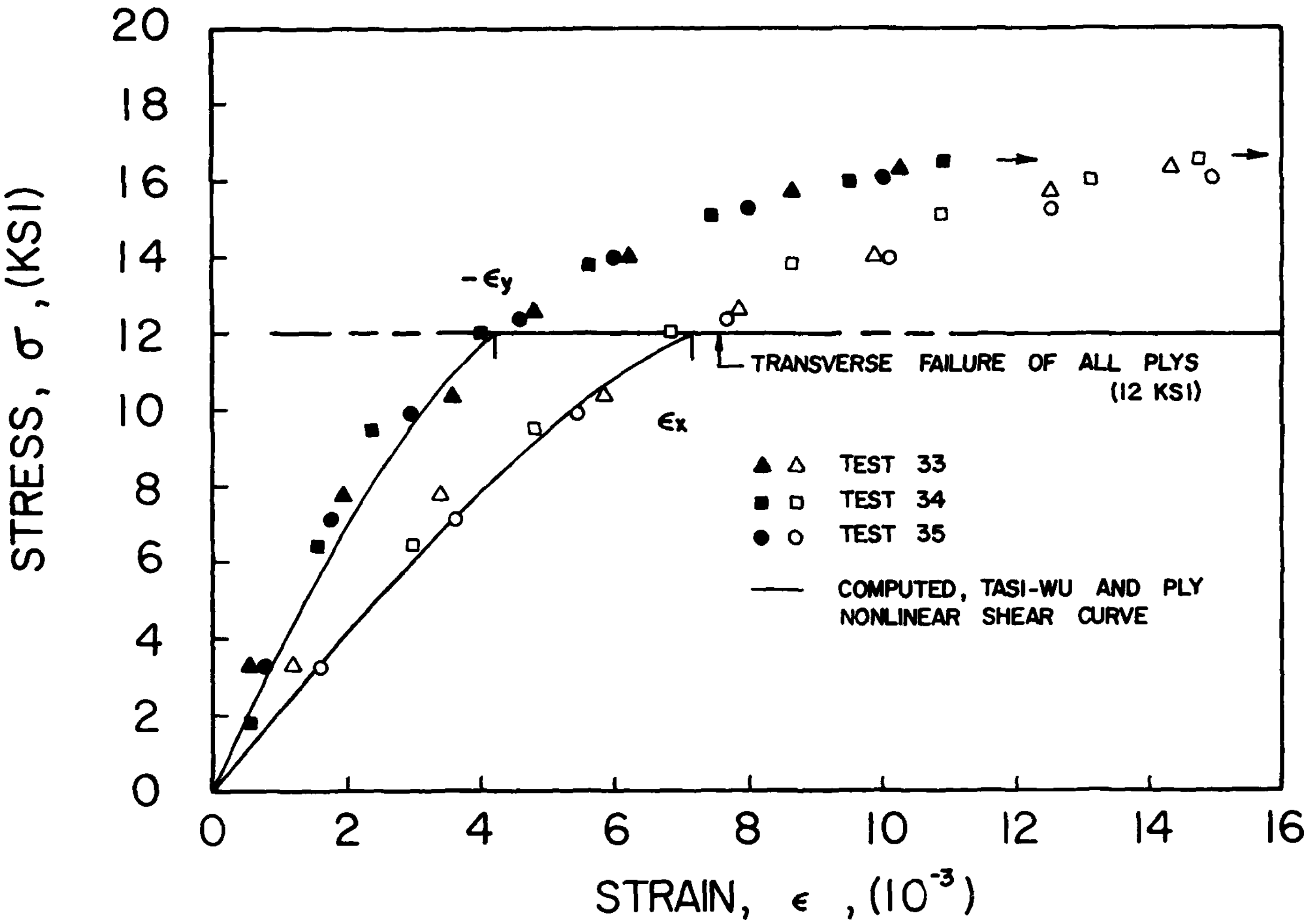

Figure 43. Stress-Strain Response of the $[\pm 45]_s$, XP-250 Glass-Epoxy Laminate--Initial Portion

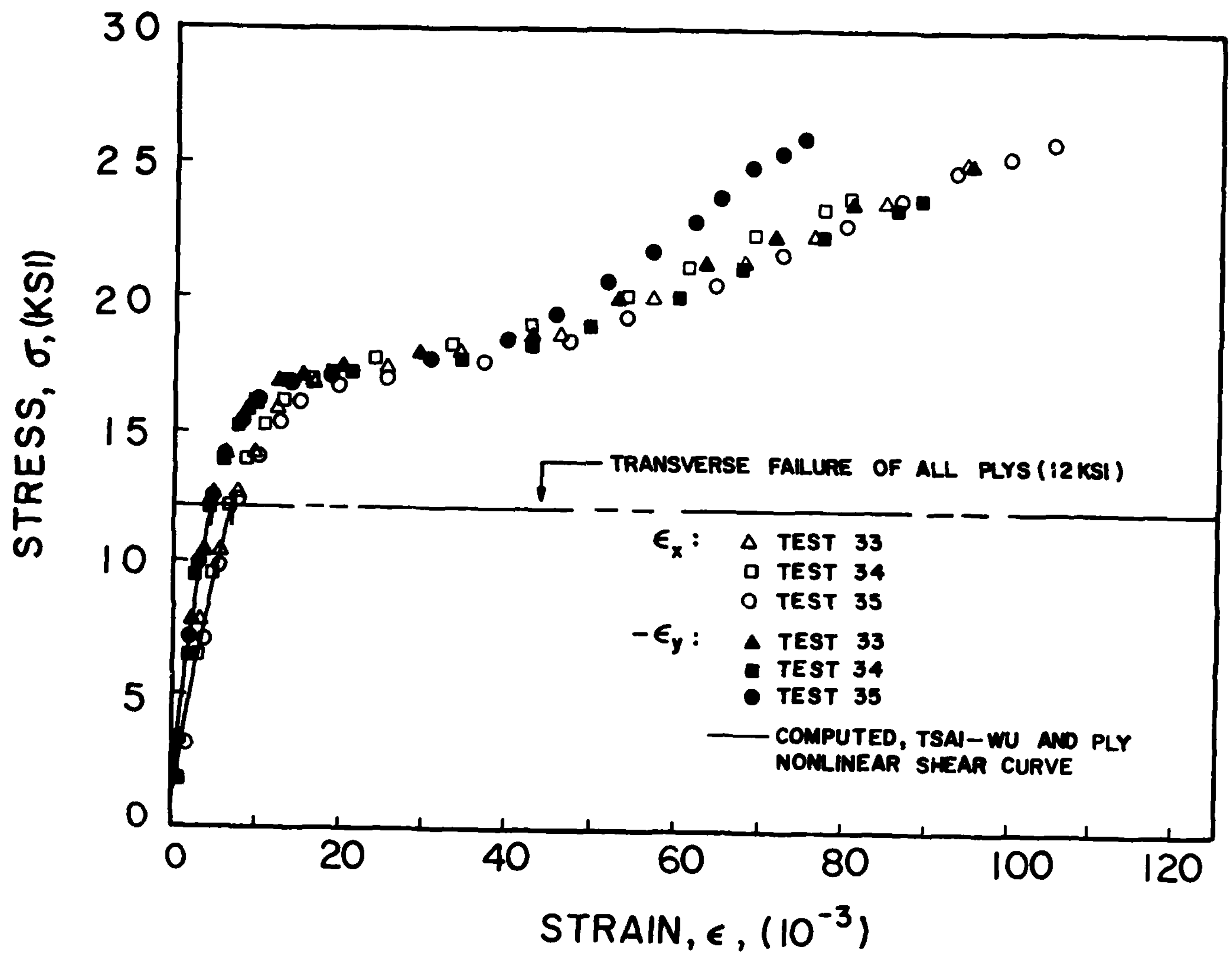

Figure 44. Stress-Strain Response of the $[\pm 45]_s$, XP-250 Glass-Epoxy Laminate--Full Curve

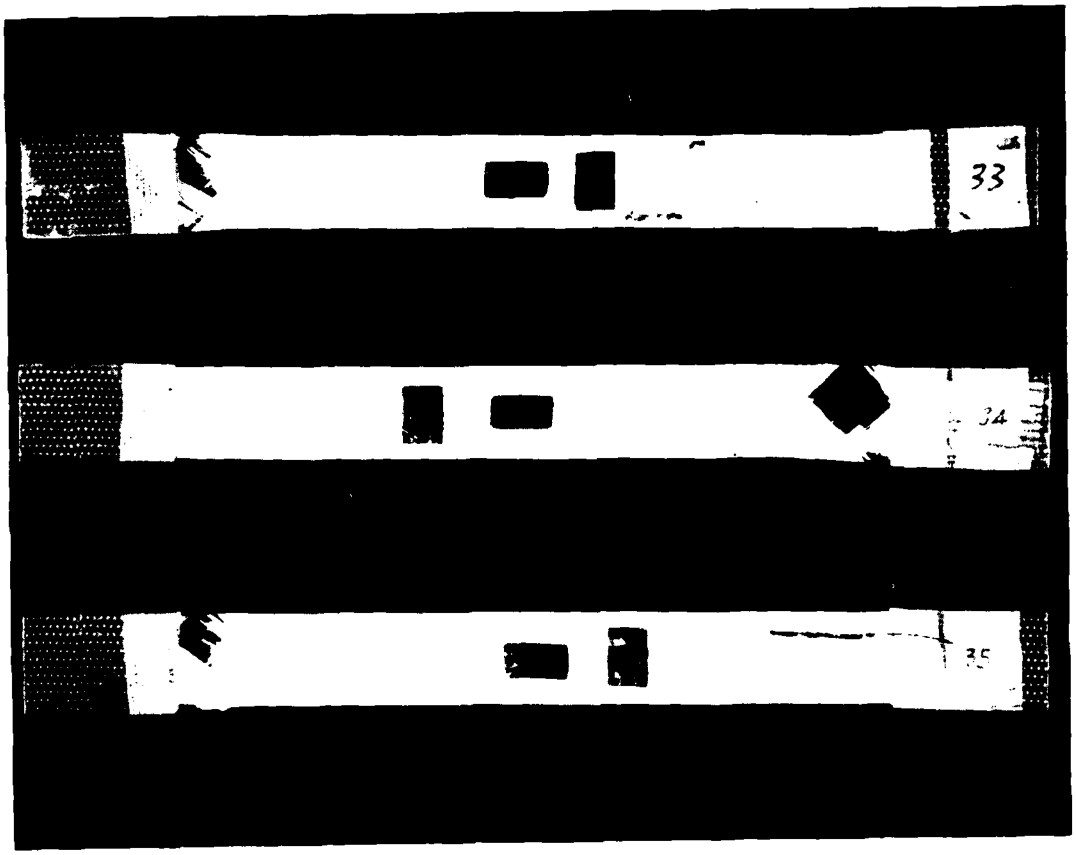

Figure 45. The $[\pm 45]_s$ XP-250 Glass-Epoxy Tension Coupons After Failure

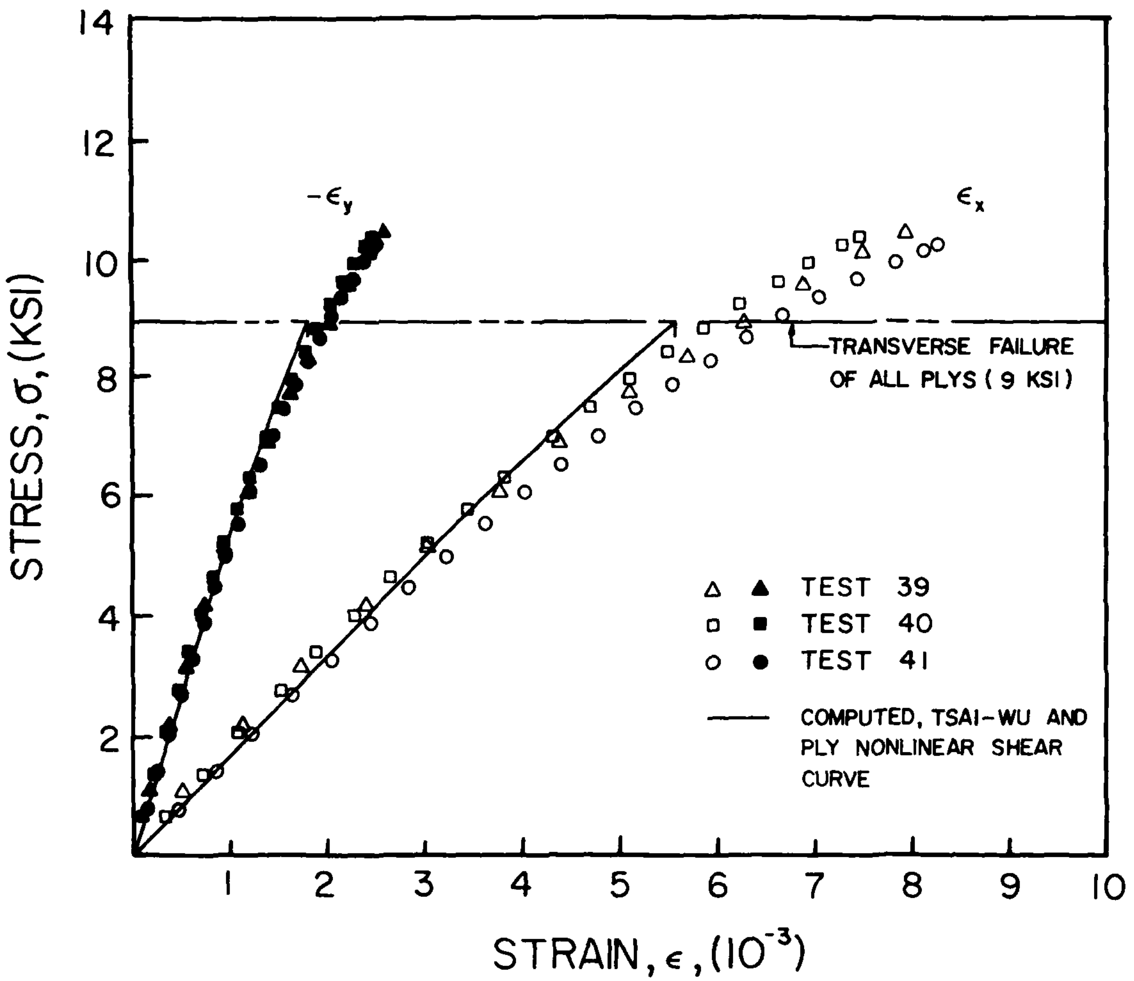

Figure 46. Stress-Strain Response of the $[\pm 60]_s$, XP-250 Glass-Epoxy Laminate

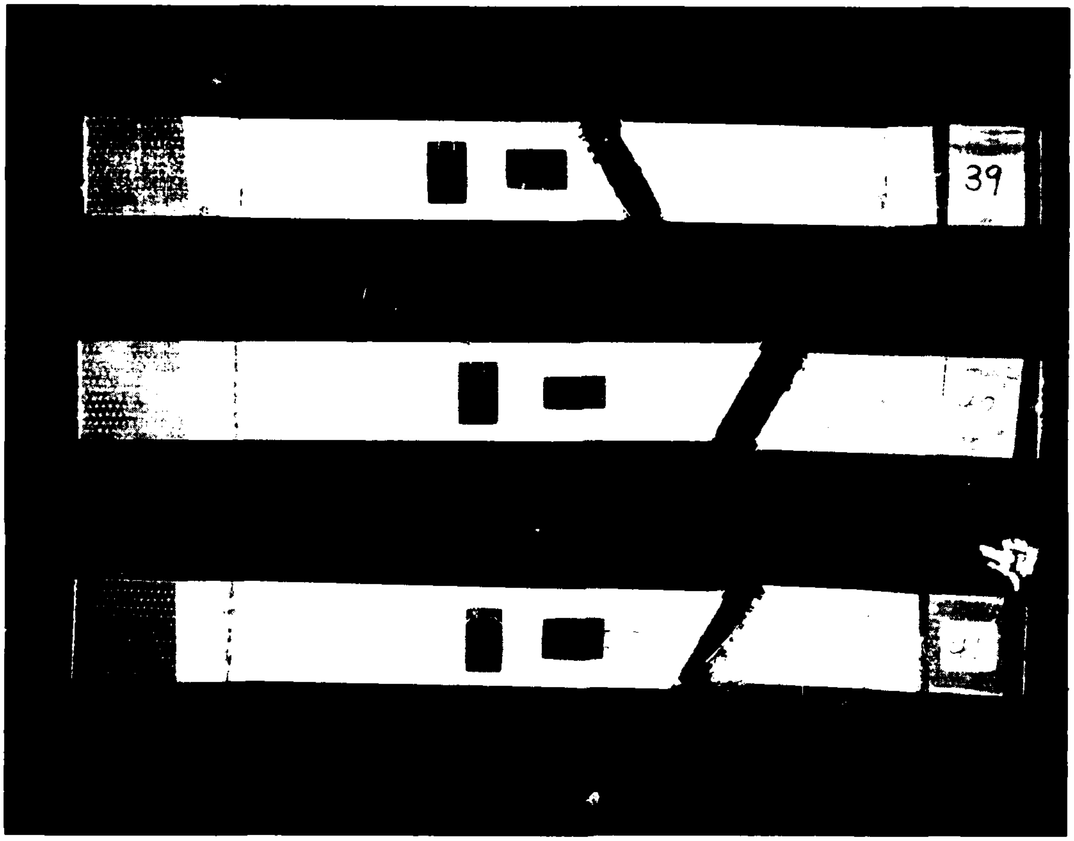

Figure 47. The $[\pm 60]_s$ XP-250 Glass-Epoxy Tension Coupons After Failure

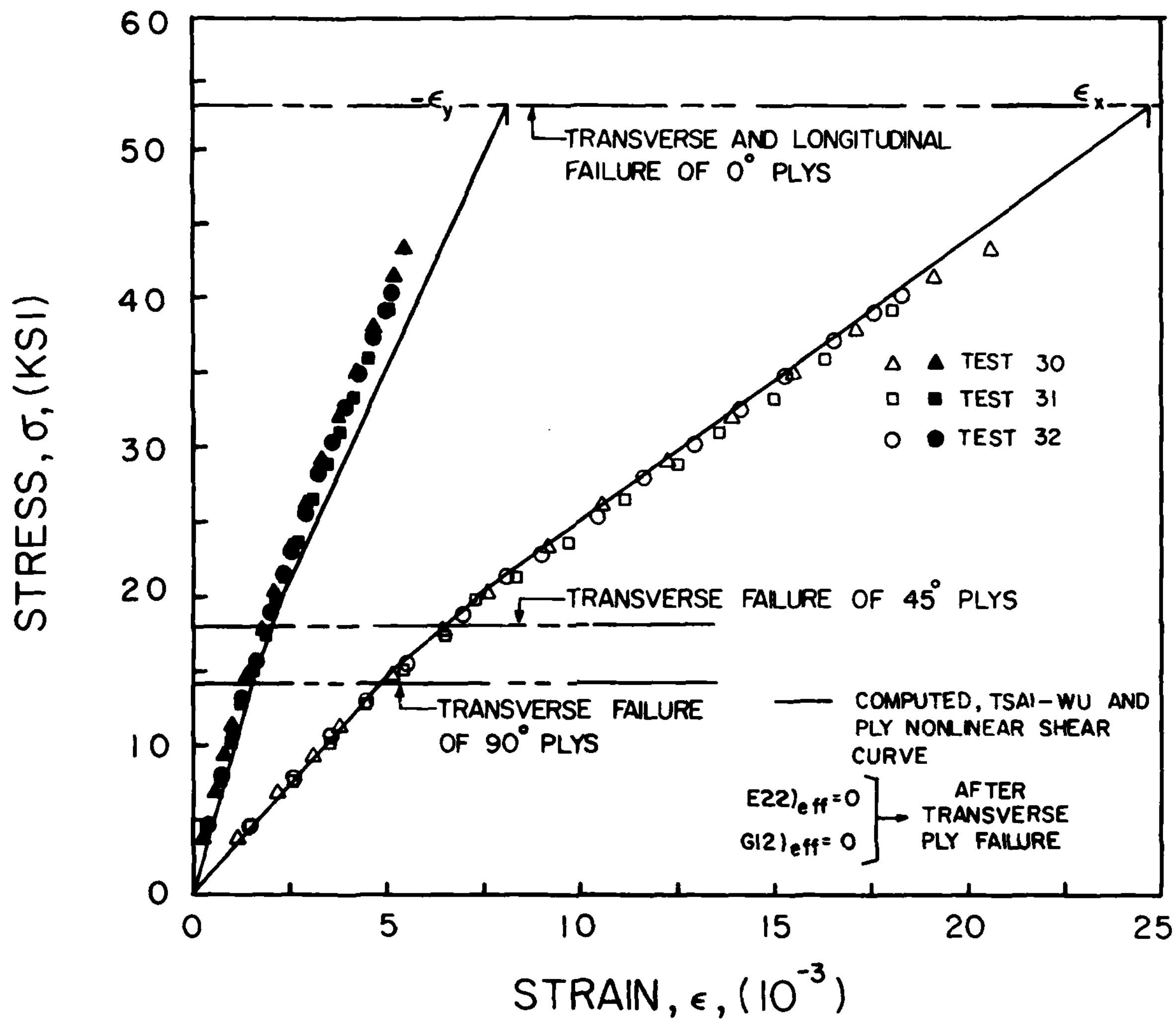

Figure 48. Stress-Strain Response of the $[0/\pm45/90]_s$, XP-250 Glass-Epoxy Laminate

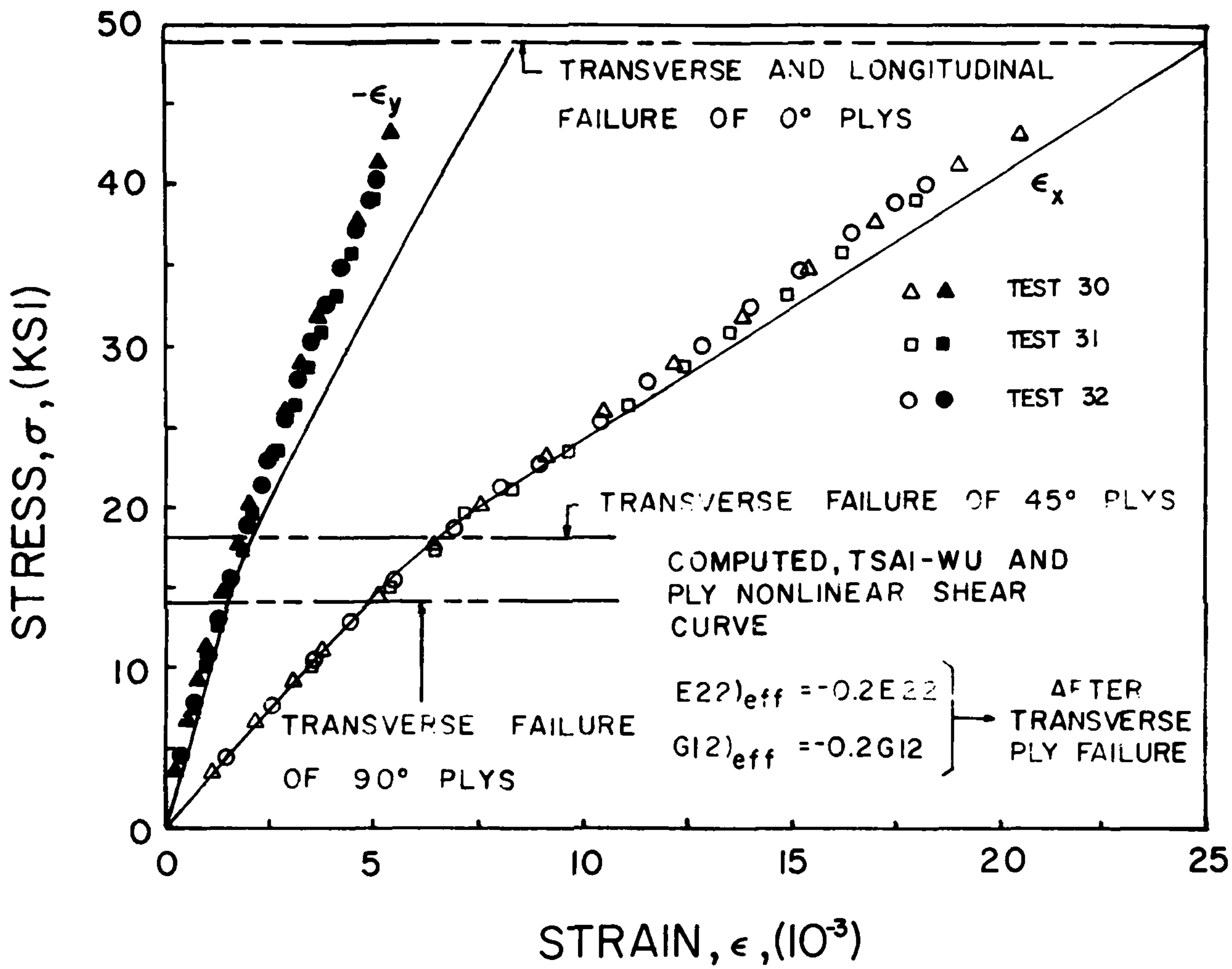

Figure 49. Effect of Failed-Ply Unloading on the Computed Strain Response of the $[0/\pm45/90]_s$ XP-250 Glass-Epoxy Laminate

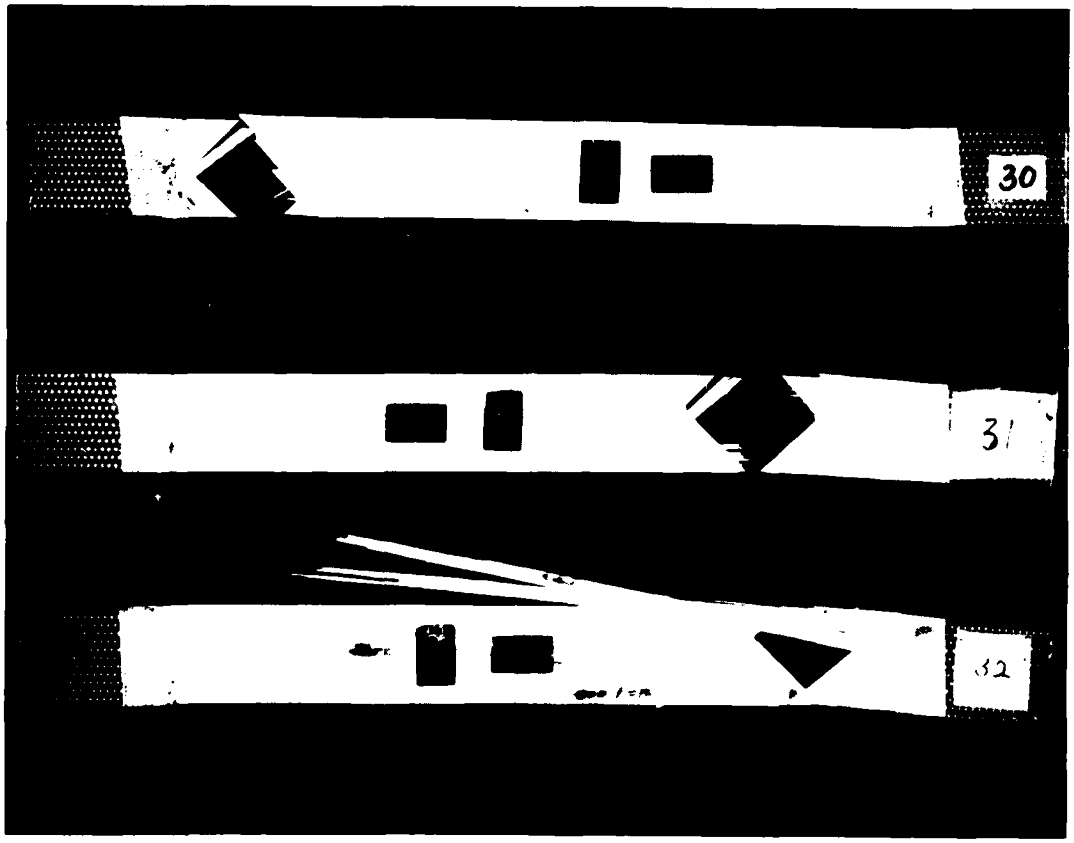

Figure 50. The $[0/\pm45/90]_s$ XP-250 Glass-Epoxy Tension Coupons After Failure

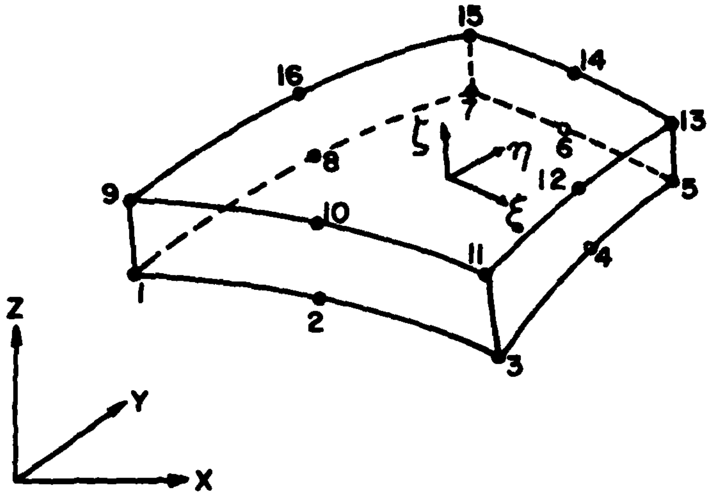

Figure 51. The 16-node Solid Element

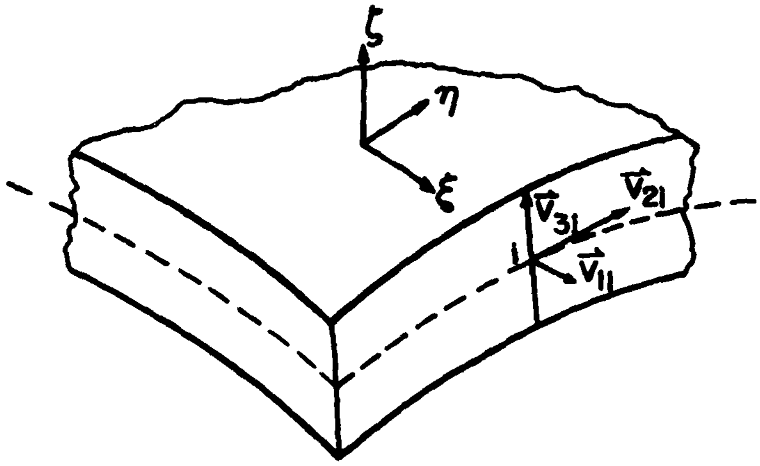

Figure 52. Local and Global Coordinates

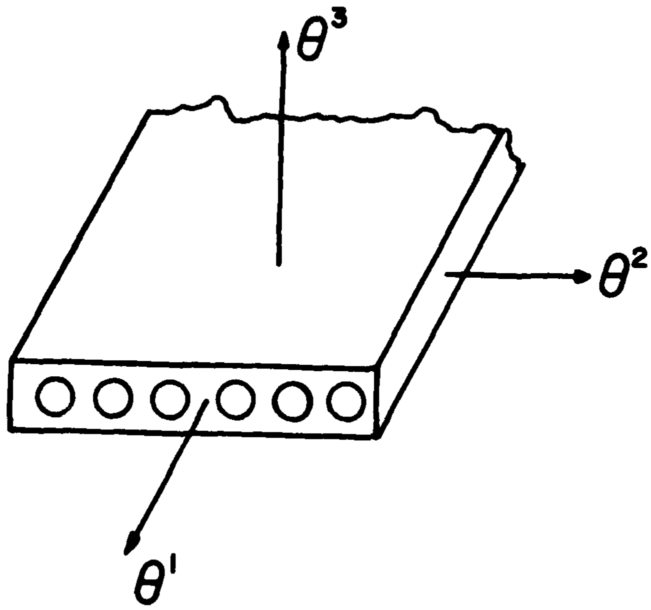

Figure 53. The Lamina Principal Axes of Elastic Symmetry

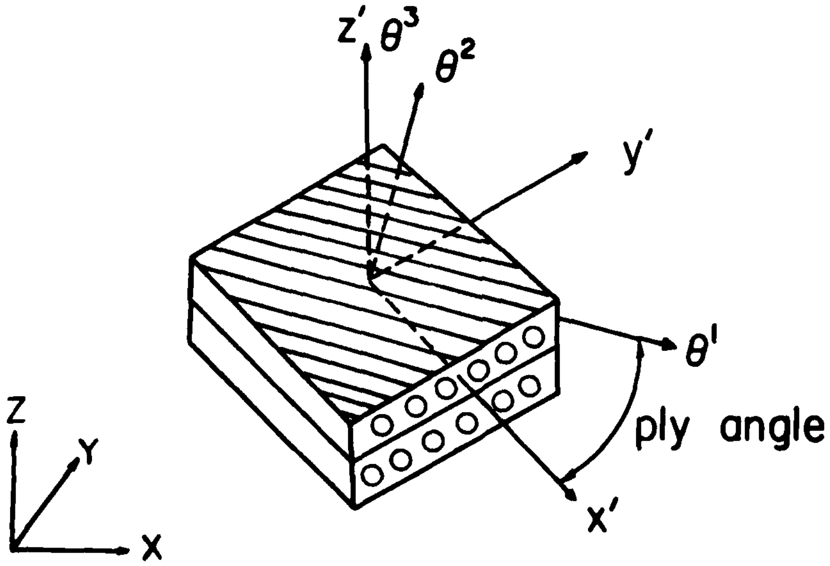

Figure 54. Relationship of Lamina Principal Axes to Shell Coordinates

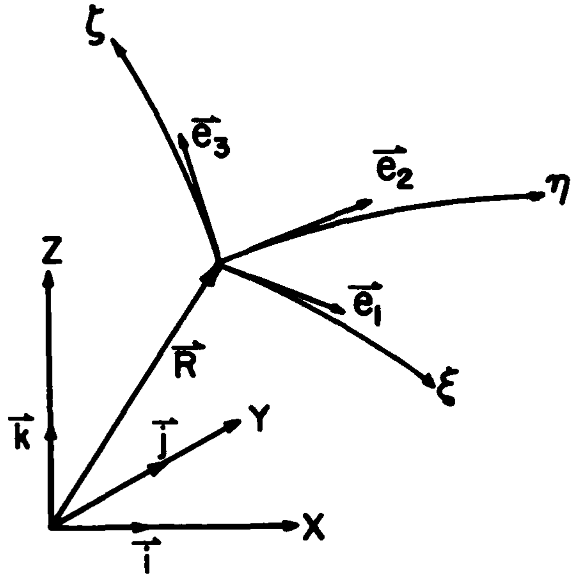

Figure 55. Intrisic Shell Coordinate Axes

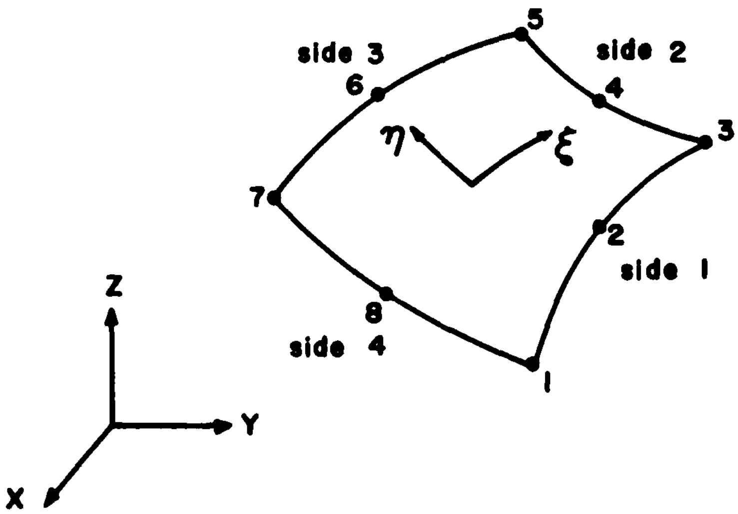

Figure 56. Possible Region for the Quadrilateral

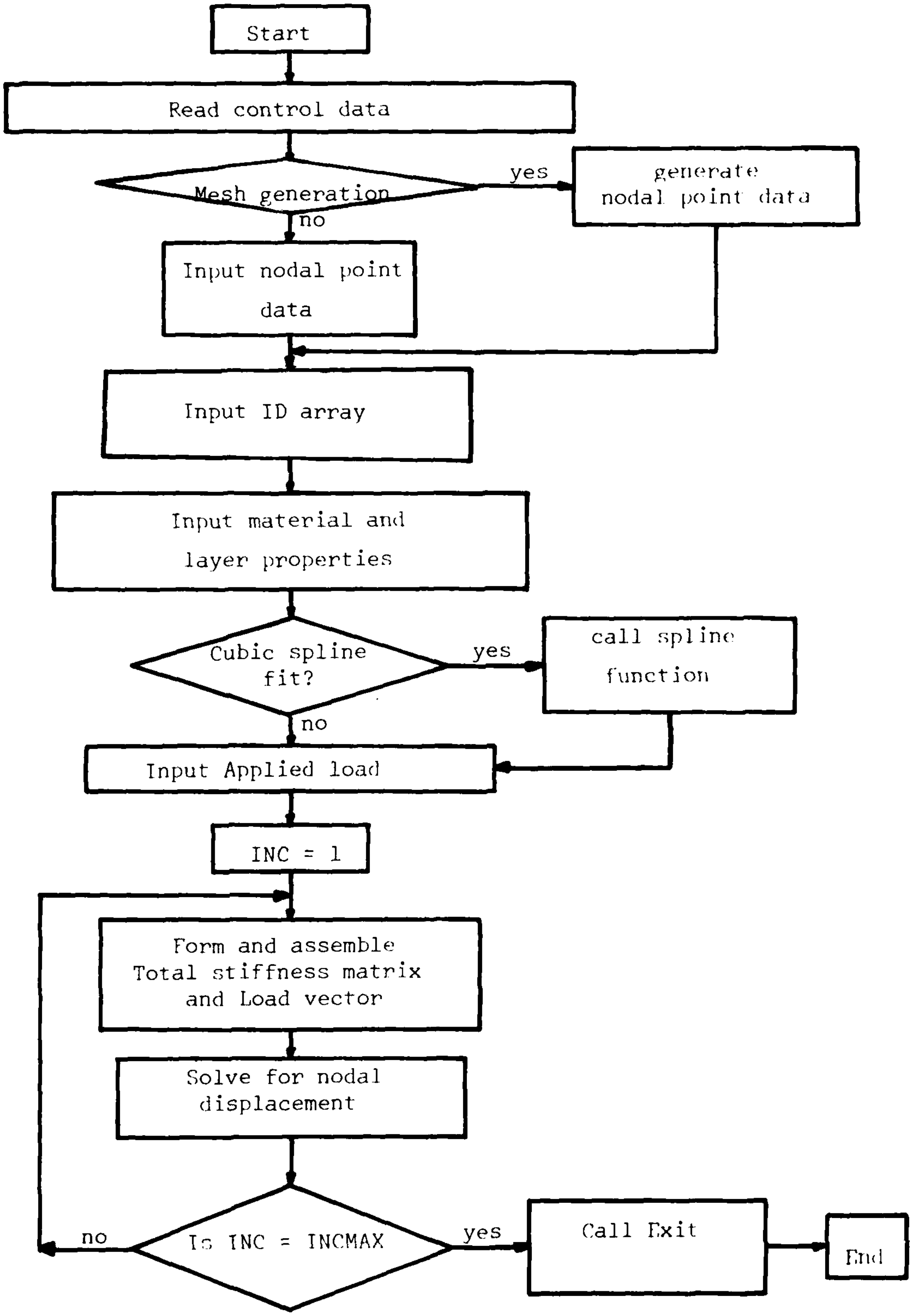

Figure 57. The Flow Chart of the Computer Program

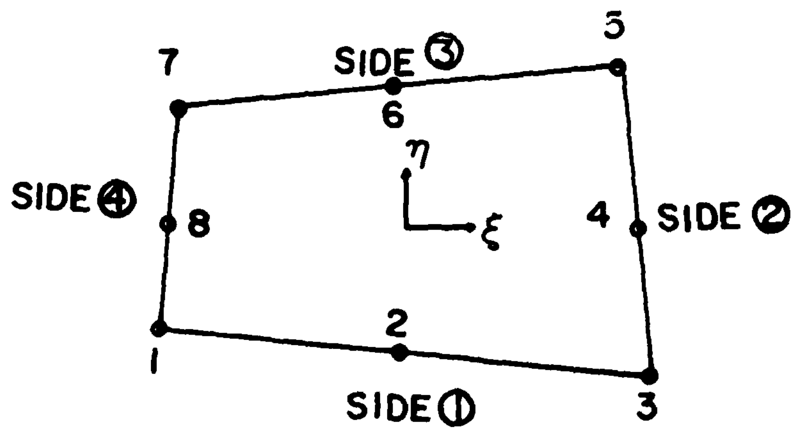

Figure 58. The Sides of a Quadrilateral Region

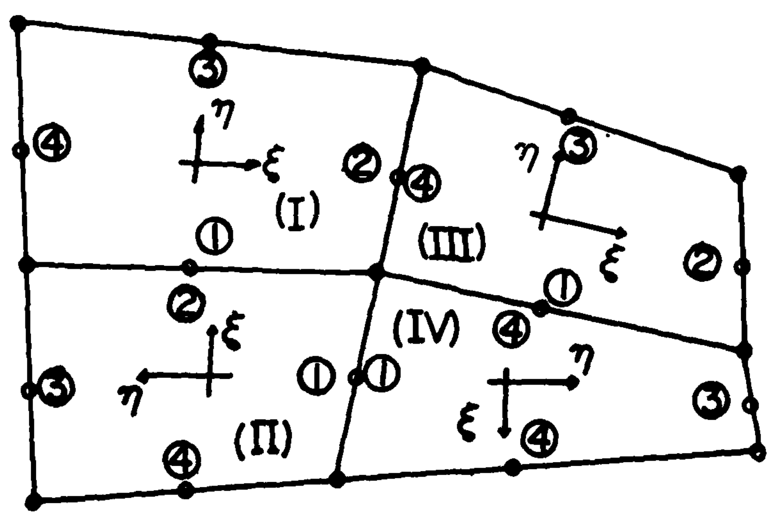

Figure 59. A Connected Set of Quadrilateral Regions

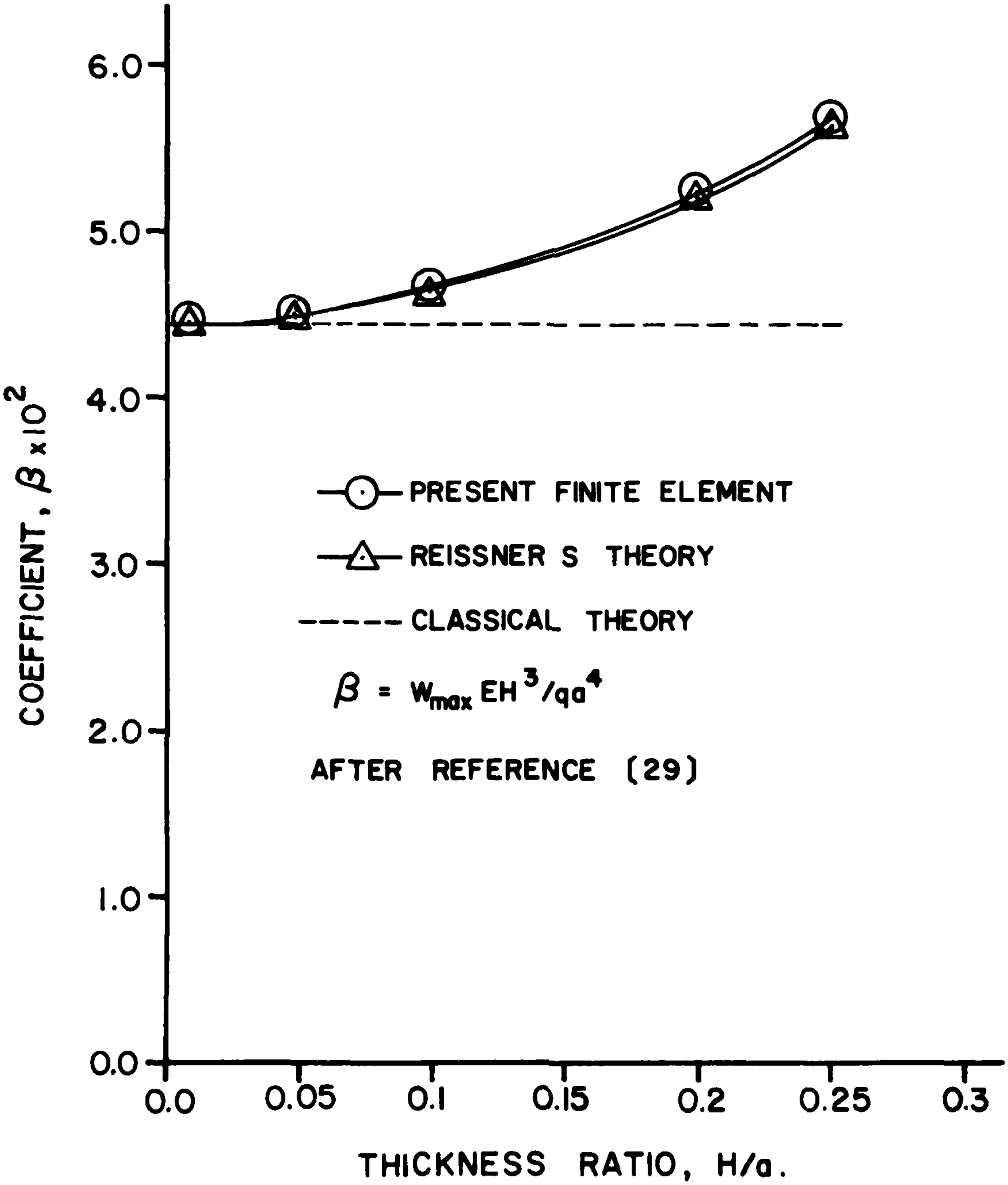

Figure 60. Influence of Transverse Shear on Maximum Deflection of a Homogeneous Simply Supported Plate

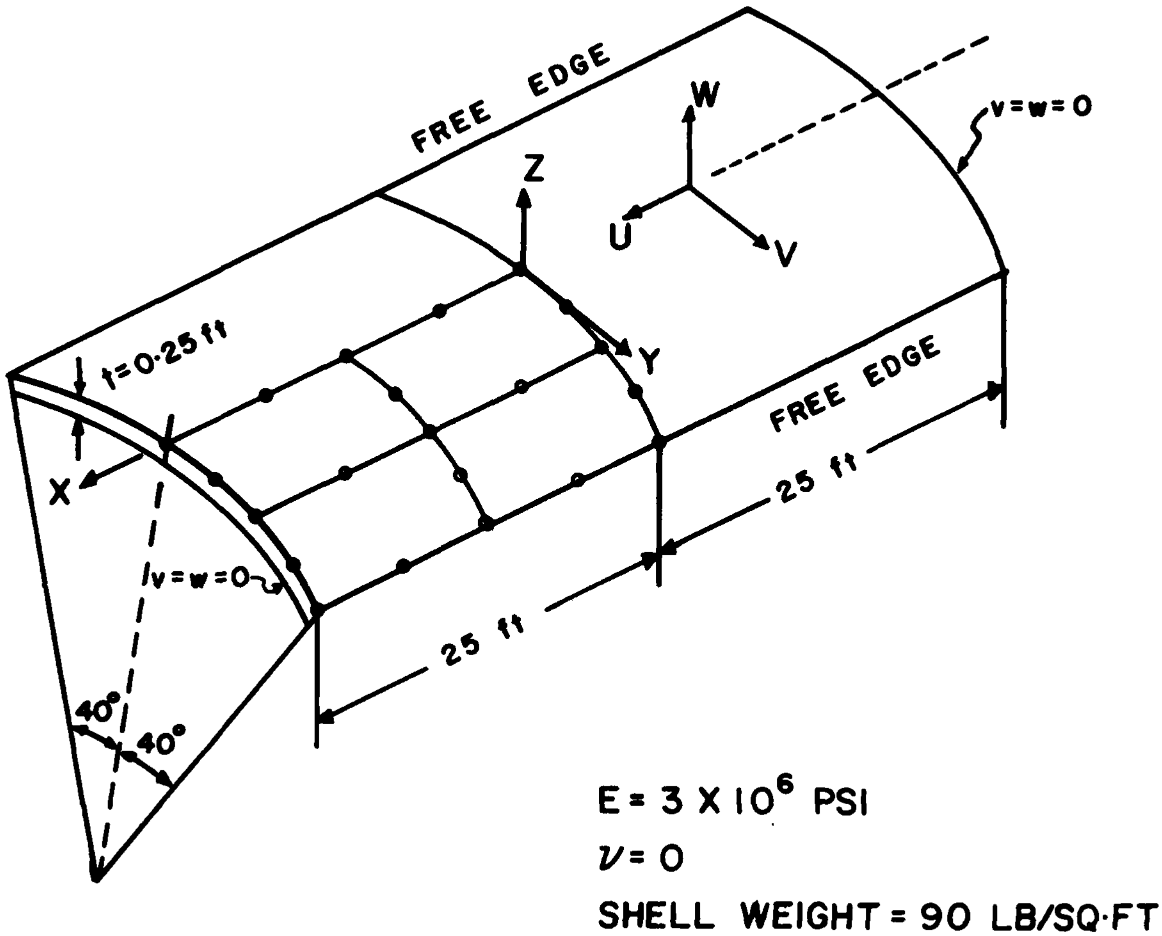

Figure 61. A Cylindrical Shell Roof

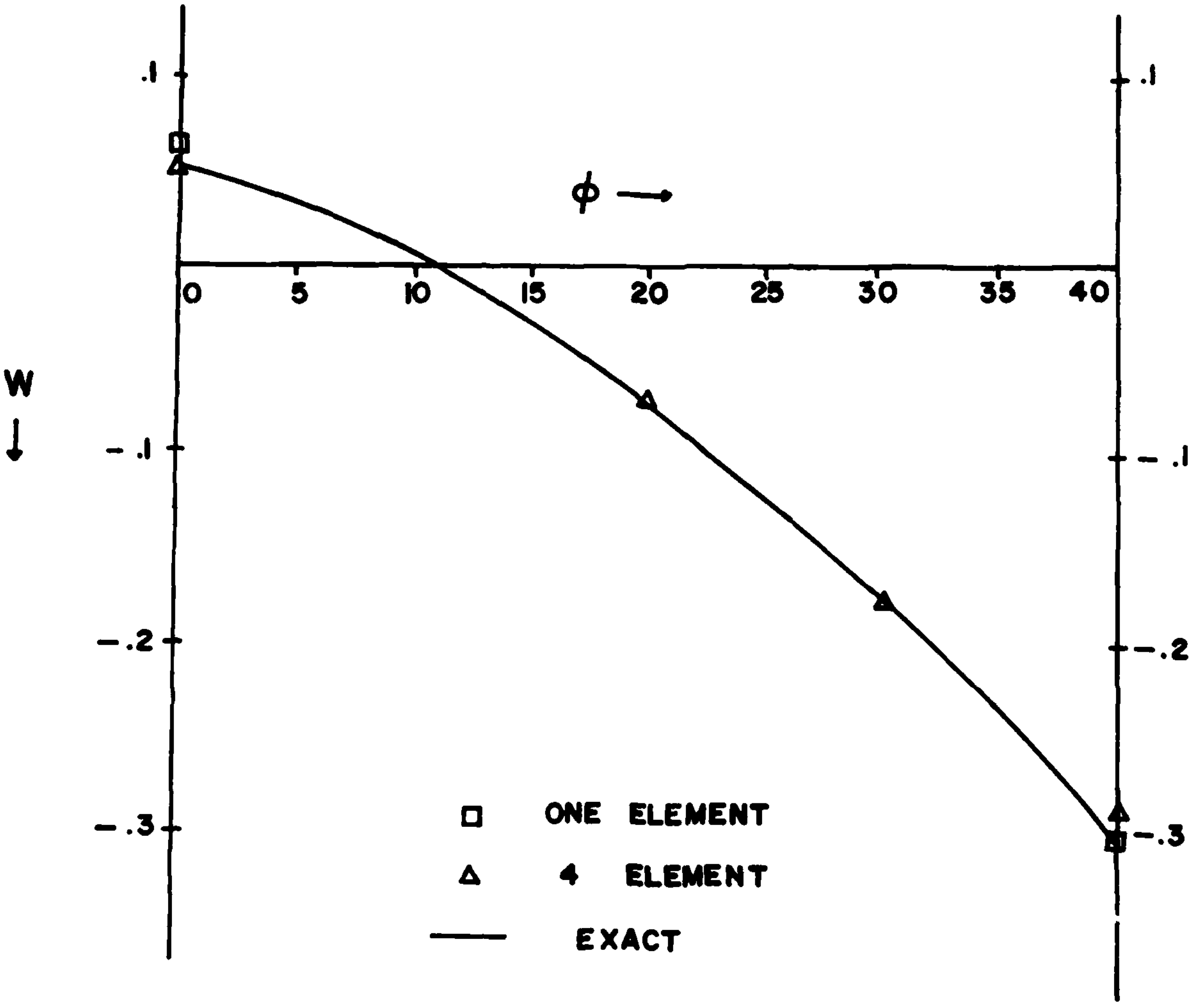

Figure 62. Midspan Vertical Displacement for the Cylindrical Shell Roof

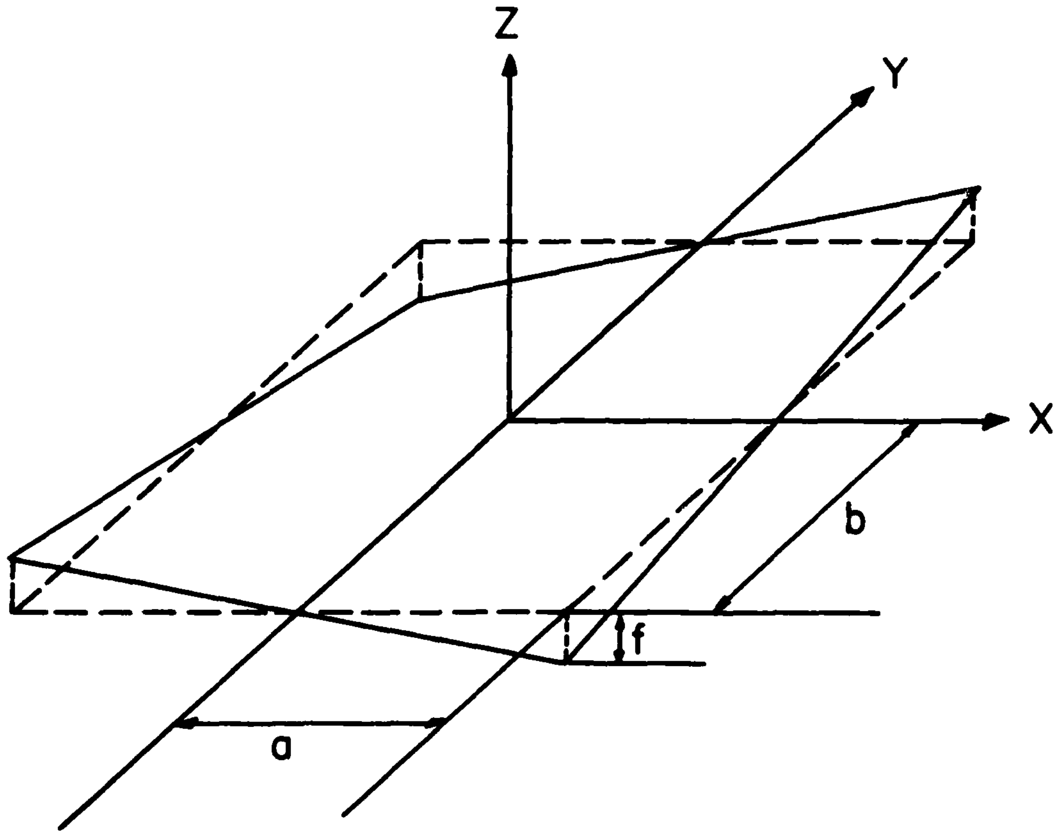

Figure 63. The Geometry of a Hyperbolic Paraboloid

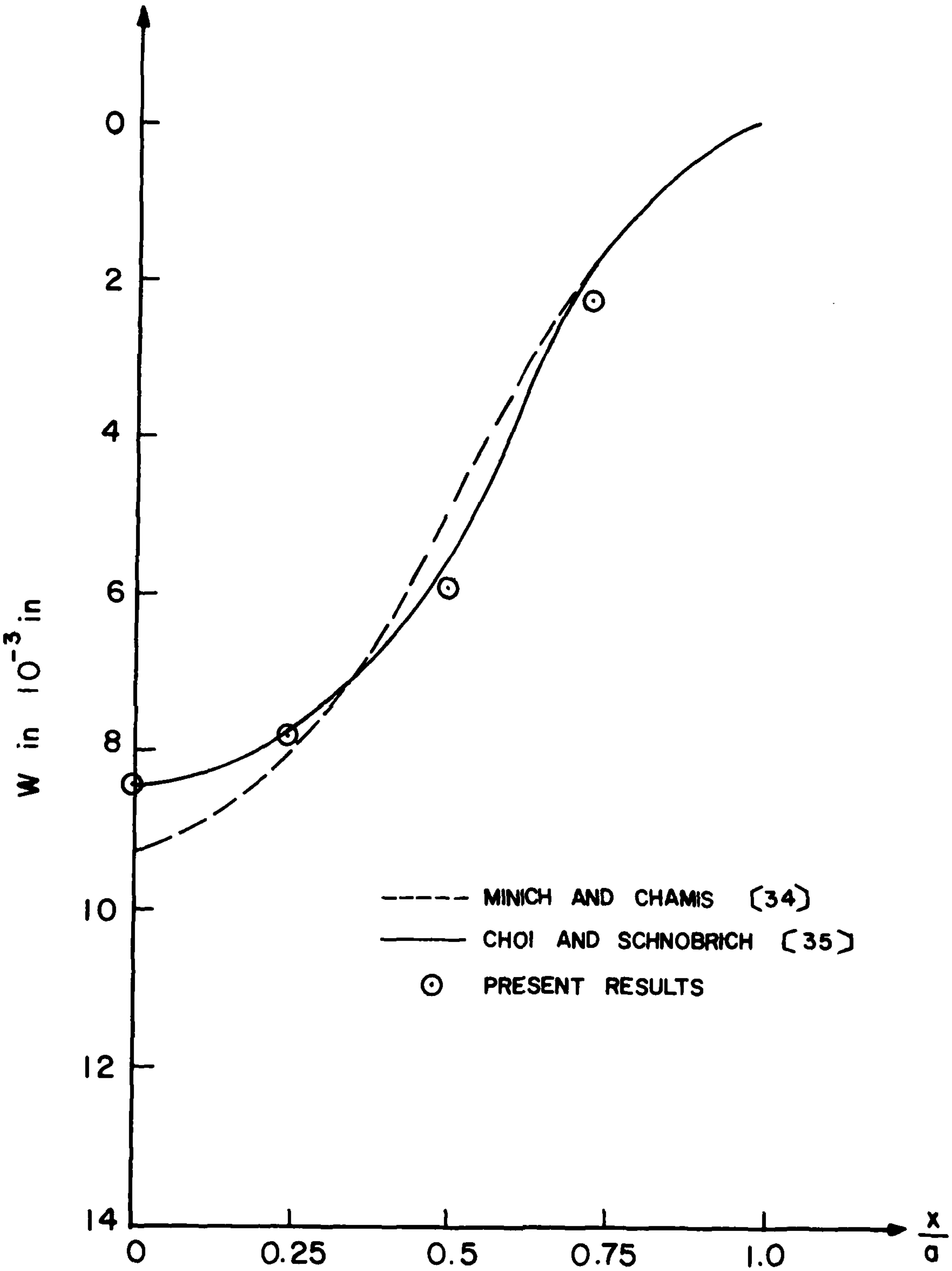

Figure 64. Vertical Deflection Across the Midspan of a Clamped Hyperbolic Paraboloid Under Uniform Load

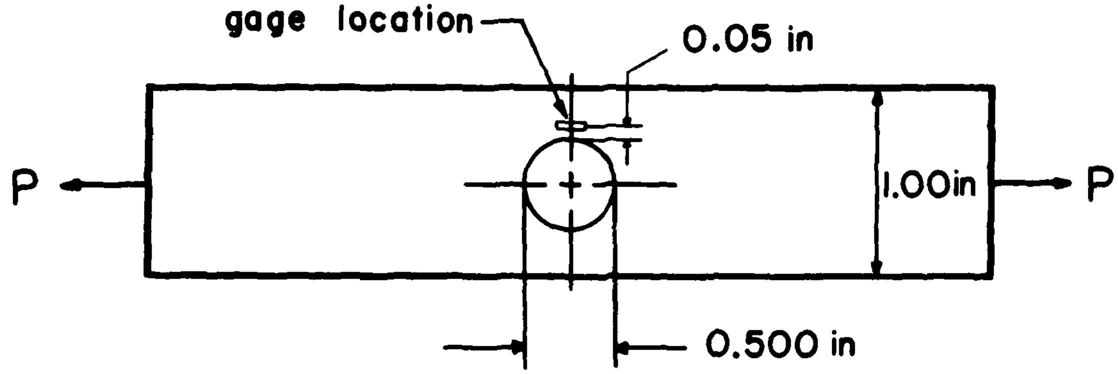

Figure 65. Coupon Dimensions for the $[0/\pm 45/90]_s$ Glass-Epoxy Laminate with a Hole

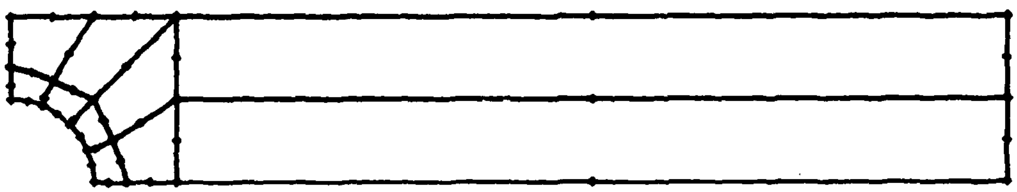

Figure 66. Mesh Layout for the $[0/\pm 45/90]_s$ Coupon with a Hole

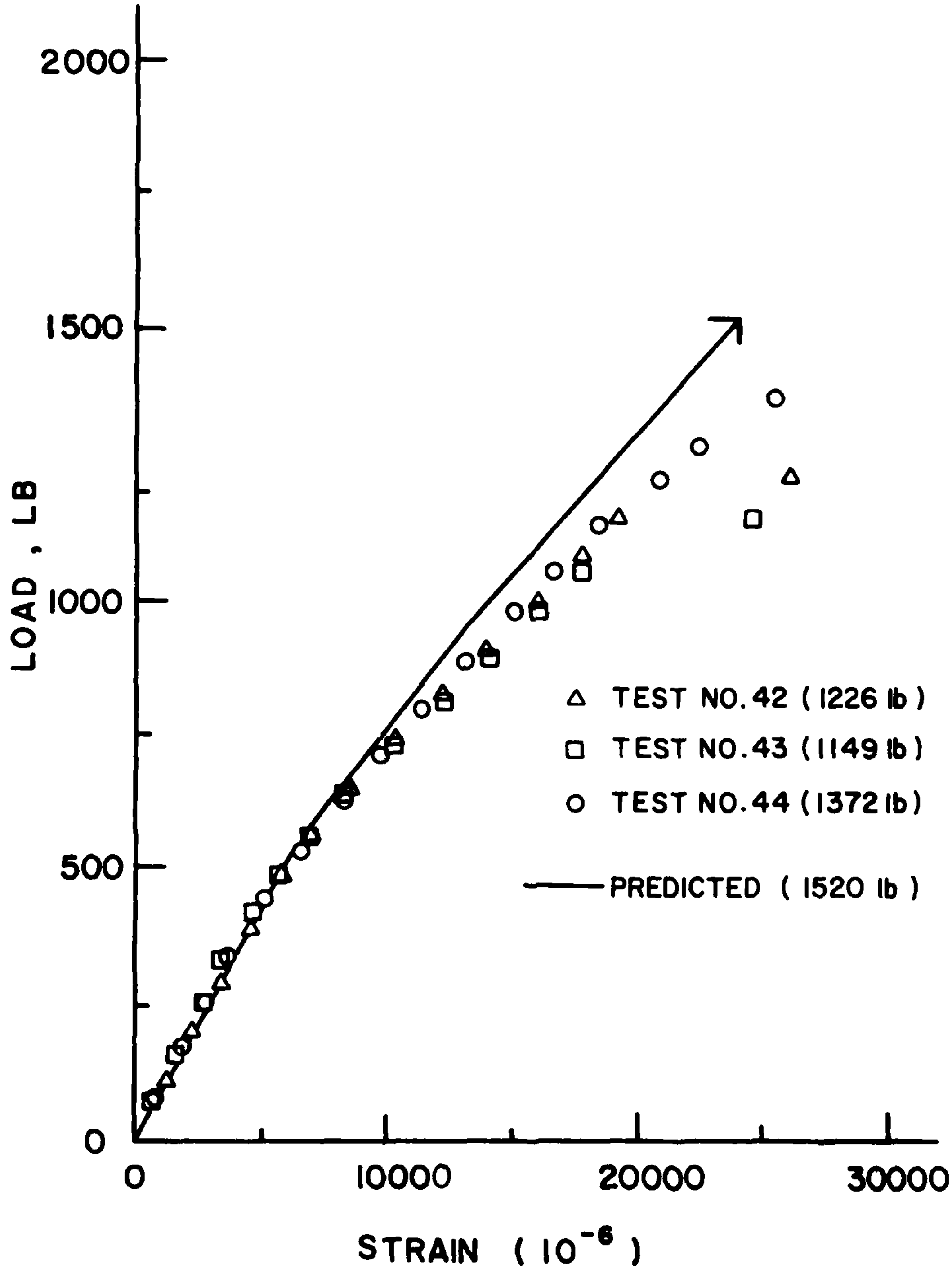

Figure 67. Comparison of the Computed and Test Strain Near a Hole in a $[0/\pm45/90]_s$ Glass-Epoxy Laminate

Appendix A

Data Input for the Program

Card 1 TITLE (13A6)
- Col. 1-70 Alphanumeric statement
- Col. 70-78 "MESH ONLY" if only the mesh generation is desired

Card 2 General Control Card (5I5)
- Col. 1-5 NNP, Number of nodal points
- Col. 6-10 NEL, Number of elements
- Col. 11-15 NMAT, Number of different filamentary composite material
- Col. 16-20 NSHELL, 0 for shell analysis, 1 for plate analysis
- Col. 21-25 NFLAG, 1 for Hill criterion, 2 for Tsai-Wu criterion
- Leave Col. 1-10 blank for mesh generation

Card 3 Load Control Card (6I5)
- Col. 1-5 LD, Load identification 1 for uniform load in x, y, z, direction, 2 for uniform normal pressure, 3 for non-uniform normal load, 4 for concentrated load, 5 for edge pressure
- Col. 6-10 NELPL, Number of element with uniform or non-uniform load
- Col. 11-15 NEDGEL, Number of edge pressure boundary conditions
- Col. 15-20 NLOAD, Number of concentrated loads
- Col. 20-25 INCMAX, Maximum number of increments

If INCMAX is set equal to 1 linear analysis will be executed.

Card 4 Mesh general control card (2I5)
- Col. 1-5 INRG, Number of region
- Col. 6-10 INBP, Number of boundary points to be input

Card 5 X-coordinates of the boundary nodes (8FIO.0)

Card 6 Y-coordinates of the boundary nodes (8FIO.0)

Card 7 Z-coordinates of the boundary nodes (8FIO.0)

This format is repeated until all the nodal values are read.

Card 8 Regions connectivity data (5I5)
- Col. 1-5 NRG, Region number
- Col. 6-10 Four connectivity numbers for a region one for each side.
- Col. 11-15 Each value is the number of the region connected to a
- Col. 16-20 particular side. The sides of the quadrilatural region
- Col. 21-25 are labeled as shown in Figure 58.
- See example for the determination of the connectivity data.

Card 9 Region data (11I5)

Col. 1-5 NRG, Region number
Col. 6-10 NROWS, Number of rows of nodes
Col. 11-15 NCOL, Number of columns of nodes
Col. 16-20
Col. 21-25
Col. 26-30 NDN Global node numbers used to define the quadrilateral.
Col. 31-35
Col. 36-40
Col. 41-45
Col. 46-50
Col. 51-55

Replace Card 4 through Card 9 with the following data Cards if mesh generation is not used. (Substitute cards are indicated by an asterick.)

* Card 4 Nodal coordinates card (A1, I4, 5X,3F10.0, I5) (one for each node)

Col. 2-5 N, Node number
Col. 6-10 Leave blank
Col. 11-20 X(N) X-coordinate
Col. 21-30 Y(N) Y-coordinate
Col. 31-40 Z(N) Z-coordinate
Col. 41-45 KN Node number increment

Nodal coordinate card need not be input in node order sequence, however, all nodal coordinates must be defined. Joint data for a series of nodes may be generated from information given on two cards in sequence:

Card 1 N_1 . . . . .KN_1

Card 2 N_2 . . . . .KN_2

KN_2 is the mesh generation parameter given on the second Card of the sequence. The first generated node is $N_1 + (1 \times KN_2)$; the second generated node is $N_1 + (2 \times KN_2)$; etc. Generation continues until node number $N_2 - KN_2$ is established. Note that the node difference $N_2 - N_1$ must be evenly divisibly by KN_2.

* Card 5 Nodal connectivity card (9I5) (one for each element)

Col. 1-5 N, Element number
Col. 6-10 NOD (N,1)
Col. 11-15 NOD (N,2)
Col. 16-20 NOD (N,3)
Col. 21-25 NOD (N,4) Global nodal point number corresponding
Col. 26-30 NOD (N,5) to element nodes
Col. 31-35 NOD (N,6)
Col. 36-40 NOD (N,7)
Col. 41-45 NOD (N,8)

Card 10 Nodal ID Card (7I5) (one for each node)

Col. 1-5 N, Node number
Col. 6-10 ID(N,1) x-translation boundary condition code
Col. 11-15 ID(N,2) y-translation boundary condition code
Col. 16-20 ID(N,3) z-translation boundary condition code
Col. 21-25 ID(N,4) α-rotation boundary condition code
Col. 26-30 ID(N,5) β-rotation boundary condition code
Col. 31-35 KN Node number increment

Note that an unspecified (ID = 0) degree of freedom is free to translate or rotate as the solution dictates. Delated (ID = 1) degrees of freedom are removed from the final set of equilibrium equations. ID = -1 is used in the generation of boundary condition code 1. Generation of the boundary code is used when a series of nodal cards all have fixity in a given direction. For example, a flat plate lying in the x-y plane subjected to plane stress state will have ID(N,3) = ID(N,4) = ID(N,5) = 1 for all the nodes. Rather than punching "1" in column 20, 25, 30 on all the cards it is possible to just punch "-1" in the column 19-20, 24-25, 29-30 of the first nodal card and enter 1 for KN in the last nodal card. The program will set ID(N,3) = ID(N,4) = ID(N,5) = -1 on all of the intervening cards. A code of -1 is then interpreted in the same way as +1 (i.e. fixed).

Card 11 Material Property card (8F10.0) (one for each type of material)

Col. 1-10 E(I) E_L longitudinal Young's modulus
Col. 11-20 PR(I) VTL Major Poisson's ratio
Col. 21-30 E2(I) E_T transverse Young's modulus
Col. 31-40 G1(I) GLT shear modulus in the L-T plane of the unidirectional composite
Col. 41-50 G2(I) GT shear modulus
Col. 51-60 VTT minor Poisson's ratio
Col. 61-70 WRANG(I) ply angle

Note that a different ply angle is considered to be a different material. The ply angle is defined by the angle between the intrinsic coordinates and the principal material coordinates.

Card 12 Yield strength for unidirectional composite (8FI0.0) (one for each type of material)

Col. 1-10 YLDX tensile yield stress in longitudinal direction
Col. 11-20 YLDY tensile yield stress in transverse direction
Col. 21-30 YLDS shear yield stress in L-T plane
Col. 31-40 YLDXX compressive yield stress in longitudinal direction
Col. 41-50 YLDYY compressive yield stress in transverse direction

Omit card 11 if INCMAX = 1.

Card 13 Layer information card (3I5) (one card for each element)
    Col. 1-5   L Element number
    Col. 6-10 NLAYER Number of layers
    Col. 11-15 KN Generation code

If KN is left blank, one card is needed for each element. If KN is set equal to 1, only the first element in the series need be provided. The other will be set equal to the first element.

Card 14 Layer property set (2I5, Fio.4, I5) (one set for each element)
    Col. 1-5   LN Layer number
    Col. 6-10 MTYPE Material type number
    Col. 11-20 THL Thickness of the layer
    Col. 21-25 KN Generation code

KN is defined the same way as in Card 12. If KN is left blank one set of cards is needed for each element. If KN is set equal to one at the last card of the first set, then only the first set is needed for the first element.

Card 15 Cubic spline control card (I5, 5X, 2F10.0)
    Col. 1-5   N Number of segments of stress-strain curve to be fit
    Col. 6-10 Leave blank
    Col. 11-20 E The initial shear modulus
    Col. 21-30 ES The last shear modulus

Card 16 Discreet values from the shear curve (2F10.0) (one for each station)
    Col. 1-10 F(I) Value of shear stress at station I
    Col. 11-20 X(I) The corresponding shear strain

Omit Card 15 and 16 if INCMAX = 1.

Card 17 Concentrated load card (I5, 5X, 3F01.4) (one for each load)
    Col. 1-5 ND Node number where load applied
    Col. 6-10 Leave blank
    Col. 11-20 IDIRN Direction of the applied load
        1 for x-direction
        2 for y-direction
        3 for z-direction
    Col. 21-20 FLOAD Magnitude of the applied force, positive if in the positive direction of the axis, negative if opposite to the direction of axis

Card 18 Distributed body load card (I5, 5X, 3F10.4, I5) (one for each element)
    Col. 1-5   L Element number
    Col. 6-10 Leave blank
    Col. 11-20 Px x-component of the body force per unit volume
    Col. 21-30 Py y-component of the body force per unit volume
    Col. 31-40 Pz z-component of the body force per unit volume
    Col. 41-45 KN generation code

Omit card 18 if LD $\neq$ 1.

Card 19 Edge pressure load card (2I5, F10.4) (one for each load)
Col. 1-5 L Element number
Col. 6-10 ISIDE Side number
Col. 11-20 PMLD Edge pressure positive if in the same direction as the outward normal of the edge surface

Omit Card 19 if LD ≠ 5.

Card 20 Surface pressure load card (I5, 5X, F10.4, I5) (one for each element)
Col. 1-5 L Element number
Col. 6-10 Leave blank
Col. 11-20 PN Surface pressure, positive if in the same direction as the outward normal of the surface
Col. 21-25 KN Generation code

Card 21 Non-uniform surface load set (I5, 1, 8F10.0) (two for each element)
Col. 1-5 L Element number

Card 22 (Continuation of Card 21)
Col. 1-10 PU(L, 1)
Col. 11-20 PU(L, 2)
Col. 21-30 PU(L, 3)
Col. 31-40 PU(L, 4) Pressure intensity at the eight nodes of
Col. 41-50 PU(L, 5) the element.
Col. 51-60 PU(L, 6)
Col. 61-70 PU(L, 7)
Col. 71-80 PU(L, 8)

Omit Card 20 and 21 if LD ≠ 3.

Note on Region Connectivity Data for Mesh Generation

A domain is generally modeled using several quadrilateral regions connected to one another along one or more sides. The possibility of a common boundary between two regions requires that certain information be provided. The determination of this connectivity data is best illustrated through an example as the four region body in Figure 59. The ξ η coordinate system and the region number have been assigned. The sides of each region are indicated by the number 1 to 4. The connectivity data for the four region body is as follows:

Region	1	2	3	4
1	2	3	0	0
2	4	1	0	0
3	4	0	0	1
4	2	0	0	3

The first line of data states that side one of region one is connected to region two and that side two of region one is connected to region three. The two zero values indicate that sides three and four of region one are not connected to any region. There is one line of data for each region.

APPENDIX B

```
$RESET LIST
FILE  1(TITLE="CH/TAPE",KIND=DISK,FILETYPE=7)
      COMMON/SET2/INC,NFLAG,YLDX(4),YLDY(4),YLDS(4),YLDXX(4)
     1,            YLDYY(4),SUMS(100,8,3),KOUNT(100),
     2 KOUNTF(100),NFAIL(100,8),NYIELD(100,8)
     3,SUMSIG(100,8,3),SUMSTN(100,20),SUMEX(100,20)
     4,SUMSX2(100,20)
      COMMON/H1/ X(163),Y(163),Z(163),ID(163,5)
      COMMON/H3/E(4),PR(4),NOD(44,8),MTYPE(3,44),TH(44),SE
     1(45,45),             PX(44),PY(44),PZ(44),NLAYER(44),THL
     2(8,44)              ,E2(4),G1(4),G2(4),PR2(4),WRANG(4)
      COMMON/SPN/DDD(200),NN3,E5
      DIMENSION TITLE(13)
      DIMENSION F(5),S(320,80),LM(40),FF(45),R(320),SI(9),TI
     1(5)             ,AA(2),FFF(6),AX(136)
      COMMON/G/AMN(163,6),PM(44,4)
      COMMON/P/NSHELL,N9,NEDGEL,KOUNTY,KOUN
      COMMON/SOL/RR(302)
      COMMON/TEST/INCMAX
      COMMON/LOAD/PN(44),PU(44,8)
      COMMON/LOADGH/LD,NEQ,NLOAD,NEL,NELPL,NNP
      DATA AA/-.57735027,.57735027/
      DATA IPRC/1HF/
      DATA WORD1/6HH ONLY/
      N9=8
      NFE=8
      NES=320
      NEC=80
      READ(5,901)(TITLE(I),I=1,13)
      WRITE(6,901)(TITLE(I),I=1,13)
  901 FORMAT(13A6)
      READ (5,5)NNP,NEL,NMAT,NSHELL,NFLAG
      READ(5,6)LD,NELPL,NEDGEL,NLOAD,INCMAX,NELSP
      IF(NELPL.EQ.0)NELPL=NEL
    6 FORMAT(6I5)
      IF(NFLAG.EQ.0) NFLAG=2
      WRITE(6,2000)NNP,NEL,NMAT,NEDGEL,NLOAD,NSHELL,NFLAG
     1,INCMAX      ,LD
      NTDF=5*NNP
        IF(NNP.NE.0.AND.NEL.NE.0)GO TO 300
C**   MESH GENERATION
      CALL MESH8(X,Y,Z,NOD,NNP,NEL,44,TITLE)
      IF(TITLE(13).EQ.WORD1) CALL EXIT
      NTDF=5*NNP
      IF(NELPL.EQ.0) NELPL=NEL
      GO TO 305
  300 CONTINUE
C**   INPUT NODAL  COORDINATES
      CALL  INPUT(X,Y,Z,NNP)
C**   INPUT ELEMENT CONNECTIVITY DATA
      DO 620 M=1,NEL
```

```
      READ (5,615)N,(NOD(N,I),I=1,8)
      WRITE(6,615)N,(NOD(N,I),I=1,8)
  620 CONTINUE
  305 CONTINUE
C**   INPUT ID CODES
      CALL INID(ID,NNP,NEQ)
  615 FORMAT(9I5)
      WRITE(6,2010)
      WRITE(6,2005)(N,(ID(N,I),I=1,5),X(N),Y(N),Z(N),N=1
     1,NNP)
 2005 FORMAT(6I5,5X,3F13.3)
 9020 FORMAT(1H1)
      WRITE(6,2020)
      WRITE(6,2025)(N,(NOD(N,I),I=1,8),N=1,NEL)
      WRITE(6,2030)
C**   INPUT MATERIAL DATA
      DO 5 I=1,NMAT
      READ (5,3)  E(I),PR(I),E2(I),G1(I),G2(I),PR2(I),WRANG
     1(I)
      IF(INCMAX.NE.1)READ(5, 3)YLDX(I),YLDY(I),YLDS(I),YLDXX
     1(I),YLDYY(I)
      WRITE(6,2035)I,  E(I),PR(I),E2(I),G1(I),G2(I),PR2(I)
     1,WRANG(I),          YLDX(I),YLDY(I),YLDS(I),YLDXX(I)
     2,YLDYY(I)
    5 CONTINUE
    3 FORMAT(8F10.0)
    4 FORMAT(I5,12E10.3)
      KN=0
      WRITE(6,2040)
C**   INPUT NUMBER OF LAYER FOR EACH ELEMENT
      DO 17 M=1,NEL
      IF(KN.EQ.0)READ (5,28)L,NLAYER(L),KN
      IF(KN.EQ.0)GO TO 27
      NLAYER(M)=NLAYER(1)
   27 CONTINUE
   17 WRITE(6,2045)M,NLAYER(M),KN
   28 FORMAT(3I5)
      KN=0
      WRITE(6,2050)
      DO 420 M=1,NEL
      NPLY=NLAYER(M)
      TL=0.
C**   INPUT MATERIAL TYPE AND THICKNESS OF EACH LAYER
      DO 410 LA=1,NPLY
       IF(KN.EQ.0)READ(5,12)LN,MTYPE(LN,M),THL(LN,M),KN
      IF(KN.EQ.0) GO TO 411
      MTYPE(LA,M)=MTYPE(LA,1)
      THL(LA,M)=THL(LA,1)
  411 TL=TL+THL(LA,M)
  410 WRITE(6,2055)M,LA,MTYPE(LA,M),THL(LA,M),KN
      TH(M)=TL
```

```
  420 CONTINUE
   12 FORMAT(2I5,F10.4,I5)
      IF(INCMAX.EQ.1) GO TO 3030
C**   CALL CUBIC SPLINE FIT
      CALL SPLINE(DDD(1),DDD(51),DDD(101),DDD(151),NN3,E5)
 3030 CONTINUE
C**   INPUT LOADING
      CALL INLOAD(R,PX,PY,PZ,PM,PN,FU,NEDGEL)
      MBAND=0
      LIM=NPE*5
      KOUNTY=0
      DO 905 M=1,NEL
      KOUNTF(M)=0
      KOUNT(M)=0
      DO 905 L=1,NPLY
      SUMSTN(M,L)=0.
      SUMEX(M,L)=0.
      SUMSX2(M,L)=0.
      DO 905 I=1,3
      SUMSIG(M,L,I)=0.
  905 SUMS(M,L,I)=0.
      DO 600 INC=1,INCMAX
      DO 605 I=4,6
  605 FFF(I)=0.
      IF(INC.GE.2.AND.KOUNTY.NE.1)GO TO 505
      DO 11 I1=1,NEQ
      RF(I1)=R(I1)
      DO 11 J1=1,NOC
   11 S(I1,J1)=0.
      DO 500 M=1,NEL
      DO 501 IV=1,NPE
      I1=5*(IV-1)
      N1=NOD(M,IV)
      DO 501 JV=1,5
      IJ=I1+JV
  501 LM(IJ)=ID(N1,JV)
   21 FORMAT(20I5)
C**   CALCULATE BANDWIDTH AND ELEMENT STIFFNESS
      CALL BANCAL (MBAND,LM,NPE)
      CALL ELEMNT(M,FF)
      DO 415 LL=1,LIM
      I=LM(LL)
      IF(I.LE.0) GO TO 415
      RF(I)=RF(I)+FF(LL)
      DO 400 MM=1,LIM
      J=LM(MM)-I+1
      IF(J.LE.0) GO TO 400
      S(I,J)=S(I,J)+SE(LL,MM)
  400 CONTINUE
  415 CONTINUE
  500 CONTINUE
```

```
   18 FORMAT(1X,5H NEQ=,I5,5X,7H MBAND=,I5)
C**    DISPLACEMENT CACULATION
       CALL BANSOL(1,MBAND,NEQ,RR,S,NDR,NDC)
       CALL BANSOL(2,MBAND,NEQ,RR,S,NDR,NDC)
       WRITE(6,2060)
  505  CONTINUE
       DO 777 N=1,NNP
       DO 776 J=1,5
       F(J)=0.
       II=ID(N,J)
       IF(II.EQ.0) GO TO 776
       F(J)=RR(II)
  776  CONTINUE
       DO 778 I=1,3
  778  FFF(I)=F(I)
       FFF(4)=AMN(N,1)*F(4)+AMN(N,4)*F(5)
       FFF(5)=AMN(N,2)*F(4)+AMN(N,5)*F(5)
       FFF(6)=AMN(N,3)*F(4)+AMN(N,6)*F(5)
       IF(INC.EQ.1)WRITE(6,902)N,(FFF(I6),I6=1,6)
  777  CONTINUE
       IF(INCMAX.EQ.1)WRITE(6,2070)
       IF(INC.EQ.2)WRITE(6,2080)
C**    STRESS CACULATION
       DO 800 M=1,NEL
       CALL STRESS(M,NELSP)
  800  CONTINUE
       DO 1777 N=1,NNP
       DO 1776      J=1,5
       F(J)=0.
       II=ID(N,J)
       IF(II.EQ.0) GO TO 1776
       F(J)=RR(II)
 1776  CONTINUE
       X(N)=X(N)+F(1)
       Y(N)=Y(N)+F(2)
       Z(N)=Z(N)+F(3)
 1777  CONTINUE
  902  FORMAT(1X,I5,3F14.4,4X,3E14.4)
  600  CONTINUE
 2000  FORMAT(1H1     1X,37HC O N T R O L   I N F O R M A T I
     1 O N          //     1X,21HNUMBER OF NODAL POINT 29
     2(1H.)          1H= I5 /    1X,18HNUMBER OF ELEMENT 32
     3(1H.)                  1H= I5 /     1X,18HNUMBER OF
     4 MATERIAL 32(1H.)                1H= I5/      1X,32HNO.
     5 OF ELEMENT WITH EDGE LOADING 18(1H.)1H= I5 /      1X
     6,24HNO. OF CONCENTRATED LOAD 26(1H.)           1H= I5 /
     7    1X,6HNSHELL 44(1H.)                              1H=
     8 I5 /      1X,27H  EQ., 0 FOR SHELL ANALYSIS
     9          /      1X,28H   EQ., 1 FOR PLATE ANALYSIS
     1            /      1X,5HNFLAG 45(1H.)
     2              1H= I5 /      1X,22H  EQ., 1 HILL CRITERIA
```

```
     3                    /      1X,25H   EQ.. 2 TSAI-WU
     4 CRITERIA                           /      1X,18HMAX.
     5 INCREMENT NO. 32(1H.)                   1H= I5 /      1X
     6,9HLOAD TYPE 41(1H.)      1H= I5 /      1X 44H  EQ.. 1
     7 DISTRIBUTED LOAD IN X Y Z DIRECTION  /       1X 20H
     8 EQ.. 2 NORMAL LOAD  /       1X 36H  EQ.. 3 NONUNIFORM
     9 DISTRIBUTED LOAD  /       1X 26H  EQ.. 4 CONCENTRATED
     1 LOAD  /       1X 18H  EQ.. 5 EDGE LOAD /       )
2025 FORMAT(I5,5X,8I5)
2030 FORMAT( //      1X 8HMATERIAL 10X 1HE 8X 2HE2 8X 2HPR
     1 8X 2HG1      8X,2HG2 7X 3HPR2 5X 5HWRANG      6X 4HYLDX
     2 6X 4HYLDY 6X 4HYLDS 5X 5HYLDXX 5X 5HYLDYY  /       1X
     3 7H NUMBER       )
2035 FORMAT(I5,7X,12E10.3)
2020 FORMAT( 1H1       34H...8 NODE THICK SHELL ELEMENT DATA
     1                //       1X 7HELEMENT 15X 12HCONNECTIVITY
     2                    /      1X,5H   NO.      48H         1
     3 2     3     4     5     6     7     8       )
2010 FORMAT( ////      1X,20HGENERATED NODAL DATA
     1                ////      1X,16HEQUATION NUMBERS
     2            ////      1X,31HNODE   DEGREE OF FREEDOM
     3  12X      1X,23HNODAL POINT COORDINATES
     4          /       1X 34HNUMBER  X     Y     Z  ALPHA BATA
     5 9X 1HX12X 1HY 12X 1HZ       )
2040 FORMAT(////      1X 22HELEMENT    LAYER      KN  /      1X
     1 16H    NO.       NO.          /,)
2045 FORMAT(1X,I5,5X,I3,7X,I2)
2050 FORMAT(////      1X 39HELEMENT    LAYER    MATERIAL
     1 THICKNESS  /       1X 16H    NO.         NO.    /,)
2055 FORMAT(1X,I5,5X,I3,7X,I3,8X,F10.4,I5)
2060 FORMAT(1H1      1X 40H N O D E    D I S P L A C E M E N
     1 T S / R      1X 40H O T A T I O N
     2          //      1X 40H  NODE              X-            Y
     3 1X 40H  Z-                X-               Y      1X 40H
     4 Z-                                           /        1X
     5 40HNUMBER    TRANSLATION   TRANSLATION   TRA       1X
     6 40HNSLATION        ROTATION        ROTATION      1X 40H
     7 ROTATION                                     /       )
2070 FORMAT(1H11X 48H...8-NODE THICK SHELL ELEMENT STRESS
     1 COMPUTED AT1X 8HCENTROID // 1X 14HELEMENT LAYER 18X
     2 6HSIG-XX 8X 1HS        49HIG-YY               SIG-ZZ
     3     SIG-XY             S       21HIG-YZ              SIG-ZX
     4                       /)
2080 FORMAT(1H1       1X 43H INC EL. NO.  LAYER  YIELD
     1 SIGX           SIGY51H          SIGXY          S1
     2 S2              S1216H          STRAIN/)
      CALL EXIT
      END
      SUBROUTINE ELEMNT(MM,F)
      COMMON/SET2/INC,NFLAG,YLDX(4),YLDY(4),YLDS(4),YLDXX(4)
     1,            YLDYY(4),SUMS(100,8,3),KOUNT(100),
```

```
     2 KOUNTF(100),NFAIL(100,8),NYIELD(100,8)
     3,SUMSIG(100,9,3),SUMSTN(100,20),SUMEX(100,20)
      COMMON/YIELD/LL,MT,EL,ET,GLT,VTL,VTT,G23,G13,AL1,IPC
      COMMON/H1/X(163),Y(163),Z(163),ID(163,5)
      COMMON/H2/XL(9),YL(9),ZL(9),V1(9),V2(9),V3(9),
     1  JAC(3,3),N(9),NS(9),NT(9)          ,D1(9),D2(9),D3
     2(9),W1(9),W2(9),W3(9)
      COMMON/H22/TT,U11,U21,U31,U12,U22,U32,I
      COMMON/H3/E(4),PR(4),NOD(44,8),MTYPE(3,44),TH(44),SE
     1(45,45),              PX(44),PY(44),PZ(44),NLAYER(44),THL
     2(8,44)             ,E2(4),G1(4),G2(4),PR2(4),WRANG(4)
     3        ,Q(6,6),H(9)
      COMMON/SPN/DDD(200),NN3,ES
      COMMON/G/AMN(163,6),PM(44,4)
      DIMENSION B(6,45),B3(6,45),KKK(6),EB(6,45),DB(6,45),EE
     1(6,6),W(2)   ,FX(45),FY(45),FZ(45),F(45),AA(2),DE(6,6)
     2,CD(6,6),DEB(6,45)   ,DEB1(6,45)             ,FF2(5)
     3     ,PO(9),FXX(9),FYY(9),FZZ(9)             ,EESAV(6,6)
     4,CESAV(6,6),DDSAV(6,6)
      COMMON/P/NSHELL,N9,NEDGEL,KOUNTY,KOUN
      COMMON/LOAD/PN(44),PU(44,8)
      COMMON/LOADGH/LD
      COMMON/K/K1,K2,K3,K4,K5
      DATA W/1.,1./
      DATA AA/-.57735027,.57735027/
      REAL N,NS,NT,JAC,NU12,NU21
      NNN=INC-1
      N45=N9*5
      DO 100 I1=1,8
      XL(I1)=X(NOD(MM,I1))
      YL(I1)=Y(NOD(MM,I1))
      ZL(I1)=Z(NOD(MM,I1))
      PO(I1)=PU(MM,I1)
  100 CONTINUE
  105 FORMAT(8F10.0)
      XL(9)=-(XL(1)+XL(3)+XL(5)+XL(7))/4.+(XL(2)+XL(4)+XL(6)
     1+XL(8))/2.
      YL(9)=-(YL(1)+YL(3)+YL(5)+YL(7))/4.+(YL(2)+YL(4)+YL(6)
     1+YL(8))/2.
      ZL(9)=-(ZL(1)+ZL(3)+ZL(5)+ZL(7))/4.+(ZL(2)+ZL(4)+ZL(6)
     1+ZL(8))/2.
      PO(9)=-(PO(1)+PO(3)+PO(5)+PO(7))/4.+(PO(2)+PO(4)+PO(6)
     1+PO(8))/2.
      GO TO (1,2,6,6,6),LD
    1 CONTINUE
      PTX=PX(MM)
      PTY=PY(MM)
      PTZ=PZ(MM)
      GO TO 6
    2 CONTINUE
      PNLJAC=PN(MM)
```

```
    5 CONTINUE
      DO 26 K=1,N45
      F(K)=0.
      FX(K)=0.
      FY(K)=0.
      FZ(K)=0.
      DO 26 L=1,N45
   26 SE(K,L)=0.
      DO 25 K=1,6
      DO 25 L=1,6
      DE(K,L)=0.
      CE(K,L)=0.
   25 EE(K,L)=0.
      NPLY=NLAYER(MM)
      TT=TH(MM)
      H(1)=-TT/2.
      DO 350 I=1,NPLY
  350 H(I+1)=H(I)+THL(I,MM)
      DO 400 LL=1,NPLY
      NFAIL(MM,LL)=0
      NYIELD(MM,LL)=0
      MT=MTYPE(LL,MM)
      IF(INC.EQ.1) GO TO 6001
      SN12=SUMSTN(MM,LL)
      X1=ABS(SN12)
      CALL FUNCT(DDD(1),DDD(51),DDD(101),DDD(151),Y1,NN3,X1
     1,YP,YPP,55)
      G1(MT)=YP
      G2(MT)=YP
 6001 CONTINUE
      AL1=WHANG(MT)*3.141592654/180.
      TT1=(H(LL+1)-H(LL))/TT
      TT2=((2.*H(LL+1)/TT)**2-(2.*H(LL)/TT)**2)/4.
      TT3=((2.*H(LL+1)/TT)**3-(2.*H(LL)/TT)**3)/6.
      EL=E(MT)
      ET=E2(MT)
      VTL=PR(MT)
      VTT=PR2(MT)
      GLT=G1(MT)
      GT=G2(MT)
      IF(ET.EQ.0.)ET=EL
      IF(GLT.EQ.0.)GLT=EL/(2.*(1.+VTL))
      IF(VTT.EQ.0.) VTT=VTL
      IF(GT.EQ.0.)GT=ET/(2.*(1.+VTT))
      G23=GLT
      G13=GT
      IF(INC.EQ.1)GO TO 302
      IPC=0
      CALL YIELD(MM)
  302 CONTINUE
      CALL QMAT(Q)
```

```
      DO 520 I=1,6
      DO 520 J=1,6
      EE(I,J)=EE(I,J)+ Q(I,J)*TT1
      DE(I,J)=DE(I,J)+Q(I,J)*TT2
      DD(I,J)=DD(I,J)+Q(I,J)*TT3
  520 CONTINUE
      IF(NFAIL(MM,LL).EQ.1.AND.KOUNTF(MM).EQ.2) CALL EXIT
  400 CONTINUE
      DO 530 I=1,6
      DO 530 J=1,6
      EESAV(I,J)=EE(I,J)
      DESAV(I,J)=DE(I,J)
      DDSAV(I,J)=DD(I,J)
  530 CONTINUE
      IF(NSHELL.NE.0) GO TO 54
      CALL SURVEC(TT)
      GO TO 59
   54 CONTINUE
      DO 56 I=1,N9
      V1(I)=0.
      V2(I)=0.
   56 V3(I)=TT
   59 CONTINUE
      DO 50 I=1,6
      DO 50 J=1,N45
      BB(I,J)=0.
   50 B(I,J)=0.
      DO 200 KK=1,2
      DO 200 II=1,2
      DO 200 JJ=1,2
      SS=AA(II)
      T1=AA(JJ)
      ZK=AA(KK)
      WI=W(II)
      WJ=W(JJ)
      WK=W(KK)
      CALL SHAPE(SS,T1,ZK,DETJAC)
      DO 540 I=1,6
      DO 540 J=1,6
      EE(I,J)=EESAV(I,J)
      DE(I,J)=DESAV(I,J)
      DD(I,J)=DDSAV(I,J)
  540 CONTINUE
      IF(NSHELL.EQ.0)CALL ETRAN(EE,DE,DD)
      XMUL1=WI*WJ*WK*DETJAC
      PNN=0.
      VV1X=0.
      VV2Y=0.
      VV3Z=0.
      DO 152 I=1,N9
      VV1=V1(I)/TT
```

```
      VV2=V2(I)/TT
      VV3=V3(I)/TT
      VV1X=VV1X+VV1*N(I)
      VV2Y=VV2Y+VV2*N(I)
      VV3Z=VV3Z+VV3*N(I)
      IF(LD.EQ.3) PNN=PNN+PD(I)*N(I)
  152 CONTINUE
      DO 57 I=1,N9
      IF(NSHELL.NE.0) GO TO 61
      U11=D1(I)
      U21=D2(I)
      U31=D3(I)
      U12=-W1(I)
      U22=-W2(I)
      U32=-W3(I)
      GO TO 57
   61 CONTINUE
      U11=0.
      U21=1.
      U31=0.
      U12= 1.
      U22=0.
      U32=0.
   57 CONTINUE
      IF(I.EQ.9) GO TO 55
      K=NOD(MM,I)
      AMN(K,1)=U11
      AMN(K,2)=U21
      AMN(K,3)=U31
      AMN(K,4)=-U12
      AMN(K,5)=-U22
      AMN(K,6)=-U32
   55 CONTINUE
      CALL BMAT(B,BB)
      GO TO(16,12,13,16,16),LD
   12 CONTINUE
      PTX=PNLOAD*VV1X
      PTY=PNLOAD*VV2Y
      PTZ=PNLOAD*VV3Z
      GO TO 16
   13 PTX=PNN*VV1X
      PTY=PNN*VV2Y
      PTZ=PNN*VV3Z
   16 CONTINUE
      FX(K1)=N(I)*PTX
      FY(K2)=N(I)*PTY
      FZ(K3)=N(I)*PTZ
      FX(K4)=N(I)*U11*TT*WK*PTX*.5
      FX(K5)=N(I)*U12*TT*WK*PTX*.5
      FY(K4)=N(I)*U21*TT*WK*PTY*.5
      FY(K5)=N(I)*U22*TT*WK*PTY*.5
```

```
      FZ(K4)=N(I)*U31*TT*WK*PTZ*.5
      FZ(K5)=N(I)*U32*TT*WK*PTZ*.5
   50 CONTINUE
      DO 60 K=1,6
      DO 60 L=1,N45
      EB(K,L)=0.
      DEB(K,L)=0.
      DEB1(K,L)=0.
      DB(K,L)=0.
      DO 60 M=1,6
      EB(K,L)=EB(K,L)+EE(K,M)*B(M,L)
      DEB(K,L)=DEB(K,L)+DE(K,M)*BB(M,L)
      DEB1(K,L)=DEB1(K,L)+DE(K,M)*B(M,L)
   60 DB(K,L)=DB(K,L)+DD(K,M)*BB(M,L)
      DO 70 K=1,N45
      F(K)=F(K)+(FX(K)+FY(K)+FZ(K))*XMUL1
      DO 70 L=1,N45
      DUM=0.
      DUM1=0.
      DUM2=0.
      DUM3=0.
      DO 65 M=1,6
      DUM1=DUM1+B(M,K)*EB(M,L)
      DUM2=DUM2+B(M,K)*DEB(M,L)
      DUM3=DUM3+BB(M,K)*DEB1(M,L)
   65 DUM=DUM+BB(M,K)*DB(M,L)
   70 SE(K,L)=SE(K,L)+(DUM+DUM1+DUM2+DUM3)*XMUL1
      TOTALA=TOTALA+XMUL1
  200 CONTINUE
      DO 512 I=1,N45
      F(I)=F(I)/TT
  512 CONTINUE
      TOTALA=TOTALA/TT
      IF(NEDGEL.NE.0)              CALL LOCAL(FXX,FYY,FZZ,AA,W
     1,MM)
      DO 509 I=1,5
  509 FF2(I)=0.
      DO 518 I=1,N9
      FF2(1)=FXX(I)
      FF2(2)=FYY(I)
      FF2(3)=FZZ(I)
      DO 518 J=1,5
      I4=(I-1)*5+J
  518 F(I4)=F(I4)+FF2(J)
      RETURN
      END
      SUBROUTINE SHAPE(S,T,ZK,DETJAC)
      COMMON/H2/XL(9),YL(9),ZL(9),V1(9),V2(9),V3(9),
     1  JAC(3,3),N(9),NS(9),NT(9)
      DIMENSION JACI(3,3)
      DIMENSION SI(8),TI(8)
```

```
      DATA SI/-1.,0.,1.,1.,1.,0.,-1.,-1./
      DATA  TI/-1.,-1.,-1.,0.,1.,1.,1.,0./
      REAL JACI
      REAL N,NS,NT,JAC
      DO 11 I=1,8
      DUM1=1.+SI(I)*S
      DUM2=1.+TI(I)*T
      IF(I.EQ.2.OR.I.EQ.6) GO TO 13
      IF(I.EQ.4.OR.I.EQ.8) GO TO 17
      DUM3=S*SI(I)+T*TI(I)-1.
      N(I)=DUM1*DUM2*DUM3/4.
      NS(I)=(DUM1*DUM2+DUM2*DUM3)*SI(I)/4.
      NT(I)=(DUM1*DUM2+DUM1*DUM3)*TI(I)/4.
      GO TO 11
   13 DUM4=1.-S**2
      N(I)=DUM2*DUM4/2.
      NS(I)=-S*DUM2
      NT(I)=TI(I)*DUM4/2.
      GO TO 11
   17 DUM5=1.-T**2
      N(I)=DUM1*DUM5/2.
      NS(I)=DUM5*SI(I)/2.
      NT(I)=-T*DUM1
   11 CONTINUE
      N(9)=(1.-S**2)*(1.-T**2)
      NS(9)=-2.*S*(1.-T**2)
      NT(9)=-2.*T *(1.-S**2)
      DO 15 I=1,3
      DO 15 J=1,3
   15 JAC(I,J)=0.
      DO 20 I =1,8
      JAC(1,1)=JAC(1,1)+NS(I)*XL(I)+NS(I)*ZK*V1(I)/2.
      JAC(1,2)=JAC(1,2)+NS(I)*YL(I)+NS(I)*ZK*V2(I)/2.
      JAC(1,3)=JAC(1,3)+NS(I)*ZL(I)+NS(I)*ZK*V3(I)/2.
      JAC(2,1)=JAC(2,1)+NT(I)*XL(I)+NT(I)*ZK*V1(I)/2.
      JAC(2,2)=JAC(2,2)+NT(I)*YL(I)+NT(I)*ZK*V2(I)/2.
      JAC(2,3)=JAC(2,3)+NT(I)*ZL(I)+NT(I)*ZK*V3(I)/2.
      JAC(3,1)=JAC(3,1)+N(I)*V1(I)/2.
      JAC(3,2)=JAC(3,2)+N(I)*V2(I)/2.
      JAC(3,3)=JAC(3,3)+N(I)*V3(I)/2.
   20 CONTINUE
      DETJAC=JAC(1,1)*JAC(2,2)*JAC(3,3)       +JAC(2,1)*JAC(3
     1,2)*JAC(1,3)       +JAC(3,1)*JAC(1,2)*JAC(2,3)
     2-JAC(1,3)*JAC(3,1)*JAC(2,2)       -JAC(1,2)*JAC(2,1)
     3*JAC(3,3)       -JAC(2,3)*JAC(3,2)*JAC(1,1)
      JACI(1,1)= (JAC(2,2)*JAC(3,3)-JAC(2,3)*JAC(3,2))
     1/DETJAC
      JACI(2,1)=-(JAC(2,1)*JAC(3,3)-JAC(2,3)*JAC(3,1))
     1/DETJAC
      JACI(3,1)= (JAC(2,1)*JAC(3,2)-JAC(2,2)*JAC(3,1))
     1/DETJAC
```

```
      JACI(1,2)=-(JAC(1,2)*JAC(3,3)-JAC(1,3)*JAC(3,2))
     1/DETJAC
      JACI(2,2)= (JAC(1,1)*JAC(3,3)-JAC(1,3)*JAC(3,1))
     1/DETJAC
      JACI(3,2)=-(JAC(1,1)*JAC(3,2)-JAC(1,2)*JAC(3,1))
     1/DETJAC
      JACI(1,3)= (JAC(1,2)*JAC(2,3)-JAC(1,3)*JAC(2,2))
     1/DETJAC
      JACI(2,3)=-(JAC(1,1)*JAC(2,3)-JAC(1,3)*JAC(2,1))
     1/DETJAC
      JACI(3,3)= (JAC(1,1)*JAC(2,2)-JAC(1,2)*JAC(2,1))
     1/DETJAC
      DO 30  I=1,3
      DO 30  J=1,3
   30 JAC(I,J)=JACI(I,J)
      RETURN
      END
      SUBROUTINE SURFAC(XL,YL,ZL,V1,V2,V3,THICKL)
      DIMENSION XL(1),YL(1),ZL(1),V1(1),V2(1),V3(1),KPTS(9
     1,4)
      DATA KPTS/   2,3,4,5,6,9,8,9,4,              1,2,3,4,5
     1,6,7,8,3,                 8,9,2,9,4,5,6,7,6,               1
     2,2,3,4,5,6,7,8,9/
      DO 1  I=1,9
      KP1=KPTS(I,1)
      KP2=KPTS(I,2)
      KP3=KPTS(I,3)
      KP4=KPTS(I,4)
      AL1=XL(KP1)-XL(KP2)
      AM1=YL(KP1)-YL(KP2)
      AN1=ZL(KP1)-ZL(KP2)
      AL2=XL(KP3)-XL(KP4)
      AM2=YL(KP3)-YL(KP4)
      AN2=ZL(KP3)-ZL(KP4)
      AL3=AM1*AN2-AM2*AN1
      AM3=AL2*AN1-AL1*AN2
      AN3=AL1*AM2-AL2*AM1
      Z=SQRT(AL3**2+AM3**2+AN3**2)
      VV1=AL3/Z
      VV2=AM3/Z
      VV3=AN3/Z
      VV1=VV1*THICKL
      VV2=VV2*THICKL
      VV3=VV3*THICKL
      V1(I)=VV1
      V2(I)=VV2
      V3(I)=VV3
    1 CONTINUE
      RETURN
      END
      SUBROUTINE BANSOL(KKK,IBAND,NEQ,R,AK,NDR,NDC)
```

```
      DIMENSION R(1),AK(NDR,NDC)
      NRS=NEQ-1
      NR=NEQ
      IF(KKK.EQ.2) GO TO 200
      DO 120 N=1,NRS
      M=N-1
      MR=MINO(IBAND,NR-M)
      PIVOT=AK(N,1)
      DO 120 L=2,MR
      CP=AK(N,L)/PIVOT
      I=M+L
      J=0
      DO 110 K=L,MR
      J=J+1
  110 AK(I,J)=AK(I,J)-CP*AK(N,K)
  120 AK(N,L)=CP
      GO TO 400
  200 DO 220 N=1,NRS
      M=N-1
      MR=MINO(IBAND,NR-M)
      CP=R(N)
      R(N)=CP/AK(N,1)
      DO 220 L=2,MR
      I=M+L
  220 R(I)=R(I)-AK(N,L)*CP
      R(NR)=R(NR)/AK(NR,1)
      DO 320 I=1,NRS
      N=NR-I
      M=N-1
      MR=MINO(IBAND,NR-M)
      DO 320 K=2,MR
      L=M+K
  320 R(N)=R(N)-AK(N,K)*R(L)
  400 RETURN
      END
      SUBROUTINE BANCAL(MBAND,LM,NPE)
      DIMENSION LM(1)
      MIN=100000
      MAX=0
      LIM=NPE*5
      DO 100 L=1,LIM
      IF(LM(L).EQ.0) GO TO 100
      IF(LM(L).GT.MAX)MAX=LM(L)
      IF(LM(L).LT.MIN)MIN=LM(L)
  100 CONTINUE
      NDIF=MAX-MIN+1
      IF(NDIF.GT.MBAND) MBAND=NDIF
      RETURN
      END
      SUBROUTINE  STRESS(MM,NELSP)
      COMMON/SET2/INC,NFLAG,YLDX(4),YLDY(4),YLDS(4),YLDXX(4)
```

```
     1,           YLDYY(4),SUMS(100,8,3),KOUNT(100),
     2 KOUNTF(100),NFAIL(100,8),NYIELD(100,8)
     3,SUMSIG(100,8,3),SUMSTN(100,20),SUMEX(100,20)
     4 ,SUMSX2(100,20)
      COMMON/YIELD/LL,MT,EL,ET,GLT,VTL,VTT,G23,G13,AL1,IPC
      COMMON/H1/X(163),Y(163),Z(163),ID(163,5)
      COMMON/H2/XL(9),YL(9),ZL(9),V1(9),V2(9),V3(9),
     1  JAC(3,3),N(9),NS(9),NT(9)              ,O1(9),O2(9),O3
     2(9),,W1(9),W2(9),W3(9)
      COMMON/H22/TT,U11,U21,U31,U12,U22,U32,I
      COMMON/H3/E(4),PR(4),NOD(44,3),MTYPE(8,44),TH(44),SE
     1(45,45),            PX(44),PY(44),PZ(44),NLAYER(44),THL
     2(8,44)            ,E2(4),G1(4),G2(4),PR2(4),WRANG(4)
     3        ,Q(6,6),H(9)
      COMMON/SPN/ODD(200),NN3,E5
      COMMON/G/AMN(163,6),PM(44,4)
      COMMON/TEST/INCMAX
      COMMON/K/K1,K2,K3,K4,K5
      DIMENSION B(6,45),BB(6,45),KKK(6),EB(6,45),DB(6,45),EE
     1(6,6),W(2)           ,D(45),AAA(1),           SIGN(6)
     2,SIGM(6),STN(6),STL(6),ST(6),SIG(6),STR(3),
     3 SIGG(3),XI(9),YI(9),ZI(9)           ,SI(9),TI(9),STL2
     4(6),STN2(6),SIG2(6)
      COMMON/P/NSHELL,N9,NEDGEL,KOUNTY,KOUN
      COMMON/SOL/U(302)
      DATA SI/-1.,0.,1.,1.,1.,0.,-1.,-1.,0./
      DATA TI/-1.,-1.,-1.,0.,1.,1.,1.,0.,0./
      DATA W/1.,1./
      REAL N,NS,NT,JAC,NU12,NU21
      N45=40
      NNN=INC-1
      DO 100 I1=1,8
      XL(I1)=X(NOD(MM,I1))
      YL(I1)=Y(NOD(MM,I1))
      ZL(I1)=Z(NOD(MM,I1))
  100 CONTINUE
      XL(9)=-(XL(1)+XL(3)+XL(5)+XL(7))/4.+(XL(2)+XL(4)+XL(6)
     1+XL(8))/2.
      YL(9)=-(YL(1)+YL(3)+YL(5)+YL(7))/4.+(YL(2)+YL(4)+YL(6)
     1+YL(8))/2.
      ZL(9)=-(ZL(1)+ZL(3)+ZL(5)+ZL(7))/4.+(ZL(2)+ZL(4)+ZL(6)
     1+ZL(8))/2.
      TT=TH(MM)
      IF(NSHELL.NE.0) GO TO 54
      CALL SURVEC(TT)
      GO TO 59
   54 CONTINUE
      DO 360 I=1,N9
      V1(I)=0.
      V2(I)=0.
  360 V3(I)=TT
```

```
   59 CONTINUE
      NPLY=NLAYER(MM)
      H(1)=-TT/2.
      DO 350 I=1,NPLY
  350 H(I+1)=H(I)+THL(I,MM)
      DO 400 LL=1,NPLY
      DO 5 K=1,6
      DO 5 L=1,6
    5 EE(K,L)=0.
      MT=MTYPE(LL,MM)
      IF(INC.EQ.1) GO TO 6001
      SN12=SUMSTN(MM,LL)
      X1=ABS(SN12)
      CALL FUNCT(DDD(1),DDD(51),DDD(101),DDD(151),Y1,NN3,X1
     1,YP,YPP,ES)
      G1(MT)=YP
      G2(MT)=YP
 6001 CONTINUE
      AL=WRANG(MT)
      AL1=WRANG(MT)*3.141592654/180.
      AAA(1)=(H(LL)+H(LL+1))/TT
      EL=E(MT)
      ET=E2(MT)
      VTL=PR(MT)
      VTT=PR2(MT)
      GLT=G1(MT)
      GT=G2(MT)
      IF(ET.EQ.0.)ET=EL
      IF(GLT.EQ.0.)GLT=EL/(2.*(1.+VTL))
      IF(VTT.EQ.0.) VTT=VTL
      IF(GT.EQ.0.)GT=ET/(2.*(1.+VTT))
      G23=GLT
      G13=GT
      IF(INC.EQ.1) GO TO 302
      IFC=1
      CALL YIELD(MM)
  302 CONTINUE
      CALL QMAT(Q)
      DO 520 I=1,6
      DO 520 J=1,6
      EE(I,J)=EE(I,J)+Q(I,J)
  520 CONTINUE
      DO 50 I=1,6
      DO 50 J=1,N45
      BE(I,J)=0.
   50 B(I,J)=0.
      NNK=1
      IF(NELSP.NE.0) NNK=2
      DO 633 KK=1,NNK
      S=0.
      T=0.
```

```
      IF(KK.EQ.1 ) GO TO 601
      S=SI(NELSP)
      T=TI(NELSP)
  601 CONTINUE
      ZK=AAA(1)
      CALL SHAPE(S,T,ZK,DETJAC)
      DO 52 I=1,8
      IF(NSHELL.NE.0) GO TO 53
      U11=D1(I)
      U21=D2(I)
      U31=D3(I)
      U12=-W1(I)
      U22=-W2(I)
      U32=-W3(I)
      GO TO 57
   53 CONTINUE
      U11=0.
      U21=1.
      U31=0.
      U12= 1.
      U22=0.
      U32=0.
   57 CONTINUE
      CALL BMAT(B,BB)
   52 CONTINUE
      DO 61 K=1,6
      DO 61 M=1,N45
   61 BB(K,M)=ZK*BB(K,M)
      DO 3 L9=1,8
      L1=NOD(MM,L9)
      L2=5*(L9-1)
      DO 3 L3=1,5
      L5=L2+L3
      D(L5)=0.
      L4=ID(L1,L3)
      IF(L4.EQ.0)GO TO 3
      D(L5)=U(L4)
    3 CONTINUE
      IF(KK.EQ.2) GO TO 630
      DO 600 K=1,6
      DUM=0.
      DO 600 L=1,N45
      DUM=DUM+B(K,L)*D(L)
      DUM=DUM+BB(K,L)*D(L)
  600 STN(K)=DUM
      IF(NSHELL.EQ.0)CALL STRANS(STL,STN,AL,0,0)
      IF(NSHELL.EQ.0)GO TO 610
      DO 620 I=1,6
  620 STL(I)=STN(I)
  610 CONTINUE
      DO 625 K=1,6
```

```
      DUM=0.
      DO 625 L=1,6
      DUM=DUM+EE(K,L)*STL(L)
  625 SIG(K)=DUM
      CALL STRANS(ST,SIG,AL,1,1)
      IF(INCMAX.EQ.1)WRITE(6,2000)MM,LL,(SIG(I),I=1,6)
      GO TO 633
  630 CONTINUE
      DO 640 K=1,6
      DUM=0.
      DO 640 L=1,N45
      DUM=DUM+B(K,L)*D(L)
      DUM=DUM+BB(K,L)*D(L)
  640 STN2(K)=DUM
      IF(NSHELL.EQ.0) CALL STRANS(STL2,STN2,0.,0,0)
      IF(NSHELL.EQ.0) GO TO 650
      DO 645 I=1,6
  645 STL2(I)=STN2(I)
  650 CONTINUE
      DO 655 K=1,6
      DUM=0.
      DO 655 L=1,6
      DUM=DUM+EE(K,L)*STL2(L)
  655 SIG2(K)=DUM
      IF(INCMAX.EQ.1) WRITE(6,2000) MM,LL,(SIG2(I),I=1,6)
  633 CONTINUE
      EXX=STL2(1)
      SUMEX(MM,LL)=SUMEX(MM,LL)+EXX
      SX2=STL(1)
      SUMSX2(MM,LL)=SUMSX2(MM,LL)+SX2
      DSN12=2.*(STL(2)-STL(1))*SN*CS+STL(4)*(CS2-SN2)
      STR(1)=ST(1)
      STR(2)=ST(2)
      STR(3)=ST(4)
      SIGG(1)=SIG(1)
      SIGG(2)=SIG(2)
      SIGG(3)=SIG(4)
      SUMSTN(MM,LL)=SUMSTN(MM,LL)+DSN12
      DO 635 I=1,3
      SUMS(MM,LL,I)=SUMS(MM,LL,I)+STR(I)
  635 SUMSIG(MM,LL,I)=SUMSIG(MM,LL,I)+SIGG(I)
 2000 FORMAT(2I5,18X,6E15.4)
 1632 FORMAT(1X,I5,5E18.6)
  400 CONTINUE
      RETURN
      END
      SUBROUTINE LOCAL(PRX,PRY,PRZ,AA,WW,MM)
      COMMON/A/Q(9),XX(9),YY(9),ZZ(9),V1(9),V2(9),V3(9)
      COMMON/G/AMN(153,5),PNN(44,4)
      COMMON/H2/XX2(9),YY2(9),ZZ2(9),W1(9),W2(9),W3(9)
      DIMENSION XL(9),YL(9),NFPOIN(4,3),          XX1(9),XX3
```

```
     1(9),YY1(9),YY3(9),ZZ1(9),ZZ3(9),          PRX(1),PRY
     2(1),PRZ(1),ZL(9),           PLX(10),PLY(10),PLZ(10),
     3        WX(9),WY(9),WZ(9),           NELEM(3,3),NFP(9)
     4,AA(1),WW(1)            ,PL1(9),PL2(9),PL3(9)
      DATA NELEM / 5,6,7,              4,0,8,                3,2
     1,1/
      DATA NFPOIN /5,7,1,3,             6,8,2,4,
     1 7,1,3,5/
      DATA NFP/1,2,3,6,9,8,7,4,5/
      DO 11       I=1,9
      PRX(I)=0.
      PRY(I)=0.
      PRZ(I)=0.
   11 CONTINUE
      DO 10 I=1,9
      XX3(I)=XX2(I)+W1(I)*.5
      XX1(I)=XX2(I)-W1(I)*.5
      YY3(I)=YY2(I)+W2(I)*.5
      YY1(I)=YY2(I)-W2(I)*.5
      ZZ3(I)=ZZ2(I)+W3(I)*.5
      ZZ1(I)=ZZ2(I)-W3(I)*.5
   10 CONTINUE
      DO 17 IN=1,4
      PN=PNN(MM,IN)
      IF(PN.EQ.0.)GO TO 16
      K1=1
      K2=4
      K3=7
      DO 7 J=1,3
      K=NFPOIN(IN,J)
    3 XL(K1)=XX1(K)
      XL(K2)=XX2(K)
      XL(K3)=XX3(K)
      YL(K1)=YY1(K)
      YL(K2)=YY2(K)
      YL(K3)=YY3(K)
      ZL(K1)=ZZ1(K)
      ZL(K2)=ZZ2(K)
      ZL(K3)=ZZ3(K)
      K1=K1+1
      K2=K2+1
      K3=K3+1
    7 CONTINUE
      DO 14 I=1,9
      K=NFP(I)
      XX(I)=XL(K)
      YY(I)=YL(K)
      ZZ(I)=ZL(K)
   14 CONTINUE
      CALL SURFAC(XX,YY,ZZ,V1,V2,V3,1.)
      DO 121 I=1,9
```

```
      PLX(I)=0.
      PLY(I)=0.
      PLZ(I)=0.
  121 CONTINUE
      AREA=0.
      DO 300 KK=1,2
      DO 300 II=1,2
      DO 300 JJ=1,2
      SS=AA(II)
      T1=AA(JJ)
      ZK=AA(KK)
      WII=WW(II)
      WJJ=WW(JJ)
      WKK=WW(KK)
      CALL SHAP2(SS,T1,ZK,DETJAC)
      XMUL1=WII*WJJ*WKK*DETJAC
      AREA=AREA+XMUL1
      DO 311 I=1,9
      VS=(V1(I)**2+V2(I)**2+V3(I)**2)**.5
      VV1=V1(I)/VS
      VV2=V2(I)/VS
      VV3=V3(I)/VS
      PL1(I)=PN*VV1*Q(I)
      PL2(I)=PN*VV2*Q(I)
      PL3(I)=PN*VV3*Q(I)
  311 CONTINUE
      DO 312 I=1,9
      PLX(I)=PLX(I)+PL1(I)*XMUL1
      PLY(I)=PLY(I)+PL2(I)*XMUL1
      PLZ(I)=PLZ(I)+PL3(I)*XMUL1
  312 CONTINUE
  300 CONTINUE
      PLX(10)=0.
      PLY(10)=0.
      PLZ(10)=0.
      DO 321 J=1,3
      K=NFPOIN(IN,J)
      K1=NELEM(1,J)
      K2=NELEM(2,J)
      K3=NELEM(3,J)
      IF(K2.EQ.0) K2=10
      PRX1=PLX(K1)
      PRX2=PLX(K2)
      PRX3=PLX(K3)
      PRX(K)=PRX(K)+PRX1+PRX2+PRX3
      PRY1=PLY(K1)
      PRY2=PLY(K2)
      PRY3=PLY(K3)
      PRY(K)=PRY(K)+PRY1+PRY2+PRY3
      PRZ1=PLZ(K1)
      PRZ2=PLZ(K2)
```

```
      PRZ3=PLZ(K3)
      PRZ(K)=PRZ(K)+PRZ1+PRZ2+PRZ3
  321 CONTINUE
   16 CONTINUE
   17 CONTINUE
      RETURN
      END
      SUBROUTINE SHAP2(S,T,ZK,DETJAC)
      COMMON/A/N(9),XL(9),YL(9),ZL(9),V1(9),V2(9),V3(9)
      DIMENSION SI(8),TI(8),NS(9),NT(9),JAC(3,3)
      DATA SI/-1.,0.,1.,1.,1.,0.,-1.,-1./
      DATA TI/-1.,-1.,-1.,0.,1.,1.,1.,0./
      REAL N,NS,NT,JAC
      DO 11 I=1,8
      DUM1=1.+SI(I)*S
      DUM2=1.+TI(I)*T
      IF(I.EQ.2.OR.I.EQ.6) GO TO 13
      IF(I.EQ.4.OR.I.EQ.8) GO TO 17
      DUM3=S*SI(I)+T*TI(I)-1.
      N(I)=DUM1*DUM2*DUM3/4.
      NS(I)=(DUM1*DUM2+DUM2*DUM3)*SI(I)/4.
      NT(I)=(DUM1*DUM2+DUM1*DUM3)*TI(I)/4.
      GO TO 11
   13 DUM4=1.-S**2
      N(I)=DUM2*DUM4/2.
      NS(I)=-S*DUM2
      NT(I)=TI(I)*DUM4/2.
      GO TO 11
   17 DUM5=1.-T**2
      N(I)=DUM1*DUM5/2.
      NS(I)=DUM5*SI(I)/2.
      NT(I)=-T*DUM1
   11 CONTINUE
      N(9)=(1.-S**2)*(1.-T**2)
      NS(9)=-2.*S*(1.-T**2)
      NT(9)=-2.*T*(1.-S**2)
      DO 15 I=1,3
      DO 15 J=1,3
   15 JAC(I,J)=0.
      DO 21 I=1,8
      JAC(1,1)=JAC(1,1)+NS(I)*XL(I)+NS(I)*ZK*V1(I)/2.
      JAC(1,2)=JAC(1,2)+NS(I)*YL(I)+NS(I)*ZK*V2(I)/2.
      JAC(1,3)=JAC(1,3)+NS(I)*ZL(I)+NS(I)*ZK*V3(I)/2.
      JAC(2,1)=JAC(2,1)+NT(I)*XL(I)+NT(I)*ZK*V1(I)/2.
      JAC(2,2)=JAC(2,2)+NT(I)*YL(I)+NT(I)*ZK*V2(I)/2.
      JAC(2,3)=JAC(2,3)+NT(I)*ZL(I)+NT(I)*ZK*V3(I)/2.
      JAC(3,1)=JAC(3,1)+N(I)*V1(I)/2.
      JAC(3,2)=JAC(3,2)+N(I)*V2(I)/2.
      JAC(3,3)=JAC(3,3)+N(I)*V3(I)/2.
   21 CONTINUE
      DETJAC=JAC(1,1)*JAC(2,2)*JAC(3,3)             +JAC(2,1)
```

```
     1*JAC(3,2)*JAC(1,3)          +JAC(3,1)*JAC(1,2)*JAC(2
     2,3)           -JAC(1,3)*JAC(3,1)*JAC(2,2)          -JAC
     3(1,2)*JAC(2,1)*JAC(3,3)          -JAC(2,3)*JAC(3,2)
     4*JAC(1,1)
      RETURN
      END
      SUBROUTINE QMAT(Q)
      COMMON/YIELD/LL,MT,EL,ET,GLT,VTL,VTT,G23,G13,AL1,IPC
      DIMENSION Q(6,6)
      DO 420 I=1,6
      DO 420 J=1,6
  420 Q(I,J)=0.
      CS=COS(AL1)
      SN=SIN(AL1)
      CS2=CS*CS
      CS3=CS2*CS
      CS4=CS2*CS2
      SN2=SN*SN
      SN3=SN2*SN
      SN4=SN2*SN2
      XK=1./(EL*(1.-VTT**2)-2.*ET*VTL**2*(1.+VTT))
      C11=EL**2*(1.-VTT**2)*XK
      C12=ET*EL*VTL*(1.+VTT)*XK
      C13=C12
      C23=ET*(EL*VTT+ET*VTL**2)*XK
      C22=ET*(EL-ET*VTL**2)*XK
      C33=C22
      Q11=C11-C13*C13/C33
      Q12=C12-C13*C23/C33
      Q22=C22-C23*C23/C33
      Q66=GLT
      U1=Q12+2.*Q66
      U2=Q11+Q22-4.*Q66
      U3=Q11-Q12-2.*Q66
      U4=Q12-Q22+2.*Q66
      U5=Q11+Q22-2.*Q12-2.*Q66
      Q(1,1)= Q11*CS4+2.*U1*SN2*CS2+Q22*SN4
      Q(1,2)= U2*SN2*CS2+Q12*(SN4+CS4)
      Q(2,2)=Q11*SN4+2.*U1*SN2*CS2+Q22*CS4
      Q(1,4)= U3*SN*CS3+U4*SN3*CS
      Q(2,4)= U3*SN3*CS+U4*SN*CS3
      Q(4,4)= U5*SN2*CS2+Q66*(SN4+CS4)
      Q(4,1)=Q(1,4)
      Q(4,2)=Q(2,4)
      Q(2,1)=Q(1,2)
      Q(5,5)=(G23*CS2+G13*SN2)*5./6.
      Q(6,6)=(G23*SN2+G13*CS2)*5./6.
      Q(5,6)=((G23-G13)*CS*SN)*5./6.
      Q(6,5)=Q(5,6)
      RETURN
      END
```

```
      SUBROUTINE SPLINE(D,S,F,X,N,E5)
      DIMENSION B(50),C(50),D(50),A(50),F(50),S(50),X(50)
      WRITE(6,185)
  185 FORMAT(////,1X26HDATA FOR CUBIC SPLINE FIT     /
     1 1X43H NUMBER OF SEGMENT GI                   GF //
     2  )
      READ(5,186)N,E,E5
  186 FORMAT(I5,5X,2F10.0)
      WRITE(6,187) N,E,E5
 187  FORMAT(I5,5X,2E20.7)
      N1=N+1
      WRITE(6,261) N1
  261 FORMAT(10H THERE ARE,I2,7H POINTS)
      WRITE(6,330)
  330 FORMAT(37H INPUT MAG. AND INTERVAL STARING AT 1   )
      WRITE(6,340)
  340 FORMAT(6X,4HF(I),17X,4HS(I)   )
      READ (5,380)(F(I),X(I),I=1,N1)
  380 FORMAT(2F10.0)
      WRITE(6,381) (F(I),X(I),I=1,N1)
 381  FORMAT((2E20.7))
      DO 217     I=1,N
      S(I)=X(I+1)-X(I)
  217 CONTINUE
      A(1)=0.
      C(N1)=0.
      B(1)=S(1)/3.
      B(N1)=S(N)/3.
      DO 540 I=1,N
      C(I)=S(I)/6.
      A(I+1)=C(I)
      K=I+1
      IF(I.EQ.N) GO TO 540
      B(K)=(S(I)+S(K))/3.
      D(K)=(F(K+1)-F(K))/S(K)-(F(K)-F(K-1))/S(I)
  540 CONTINUE
      D(1)=(F(2)-F(1))/S(1)-E
      D(N1)=E5-(F(N1)-F(N))/S(N)
      DO 900 I=2,N1
      B(I)=-B(I)/A(I)
      C(I)=-C(I)/A(I)
      D(I)=-D(I)/A(I)
  900 CONTINUE
      CALL SOLVE(B,C,D,N1,50)
      RETURN
      END
      SUBROUTINE FUNCT(D,S,F,X,Y,N,X1,YP,YPP,E5)
      DIMENSION D(1),S(1),F(1),X(1)
      DO 2020 I=1,N
      IF(X1.GT.X(I+1)) GO TO 2020
      Y1=D(I)*(X(I+1)-X1)**3/(6.*S(I))
```

```
      Y2=D(I+1)*(X1-X(I))**3/(6.*S(I))
      Y3=(F(I+1)/S(I)-D(I+1)*S(I)/6.)*(X1-X(I))
      Y4=(F(I)/S(I)-D(I)*S(I)/6.)*(X(I+1)-X1)
      Y=Y1+Y2+Y3+Y4
      Y1=-(D(I)*(X(I+1)-X1)**2)/(2.*S(I))
      Y2=D(I+1)*(X1-X(I))**2/(2.*S(I))
      Y3=(F(I+1)-F(I))/S(I)
      Y4=-S(I)*(D(I+1)-D(I))/6.
      YF=Y1+Y2+Y3+Y4
      Y1=D(I)*(X(I+1)-X1)/S(I)
      Y2=D(I+1)*(X1-X(I))/S(I)
      YFP=Y1+Y2
      GO TO 2350
 2020 CONTINUE
      IF(X1 .GT. X(N+1))    YP=E5
 2360 CONTINUE
      RETURN
      END
         SUBROUTINE SOLVE(B,C,D,N1,ND)
      DIMENSION B(ND),C(ND),D(ND)
      DO 1240 I=1,N
      N=N1-1
      B(I+1)=B(I)*B(I+1)+C(I)
      C(I+1)=B(I)*C(I+1)
      D(I+1)=B(I)*D(I+1)+D(I)
 1240 CONTINUE
      C(N1)=0.
      D(N1)=D(N1)/B(N1)
      DO 1380 J=1,N
      I=N1-J
      D(I)=(D(I)-C(I)*D(I+1))/B(I)
 1380 CONTINUE
      RETURN
      END
      SUBROUTINE YIELD(MM)
      COMMON/SET2/INC,NFLAG,YLDX(4),YLDY(4),YLDS(4),YLDXX(4)
     1,          YLDYY(4),SUMS(100,8,3),KOUNT(100),
     2 KOUNTF(100),NFLAIL(100,8),NYIELD(100,8)
     3,SUMSIG(100,8,3),SUMSTN(100,20),SUMEX(100,20)
     4 ,SUMSX2(100,20)
      COMMON/YIELD/LL,MT,EL,ET,GLT,VTL,VTT,G23,G13,AL1,IPC
      COMMON/P/NSHELL,N9,NEDGEL,KOUNTY,KOUN
      DATA ONE,TWO,BLAN/6HYEILD*,6HFAIL**,1H /
      NNN=INC-1
      SS=YLDS(MT)
      STT=YLDS(MT)
      F1=1./YLDX(MT)-1./YLDXX(MT)
      F2=1./YLDY(MT)-1./YLDYY(MT)
      F3=1./SS-1./STT
      F11=1./(YLDX(MT)*YLDXX(MT))
      F22=1./(YLDY(MT)*YLDYY(MT))
```

```
      F33=1./(SS*STT)
      F12=0.
      S1=SUMS(MM,LL,1)
       S2=SUMS(MM,LL,2)
      S12=SUMS(MM,LL,3)
      SIGX=SUMSIG(MM,LL,1)
      SIGY=SUMSIG(MM,LL,2)
      SIGXY=SUMSIG(MM,LL,3)
      EXX=SUMEX(MM,LL)
      SX2=SUMSX2(MM,LL)
      IF(NFLAG.EQ.2) GO TO 309
      PC=(S1/YLDX(MT))**2+(S2/YLDY(MT))**2     -S1*S2/(YLDX
     1(MT)*YLDX(MT))+(S12/SS)**2
      GO TO 312
  309 PC=F1*S1+F2*S2+F3*S12             +F11*S1**2+F22*S2**2
     1        +F33*S12**2+2.*F12*S1*S2
  312 CONTINUE
      TAG=BLAN
      IF(PC.LT.1) GO TO 301
      IF(S1.GT.0.) GO TO 307
      XXX=-YLDXX(MT)
      IF(S1.GT.XXX) GO TO 305
      GO TO 308
  307 IF(S1.LT.YLDX(MT)) GO TO 305
  308 EL=100.
      ET=100.
      GLT=100.
      VTL=0.
      VTT=0.
      G23=100.
      G13=100.
      TAG=TWO
      GO TO 306
  305  ET=100.
      GLT=100.
      VTL=0.
      VTT=0.
      G23=100.
      TAG=ONE
  306  KOUNTY=1
  301 CONTINUE
      IF(IPC.EQ.1)WRITE(6,580)          NNN,MM,TAG,LL,PC
     1,SIGX,SIGY,SIGXY,S1,S2,S12,SX2,EXX
  580 FORMAT(1X,2I5,A6,I2,5X,F5.2,8E13.4)
      RETURN
      END
      SUBROUTINE INLOAD(R,PX,PY,PZ,PM,PN,PU,NEDGEL)
      COMMON/LOADGH/LD,NEQ,NLOAD,NEL,NELPL,NNP
      DIMENSION R(302),PX(44),PY(44),PZ(44),PM(44,4),PN(44)
     1         ,PU(44,8),NSIDE(4)
      COMMON/H1/X(163),Y(163),Z(163),ID(163,3)
```

```
      DATA NSIDE/3,4,1,2/
      WRITE(6,1050)
      GO TO (1,2,3,4,5,9,9,9,9),LD
    4 CONTINUE
      WRITE(6,1051)
      DO 10 I=1,NEQ
   10 R(I)=0.
      DO 220 L=1,NLOAD
      READ(5,1000)ND,IDIRN,FLOAD
      WRITE(6,1070)ND,IDIRN,FLOAD
      II=ID(ND,IDIRN)
      IF(II)220,220,240
  240 R(II)=R(II)+FLOAD
  220 CONTINUE
      RETURN
    1 CONTINUE
      DO 390 M=1,NEL
      WRITE(6,1070)
      PX(M)=0.
      PY(M)=0.
      PZ(M)=0.
  390 CONTINUE
      KN=0
      DO 420 I=1,NELPL
      IF(KN.EQ.0)READ(5,1001)L,PX(L),PY(L),PZ(L),KN
      IF(KN.EQ.0) GO TO 410
      PX(I)=PX(1)
      PY(I)=PY(1)
      PZ(I)=PZ(1)
  410 WRITE(6,1001)L,PX(L),PY(L),PZ(L),KN
  420 CONTINUE
      RETURN
    5 CONTINUE
      WRITE(6,1080)
      DO 380 M=1,NEL
      DO 380 L=1,4
  380 PM(M,L)=0.
      DO 370 M=1,NEDGEL
      READ(5,1010)L,ISIDE,PMLD
      WRITE(6,1015)L,ISIDE,PMLD
      NSID=NSIDE(ISIDE)
      PM(L,NSID)=PMLD
  370 CONTINUE
      RETURN
    2 CONTINUE
      WRITE(6,1090)
      KN=0
      DO 500 M=1,NEL
      IF(KN.EQ.0)READ(5,1030)L,PN(L),KN
       IF(KN.EQ.0) GO TO 450
      PN(M)=PN(1)
```

```
  450 WRITE(6,1030) M,PN(M),KN
  500 CONTINUE
      RETURN
    3 CONTINUE
      WRITE(6,2000)
      DO 510 I=1,NELPL
      READ(5,1040) L,(PU(L,J),J=1,8)
      WRITE(6,1040) L,(PU(L,J),J=1,8)
  510  CONTINUE
    9 CONTINUE
      RETURN
 1015 FORMAT(1X,I5,I7,5X,F12.4)
 1000 FORMAT(I5,5X,3F10.4)
 1001 FORMAT(I5,5X,3F10.4,I5)
 1010 FORMAT(2I5,F10.4)
 1030 FORMAT(I5,5X,F10.4,I5)
 1040 FORMAT(I5,/,8F10.4)
 1061 FORMAT(      1X,20HCONCENTRED LOAD                  ////
     1     1X 29H NODE       DIRECTION        LOAD         /
     2 1X 32HNUMBER                     MAGNITUDE      //       )
 1070 FORMAT(      1X 20HDISTRIBUTED LOAD                ////
     1 1X 41HELEMENT       PX          PY          PZ    KN     /
     2    1X 10H    NO.             )
 1080 FORMAT(      1X 20HE D G E  L O A D          ////      1X
     1 40HELEMENT  SIDE      LOAD                            /
     2 1X 40H  NO.            MAGNITUDE                       /
     3    )
 1090 FORMAT(      1X 11HNORMAL LOAD                             //
     1//      1X30HELEMENT     PN           KN
     2 /      1X 5H  NO.     /     )
 2000 FORMAT(      1X 35HNONUNIFORM DISTRIBUTED LOAD
     1 /      1X 48HELEMENT          PRESSURE INTENSITY AT
     2 LOCAL COOR.  /      1X 45H  NO.    1     2     3     4
     3 5     6     7     8    /     )
 1050 FORMAT(1H1      1X 27HL O A D   T Y P E    D A T A
     1  ////      )
      END
      SUBROUTINE INPUT(X,Y,Z,NNP)
      DIMENSION IPRC(1),X(163),Y(163),Z(163)
      DATA IPRC/1HF/
      RAD=ATAN(1.0)/(45.0)
      NOLD=0
      WRITE(6,2030)
   10 CONTINUE
      READ (5,1000)IT,N,X(N),Y(N),Z(N),KN
 1000 FORMAT(A1,I4,5X,3F10.0,I5)
      WRITE(6,2002)IT,N,X(N),Y(N),Z(N),KN
 2002 FORMAT(1X,A1,I4,3F12.4,I5)
      IF(NOLD.EQ.0) GO TO 50
      IF(KN.EQ.0) GO TO 50
      NUM=(N-NOLD)/KN
```

```
      NUMN=NUM-1
      IF(NUMN.LT.1) GO TO 50
      XNUM=NUM
      DX=(X(N)-X(NOLD))/XNUM
      DY=(Y(N)-Y(NOLD))/XNUM
      DZ=(Z(N)-Z(NOLD))/XNUM
      K=NOLD
      DO 30 J=1,NUMN
      KK=K
      K=K+KN
      X(K)=X(KK)+DX
      Y(K)=Y(KK)+DY
      Z(K)=Z(KK)+DZ
   30 CONTINUE
   50 NOLD=N
      IF(IT.NE.IPRC(1))GO TO 60
      IF(KN.EQ.0)GO TO 70
      DO 29 J=1,NUMN
      K=N-J*KN
      DUM=Z(K)*RAD
      Z(K)=Y(K)*COS(DUM)
      Y(K)=Y(K)*SIN(DUM)
   29 CONTINUE
   70 CONTINUE
      DUM=Z(NOLD)*RAD
      Z(NOLD)=Y(NOLD)*COS(DUM)
      Y(NOLD)=Y(NOLD)*SIN(DUM)
   60 NOLD=N
      IF(N.NE.NNP)GO TO 10
      RETURN
 2030 FORMAT(////,1X 22HNODAL POINT INPUT DATA /         1X
     1,40H NODE   NODAL POINT COORDINATES               /
     2 1X 43HNUMBER        X               Y         Z          KN/
     3  )
      END
      SUBROUTINE INID(ID,NNP,NEQ)
      DIMENSION ID(163,5)
      NOLD=0
      WRITE(6,2035)
   15 CONTINUE
      READ(5,1005) N,(ID(N,I),I=1,5),KN
 1005 FORMAT(7I5)
      WRITE(6,2006)N,(ID(N,I),I=1,5),KN
 2006 FORMAT(1X,7I5)
      IF(NOLD.EQ.0)GO TO 55
      DO 20 I=1,5
      IF(ID(N,I).EQ.0.AND.ID(NOLD,I).LT.0)                  ID(N
     1,I)=ID(NOLD,I)
   20 CONTINUE
      IF(KN.EQ.0) GO TO 55
      NUM=(N-NOLD)/KN
```

```
      NUMN=NUM-1
      IF(NUMN.LT.1) GO TO 55
      K=NOLD
      DO 35 J=1,NUMN
      KK=K
      K=K+KN
      DO 35 I=1,5
      ID(K,I)=ID(KK,I)
      IF(ID(K,I).GT.1)ID(K,I)=ID(KK,I)+KN
   35 CONTINUE
   55 NOLD=N
      IF(N.NE.NNP) GO TO 15
      WRITE(6,2040)
      WRITE(6,2010)(N,(ID(N,I),I=1,5),N=1,NNP)
 2010 FORMAT(6I5)
      NEQ=0
      DO 62 N=1,NNP
      DO 62 I=1,5
      ID(N,I)=IABS(ID(N,I))
      IF(ID(N,I)-1)57,58,59
   57 NEQ=NEQ+1
      ID(N,I)=NEQ
      GO TO 62
   58 ID(N,I)=0
      GO TO 62
   59 ID(N,I)=-ID(N,I)
   62 CONTINUE
 2035 FORMAT(///,1X 20HINPUT ID CODES
     1          /      1X 40H NODE   BOUNDARY CONDITION CODES
     2                    /       1X 40HNUMBER    X     Y     Z
     3 ALPHA BATA   KN            /       )
 2040 FORMAT(//1X,40HGENERATED ID CODES
     1    /       1X 40H NODE   BOUNDARY CONDITION CODES
     2              /       1X 40HNUMBER    X     Y     Z  ALPHA BATA
     3                    /)
      RETURN
      END
      SUBROUTINE SURVEC(THICK)
      COMMON/H2/XL(9),YL(9),ZL(9),V1(9),V2(9),V3(9),JAC(3,3)
     1,       N(9),NS(9),NT(9),U1(9),U2(9),U3(9),W1(9),W2(9)
     2,W3(9)
      DIMENSION SI(8),TI(8)
      REAL N,NS,NT,JAC
      REAL L1,L2,L3,M1,M2,M3,N1,N2,N3
      DATA SI/-1.,0.,1.,1.,1.,0.,-1.,-1./
      DATA  TI/-1.,-1.,-1.,0.,1.,1.,1.,0./
      DO 30 II=1,8
      S=SI(II)
      T=TI(II)
      DO 11 I=1,8
      SUM1=1.+SI(I)*S
```

```
      DUM2=1.+TI(I)*T
      IF(I.EQ.2.OR.I.EQ.6) GO TO 13
      IF(I.EQ.4.OR.I.EQ.8) GO TO 17
      DUM3=      S*SI(I)+      T*TI(I)-1.
      N(I)=DUM1*DUM2*DUM3/4.
      NS(I)=(DUM1*DUM2+DUM2*DUM3)*SI(I)/4.
      NT(I)=(DUM1*DUM2+DUM1*DUM3)*TI(I)/4.
      GO TO 11
   13 DUM4=1.-      S**2
      N(I)=DUM2*DUM4/2.
      NS(I)=-      S*DUM2
      NT(I)=TI(I)*DUM4/2.
      GO TO 11
   17 DUM5=1.-      T**2
      N(I)=DUM1*DUM5/2.
      NS(I)=DUM5*SI(I)/2.
      NT(I)=-      T*DUM1
   11 CONTINUE
      XXI=0.
      YXI=0.
      ZXI=0.
      XET=0.
      YET=0.
      ZET=0.
      DO 20 I=1,8
      XXI=XXI+NS(I)*XL(I)
      YXI=YXI+NS(I)*YL(I)
      ZXI=ZXI+NS(I)*ZL(I)
      XET=XET+NT(I)*XL(I)
      YET=YET+NT(I)*YL(I)
      ZET=ZET+NT(I)*ZL(I)
   20 CONTINUE
      DL=(XXI*XXI+YXI*YXI+ZXI*ZXI)**.5
      L1=XXI/DL
      M1=YXI/DL
      N1=ZXI/DL
      U1(II)=L1
      U2(II)=M1
      U3(II)=N1
      DL=(XET*XET+YET*YET+ZET*ZET)**.5
      L2=XET/DL
      M2=YET/DL
      N2=ZET/DL
      W1(II)=L2
      W2(II)=M2
      W3(II)=N2
      L3=M1*N2-M2*N1
      M3=L2*N1-N2*L1
      N3=L1*M2-M1*L2
      V1(II)=L3*THICK
      V2(II)=M3*THICK
```

```
      V3(II)=N3*THICK
30    CONTINUE
      RETURN
      END
      SUBROUTINE ETRAN(E,DE,D)
      COMMON/H2/XL(9),YL(9),ZL(9),V1(9),V2(9),V3(9),
     1  JAC(3,3),N(9),NS(9),NT(9)
      COMMON/DC/L1,L2,L3,M1,M2,M3,N1,N2,N3
      DIMENSION  E(6,6),DE(6,6), D(6,6), DTE(6,6),DETE(6,6)
     1,TE(6,6),            ETE(6,6)
      REAL N,NS,NT,JAC
      REAL L1,L2,L3,M1,M2,M3,N1,N2,N3
      XXI=0.
      YXI=0.
      ZXI=0.
      XET=0.
      YET=0.
      ZET=0.
      DO 20 I=1,8
      XXI=XXI+NS(I)*XL(I)
      YXI=YXI+NS(I)*YL(I)
      ZXI=ZXI+NS(I)*ZL(I)
      XET=XET+NT(I)*XL(I)
      YET=YET+NT(I)*YL(I)
      ZET=ZET+NT(I)*ZL(I)
20    CONTINUE
      DL=(XXI*XXI+YXI*YXI+ZXI*ZXI)**.5
      L1=XXI/DL
      M1=YXI/DL
      N1=ZXI/DL
      DL=(XET*XET+YET*YET+ZET*ZET)**.5
      L2=XET/DL
      M2=YET/DL
      N2=ZET/DL
      L3=M1*N2-M2*N1
      M3=L2*N1-N2*L1
      N3=L1*M2-M1*L2
      L2=M3*N1-N3*M1
      M2=L1*N3-L3*N1
      N2=L3*M1-M3*L1
      CALL TMAX(TE,1.,2.)
      DO 100 I=1,6
      DO 100 J=1,6
      ETE(I,J)=0.
      DETE(I,J)=0.
      DTE(I,J)=0.
      DO 100 M=1,6
      ETE(I,J)=ETE(I,J)+E(I,M)*TE(M,J)
      DETE(I,J)=DETE(I,J)+DE(I,M)*TE(M,J)
       DTE(I,J)= DTE(I,J)+ D(I,M)*TE(M,J)
100   CONTINUE
```

```
      DO 200 I=1,6
      DO 200 J=1,6
      E(I,J)=0.
      DE(I,J)=0.
       D(I,J)=0.
      DO 200 M=1,6
      E(I,J)=E(I,J)+TE(M,I)*ETE(M,J)
      DE(I,J)=DE(I,J)+TE(M,I)*DETE(M,J)
      D(I,J)=D(I,J)+TE(M,I)*DTE(M,J)
  200 CONTINUE
      RETURN
      END
      SUBROUTINE STRANS(TT,SIG,AL,KK,KKK)
      COMMON/H2/X(9),Y(9),Z(9),V1(9),V2(9),V3(9),
     1 JAC(3,3),N(9),NS(9),NT(9)
 1776 CONTINUE
      COMMON/DC/L1,L2,L3,M1,M2,M3,N1,N2,N3
      DIMENSION T(6,6),TT(6),SIG(6)
      REAL N,NS,NT,JAC
      REAL L1,M1,N1,      L2,M2,N2,      L3,M3,N3
      IF(KK.EQ.0)GO TO 2
      PI=3.141592654
      B=AL*PI/180.
      L1=COS(B)
      M1=SIN(B)
      N1=0.
      L2=-SIN(B)
      M2=COS(B)
      N2=0.
      L3=0.
      M3=0.
      N3=1.
      GO TO 3
    2 CONTINUE
      DX=0.
      DY=0.
      DZ=0.
      DO 10 I=1,8
      DX=DX+NS(I)*X(I)
      DY=DY+NS(I)*Y(I)
   10 DZ=DZ+NS(I)*Z(I)
      DL=(DX*DX+DY*DY+DZ*DZ)**.5
      L1=DX/DL
      M1=DY/DL
      N1=DZ/DL
      DX=0.
      DY=0.
      DZ=0.
      DO 20 I=1,6
      DX=DX+NT(I)*X(I)
      DY=DY+NT(I)*Y(I)
```

```
20    DZ=DZ+NT(I)*Z(I)
      DL=(DX*DX+DY*DY+DZ*DZ)**.5
      L2=DX/DL
      M2=DY/DL
      N2=DZ/DL
      L3=M1*N2-M2*N1
      M3=L2*N1-N2*L1
      N3=L1*M2-M1*L2
      L2=M3*N1-N3*M1
      M2=L1*N3-L3*N1
      N2=L3*M1-M3*L1
    3 CONTINUE
      IF(KKK.EQ.0) GO TO 5
      C=2.
      C=1.
      GO TO 6
5     CONTINUE
      C=1.
      D=2.
6     CONTINUE
      CALL TMAX(T,C,D)
      DO 1 I=1,6
      TT(I)=0.
      DO 1 J=1,6
      TT(I)=TT(I)+T(I,J)*SIG(J)
    1 CONTINUE
      RETURN
      END
      SUBROUTINE TMAX(T,C,D)
      DIMENSION T(6,6)
      COMMON/DC/L1,L2,L3,M1,M2,M3,N1,N2,N3
      REAL L1,L2,L3,M1,M2,M3,N1,N2,N3
      T(1,1)=L1**2
      T(1,2)=M1**2
      T(1,3)=N1**2
      T(1,4)=C*L1*M1
      T(1,5)=C*M1*N1
      T(1,6)=C*N1*L1
      T(2,1)=L2**2
      T(2,2)=M2**2
      T(2,3)=N2**2
      T(2,4)=C*L2*M2
      T(2,5)=C*M2*N2
      T(2,6)=C*N2*L2
      T(3,1)=L3**2
      T(3,2)=M3**2
      T(3,3)=N3**2
      T(3,4)=C*L3*M3
      T(3,5)=C*M3*N3
      T(3,6)=C*N3*L3
      T(4,1)=L1*L2*D
```

```
      T(4,2)=M1*M2*D
      T(4,3)=N1*N2*D
      T(4,4)=L1*M2+L2*M1
      T(4,5)=M1*N2+M2*N1
      T(4,6)=N1*L2+N2*L1
      T(5,1)=L2*L3*D
      T(5,2)=M2*M3*D
      T(5,3)=N2*N3*D
      T(5,4)=L2*M3+L3*M2
      T(5,5)=M2*N3+M3*N2
      T(5,6)=N2*L3+N3*L2
      T(6,1)=L3*L1*D
      T(6,2)=M3*M1*D
      T(6,3)=N3*N1*D
      T(6,4)=L3*M1+L1*M3
      T(6,5)=M3*N1+M1*N3
      T(6,6)=N3*L1+N1*L3
      RETURN
      END
      SUBROUTINE BMAT(B,BB)
      DIMENSION B(6,45),BB(6,45),KKK(5)
      COMMON/K/K1,K2,K3,K4,K5
      COMMON/H22/TT,U11,U21,U31,U12,U22,U32,I
      COMMON/H2/XL(9),YL(9),ZL(9),V1(9),V2(9),V3(9),
     1  JAC(3,3),N(9),NS(9),NT(9)
      REAL JAC,N,NS,NT
      DO 51 J=1,5
   51 KKK(J)=5*(I-1)+J
      K1=KKK(1)
      K2=KKK(2)
      K3=KKK(3)
      K4=KKK(4)
      K5=KKK(5)
      A1=JAC(1,1)*NS(I)+JAC(1,2)*NT(I)
      B1=JAC(2,1)*NS(I)+JAC(2,2)*NT(I)
      C1=JAC(3,1)*NS(I)+JAC(3,2)*NT(I)
      B(1,K1)=A1
      B(1,K4)=JAC(1,3)*N(I)*U11*TT/2.
      B(1,K5)=JAC(1,3)*N(I)*U12*TT/2.
      B(2,K2)=B1
      B(2,K4)=JAC(2,3)*N(I)*U21*TT/2.
      B(2,K5)=JAC(2,3)*N(I)*U22*TT/2.
      B(3,K3)=C1
      B(3,K4)=JAC(3,3)*N(I)*U31*TT/2.
      B(3,K5)=JAC(3,3)*N(I)*U32*TT/2.
      B(4,K1)=B1
      B(4,K2)=A1
      B(4,K4)=JAC(2,3)*N(I)*U11*TT/2.+JAC(1,3)*N(I)*U21*TT
     1/2.
      B(4,K5)=JAC(2,3)*N(I)*U12*TT/2.+JAC(1,3)*N(I)*U22*TT
     1/2.
```

```
      B(5,K2)=C1
      B(5,K3)=B1
      B(5,K4)=JAC(3,3)*N(I)*U21*TT/2.+JAC(2,3)*N(I)*U31*TT
     1/2.
      B(5,K5)=JAC(3,3)*N(I)*U22*TT/2.+JAC(2,3)*N(I)*U32*TT
     1/2.
      B(6,K1)=C1
      B(6,K3)=A1
      B(6,K4)=JAC(3,3)*N(I)*U11*TT/2.+JAC(1,3)*N(I)*U31*TT
     1/2.
      B(6,K5)=JAC(3,3)*N(I)*U12*TT/2.+JAC(1,3)*N(I)*U32*TT
     1/2.
      BE(1,K4)=A1*U11*TT/2.
      BE(1,K5)=A1*U12*TT/2.
      BE(2,K4)=B1*U21*TT/2.
      BE(2,K5)=B1*U22*TT/2.
      BE(3,K4)=C1*U31*TT/2.
      BE(3,K5)=C1*U32*TT/2.
      BE(4,K4)=B1*U11*TT/2.+A1*U21*TT/2.
      BE(4,K5)=B1*U12*TT/2.+A1*U22*TT/2.
      BE(5,K4)=C1*U21*TT/2.+B1*U31*TT/2.
      BE(5,K5)=C1*U22*TT/2.+B1*U32*TT/2.
      BE(6,K4)=C1*U11*TT/2.+A1*U31*TT/2.
      BE(6,K5)=C1*U12*TT/2.+A1*U32*TT/2.
      RETURN
      END
      SUBROUTINE MESH8(XX,YY,ZZ,NOD,NEQ,NEL,ND,TITLE)
      DIMENSION TITLE(13),XP(100),YP(100),XPG(13),YPG(13),N
     1(12),NON(12)
      DIMENSION NN(21,21),YC(21,21),XC(21,21),NNB3(20,4,21)
     1,JT(20,4)
      DIMENSION LB(8),NE(400),XE(400),YE(400),NF(8),ICOMP(4
     1,4)
      DIMENSION XX(1),YY(1),NOD(ND,8)
      DIMENSION ZP(100),ZPG(13),ZE(400),ZZ(1),ZC(21,21)
      REAL N
      DATA ICOMP/-1,1,1,-1,1,-1,-1,1,1,-1,-1,1,-1,1,1,-1/
      DATA NBW/0/,NB/0/
      DATA Z,U,V,W/0.,0.,0.,0./
      REWIND 1
      NEQ=0
      NEL=0
      NEN=8
      WRITE(6,17) (TITLE(I),I=1,11)
   17 FORMAT(1X,'MESH GENERATION FOR'11A6,/)
      READ (5,1) INRG,INBP,NBN
    1 FORMAT(4I5)
      READ(5,3)(XP(I),I=1,INBP)
      READ(5,3)(YP(I),I=1,INBP)
      READ(5,3)(ZP(I),I=1,INBP)
      IF(NBN.EQ.0) NBN=8
```

```
    3 FORMAT(8F10.5)
      DO 2 I=1,INRG
    2  READ(5,8) NRG,(JT(NRG,J),J=1,4)
    8 FORMAT(5I5)
      WRITE(6,36)
   36 FORMAT(1H0////1X,"GLOBAL COORDINATES"//1X,"NUMBER X
     1 COORD     Y COORD     ")
      WRITE(6,30) (I,XP(I),YP(I),ZP(I),I=1,INBP)
   30 FORMAT (2X,I3,7X,F7.2,5X,F7.2,5X,F7.2)
      WRITE(6,21)
   21 FORMAT(//1X,17HCONNECTIVITY DATA/1X,41HREGION     SIDE
     1  1       2        3       4    )
      DO26I=1,INRG
   26 WRITE(6,22) I,(JT(I,J),J=1,4)
   22 FORMAT(2X,I3,14X,4(I2,5X))
      DO16KK=1,INRG
      READ(5,4) NRG,NROWS,NCOL,(NON(I),I=1,NBN)
    4 FORMAT(15I5)
      WRITE(6,18) NRG,NROWS,NCOL,(NON(I),I=1,NBN)
   18 FORMAT(1H0///1X,12H***   REGION ,I2,6H   ****//10X,I2,5H
     1 ROWS,10X,I2,8H COLUMNS//10X,21HBOUNDARY NODE NUMBES
     2,10X,12I5)
      DO 5 I=1,NBN
      II=NON(I)
      ZRG(I)=ZP(II)
      XRG(I)=XP(II)
    5 YRG(I)=YP(II)
      TR=NROWS-1
      DETA=2./TR
      TR=NCOL-1
      DSI=2./TR
      DO12I=1,NROWS
      TR=I-1
      ETA=1.-TR*DETA
      DO12J=1,NCOL
      TR=J-1
      SI=-1.+TR*DSI
      IF(NBN.EQ.8) GO TO 1012
      N(1)=(1.-SI)*(1.-ETA)*(-10.+9.*(SI*SI+ETA*ETA))/32.
      N(2)=9.*(1.-ETA)*(1.-SI*SI)*(1.-3.*SI  )/32.
      N(3)=9.*(1.-ETA)*(1.-SI*SI)*(1.+3.*SI  )/32.
      N(4)=(1.+SI)*(1.-ETA)*(-10.+9.*(SI*SI+ETA*ETA))/32.
      N(5)=9.*(1.+SI)*(1.-ETA*ETA)*(1.-3.*ETA)/32.
      N(6)=9.*(1.+SI)*(1.-ETA*ETA)*(1.+3.*ETA)/32.
      N(7)=(1.+SI)*(1.+ETA)*(-10.+9.*(SI*SI+ETA*ETA))/32.
      N(8)=9.*(1.+ETA)*(1.-SI*SI)*(1.+3.*SI)/32.
      N(9)=9.*(1.+ETA)*(1.-SI*SI)*(1.-3.*SI)/32.
      N(10)=(1.-SI)*(1.+ETA)*(-10.+9.*(SI*SI+ETA*ETA))/32.
      N(11)=9.*(1.-SI)*(1.-ETA*ETA)*(1.+3.*ETA)/32.
      N(12)=9.*(1.-SI)*(1.-ETA*ETA)*(1.-3.*ETA)/32.
      GO TO 1013
```

```
1012 CONTINUE
     N(1)=-0.25*(1.-SI)*(1.-ETA)*(SI+ETA+1.)
     N(2)=0.50*(1.-SI**2)*(1.-ETA)
     N(3)=0.25*(1.+SI)*(1.-ETA)*(SI-ETA-1.)
     N(4)=0.50*(1.+SI)*(1.-ETA**2)
     N(5)=0.25*(1.+SI)*(1.+ETA)*(SI+ETA-1.)
     N(6)=0.50*(1.-SI**2)*(1.+ETA)
     N(7)=0.25*(1.-SI)*(1.+ETA)*(ETA-SI-1.)
     N(8)=0.50*(1.-SI)*(1.-ETA**2)
1013 CONTINUE
     ZC(I,J)=0.
     XC(I,J)=0.
     YC(I,J)=0.0
     DO 12 K=1,NRN
     ZC(I,J)=ZC(I,J)+ZRG(K)*N(K)
     XC(I,J)=XC(I,J)+XRG(K)*N(K)
  12 YC(I,J)=YC(I,J)+YRG(K)*N(K)
     KN1=1
     KS1=1
     KN2=NROWS
     KS2=NCOL
     DO 50 I=1,4
     NRT=JT(NRG,I)
     IF(NRT.EQ.0.OR.NRT.GT.NRG) GO TO 50
     DO 56 J=1,4
  56 IF(JT(NRT,J).EQ.NRG) NRTS=J
     K=NCOL
     IF(I.EQ.2.OR.I.EQ.4) K=NROWS
     JL=1
     JK=ICOMP(I,NRTS)
     IF(JK.EQ.-1) JL=K
     DO 44 J=1,K
     GO TO (45,46,47,48),I
  45 NN(NROWS,J)=NNRB(NRT,NRTS,JL)
     KN2=NROWS-1
     GO TO 44
  46 NN(J,NCOL)=NNRB(NRT,NRTS,JL)
     KS2=NCOL-1
      GO TO 44
  47 NN(1,J)=NNRB(NRT,NRTS,JL)
     KN1=2
     GO TO 44
  48 NN(J,1)=NNRB(NRT,NRTS,JL)
     KS1=2
  44 JL=JL+JK
  50 CONTINUE
     IF (KN1.GT.KN2) GO TO 105
     IF (KS1.GT.KS2) GO TO 105
     DO 10 I=KN1,KN2
     II=(I/2)*2
     DO 10 J=KS1,KS2
```

```
      JJ=(J/2)*2
      IF(I.EQ.II.AND.J.EQ.JJ) GO TO 1001
      NE=NB+1
      NN(I,J)=NB
      GO TO 10
 1001 NN(I,J)=0
   10 CONTINUE
      DO 42 I=1,NCOL
      NNRB(NRG,1,I)=NN(NROWS,I)
   42 NNRB(NRG,3,I)=NN(1,I)
      DO 43 I=1,NROWS
      NNRB(NRG,2,I)=NN(I,NCOL)
   43 NNRB(NRG,4,I)=NN(I,1)
      DO 210 I=1,NROWS
      DO 210 J=1,NCOL
      IF(NEQ.GT.NN(I,J)) GO TO 210
      NEQ=NN(I,J)
  210 CONTINUE
  105 CONTINUE
      K=1
      DO 54 I=1,NROWS
      DO 54 J=1,NCOL
      IF(NN(I,J).EQ.0) GO TO 54
      XE(K)=XC(I,J)
      YE(K)=YC(I,J)
      ZE(K)=ZC(I,J)
      NE(K)=NN(I,J)
      K=K+1
   54 CONTINUE
      L=NROWS-1
      DO 151 I=1,L,2
      DO 151 J=3,NCOL,2
      NR(1)=(NCOL+(NCOL+1)/2)*(1+I/2)+J-2
      NR(2)=NR(1)+1
      NR(3)=NR(2)+1
      NR(4)=NCOL*(1+I/2)+((NCOL+1)/2)*(I/2)+J-(J/2)
      NR(5)=(NCOL+(NCOL+1)/2)*(I/2)+J
      NR(6)=NR(5)-1
      NR(7)=NR(6)-1
      NR(8)=NR(4)-1
      NEL=NEL+1
      J1=NR(1)
      J2=NR(2)
      J3=NR(3)
      J4=NR(4)
      J5=NR(5)
      J6=NR(6)
      J7=NR(7)
      J8=NR(8)
      LB(1)=IABS(NE(J1)-NE(J2))+1
      LB(2)=IABS(NE(J2)-NE(J3))+1
```

```
      LE(3)=IABS(NE(J3)-NE(J4))+1
      LE(4)=IABS(NE(J4)-NE(J5))+1
      LE(5)=IABS(NE(J5)-NE(J6))+1
      LE(6)=IABS(NE(J6)-NE(J7))+1
      LE(7)=IABS(NE(J7)-NE(J8))+1
      LE(8)=IABS(NE(J8)-NE(J1))+1
      DO 207 IK=1,8
      IF(LE(IK).LE.NBW) GO TO 207
      NBW=LE(IK)
      NELBW=NEL
  207 CONTINUE
      XX(NE(J1))=XE(J1)
      XX(NE(J2))=XE(J2)
      XX(NE(J3))=XE(J3)
      XX(NE(J4))=XE(J4)
      XX(NE(J5))=XE(J5)
      XX(NE(J6))=XE(J6)
      XX(NE(J7))=XE(J7)
      XX(NE(J8))=XE(J8)
      YY(NE(J1))=YE(J1)
      YY(NE(J2))=YE(J2)
      YY(NE(J3))=YE(J3)
      YY(NE(J4))=YE(J4)
      YY(NE(J5))=YE(J5)
      YY(NE(J6))=YE(J6)
      YY(NE(J7))=YE(J7)
      YY(NE(J8))=YE(J8)
      ZZ(NE(J1))=ZE(J1)
      ZZ(NE(J2))=ZE(J2)
      ZZ(NE(J3))=ZE(J3)
      ZZ(NE(J4))=ZE(J4)
      ZZ(NE(J5))=ZE(J5)
      ZZ(NE(J6))=ZE(J6)
      ZZ(NE(J7))=ZE(J7)
      ZZ(NE(J8))=ZE(J8)
      NOD(NEL,1)=NE(J1)
      NOD(NEL,2)=NE(J2)
      NOD(NEL,3)=NE(J3)
      NOD(NEL,4)=NE(J4)
      NOD(NEL,5)=NE(J5)
      NOD(NEL,6)=NE(J6)
      NOD(NEL,7)=NE(J7)
      NOD(NEL,8)=NE(J8)
  270 CONTINUE
  151 CONTINUE
   16 CONTINUE
      WRITE(1,500) NEL,NEQ
  500 FORMAT(2I5)
      DO 220 I=1,NEQ
      WRITE(1,501) XX(I),YY(I),ZZ(I),U,V,W
  220 CONTINUE
```

```
501 FORMAT(8F10.4)
    DO 230 I=1,NEL
    WRITE(1,502) (NOD(I,J),J=1,NEN)
230 CONTINUE
502 FORMAT(8I5)
    CLOSE(1,DISP=KEEP)
    RETURN
    END
```

END

FILMED

2-83

DTIC